Electroweak Radiative Corrections and Effective Field Theories

Dissertation

zur Erlangung des Doktorgrades
an der Fakultät für Mathematik,
Informatik und Naturwissenschaften

Fachbereich Physik
der Universität Hamburg

vorgelegt von
Benoît Assi

Hamburg
2021

Gutachter der Dissertation:	Prof. Dr. Bernd Kniehl Prof. Dr. Sven-Olaf Moch
Prüfungskommission:	Prof. Dr. Bernd Kniehl Prof. Dr. Sven-Olaf Moch Prof. Dr. Dieter Horns Prof. Dr. Caren Hagner Prof. Dr. Elisabetta Gallo
Vorsitzender der Prüfungskommission:	Prof. Dr. Dieter Horns
Datum der Disputation:	18.08.2021
Vorsitzender des Promotionsausschusses Physik:	Prof. Dr. Wolfgang Hansen
Leiter des Fachbereichs Physik:	Prof. Dr. Michael Potthoff
Dekan der Fakultät MIN:	Prof. Dr. Heinrich Graener

To my grandmother Alice, who loved nature beyond reason.

Abstract

The Standard Model (SM) of particle physics can be divided into the strong sector and the electroweak (EW) sector. The strong interactions governed by Quantum Chromodynamics (QCD) have an out-sized influence on high energy predictions relative to the EW interactions. Thanks to the enormous effort in the precision analysis of QCD, we are now reaching a turning point in which EW uncertainty is of the same or higher order. Our goal is to further develop the progress of describing the EW sector's role, particularly with regards to heavy fields in the SM and beyond.

In this thesis, we begin by deriving the static potential of a heavy field in theories exhibiting spontaneous symmetry breaking. We then use our findings to calculate the potential of a heavy quark-antiquark pair in the Standard Model at EW one-loop order. We do so in both the Wilson loop and scattering amplitude approaches and discuss the limitations of the Wilson loop approach. As the field content of the SM is extensive, similar studies in a large set of models are now achievable by varying the appropriate couplings and group theory factors. We then present the leading EW corrections to the short-distance heavy quark mass definitions. We achieve this with the heavy meson static potential as well as its binding and residual kinetic energy. These energies form the building blocks of most short-distance mass definitions. We explain how attaining the EW contributions to these energies leads to additional corrections to the masses. We determine that the leading EW corrections are of the same strength as their next-to-leading pure QCD counterparts. Next, we consider the leading electroweak corrections to the heavy quark effective theory and non-relativistic QCD Lagrangian. These corrections appear in the Wilson coefficients of the heavy quark operators at one-loop order. Due to Parity violation in the SM, operators up to this order include new parity-violating terms. We derive these analogously to the parity-preserving QCD result at one-loop order. Pushing the previous analysis to two-loop order and generalising, we compute the massive gauge and scalar corrections to form factors in both the Sudakov and threshold regimes up to and including two-loop orders. The corrections are calculated for processes involving two external fermions and scalars in the spontaneously broken $SU(N)$-Higgs model, examining a set of composite operators. We further discuss how form factors in our toy model can be mapped to the Standard Model and beyond. Lastly, we determine the master integrals for vertex and propagator diagrams appearing in effective field theories containing heavy fields. The integrals involve at least one heavy line, and the standard lines include an arbitrary mass scale. We employ modern methods to tackle these two-loop integrals, including differential equations and dimensional recurrence relations.

Zusammenfassung

Das Standardmodell (SM) der Teilchenphysik und seine Vorhersagen lassen sich in den starken und elektroschwachen (EW) Sektor unterteilen. Wie der Name schon sagt, haben starke Wechselwirkungen, die von der Quantenchromodynamik (QCD) gesteuert werden, einen übergroßen Einfluss auf die Dynamik und folglich auf Präzisionsstudien. Dank des enormen Aufwands bei Präzisionsanalysen in der QCD erreichen wir jetzt einen Wendepunkt, an dem die EW-Unsicherheit gleich oder höhr ist. Unser Ziel ist es, Teil des Fortschritts an dieser neuen Grenze bei der Beschreibung der Rolle des EW-Sektors zu sein, insbesondere in Bezug auf schwere Felder im SM und darüber hinaus.

In dieser Arbeit leiten wir zunächst das statische Potential eines schweren Feldes in Theorien ab, die spontane Symmetriebrechung aufweisen. Wir verwenden unsere Ergebnisse dann, um das Potenzial eines schweren Quark-Antiquark-Paares im SM in der EW Ein-Schleifen-Ordnung zu berechnen. Wir tun dies sowohl im Wilson-Loop- als auch im Streuamplitudenansatz und diskutieren die Einschränkungen des Wilson-Loop-Ansatzes. Da der Feldinhalt des SM umfangreich ist, können jetzt analoge Ergebnisse zu unseren in einer großen Anzahl von Modellen erzielt werden, indem die entsprechenden Kopplungen und gruppentheoretischen Faktoren variiert werden. Anschließend präsentieren wir die führenden EW Korrekturen für die Kurz-Abstands-Definitionen schwerer Quarkmassen. Dies erhalten wir mit dem starken statischen Mesonenpotential sowie seiner Bindungs- und restlichen kinetischen Energie. Diese Energien bilden die Bausteine der meisten Massendefinitionen für kurze Abstände. Wir erklären, wie die Berechnung der EW Beiträge zu diesen Energien zu analogen Korrekturen der Massen führt. Wir stellen fest, dass die führenden EW Korrekturen dieselbe Stärke haben wie ihre nächstführenden Gegenstücke in der reinen QCD. Als nächstes betrachten wir die führenden EW Korrekturen zu den Lagrangedichten der *heavy quark effective theory* und der nichtrelativistischen QCD. Diese Korrekturen treten in den Wilson-Koeffizienten der Operatoren für schwere Quarks in der Ein-Schleifen-Ordnung auf. Aufgrund der Parität-Verletzung im SM enthalten die Operatoren zu dieser Ordnung parität-verletztende Terme. Wir leiten diese analog zum parität-erhaltenden QCD-Ergebnis in der Ein-Schleifen-Ordnung ab. Indem wir die vorherige Analyse auf die Zwei-Schleifen-Ordnung ausdehnen und verallgemeinern, berechnen wir die von massiven Eich- und Skalarbosonen herrührenden Korrekturen zu den Formfaktoren sowohl im Sudakov- als auch im Schwellenregime bis einschließlich zur Zwei-Schleifen-Ordnung. Die Korrekturen werden für Prozesse berechnet, an denen zwei externe Fermionen und Skalare im spontan gebrochenen $SU(N)$-Higgs-Modell beteiligt sind, wobei eine Reihe von zusammengesetzten Operatoren untersucht wird. Wir diskutieren weiter, wie Formfaktoren in unserem Spielzeugmodell auf das SM und darüber hinaus abgebildet werden können. Zuletzt bestimmen wir die Master-Integrale für Vertex- und Propagator-Diagramme, die in effektiven Feldtheorien mit schweren Feldern auftreten. Die Integrale umfassen mindestens eine schwere Linie, und die Standardlinien enthalten eine beliebige Massenskala. Wir verwenden moderne Methoden, einschließlich Differentialgleichungen und *Dimensional Recurrence*-Relationen, um diese Integrale bis zur Zwei-Schleifen-Ordnung auszuwerten.

Publication List

- B. Assi, B.A. Kniehl. 2020. "Matching the Standard Model to HQET and NRQCD". *hep-ph/2011.06447, DESY pre-print:20-211*
- B. Assi, B.A. Kniehl, O. Veretin. 2020. "Static Potential of the Standard Model and Spontaneously Broken Theories". *hep-ph/2011.06437, DESY pre-print:20-212*
- B. Assi, B.A. Kniehl. 2020. "Electroweak Form Factor in Sudakov and Threshold Regimes with Effective Field Theories". *hep-ph/2011.14933, DESY pre-print:20-213*
- B. Assi, B.A. Kniehl. 2021. "Electroweak Corrections to Heavy Quark Mass Definitions". *In Preparation*
- B. Assi, B.A. Kniehl, A. Onischenko. 2021. "Massive Two-Loop Heavy Particle Diagrams". *In Preparation*

This thesis is based on the work listed here, including ongoing work, reflecting the author's contributions.

Acknowledgements

My time in Hamburg as a PhD student over the last three years has been exceptionally formative and inspiring. For the people who have guided, supported and collaborated with me throughout this experience, I will now take the time to sincerely thank. First and foremost, I would like to thank Bernd Kniehl for his guidance, care, honesty and relentless encouragement. He taught me the incredible value of conceptual thinking and was always eager to discuss problems, no matter how small. I am grateful to him for fostering my creativity and, most significantly, encouraging me to persevere through moments of self-doubt. Secondly, I would like to thank Oleg Veretin, who was always willing to lend me some of his extraordinary technical expertise. His patience and humour are unmatched and very appreciated. My many questions and our long discussions now form the basis of my technical understanding. Thirdly, I would like to thank Sven-Olaf Moch for co-supervising me, his advice I always placed in high regard, and I am grateful for his kindness, patience and career support. As for the remaining members of our group, I would like to thank Maxim Nefedov, Vitaly Magerya and Zhiguo He, for their friendship and our many fruitful discussions. Lastly, a thank you to my recent collaborator abroad, Andrei Onischenko, whose skill and competence continually impresses me.

Contents

List of Figures

List of Tables

Chapter 1

Introduction

The immense success of the *Standard Model* (SM) of particle physics and its ability to withstand experimental scrutiny have puzzled theorists for decades. We know, however, that the SM is incomplete as it does not incorporate all known fundamental phenomena. The last piece of the Standard Model was confirmed in the discovery of the Higgs boson by the international scientific collaboration at the *Large Hadron Collider* (LHC) [1,2]. Although the Higgs field was predicted nearly 50 years prior [3,4], the immense precision requirements from both theory and experiment are what ultimately lead to its confirmation as part of nature. Thus, the current state of particle physics is mainly focused on precision studies of the Standard Model. In the quest to attain higher precision, we must refine our understanding of *quantum field theory* (QFT) and account for the tiniest corrections wherein anomalies may lie, revealing potential answers to remaining mysteries.

One can argue that the most glaring evidence of the incompleteness of the SM is the recent experimental observation of *neutrino oscillations* [5–7]. This implies that each neutrino is equipped with a unique non-zero mass, which is in direct contradiction with the SM prediction of massless neutrinos. The evidence of neutrino oscillations was generated from studies on the smallest (quantum) scales. In contrast, SM incompleteness also occurs on the largest (classical) scales. Astronomical and cosmological observations no longer agree with astrophysical predictions [8], derived using *general relativity* (GR) [9]. More specifically, if one considers particles that are allowed by the Standard Model, there is a sizeable apparent mass difference between theory and experiment. This implies that new matter, known as *dark matter* (DM), exists [10, 11]. These observations shake the foundations of either the SM or GR or both. If the discrepancy arises from the SM, then new field(s) must be introduced and accounted for by detection. Otherwise, general relativity must be modified in some consistent fashion to explain the discrepancy.

Sticking to the gravitational track, herein lies the most well-known puzzle of fundamental theory: the SM does not include gravity, which starts to play a role in fundamental interactions at the so-called *Planck scale*, $M_{\mathrm{P}} \sim 10^{16}$ TeV. The fundamental incompatibility lies in the fact that the SM is a perturbative QFT, whereas GR is inherently non-perturbative. Attempting to quantise gravity in GR as a field perturbatively yields unphysical predictions near M_{P} [12–14]. Many proposed solutions have been introduced to describe gravity fundamentally [15–18], but testing their predictions which would occur near M_{P} is far from reach currently. For comparison,

the recent Higgs discovery was achieved by a proton-proton collisions at the LHC with *centre-of-mass* (COM) energies, $\sqrt{s} = 7$ TeV, to discover the Higgs particle of mass $M_H \sim 0.1$ TeV [19]. This is by no means an exhaustive list and there are many more arguments for physics *beyond the Standard Model* (BSM), such as dark energy or the cosmological constant problem, the hierarchy problem, and grand unification [20–22].

One is then left wondering how to tackle such discrepancies and investigate their fundamental nature. In principle, there are two ways to search for discrepancies, either directly or indirectly. Direct searches for BSM physics involve scanning cross-sections and searching for novel field resonances not permitted by the SM alone. The issue is that the energy of the process limits this and experiments cannot reach arbitrarily high energy scales. In contrast, indirect searches rely on precision alone and allow one to scan significantly higher energies than an experiment can reach. This advantage can be stated heuristically, if the energy scale of new physics is $\Lambda_{\rm BSM}$ and the *electroweak* (EW) scale is $\Lambda_{\rm EW} \sim M_H$ then the observable uncertainty needs to be of $\mathcal{O}(M_H/\Lambda_{\rm BSM})$. For instance, given a high precision study that reduces the uncertainty of a collider observable to a single per cent, one can probe effects occurring at one-hundred fold $\Lambda_{\rm EW}$ which is $\Lambda_{\rm BSM} \sim$ TeV. In this case, indirect effects of BSM physics again are seen by any discrepancies which implies virtual contributions from BSM physics.

More recently, the incredible utility of indirect searches through precision studies has been exemplified in the possible detection of unknown physics. The comparison of high precision SM determinations of the *anomalous magnetic moment* (AMM) and lepton-flavour universality are showing discrepancies with measurements at various experiments [23–26]. If further studies prove one or more of these discrepancies to be true, this would be an incredible success as it would not only call for extensions to the SM but said extensions could also explain discrepancies previously pointed to [27–31]. We end this motivation by adding that BSM searches are not the sole reason for precision studies. For instance, the critical question of the stability of the EW vacuum depends on reducing the uncertainty of the top quark and Higgs masses [32–34]. Thus, we have an abundance of reasons to minimise uncertainties in our theoretical predictions to match current and future-planned high precision experiments.

In performing precision studies with the SM, it is convenient to separate its two sectors, namely the strong and the EW sector. The strong sector is described by *quantum chromodynamics* (QCD) and the remaining SM interactions are all governed by the EW sector. It is well understood that the pure QCD radiative corrections are dominant at high energies and therefore have leading uncertainty. Thus, it has been the quest of many to reduce said uncertainty by going beyond *leading order* (LO) in perturbation theory when determining QCD-dependent quantities and observables. This goal takes us to the realm of higher-order radiative corrections and the art of calculating multi-loop processes at *next-to leading order* (NLO) and beyond. Thanks to a plethora of modern analytical and numerical methods [35–37], we are now able to study processes and determine quantities at a very high perturbative order, for instance, the *beta function* of QCD is now known to five-loop order [38]. Given this exceptional progress in the QCD sector, it is becoming abundantly clear that observable uncertainties from the EW sector are becoming significant enough to consider in comparison. Based on the ratio of strong and EW couplings, the rule of thumb is that EW corrections are sub-leading by an order of magnitude relative to pure QCD corrections. For this reason, to bring the SM observable uncertainty down

to the level attained with QCD alone, we must begin to consider EW corrections beyond LO and even NLO.

In this thesis, we pursue the end of incorporating EW effects to well-understood quantities, processes and *effective field theories* (EFTs) in QCD. We begin by considering heavy fields such as the top quark in the SM. Our analysis centres on determining the EW corrections to the potential of a heavy meson (or so-called static potential) in the large mass and small quark velocity limit. The most well-known static potential is that of *quantum electrodynamics* (QED), which is simply the Coulomb potential to all orders [39]. On the other hand, due to the presence of colour, QCD is the non-Abelian analogue of QED. Thus, the QCD static potential does depend on higher-order calculations and is known to three-loop order [40, 41]. The potential is valuable as it allows one to study the fundamental properties of a given theory in the *non-relativistic* (NR) limit. We then investigate analogous corrections for a heavy meson's *binding energy* (BE) and *residual kinetic energy* (KE) [42, 43]. Armed with these energetic quantities, we consider applications, mainly how they affect the short-distance heavy quark mass definitions and NR effective theories.

A precise determination of quark masses has been of particular interest due to their fundamental nature as SM Lagrangian parameters and constraining flavour *beyond the Standard Model* [22, 44]. The focus on heavy quarks (top, bottom and charm) is due to their large masses which means they can have a large influence on observables. Thus, uncertainty reduction in this case is of particular importance. For instance, the top quark mass is required to very high precision in the combined EW fits [45, 46]. These fits were employed to attain indirect information on the Higgs mass and currently serve as SM consistency checks. Moreover, on the conceptual front, the traditional definition of particle mass as the pole of the field propagator is no longer applicable in the case of heavy quarks. This definition is lacking due to spurious non-perturbative *infrared* (IR) divergences arising at higher-loop orders [47].

Thus, new, so-called short-distance masses must be defined in a way that distinguishes between *ultraviolet* (UV) and IR physics. In this thesis, we are primarily interested in the largest parameter in the SM, the mass of the top quark. Determining the top mass precisely is crucial for consistency checks of the SM [48–50], and is the dominant uncertainty in studies of EW vacuum stability [33, 51, 52]. We are also interested in the bottom quark, which has the second largest mass and lies in the same generation as the top quark. High power factors of said mass appear in many important processes, such as B-meson and Higgs boson decays, which are highly coveted for indirect BSM searches [53–55]. Thus, precise theoretical mass predictions are of immense value and even defining a well-behaved perturbative quark mass is problematic. Many successful proposals have been considered and studied to very high precision in pure QCD [56–60]. We thus focus on EW corrections in this thesis for a portion of widely-employed heavy quark mass schemes.

The second point of focus in this thesis lies on the front of EFTs, which have proven highly effective for precision studies. The EFT framework exploits the persisting fact that exciting and unique physics occurs at all distances, times and energy scales. If one wants to probe a particular scale of interest, EFTs allow the so-called integrating out of irrelevant scales. I.e. relegate degrees of freedom present beyond the scale of interest to multiplicative *Wilson* or so-called *matching coefficients* in the EFT Lagrangian [61, 62]. In general, an EFT can be either constructed from the top-down or the bottom-up.

In a bottom-up EFT, the UV theory is either known but lacks a low energy description or is entirely unknown. Using an EFT, in this case, is convenient as no commitment to a particular model is necessary, and one can work off what is established. For instance, the *Standard Model effective field theory* (SMEFT) is one such model-independent EFT consisting of the SM itself along with higher-dimensional operators [63]. On the other hand, a top-down EFT is helpful when the UV or so-called full theory is known, but we are solely interested in the low-energy or IR regime. The main advantage in employing such an EFT is that its calculations of processes at lower-energies are rendered much simpler. Thus, one can immediately perceive the utility of the top-down approach for precision studies as the goal is to attain higher orders in the perturbative expansion. The issue with working with the full theory is that the number of amplitudes to determine increases exponentially at each order, which can easily become an impossible task computationally. The EFT framework grants one the luxury of reducing the field content to only what is relevant at the low-energy scale and therefore eliminating many degrees of freedom that are present in the full theory, simplifying calculations significantly [64–67].

In this thesis, we are more concerned with the top-down approach and, in particular, the NR regime. We begin by considering the leading EW radiative corrections to *heavy quark effective theory* (HQET) [64, 68–72], and *non-relativistic quantum chromodynamics* (NRQCD) [73, 74]. These corrections appear at one-loop order in the matching coefficients of the HQET/NRQCD Lagrangian. We then further generalise our EFT analysis to two-loop orders in both the NR and Sudakov energetic regimes. The *Sudakov regime* is appropriate when the COM energy of a process is large compared to the theory's predicted masses [75, 76]. For instance, when considering LHC partonic processes, the COM energy is $\sqrt{s} \sim 14$ TeV, which is an order of magnitude above the largest SM masses. In this way, our analysis applies to both current LHC processes in the Sudakov regime and future high precision collider processes in the NR regime.

To perform our two-loop study, we work with the $SU(N)$-Higgs model instead of the full SM, as it is more versatile and can be mapped both to the SM and BSM theories. We then employ a sequence of EFTs at each scale for different mass hierarchies and determine the Wilson coefficients to two-loop orders. In the EFT sector of the matching calculation, we come across two-loop diagrams which require modern multi-loop techniques to determine. These diagrams are UV model-independent and appear in all EFTs containing both heavy fields and a mass scale. Therefore it would be useful to evaluate all diagrams of these types, and we do so with the help of modern techniques. Upon analysis, we find that the methods that work best to solve such integrals are a combination of the differential equations approach and *dimensional recurrence relations* [77, 78]. These two methods have seen enormous success in the current multi-loop era [79–83], and we further demonstrate their utility here in the realm of EFT. We now turn to a brief survey of the research, which outlines the content of each chapter.

Outline

This thesis is structured as follows. In Chapter 2 we introduce the SM of particle physics, describing its properties and symmetries as well as the parameters and field content of the SM Lagrangian. We then outline the concept of renormalisation and the running of couplings. From there, we argue the need for short-distance mass definitions when studying heavy quarks. We close by digging deeper at hints for BSM physics. Chapter 3 describes the framework of EFTs, delving into the effective theories we employ in this thesis. In particular, we describe HQET along with its extensions to heavy particles of differing spin, NRQCD and soft-collinear effective theory (SCET). After these introductory chapters, we proceed to the main results. In Chapter 4, we introduce the static potential, re-deriving it for QED and QCD up to NLO. From there, we determine how the EW corrections play a role at NLO and consider applications. In Chapter 5 we derive the heavy meson binding and residual kinetic energy then determine the leading EW corrections to said energies. With these energies, we evaluate and analyse the leading EW corrections to commonly used short-distance mass schemes. At this juncture, our analysis shifts focus entirely to EFTs. In Chapter 6 we reproduce the HQET/NRQCD Lagrangian for heavy quarks. In doing so, we determine the matching coefficients from the full SM to one-loop EW order. Moreover, we find the EFT Lagrangian must be extended to include additional operators, which we determine and match to the full theory. Generalising our EW analysis in Chapter 7, we perform matching and running with a sequence of EFTs up to two-loop orders with a range of composite operators. We consider both heavy fermions and scalars, various mass hierarchy scales and two distinct energetic regimes. Lastly, Chapter 8 is devoted to evaluating massive two-loop diagrams with heavy fields, some of which are needed in Chapter 7. The calculation is achieved with modern multi-loop techniques, which we introduce and employ in our analysis. We then conclude and discuss possible future directions in Chapter 9. The Appendices include theoretical frameworks employed, technical details and further insights on the calculations performed in this thesis.

Chapter 2

The Standard Model and Beyond

This chapter sets the stage for research presented throughout this thesis. In Section 2.1 we introduce the Standard Model of particle physics, describing the concept of *gauge symmetries* and presenting the field content in the form of its Lagrangian. We outline the concept of renormalisation and the running of couplings in Section 2.2 and focus on mass definitions and the case for short-distance masses in Section 2.3. We end this chapter by discussing hints of new physics in Section 2.4.

2.1 The Standard Model of Particle Physics

The SM is a fundamental quantum theory that describes the interactions of elementary fields obeying relativistic mechanics under local gauge groups. As any QFT, once defined, the SM must undergo a quantisation procedure, detailed in Ref. [84]. Since this section entails a brief introduction, we will hone in on the SM Lagrangian, decoding its various sectors. The key feature of the SM is that it is a chiral gauge theory that completely describes the directly observed fundamental phenomena of strong and EW interactions, *spontaneous symmetry breaking* (SSB), *quark confinement*, *flavour physics*, etcetera. The SM gauge group can be split in two parts, $SU(N_c)$ describing the strong interactions of QCD [85–88], and $SU(2)_L \times U(1)_Y$ encoding the EW interactions [89–91].

The field content of the SM is divisible into two classes, the *fermions* of half-integer spin and the *bosons* of integer spin. The fermions, also known as matter fields, are equipped with spin-1/2; the *scalar* and *vector* bosons are spin-0 and spin-1, respectively. SM fermions come in two types, *quarks* and *leptons*, each a family of six particles (known as *flavours*) and their corresponding *anti-particles* (distinguished by opposite electric charge). The flavours are further grouped into quark couplets of up-type and down-type known as *generations*. In order of increasing mass, the three *up-type* quarks are up, charm and top, labelled by (u, c, t); and the three *down-type* quarks are down, strange and bottom, labelled by (d, s, b). Unlike leptons, quarks are colour charged under the $SU(N_c)$ gauge group in the *fundamental* representation and are equipped with $N_c = 3$ separate *colour* charges. Moreover, quarks are electrically charged under $U(1)_Q$ where up-type and down-type quarks have electric charge, $Q = 2/3$ and $Q = -1/3$, respectively. Thus, the sole differentiating factor between quark generations is, in fact, their masses.

In the case of leptons, they are distinguishable by their electric charge. Analogous to the up-type and down-type description of quarks, we have charged and neutral leptons or neutrinos. All

Field	$SU(3)_C$	$SU(2)_L$	Y	Q	I_3
$\begin{pmatrix} u \\ d \end{pmatrix}_L, \begin{pmatrix} c \\ s \end{pmatrix}_L, \begin{pmatrix} t \\ b \end{pmatrix}_L$	**3**	**2**	1/6	2/3 −1/3	1/2 −1/2
u_R, c_R, t_R	**3**	**1**	2/3	2/3	-
d_R, s_R, b_R	**3**	**1**	−1/3	−1/3	-
$\begin{pmatrix} e \\ \nu_e \end{pmatrix}_L, \begin{pmatrix} \mu \\ \nu_\mu \end{pmatrix}_L, \begin{pmatrix} \tau \\ \nu_\tau \end{pmatrix}_L$	**1**	**2**	−1/2	−1 0	−1/2 1/2
e_R, μ_R, τ_R	**1**	**1**	−1	−1	-

Table 2.1: Fermionic fields and their represention under local gauge groups of the SM. The triplet, doublet and singlet representations of a given group are labelled by **3**, **2** and **1**. I_3 corresponds to the third isospin component and $Y = Q - I_3$ is the hypercharge in our convention.

charged leptons have $Q = -1$ while neutrinos are uncharged and do not interact under the gauge group of electromagnetism (EM). Again, in order of increasing mass, the three charged leptons are the electron, muon and tau, labelled by (e, μ, τ). The three neutrinos, named according to their respective generations, are the electron-, muon- and tau-neutrinos, labelled by $(\nu_e, \nu_\mu, \nu_\tau)$. Although it has been recently confirmed in several experiments that neutrinos oscillate, implying they have mass [5,6,92], the SM lacks a description of this feature. As we neglect neutrino masses in this thesis, we leave the treatment of massive neutrinos to Ref. [93]. Therefore, the only massive leptons are the charged ones, and as in the case of quarks, mass is the sole distinguishing factor between lepton generations. We present the SM fermions and their representations under local gauge groups in Table 2.1.

2.1.1 Gauge Symmetry

Before exploring the various sectors of the SM Lagrangian, we need to unpack the concept of *gauge symmetry* [94]. Given a Lagrangian, a *global* symmetry group describes a class of transformations that leave the Lagrangian invariant. Global symmetries are non-local, meaning they are independent of coordinates of space and time in the Lagrangian formulation of a theory. One may also consider *local* symmetries where the group transformation is coordinate dependent. In turn, one can enforce invariance under said local gauge transformation. This procedure is known as achieving *local gauge invariance* under a symmetry group, and in doing so, one passes to a reduced phase space with fewer canonical degrees of freedom.

To illustrate this feature let us consider the example of a fermion labelled by a *Dirac spinor*, ψ^α, with four complex components labelled by a spinor index, $\alpha = 1, \ldots, 4$, and mass, m. The free Lagrangian is then given by the *Dirac Lagrangian*,

$$\mathcal{L}_0 = \bar{\psi}^\alpha (i\partial\!\!\!/ - m)\psi^\alpha, \tag{2.1}$$

where $\bar{\psi} = \psi^\dagger \gamma_0$ and given an arbitrary four-vector v, $v\!\!\!/ = \gamma_\mu v^\mu$ and γ_μ are *Dirac matrices*. Let us now perform a infinitesimal local symmetry group transformation,

$$\psi_\alpha \to e^{i\theta(x)}\psi^\alpha = \psi_\alpha + i\theta^a(x) T^a_{\alpha\beta}\psi^\beta, \tag{2.2}$$

with infinitesimal coordinate dependent parameters $\theta(x)$ and T^a are constant transformations matrices, known as group generators, in the fundamental representation of the group. Note that if $\theta(x)$ is constant then the Dirac Lagrangian is invariant under the symmetry transformation, meaning it is a global symmetry. By promoting $\theta(x)$ to being coordinate dependent, we are now considering a local symmetry. In this case the Dirac Lagrangian is no longer invariant and transforms as,

$$\mathcal{L}_0 \to \mathcal{L}_0 + i(\partial_\mu \theta^a(x))\bar{\psi}^\alpha \gamma^\mu T^a_{\alpha,\beta}\psi^\beta. \tag{2.3}$$

We can thus employ *Noether's theorem*, which states that the new term appearing under the local transformation,

$$J^a_\mu = i(\partial_\mu \theta^a(x))\bar{\psi}^\alpha \gamma^\mu T^a_{\alpha,\beta}\psi^\beta \tag{2.4}$$

is a conserved current with $\partial^\mu J^a_\mu = 0$. As our goal is to enforce local gauge invariance on our free Lagrangian, the introduction of a new field, $A^a_\mu(x)$ is necessary, that is defined by its ability to cancel J^a_μ once the local gauge transformation is applied.

Before describing $A^a_\mu(x)$, we need to introduce the adjoint representation. In physics, it is often the case that symmetry groups being considered are so-called Lie groups [95]. These groups are defined by the matrices, T^a, obeying a so-called Lie Algebra,

$$\left[T^a, T^b\right] = if^{abc}T^c, \tag{2.5}$$

with constants, f^{abc}, known as structure constants. The structure constants define another useful representation of a Lie group, the so-called Adjoint representation, with generators,

$$(T^a)^{bc} = -if^{abc}, \tag{2.6}$$

of dimension equivalent to its symmetry group. With this additional construction at hand, we may now proceed with defining the new field.

As our goal is to cancel the Noether current in Eq. (2.3), $A^a_\mu(x)$ must carry the same group index, meaning it will not be invariant under group transformation. However, the new field is not in the fundamental representation; instead, it is chosen to transform in the *adjoint* representation,

$$A^a_\mu \to A^a_\mu + \partial_\mu \theta^a + i\theta^b (T^b)^{ac} A^c_\mu = A^a_\mu - \partial_\mu \theta^a - \theta^b f^{bac} A^c_\mu. \tag{2.7}$$

The field, $A^c_\mu(x)$, chosen as such is known as a gauge field of the group [84]. The gauge field is solely dependent on the group symmetry being considered and we can now define further quantities of interest associated to such fields. The first is the so-called *covariant derivative*,

$$D_\mu = \partial_\mu + iA^a_\mu T^a_{\alpha\beta}, \tag{2.8}$$

then combining Eqs. (2.2) and (2.7),

$$\begin{aligned} D_\mu\psi_\alpha \to D_\mu\psi_\alpha + i(\partial_\mu\theta^a)T^a_{\alpha\beta}\psi^\beta - A^a_\mu T^a_{\alpha\beta}(\partial_\mu\theta^b)(T^b)^\beta_\sigma\psi^\sigma - i\partial_\mu\theta^a T^a_{\alpha\beta}\psi^\beta \\ - i\theta^b f^{bac}T^a_{\alpha\beta}A^c_\mu T^a_{\alpha\beta}\psi^\beta_i \qquad (2.9) \\ = D_\mu\psi^\alpha + i\theta^a T^a_{\alpha\beta}D_\mu\psi^\beta, \qquad (2.10) \end{aligned}$$

and therefore, $D_\mu \psi^\alpha$ transforms identically to ψ^α. Whence, replacing the partial derivative in the free Lagrangian with a covariant derivative results in a new Lagrangian which exhibits invariance under local symmetry transformations,

$$\mathcal{L} = \bar{\psi}\left(i\not{D} - m\right)\psi, \tag{2.11}$$

with spinor indices suppressed. We re-iterate the difference here is the inclusion of a gauge field and by inspection of $\mathcal{K}$, the gauge field interact with the Dirac fermions, thus, we no longer have a free Lagrangian but an interacting one. By the lack of a gauge field kinetic term in Eq. (2.11), however, we can see that $\mathcal{L}$ is incomplete. This brings us to the second quantity of interest we introduce, the *field strength tensor*,

$$F_{\mu\nu} = F^a_{\mu\nu}T^a = i\left[D_\mu, D_\nu\right] = \partial_\mu A_\nu - \partial_\nu A_\mu - i\left[A_\mu, A_\nu\right] \tag{2.12}$$

$$= F^a_{\mu\nu}T^a = \partial_\mu A^a_\nu - \partial_\nu A^a_\mu + f^{abc}A^b_\nu A^c_\nu, \tag{2.13}$$

the components of which transform locally under the symmetry group as,

$$F^a_{\mu\nu} \to F^a_{\mu\nu} - f^{abc}\theta^b F^c_{\mu\nu}. \tag{2.14}$$

Therefore, we now are in possession of a kinetic term for the gauge field by contraction of the field strength tensor and may write down the complete, parity conserving [96], Lagrangian for mass dimension $\mathcal{D} \leq 4$,

$$\mathcal{L} = -\frac{1}{4}F^a_{\mu\nu}F^{a,\mu\nu} + \bar{\psi}\left(i\not{D} - m\right)\psi. \tag{2.15}$$

The first term in Eq. (2.15) is also invariant under local symmetry group transformations. Notice the lack of a mass term for the gauge field, of the form $m_A^2 A^a_\mu A^{a,\mu}$, although it is valid in $\mathcal{D} \leq 4$, we can immediately see that it is not invariant under a local symmetry transformation. Thus the gauge field must be massless.

Throughout this illustration, we considered Lie groups in general. However, implicitly we restricted ourselves to $SU(N)$ with $a = 1, \ldots, N^2 - 1$, defined as the group of unitary matrices, $U(N)$, with unit determinant. The reason is that the Dirac Lagrangian's global symmetry is $SU(N)$. In general, when working in the SM, the main symmetry groups that are imposed are $SU(N)$ for $N = 1, 2, 3$ and $SO(1, 3)$ for space-time, known as *Poincaré symmetry* [97].

We may now end with the case of a finite group symmetry transformation, to ensure our Lagrangian is not solely invariant in the infinitesimal case. The Dirac spinor transformation can be written with spinor indices suppressed as,

$$\psi \to U\psi = \exp\left[i\theta^a T^a\right]\psi_i, \tag{2.16}$$

such that $U \in SU(N)$. Moreover, the transformations of the gauge field and field strength tensor are given by,

$$A^a_\mu T^a \to U A^a_\mu T^a U^\dagger - i(\partial_\mu U)U^\dagger, \tag{2.17}$$

$$F^a_{\mu\nu}T^a \to U F^a_{\mu\nu}T^a U^\dagger \tag{2.18}$$

and therefore, upon simplification the covariant derivative of ψ transforms as,

$$D_\mu \psi \to U D_\mu \psi. \tag{2.19}$$

Whence the complete Lagrangian given in Eq. (2.15) can be transformed piece-wise, and by inspection, it remains invariant under the finite symmetry transformation. We may now proceed to the SM, gauging its group symmetries and determining its associated gauge fields.

2.1.2 The Standard Model Lagrangian

The SM is equipped with global $SU(3)_c \times SU(2)_L \times U(1)_Y$ symmetry. The $SU(2)_L \times U(1)_Y$ group defines the *chiral* nature of the SM, in which different field transform under the fundamental representations of either $SU(2)_L$ or $U(1)_Y$. Fields that transform under $SU(2)_L$ and $U(1)_Y$ are known as *left-* and *right-handed* fields, respectively. Only fermions exhibit chirality, and the labelling convention is given by,

$$\psi_{R/L} = P_{R/L} = \frac{1}{2}\left(1 \pm \gamma_5\right)\psi, \quad \gamma_5 = i\gamma^0\gamma^1\gamma^2\gamma^3, \tag{2.20}$$

which transform accordingly under $SU(2)_L \times U(1)_Y$ but identically under $SU(3)_C$. We again refer to Table 2.1 for SM fermions to see how they transform under each group. The procedure of localising a global symmetry and gauging the local symmetry as introduced in Section 2.1.1 will now be employed in the case of the SM. The outcome will be the introduction of SM gauge fields and couplings; we will also interpret the interaction terms that arise in the Lagrangian.

Strong Sector

Let us begin with the quark sector of the SM and construct QCD, which is a consequence of gauging local $SU(3)_C$ symmetry. Quarks are fermions that transform under the fundamental representation of $SU(3)_C$, and all six can be grouped under a label, q_f, where f denotes the six possible flavours. Thus, we can write the non-trivial transformation of a quark in $SU(3)_C$ as,

$$q_f \to U q_f = \exp\left[i\theta^a T^a\right] q_f, \tag{2.21}$$

with generators, $T^a = \lambda^a/2$ in the $SU(3)_C$ adjoint representation, such that $a = 1, \ldots, 8$ and λ^a are given by the *Gell-Mann* matrices. Upon gauging the symmetry in the quark Dirac Lagrangian, analogous to the illustration in Section 2.1.1, the *gluon* or gauge field, G^a_μ, of $SU(3)_C$ appears. The eight gluons of the SM are so-called vector bosons and are the mediators of all QCD interactions. The transformation of gluons is under the adjoint representation of $SU(3)_C$ and is given by Eq. (2.17),

$$G^a_\mu T^a \to U G^a_\mu T^a U^\dagger + \frac{i}{g_s}(\partial_\mu U)U^\dagger. \tag{2.22}$$

Note the inclusion of g_s, as one is free to multiply by a constant, dimensionless parameter known as the *strong coupling constant*. A coupling constant is always included in field theories as it allows one to tune the strength of an interaction. The gluon field strength tensor, $G^a_{\mu\nu}$, on the other hand, transforms according to Eq. (2.18),

$$G^a_{\mu\nu} = \partial_\mu G^a_\nu - \partial_\nu G^a_\mu + g_s G^b_\mu G^c_\nu f^{abc}, \tag{2.23}$$

with structure constants, $f^{abc} \in \mathbb{R}$, of $SU(3)_C$, which are totally anti-symmetric. We may now express the QCD sector of the SM Lagrangian and expand out the terms to take note of the interactions present,

$$\begin{aligned}
\mathcal{L}_{\text{QCD}} =& -\frac{1}{4}G^a_{\mu\nu}G^{a,\mu\nu} + \bar{q}_f\left(i\not{D} - m_f\right)q_f && (2.24)\\
=& -\frac{1}{4}(\partial_\mu G^a_\nu - \partial_\nu G^a_\mu)(\partial^\mu G^{a,\nu} - \partial^\nu G^{a,\mu}) + g_s f^{abc}(\partial_\mu G^a_\nu)(G^{b,\mu}G^{c,\nu}) \\
& -\frac{g_s^2}{4}f^{abc}f^{ade}G^b_\mu G^c_\nu G^{d,\mu}G^{e,\nu} + \bar{q}_f\left(i\not{\partial} - g_s\not{G}^a T^a\right)q_f - m_f\bar{q}_f q_f. && (2.25)
\end{aligned}$$

As $SU(3)_C$ is a matrix Lie group which is non-Abelian, self-interactions between gluons occur. We see both triplet and quartic terms of gluons alone which would not arise in a an Abelian $U(1)$ theory such as QED. Moreover, we need not derive the quantum electrodynamics Lagrangian, $\mathcal{L}_{\text{QED}}$, as it is analogous to the QCD Lagrangian modulo colour indices and self-interactions among the $U(1)$ gauge fields, also known as photons.

Electroweak Sector

What remains to be gauged is the EW sector classified by its global $SU(2)_L \times U(1)_Y$ symmetry. The EW sector involves all fermions in the SM and not simply quarks, i.e. all fermions transform non-trivially under $SU(2)_L \times U(1)_Y$. Whence, we may group fermions as ones that transform in the fundamental representation of $SU(2)_L$ and $U(1)_Y$, known as *isospin-doublets*, Ψ_L, which includes all SM fermions. Furthermore, we can group those that transform as a *singlet* in $SU(2)_L$ and $U(1)_Y$ in Ψ_R, including up- and down-type quarks as well as charged leptons. The left- and right-handed representations then transform under $SU(2)_L \times U(1)_Y$ as,

$$\Psi_L \to U_L U_Y \Psi_L = \exp\left[i(\theta^i \tau^i + \rho Y_L \mathbf{1})\right] \Psi_L \tag{2.26}$$

$$\Psi_R \to U_Y \Psi_R = \exp\left[i\rho Y_R\right] \Psi_R, \tag{2.27}$$

with Y corresponding to the weak *hypercharge* and $SU(2)_L$ group generators represented by $\tau^i = \sigma^i/2$ such that σ^i are the *Pauli matrices* with $i = 1, 2, 3$. As this is a finite transformation, we take parameters θ^i and ρ to be finite. Localising this symmetry and rendering the EW Lagrangian invariant under such transformations introduces novel gauge fields, W^i_μ and B_μ which transform in the adjoint representations of $SU(2)_L$ and $U(1)_Y$, respectively. We may write these transformations as,

$$W^i_\mu \tau^i \to U_L W^i_\mu \tau^i U^\dagger + \frac{i}{g}(\partial_\mu U_L) U_L^\dagger, \tag{2.28}$$

$$B_\mu \to B_\mu - \frac{1}{g'} \partial_\mu \rho \tag{2.29}$$

in which we have introduced new parameters, g and g', which correspond to the couplings from gauging $SU(2)_L$ and $U(1)_Y$. Moreover, the kinetic terms of the Lagrangian require field strength tensors to construct, and these transform as,

$$W^i_{\mu\nu} \to \partial_\mu W^i_\nu - \partial_\nu W^i_\mu - g\epsilon^{ijk} W^j_\mu W^k_\mu, \tag{2.30}$$

$$B_{\mu\nu} \to \partial_\mu B_\nu - \partial_\nu B_\mu, \tag{2.31}$$

such that ϵ^{ijk} is the totally anti-symmetric Levi-Chevita tensor and the structure constant of $SU(2)_L$. Now that the gauge fields are defined and their properties understood, we may construct the covariant derivatives for the left- and right-handed spinors we defined,

$$D_\mu \psi_L = \left(\partial_\mu + igW^i_\mu \tau^i + ig' Y B_\mu\right) \Psi_L, \tag{2.32}$$

$$D_\mu \psi_R = \left(\partial_\mu + ig' Y B_\mu\right) \Psi_R. \tag{2.33}$$

Given these ingredients and the constraints of mass dimension, $\mathcal{D} \leq 4$, the Lagrangian of the EW sector is accordingly,

$$\mathcal{L}_{\text{EW}} = -\frac{1}{4} W^i_{\mu\nu} W^{i,\mu\nu} - \frac{1}{4} B_{\mu\nu} B^{\mu\nu} + i\bar{q}^k_L \not{D} q^k_L + i\bar{l}^k_L \not{D} l^k_L + i\bar{u}^k_R \not{D} u^k_R + i\bar{d}^k_R \not{D} d^k_R + i\bar{e}^k_R \not{D} e^k_R, \tag{2.34}$$

where the new index $k = 1, 2, 3$ denotes the generation and is summed over. Expanding each term, as in the QCD case, one can investigate the gauged $SU(2)_L \times U(1)_Y$ interactions. What is immediately apparent and novel relative to QCD, is the lack of fermionic mass terms. If one attempts to include one gauge invariance will cease to hold and thus the SM fermions are massless unless there is another mechanism in play.

2.1.3 Spontaneous Symmetry Breaking

In the previous section, we came to an impasse, massless matter fields are not physical, and thus a different sector is required, which grants fermions mass. The solution arises from SSB in the SM, first introduced by Weinberg and Salam [89–91]. In the *Weinberg-Salam model*, a complex scalar doublet, $\varphi(x)$, is included, which transforms non-trivially under the fundamental representation of $SU(2)_L \times U(1)_Y$ with weak hypercharge, $Y = 1/2$. The process of SSB occurs in many areas of physics, from cosmology to condensed matter theory [98–100]. Heuristically, SSB occurs when the Lagrangian of interest is invariant under a symmetry group transformation but contains a vacuum state that is not invariant.

To illustrate this phenomenon, let us consider the following Lagrangian,

$$\mathcal{L}_\varphi = -\frac{1}{4} W^i_{\mu\nu} W^{\mu\nu,i} - \frac{1}{4} B_{\mu\nu} B^{\mu\nu} + (D_\mu \varphi)\,(D^\mu \varphi)^\dagger - V(|\varphi|^2) \tag{2.35}$$

with potential, $V(|\varphi|^2)$, and covariant derivative given by,

$$V(|\varphi|^2) = \mu^2 |\varphi|^2 + \lambda |\varphi|^4 \tag{2.36}$$

$$D_\mu \varphi = (\partial_\mu + i g W^i_\mu \tau^i + i g' B^\mu)\varphi. \tag{2.37}$$

The newly introduced parameters, $\mu^2 < 0$ and $\lambda > 0$, are additional coupling constant to be tuned and thus the potential has minima at

$$|\varphi_0|^2 = v^2 = -\frac{\mu^2}{2\lambda}, \tag{2.38}$$

which is commonly termed the *vacuum expectation value* (VEV). As our newly introduced scalar, $\varphi(x)$, is a complex scalar doublet, it may be written in terms of four real fields as,

$$\varphi(x) = \begin{pmatrix} \varphi_1 + i\varphi_2 \\ \varphi_3 + \varphi_4 \end{pmatrix} = \exp\left[\frac{i}{\sqrt{2}v} \phi^i \tau^i\right] \begin{pmatrix} 0 \\ \frac{v+h}{\sqrt{2}} \end{pmatrix}. \tag{2.39}$$

The fields, $\phi^i(x) \in \mathbb{R}$, with $i = 1, 2, 3$ are known as *Goldstone bosons* [101, 102], and they are massless, while the field, $h(x) \in \mathbb{R}$, is massive with $M_H^2 = -\mu^2$, as is apparent upon re-insertion into Eq. (2.35). The massive field $h(x)$ is called the *Higgs boson* and has been generated dynamically by the non-zero VEV.

To make the proceeding parts of the derivation simpler, one can set $\phi^i = 0$ as these are redundant degrees of freedom. So we have fixed three out of four parameters in θ^i and ρ under $SU(2)_L \times U(1)_Y$ transformations. This choice is called *unitary gauge* in the literature, and the procedure of exploiting redundancies, in general, is known as *gauge fixing* [103]. In this gauge fixing scheme, three mass terms in Eq. (2.35) are generated,

$$\mathcal{L}_\varphi \supset (D_\mu \varphi)(D^\mu \varphi)^\dagger = g^2 \frac{v^2}{8} \left[(W^1_\mu)^2 + (W^2_\mu)^2 + (\frac{g'}{g} B_\mu - W^3_\mu)^2\right]. \tag{2.40}$$

Thus, the gauge bosons acquire the redundant degrees of freedom from fixing the Goldstone bosons and express them as mass terms. If we further define,

$$W_\mu^\pm = \frac{1}{2}(W_\mu^1 \pm iW_\mu^2), \tag{2.41}$$

$$Z_\mu = \cos\theta_w W_\mu^3 - \sin\theta_w B_\mu, \tag{2.42}$$

$$A_\mu = \sin\theta_w W_\mu^3 + \cos\theta_w B_\mu, \tag{2.43}$$

which is standard notation for the SM, with *Weinberg angle*, θ_w, defined as $\tan\theta_w = g'/g$. The gauge field A_μ corresponds to the *photon* of QED, whereas $W_\mu^\pm$ and Z^μ are the massive charged and neutral W and Z bosons that mediate the weak interaction. It then becomes immediately clear from Eq. (2.40) that we are left with one massless and three massive vector gauge bosons with masses given by,

$$M_W = \frac{1}{2}gv, \quad M_Z = \frac{1}{2\cos\theta_w}gv = \frac{M_W}{\cos\theta_w}, \quad M_A = 0. \tag{2.44}$$

The following two points can be gleamed from these masses by inspection, the first is that photons are massless and the second is that the neutral Z boson must be heavier than the $W^\pm$ bosons. To explicitly see the charge exhibited by the $W^\pm$ bosons, one can define the EM coupling as,

$$e = g\sin\theta_w = g'\cos\theta_w, \tag{2.45}$$

and expand the $W^i_{\mu\nu}W^{i,\mu\nu}$ in $\mathcal{L}_\phi$ and indeed $W^\pm$ bosons exhibit EM charge of ± 1 by inspection.

Of course, although the above Lagrangian adds value, we have not dealt with the issue of massless fermions yet. The SSB mechanism is not complete, including complex scalar fields in the Lagrangian and thus, the Higgs field as described means that new interaction terms are permitted in $\mathcal{D} \leq 4$. These terms form a new sector known as the *Yukawa sector*. If we hone in on quark masses for illustration, the terms are as follows,

$$\mathcal{L}_{\text{Yuk}} \supset -Y^u_{kj}\bar{q}^k_L\tilde{\varphi}u^j_R - Y^d_{kj}\bar{q}^k_L\varphi d^j_R + \text{h.c.} \tag{2.46}$$

The Yukawa matrices, $Y^{u,d}$, are different for up- and down-type quarks and $k, j = 1, 2, 3$ are generation labelling indices. Moreover, the field $\tilde{\varphi} = i\sigma_2\phi^*$ where σ_2 is the second Pauli matrix and the Yukawa matrices may not necessarily be diagonal in generation. Note the careful construction of the Yukawa terms and their implicit invariance under local SM group transformations. SSB in the EW sector is also known as *electroweak symmetry breaking* (EWSB), and once this is incorporated into $\mathcal{L}_{\text{Yuk}}$, we see the coveted generation of fermion mass terms,

$$\mathcal{L}_{\text{Yuk}} \supset -\frac{v}{\sqrt{2}}(Y^u_{kj}\bar{q}^k_L\tilde{\varphi}u^j_R + Y^d_{kj}\bar{q}^k_L\varphi d^j_R) + \text{h.c.} \tag{2.47}$$

One can now diagonalise the Yukawa matrices by diagonalising,

$$Y^u = S^u_L M_u S^{u\dagger}_R, \quad Y^d = S^d_L M_d S^{d\dagger}_R, \tag{2.48}$$

with unitary matrices, $S^{u,d}_{L/R}$, and $M_{u,d}$ diagonal in generation. We can then re-define the quark fields consistently in the so-called *mass eigenstate* basis [104],

$$u'_{L/R} = S^{u\dagger}_{L/R}u_{L/R}, \quad d'_{L/R} = S^{d\dagger}_{L/R}d_{L/R}, \tag{2.49}$$

which by definition diagonalises our fermion mass terms in $\mathcal{L}_{\text{Yuk}}$. Performing this change of basis from the original *flavour eigenstate* basis alters the gauge interactions non-trivially and we will investigate this now. Quarks in the flavour basis have the following gauge field interactions,

$$\mathcal{L}_{\text{EW}} \supset (\bar{u}_L \bar{d}_L)^k \left[\left(\frac{g}{2} \not{W}^3 \sigma^3 + g' Y_q \not{B} \right) + \frac{g}{2} \not{W}^1 \sigma^1 + \frac{g}{2} \not{W}^2 \sigma^2 \right] \begin{pmatrix} u_L \\ d_L \end{pmatrix}^k \tag{2.50}$$

$$+ g' \bar{u}_R^k Y_u \not{B} u_R^k + g' \bar{d}_R^k Y_d \not{B} d_R^k \tag{2.51}$$

$$= \frac{e}{\sin\theta_w} Z^\mu J_\mu^Z + e A^\mu J_\mu^{EM} + \frac{g}{\sqrt{2}} \left(\bar{u}_L^k \not{W}^+ d_L^k + \bar{d}_L^k \not{W}^- u_L^k \right), \tag{2.52}$$

with *neutral currents* given by,

$$J_\mu^Z = \frac{1}{\cos\theta_w} (J_\mu^3 - \sin^2\theta_w J_\mu^{\text{EW}}), \tag{2.53}$$

$$J_\mu^3 = \bar{\psi}_L \gamma_\mu T^3 \psi_L, \tag{2.54}$$

$$J_\mu^Z = Q_k \left(\bar{\psi}_L \gamma_\mu \psi_L + \bar{\psi}_R \gamma_\mu \psi_R \right), \tag{2.55}$$

such that $\psi^k = u^k, d^k$, $T^3 = \tau^3$ and the EM charge is given by the relation, $Q = T^3 + Y$. Conveniently, the flavour basis is diagonal in its gauge-quark interactions, this feature is no longer present in the mass basis. Upon analysis, the neutral-currents remain diagonal but not the *charged-currents*. In this basis one has to introduce a unitary matrix, $V = (S_L^u)^\dagger S_L^d$, known as the *Cabibbo-Koboyashi-Maskawa* (CKM) matrix [105, 106], in the Lagangian,

$$\mathcal{L}_{\text{EW}} \supset \frac{g}{\sqrt{2}} \left(\bar{u'}_L^k \not{W}^+ V_{\text{CKM}}^{kj} d'^j_L + \bar{d'}_L^k \not{W}^- (V_{\text{CKM}}^{kj})^\dagger u'^j_L \right). \tag{2.56}$$

The CKM matrix can be further parametrised as it contains four degrees of freedom [107],

$$V = \begin{pmatrix} V_{ud} & V_{us} & V_{ub} \\ V_{cd} & V_{cs} & V_{cb} \\ V_{td} & V_{ts} & V_{tb} \end{pmatrix} = \begin{pmatrix} c_{12}c_{13} & s_{12}c_{13} & s_{13}e^{-i\delta} \\ -s_{12}c_{23} & V_{cs} & V_{cb} \\ V_{td} & V_{ts} & V_{tb} \end{pmatrix}. \tag{2.57}$$

Angles give the four degrees of freedom, θ_{12}, θ_{13} and θ_{23} as well as a phase, δ. The phase, δ, when non-zero, causes the violation of *Charge-Parity* (CP) symmetry, which is an important and well-studied aspect of the SM [108].

Analogously with regards to leptons, the Yukawa sector contains lepton interactions similar to Eq. (2.47),

$$\mathcal{L}_{\text{Yuk}} \supset -Y_{jk}^a \bar{l}_L^j \varphi e_R^k + \text{h.c}, \tag{2.58}$$

between left-handed neutrinos and charged leptons. The lack of a second term as in Eq. (2.47) is due to right-handed neutrinos not having been previously observed and thus excluded from the SM. However, we now know that neutrinos have mass, and thus, right-handed neutrinos must be incorporated in some fashion [109].

We may now combine all the contributions discussed above into one final SM Lagrangian (in unitary gauge). Prior to SSB, the SM Lagrangian is thus given by,

$$\begin{aligned} \mathcal{L}_{\text{SM}} = & -\frac{1}{4} G_{\mu\nu}^a G^{a,\mu\nu} - \frac{1}{4} W_{\mu\nu}^i W^{i,\mu\nu} - \frac{1}{4} B_{\mu\nu} B^{\mu\nu} + |D_\mu \varphi|^2 - V(|\varphi|^2) \\ & + i(\bar{q}_L \not{D} q_L + \bar{u}_R \not{D} u_R + \bar{d}_R \not{D} d_R + \bar{l}_L \not{D} l_L + \bar{e}_R \not{D} e_R) \\ & - \left(Y^u \bar{q}_L \tilde{\varphi} u_R + Y^d \bar{q}_L \varphi d_R + Y^e \bar{l}_L \varphi e_R + \text{h.c} \right), \end{aligned} \tag{2.59}$$

with suppressed color, isospin and generation indices and the covariant derivatives are defined to act as follows,

$$D_\mu q_L = (\partial_\mu + ig'YB_\mu + ig\tau^i W_\mu^i + ig_s T^a G_\mu^a) q_L, \tag{2.60}$$
$$D_\mu u_R = (\partial_\mu + ig'YB_\mu + ig_s T^a G_\mu^a) u_R, \tag{2.61}$$
$$D_\mu d_R = (\partial_\mu + ig'YB_\mu + ig_s T^a G_\mu^a) d_R, \tag{2.62}$$
$$D_\mu l_L = (\partial_\mu + ig'YB_\mu + ig\tau^i W_\mu^i) l_L, \tag{2.63}$$
$$D_\mu e_R = (\partial_\mu + ig'YB_\mu) e_R. \tag{2.64}$$

We end this overview by noting that the SM has many properties only briefly considered here, for instance, quantisation and *gauge-fixing* (GF). For a complete review we point to Ref. [84].

2.2 Renormalisation

When dealing with perturbative QFTs such as the SM, one calculates processes that are related to observables. The perturbative expansion of a given process is achieved in powers of the small coupling constants introduced in Section 2.1. Higher-order quantum corrections, also known as *radiative corrections*, are required for high precision studies. The Lagrangian formulation contains interactions and propagating terms which can be translated diagrammatically to *Feynman diagrams*. We aptly name these *higher-loop* processes as radiative corrections are distinguished from LO or *tree-level* processes by containing loops in their diagrammatic representation. A curious fact about going beyond LO is that amplitudes from loop diagrams contain divergences from the UV regions of the momentum integrals being taken. The purpose of renormalisation is to eliminate said UV divergences by absorption into so-called *bare* parameters of the QFT Lagrangian. Every parameter, including coupling constants, masses and field content, is needed to absorb divergences and the physical Lagrangian used for predictions exhibits no UV divergences.

Aside from absorbing infinities, a renormalisation of fields, mass and couplings would still be necessary even if the loop integrals were finite [94]. The reason is that renormalisation replaces the postulated bare parameters with those experimentally observed in a mathematically consistent way. We now arrive at the notion of *renormalisable theories*: a theory is renormalisable if all its UV divergences are suppressible by a finite number of parameter re-definitions. We can reformulate this statement in terms of individual terms which describe interactions in a Lagrangian. Given an interaction term, one can inspect the mass dimension, $\mathcal{D}$, of its associated coupling constant. In checking this, if $\mathcal{D} > 0$ the interaction is deemed *relevant* if $\mathcal{D} = 0$ the interaction is *marginal* and if $\mathcal{D} < 0$ the interaction is deemed *irrelevant*. A theory is considered non-renormalisable by definition if it permits irrelevant interactions. Renormalisability is one of the crucial tests in model construction and has played a significant role in the development of QFTs [110]. The SM itself was constructed to be renormalisable as this issue was first noticed in the development of QED years prior [111, 112].

Conversely, the cancellation of UV divergences does not necessarily depend on whether a theory is renormalisable in the traditional sense of finite parameter cancellation. In principle, a non-renormalisable theory, which by definition requires infinitely many parameters to absorb its UV divergences, can still be predictive [110]. However, predictiveness only holds if one is solely interested in physics below the energy of mass scales of irrelevant couplings in a non-renormalisable

theory. I.e. given a theory with irrelevant coupling with a mass scale, Λ, one can still make predictions at energies, $E \ll \Lambda$, where the number of non-negligible, non-renormalisable interactions is finite. In this way, one can fix all parameters of a non-renormalisable theory with a finite number of measurements, although the theory will not be exact and precision is limited. We will re-interpret this notion of theories valid at specific energy scales as EFTs in Chapter 3.

Now that we have introduced the notion of renormalisation, We will discuss how it is achieved conventionally. In general, one begins by regularising the infinities with what is known in the literature as a *regularisation scheme*. The process is defined by introducing a regulator for the UV divergences, which renders their form explicit. Upon regularisation, one can then ensure that the infinities are removed by renormalisation. In our work, we employ the scheme known as *dimensional regularisation*, in which one replaces the dimension of space-time with $d = 4 - 2\epsilon$, such that $\epsilon \to 0$. In this scheme, UV divergences appear as poles in $1/\epsilon$ and are thus made explicit when calculating amplitudes.

Moreover, in dimensional regularisation, one includes an additional factor of arbitrary mass scale, $\mu^{-\epsilon}$. This scale ensures that the renormalised couplings remain dimensionless. The newly introduced scale, μ, is known as the *renormalisation scale*, and one is free to re-scale it for convenience. After regularising, the *renormalisation scheme* is set by how one chooses to absorb the explicit divergences which appear. For instance, one can employ the *minimal subtraction* (MS) scheme in which one absorbs only the divergent parts leaving the finite parts untouched. In our work, we employ the *modified minimal subtraction* ($\overline{\text{MS}}$) scheme, which is identical to the MS scheme modulo an additional re-scaling, $\mu^2 \to \mu^2 e^\gamma / 4\pi$, such that γ is Euler's constant.

2.2.1 Renormalisation

To illustrate the process of renormalisation, let us consider the renormalisable theory of QED in which the issue of UV divergences first emerged in the context of QFT. Let us examine the bare QED Lagrangian in which we identify bare parameters with nil superscript,

$$\mathcal{L}_{\text{QED}} = \bar{\psi}^0 \left(i \not{D}^0 - m_e^0 \right) \psi^0 - \frac{1}{4} F^0_{\mu\nu} F^{0,\mu\nu} \tag{2.65}$$

with bare covariant derivative, $D^0 = \partial_\mu - ie^0 A^0_\mu$, and field strength tensor, $F^0_{\mu\nu} = \partial_\mu A^0_\nu - \partial_\nu A^0_\mu$. As previously stated, all bare masses, couplings and fields are non-physical as they are not those measured by experiment. The reason being that measured parameters implicitly incorporate all higher order quantum corrections. Thus, to link theory predictions to observation one needs to renormalise each of these parameters individually. We define the following QED renormalisation constants upon dimensional regularisation, which relate the physical to the bare parameters,

$$\psi = \frac{1}{\sqrt{Z_\psi}} \psi^0, \quad A_\mu = \frac{1}{\sqrt{Z_A}} A^0_\mu, \quad e = \frac{1}{Z_e} \mu^{-\epsilon} e^0, \quad m_e = \frac{1}{Z_m} m_e^0. \tag{2.66}$$

With the above replacements one can then write the Lagrangian explicitly in terms of renormalised parameters,

$$\begin{aligned} \mathcal{L}_{\text{QED}} = {} & i\bar{\psi} \left(\not{\partial} - ie\mu^{-\epsilon} \not{A} \right) \psi - m_e \bar{\psi} \psi - \frac{1}{4} F_{\mu\nu} F^{\mu\nu} \\ & - \frac{1}{4} (Z_A - 1) F_{\mu\nu} F^{\mu\nu} + i(Z_\psi - 1) \bar{\psi} \not{\partial} \psi \\ & + e(\sqrt{Z_A} Z_\psi Z_e - 1) \mu^{-\epsilon} \bar{\psi} \not{A} \psi - m_e (Z_\psi Z_m - 1) \bar{\psi} \psi, \end{aligned} \tag{2.67}$$

with the so-called renormalisation-induced *counterterms* appearing in the second and third lines. The renormalisation constants, Z_i, are fixed by the finiteness requirement of *Green's functions*, which are time-ordered products of our renormalised fields. However, simply requiring freedom from divergence means that the renormalisation constants are not unique. Instead, they are scheme dependent quantities, meaning one can employ any *subtraction scheme* as long as consistency is maintained. For instance, one can use the $\overline{\text{MS}}$-scheme defined previously [94, 113], but others exist and are more convenient for different applications, for instance the *momentum subtraction scheme* useful for lattice studies [114]. As the $\overline{\text{MS}}$-scheme is most often used, we will employ it in our illustration, whence, re-scaling $\mu^2 \to \mu^2 e^\gamma/(4\pi)$ and choosing,

$$Z_i = 1 + \sum_{k=1}^{\infty} \frac{1}{\epsilon^k} Z_{i,k}(e), \tag{2.68}$$

such that $Z_{i,k}(e)$ are solely dependent on the EM coupling, e, and independent of ϵ. Thus, we may now see how to define the $Z_{i,k}$ in QED in the $\overline{\text{MS}}$-scheme such that the divergences are no longer present. The first appearance of a divergence always occurs at one-loop or next-to-leading order (NLO) in a perturbative expansion. For instance, if we consider Z_A for the photon field and attempt to attain it at NLO, Z_A is defined by the finiteness condition of the photon propagator,

finite = 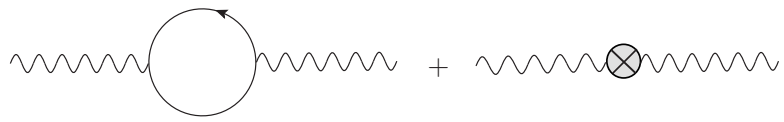 (2.69)

The first diagram gives the one-loop vacuum polarisation correction, and its corresponding counterterm (from the Lagrangian in Eq. (2.67)) is shown in the second diagram. Requiring that the sum of the two diagrams is finite in the $\epsilon \to 0$ limit up to $\mathcal{O}(\alpha_e)$ where $\alpha_e = e^2/(4\pi)$ gives,

$$Z_A = 1 - \frac{4}{3\epsilon}\frac{\alpha_e}{4\pi} + \mathcal{O}(\alpha_e^2). \tag{2.70}$$

Similarly, we obtain Z_ψ and Z_m in one fell swoop by fixing the NLO electron propagator corrections and counterterms according to finiteness,

finite = 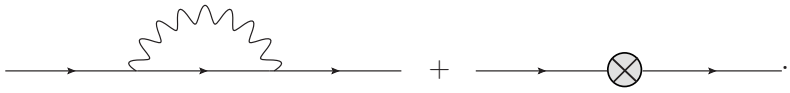 (2.71)

Again, the first diagram is simply vacuum polarisation and the second is its corresponding counterterm in Eq. (2.67). Performing the loop integral and enforcing finiteness then gives,

$$Z_\psi = 1 - \frac{1}{\epsilon}\frac{\alpha_e}{4\pi} + \mathcal{O}(\alpha_e^2), \quad Z_m = 1 - \frac{3}{\epsilon}\frac{\alpha_e}{4\pi} + \mathcal{O}(\alpha_e^2). \tag{2.72}$$

Lastly, for the coupling constant renormalisation, by inspection of Eq. (2.67), one needs to enforce finiteness on the one-loop correction to the vector current,

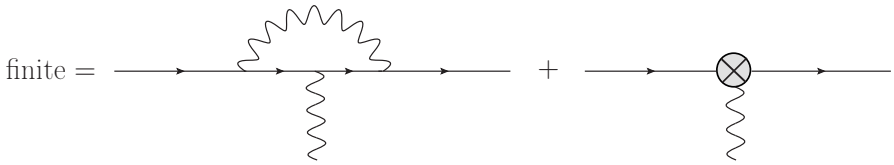

(2.73)

and upon similar calculation, one finds,

$$Z_e = 1 + \frac{2}{3\epsilon}\frac{\alpha_e}{4\pi} + \mathcal{O}(\alpha_e^2). \tag{2.74}$$

Moreover, we find a relation that holds between renormalisation constants up to $\mathcal{O}(\alpha_e)$, $Z_e = 1/\sqrt{Z_A}$. This is often the case and determining such relations beforehand is helpful in performing calculations [115].

2.2.2 Running of Couplings

We may now introduce the notion of running of couplings [116]. Given the renormalised coupling up to NLO,

$$e^0 = e\mu^\epsilon \left(1 + \frac{2}{3\epsilon}\frac{e^2}{16\pi^2} + \mathcal{O}(e^3)\right), \tag{2.75}$$

we can use the fact that μ, the renormalisation scale we introduce in dimensional regularisation, is not physical. Thus, the bare couplings must be independent of μ,

$$\frac{de^0}{d\ln\mu} = e\mu^\epsilon Z_e \left(\epsilon + \frac{1}{e}\frac{de}{d\ln\mu} + \frac{1}{Z_e}\frac{dZ_e}{d\ln\mu}\right) = 0, \tag{2.76}$$

and assuming non-zero coupling, this relation holds only if,

$$\frac{1}{e}\frac{de}{d\ln\mu} = -\epsilon - \frac{1}{Z_e}\frac{dZ_e}{d\ln\mu}. \tag{2.77}$$

We are thus left with this *renormalisation group equation* (RGE) which defines the QED *beta function* of our coupling renormalised in the $\overline{\text{MS}}$-scheme,

$$\beta(e) = \frac{de}{d\ln\mu} = -\frac{e^2}{12\pi^2} + \mathcal{O}(e^3), \tag{2.78}$$

in the limit $\epsilon \to 0$. Thus the beta function is a finite function which provides a complete description of the renormalisation scale dependence of the coupling in a particular renormalisation scheme. When calculating QED processes, the higher n-loop corrections are of the form, $\alpha_e^n \ln^k s/\mu^2$, with $k \leq n$ and $\sqrt{s}$ is the COM energy of the process of interest. Thus, to minimise large logarithms in theory predictions, the appropriate choice for renormalisation scale is $\mu^2 \sim s$.

We now re-write our RGE in Eq. (2.78) with respect to α_e as is done conventionally,

$$\beta(\alpha_e) = \frac{d\alpha}{d\ln\mu} = -2\alpha_e \left(\epsilon + \frac{\alpha_e}{4\pi}\beta_0 + \mathcal{O}(\alpha_e^2)\right), \tag{2.79}$$

such that $\beta_0 = -4/3$ and solving the RGE to NLO gives the so called running coupling,

$$\alpha_e(\mu) = \frac{2\pi}{\beta_0}\ln^{-1}\left(\mu/\Lambda_{\text{QED}}\right) \tag{2.80}$$

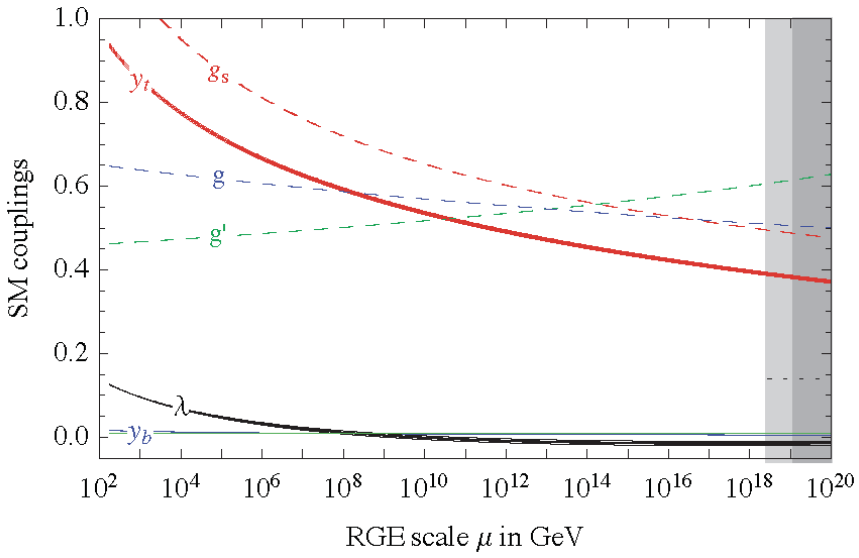

Figure 2.1: The SM running couplings with respect to renormalisation scale. The SM gauge couplings are g, g' and g_s. The top and bottom quark Yukawa couplings are represented by y_t and y_b. The Higgs potential quartic coupling is given by λ. All couplings are computed in the $\overline{\text{MS}}$-scheme up to NNLO [34].

where the coupling is no-longer a constant but renormalisation scale dependant. The newly introduced scale, Λ_{QED}, is given by the experimentally observed value of the QED coupling. We now pause to note an interesting property of Eq. (2.80), recall that α_e is necessarily a positive real number, and β_0 is negative, thus the coupling grows as energy increases. Moreover, as $\mu \to \Lambda_{\text{QED}}$, Eq. (2.80) exhibits a pole and this divergence is known as the Landau pole of the theory.

In this illustration, we focused on QED as an example; however, the SM, in turn, contains renormalisation scale-dependent couplings. As written in Section 2.1, the SM gauge couplings are g', g and g_s, also from the Yukawa sector, we have the Yukawa couplings, y_I, with I labelling massive fermions and the couplings of the *Higgs potential*. The largest Yukawa couplings are y_t, y_b and y_τ in order of decreasing mass. Each SM coupling has an associated beta function, and these have been determined in the SM to three-loop orders [117]. We present these scale-dependent couplings in Fig. 2.1 and comment on their properties. The first feature of SM running couplings to point out is the quartic coupling, λ, of the Higgs potential turning negative near 10^9 GeV. This behaviour is only exhibited by this coupling and points to the meta-stability of the EW vacuum. The precision of this stability is predominantly dependent on the Higgs and top quark mass precision determinations as shown in Fig. 2.2 from calculations to two-loop order [33, 34, 118, 119]. As for the gauge couplings, g' from gauging the $U(1)_Y$ symmetry group is non-negative and grows with energy, diverging as in QED at a *Landau pole*. The Landau pole appears past the *Planck scale* $M_{\text{P}} \sim 10^{19}$ GeV, and thus, the pole is not sufficiently well-defined as of yet unknown quantum gravitational effects will begin to take hold at this scale. The $SU(2)_L$ gauged weak coupling, g, has the interesting feature of overtaking the strong coupling near 10^{16} GeV and, unlike the hypercharge coupling, does not exhibit a Landau pole.

The remaining gauge coupling to consider is the strong coupling, g_s, which conversely to QED and hypercharge exhibits a Landau pole at small energies, $\Lambda_{\text{QCD}} \sim 10^{-1}$ GeV. Λ_{QCD} is

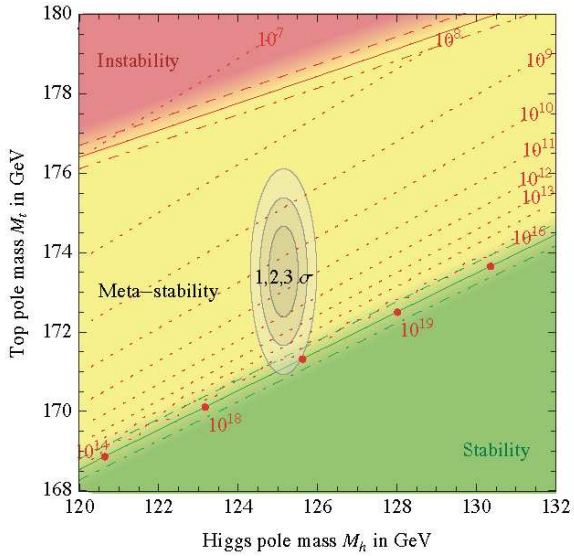

Figure 2.2: The SM vacuum phase space with respect to the top quark and Higgs masses. The plane is subdivided into regions of stability, metastability and instability. The three boundary ellipses correspond to standard deviation variations in the strong coupling indicating the dominant uncertainty in the top mass. Colour gradings correspond to the size of theoretical error from terms beyond NNLO [34].

also known as the quark *confinement scale* as it is related to the non-perturbative regime of QCD and the phenomenon of confinement. Near Λ_{QCD}, physical quark states exist in colour singlet combinations known as *hadrons*, such that no free quarks arise. For instance, the most commonly observed hadronic states are *mesons* (quark-antiquark pairs) and *baryons* (bound states of three quarks), but more exotic states such as *pentaquarks* may appear as well. On the opposite end of the energy spectrum, at high energies, the strong coupling goes to zero, and this phenomenon, which is unique to the QCD sector, is known as *asymptotic freedom* [85]. This feature is immediately apparent from the overall positive sign of the β_0 coefficient of the QCD beta function,

$$\beta_0^{\text{QCD}} = \frac{1}{3}\left(33 - 2n_f\right), \tag{2.81}$$

which can be compared to the QED case in Eq. (2.79). It is clear that Eq. (2.81) is positive for $n_f < 17$ and in the SM $n_f = 6$ which results in asymptotic freedom. This feature of QCD has been confirmed by observation and is now a consistency condition that must be satisfied for BSM theories that couple to QCD. Any reason behind the sign difference in QCD relative to QED harkens back to QCD being symmetric under a non-Abelian group. This results in the phenomenon of self-interactions among the gauge fields, which in turn impact strong coupling renormalisation as these are determined from vertex diagrams [85].

2.3 Quark Mass

In this thesis, we will mainly be interested in heavy fields, particularly the SM's heavy quarks. One of the most crucial parameters required in the study of heavy quarks is attaining a precise mass determination. The reason being that heavy quark mass is a fundamental parameter of

the SM. Moreover, it constrains BSM models with additional flavour physics [22, 44, 120, 121]. Quark masses are non-trivial to define due to the phenomenon of quark confinement, which is not exhibited by any other fields in the SM. Confinement complicates matters, as free quarks do not exist in nature, and thus, their mass can not be measured as individual entities. We briefly introduce the issues with defining a quark mass in this section; a complete review is present in Ref. [122].

We will focus on the top mass, m_t, as it is often employed in SM consistency checks [48–50]. Moreover, it is the dominant source of uncertainty when weighing the stability of the EW vacuum [33,51,52]. Secondarily, we are also concerned with the bottom quark, which is the next heaviest and lies in the same generation as the top quark. The bottom mass, m_b, is an important factor in the phenomenology of B-meson and Higgs decay as their decay widths contain large powers of m_b [53–55]. The study of B decays highly constrains elements of the CKM matrix, thereby supplying precision tests of the flavour sector in the SM [120, 123, 124].

2.3.1 Heavy-Quark Limit

Let us begin by considering the *heavy quark limit*, in which the quark mass, $m_Q \gg \Lambda_{\text{QCD}}$. In this limit, processes that occur at a scale,

$$\frac{\Lambda_{\text{QCD}}}{m_Q} \to 0, \tag{2.82}$$

are separable from confinement physics which is an IR phenomenon occurring at distance scales of $\mathcal{O}(1/\Lambda_{\text{QCD}})$. If this limit is physical, we have a large advantage as we may disentangle UV and IR physics cleanly. In the case of the top quark, $\Lambda_{\text{QCD}}/m_t \sim 10^{-3}$, which would mean minor corrections beyond LO of $< 1\%$ from this limit. On the other hand, in the case of the bottom quark, $\Lambda_{\text{QCD}}/m_b \sim 10^{-1}$ and thus the naive expectation is $\sim 10\%$ corrections. Such corrections are significant and thus $\mathcal{O}(\Lambda_{\text{QCD}}/m_b)$ corrections and higher require accounting for.

The advantage of scale separation occurring in the heavy quark limit is that quark processes are only sensitive to short-distance physics, which can be perturbatively determined. On the other hand, long-distance physics is non-perturbative and appropriate for hadronic properties, which is the purview of *lattice QCD* [125, 126]. The former case is of interest to us, and thus quantities determined by short-distance physics help probe the heavy quark masses. For instance, in the case of the bottom quark, the B-meson semi-leptonic decay width has been widely studied and shown to be a sensitive probe of m_b [127].

Complications in the heavy quark limit can arise; in particular, quantum corrections occurring at higher-loop order are indiscriminate in their probing of short- and long-distance scales. These radiative corrections result in alterations to the heavy quark limit by introducing terms that are suppressed by running coupling powers, and thus, the limit can not be taken naively. Moreover, these virtual corrections introduce energy scales aside from coupling from the SM, for instance, matter and gauge field masses. These, along with heavy quark three-momentum $\sim m_Q \boldsymbol{v}$ and kinetic energy $\sim m_Q \boldsymbol{v}^2$ enter the dynamics. Lastly, when dealing with the bottom quark, the inclusion of finite-mass effects becomes necessary and require careful consideration at each loop order [128, 129].

These complications and various scales seem to make the precision study of heavy quarks intractable. However, with the help of EFT, which we introduce in Chapter 3, the problem has proven manageable. We now proceed to the task at hand of defining mass for heavy quarks.

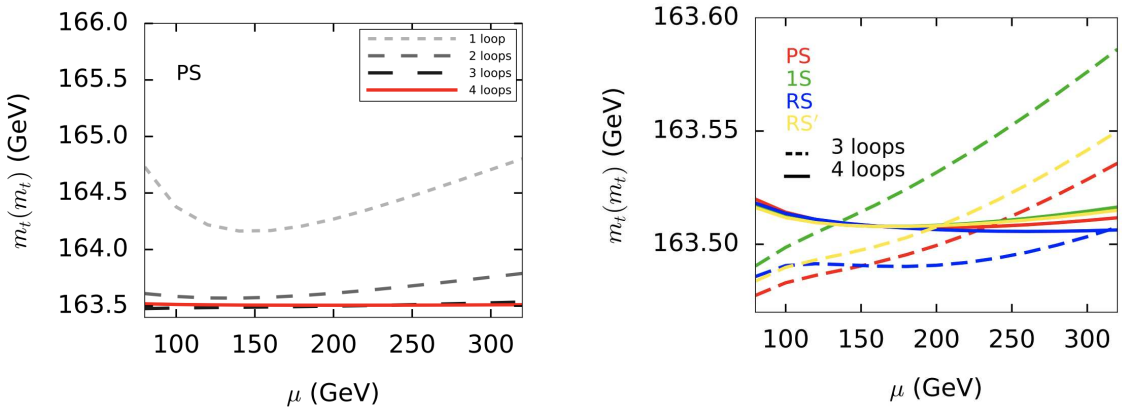

(a) (b)

Figure 2.3: (a) $\overline{\text{MS}}$ top quark mass computed from the PS mass with one- to four-loop accuracy with respect to the renormalisation scale of the $\overline{\text{MS}}$-threshold mass relation. (b) $\overline{\text{MS}}$ top quark mass computed from the PS, 1S, RS and RS′ mass with third and fourth loop accuracy with respect to renormalistion scale in the $\overline{\text{MS}}$-threshold mass relation [133].

2.3.2 Mass Definitions

As is the case for all parameters in the SM Lagrangian, quark masses are renormalised quantities. Moreover, one is free to renormalise in any well-defined fashion as long as all predictions are UV finite. This freedom turns out to be of great utility when dealing with quark masses in particular. The reason being that although any renormalisation scheme is permitted, different ones need to be applied for different purposes when dealing with quarks as predictions can become non-attainable otherwise. Various quark mass renormalisation schemes have been proposed and studied [58, 60, 94, 130–132], some of which are illustrated for m_t in Fig. 2.3 from one- to four-loop order [133, 134]. Each has its associated regimes of utility as well as properties that make them unique. We will discuss the ones employed in this thesis briefly as they are re-introduced later on in the appropriate sections.

2.3.2.1 The Pole Mass and Renormalons

The most natural definition of quark mass is arrived at from the quark *propagator* and is known as the *pole mass*, m_{pole} [135]. This is how we generally define mass in QFT and it is explicitly given by the pole solution of the quark propagator. The full quark propagator to all loop-orders can be written as,

$$iS(p, m_Q) = \frac{i}{\not{p} - m_Q - \Sigma(p, m_Q)} \tag{2.83}$$

for a quark with mass, m_Q, momentum p and *self-energy*, $\Sigma(p, m_Q)$. The pole mass is then defined by the solution to,

$$(\not{p} - m_Q - \Sigma(p, m_Q))|_{p^2 = m^2_{\text{pole}}} = 0. \tag{2.84}$$

Thus, all that is necessary to determine the pole mass up to a specific order in small couplings is the radiative corrections to self-energy diagrams. The pole mass has the advantage of being both gauge invariant [135, 136] and IR finite [137]. Moreover, for heavy quarks, one can relate the pole mass to hadron masses such as the meson mass in a perturbative expansion in $1/m_Q$ [59].

Although the pole mass is well-defined and simply determined, its perturbative relation to physical observables is known to contain ambiguities [130]. For example, consider the semi-leptonic, $b \to u$ decay width to the bottom quark pole mass, denoted m_b. At two-loop orders in QCD this relation is given by [138, 139],

$$\Gamma(b \to X_u l \bar{\nu}_l) = \frac{G_F^2 |V_{ub}|^2 m_b^5}{192\pi^3} \left(1 - 2.41\frac{\alpha_s}{\pi} + (3.39 - 3.22\beta_0)\left(\frac{\alpha_s}{\pi}\right)^2 + \mathcal{O}(\alpha_s^3, m_b^{-1})\right) \tag{2.85}$$

$$= \frac{G_F^2 |V_{ub}|^2 m_b^5}{192\pi^3}(1 - 0.17 - 0.11 + \ldots) \tag{2.86}$$

where G_F is the Fermi constant, $\alpha_s = \alpha_s(m_b) = 0.22$ and,

$$\beta_0 = 11 - \frac{2}{3}n_f, \tag{2.87}$$

is the first coefficient of the QCD beta function such that $n_f = 4$ is the number of light quark flavours. By inspection of Eq. (2.86), the two-loop terms are large and thus the perturbative series is poorly behaved although $\alpha_s/\pi \ll 1$.

This poor perturbative behaviour is endemic in the pole mass to all perturbative orders [130]. More specifically, any perturbative series relating quantities to the pole mass exhibit ambiguities of $\mathcal{O}(\Lambda_{\rm QCD}/m_{\rm pole})$. These ambiguities are expected to occur as solely asymptotic convergence is achievable with perturbation theory [39]. Furthermore, $m_{\rm pole}$ can only be defined through its relation to observable quantities, which pass on the ambiguity to the pole mass definition. This ambiguity has been studied extensively and is also known as the IR *renormalon*. The IR nature of the renormalon is due to it arising from the IR (or low-momentum) region of loop integrals at which the QCD running coupling grows large. For a more detailed review of this phenomenon, see Ref. [47].

2.3.2.2 The $\overline{\rm MS}$ Mass

The renormalon ambiguity of the pole mass arises due to its sensitivity to IR physics; this results in the notion of a *short-distance mass* definition. To define such a mass, one needs a way to separate short- from long-distance physics. Conveniently, any mass parameter which is renormalised at some scale, μ, is by definition insensitive to IR scales. Moreover, regulating perturbative calculations is most often done with dimensional regularisation, as defined in Section 2.2. Thus, the combination of dimensional regularisation and the requirement of renormalisation scale dependence leads to the $\overline{\rm MS}$-mass, labelled $\bar{m}_q(\mu)$, as being a valid quark mass candidate.

As previously introduced the $\overline{\rm MS}$-mass in the SM is defined by dimensionally regulating the SM Lagrangian and subtracting divergences in the $\overline{\rm MS}$-scheme. Moreover, as discussed in Section 2.2.1, one chooses $\mu \sim Q$ where Q is the characteristic energy scale of the physical process being studied. The RGE can be used to then relate a mass renormalised at a particular scale to one renormalised at another, performing a resummation of logarithms at all orders [140, 141]. One may then relate the $\overline{\rm MS}$-mass to the pole mass at any order. Again, sticking with our example from the previous section of bottom quarks in QCD [142–144],

$$\frac{m_b}{\bar{m}_b} = 1 + \frac{4}{3}\frac{\bar{\alpha}_s}{\pi} + (1.56\beta_0 - 3.74)\left(\frac{\bar{\alpha}_s}{\pi}\right)^2 + (1.47\beta_0^2 + 0.3\beta_1 + 0.4\beta_0 - 30)\left(\frac{\bar{\alpha}_s}{\pi}\right)^3 + \mathcal{O}(\alpha_s^4), \tag{2.88}$$

given to three-loop orders. The second coefficient of the QCD beta function is given by,

$$\beta_1 = 102 - \frac{38}{3} n_f, \tag{2.89}$$

and $\bar{\alpha}_s \equiv \alpha_s(\bar{m}_b)$, meaning the $\overline{\text{MS}}$-mass is taken to be renormalised at $\mu = \bar{m}_b(\mu)$ and thus, $\bar{m}_b \equiv \bar{m}_b(\bar{m}_b)$. With this relation we can re-express the semi-leptonic decay width of the previous section to two-loop orders [138],

$$\Gamma(b \to X_u l \bar{\nu}) = \Gamma_0 \bar{m}_b^5 (1 + 4.25 \frac{\alpha_s(m_b)}{\pi} + 4.58 \beta_0 \frac{\alpha_s(m_b)}{\pi}^2 + \mathcal{O}(\alpha_s^3)) \tag{2.90}$$

$$= \Gamma_0 \bar{m}_b^5 (1 + 0.30 + 0.19 + \mathcal{O}(\alpha_s^3)). \tag{2.91}$$

We can see a marked improvement in the asymptotic series, and it has been shown that the $\mathcal{O}(\Lambda_{\text{QCD}})$ renormalon ambiguity indeed vanishes [139]. Thus, $\overline{\text{MS}}$-pole relation seems to quell our perturbative issues, and the relation is known to four loop orders in pure QCD for the heavy quarks [133, 134]. Furthermore, as we are interested in EW corrections mainly, the $\overline{\text{MS}}$-pole relation has been determined for top and bottom quarks to two-loop precision in the full SM [145–151].

2.3.2.3 The Threshold Masses

At this point in our overview, it seems the $\overline{\text{MS}}$-mass is sufficient for all precision tests in the SM. However, as pointed out firstly in Ref. [152], the $\overline{\text{MS}}$-mass is not well behaved as well at scales below $\mu = m_Q$, where m_Q denotes the pole mass. This poor behaviour is best explained from an EFT perspective. The $\overline{\text{MS}}$-mass is defined in the full theory treating the quark as fully dynamical from a UV scale down to m_Q. Once one reaches $\mu = m_Q$, however, the appropriate theory which describes the dynamics and kinematics changes from the SM to HQET [153]. Thus, from an EFT perspective, it makes no physical sense for μ to be lowered beyond m_Q in the full theory. Furthermore, m_Q is not a running parameter in HQET and renormalising $\bar{m}_q(\mu)$ below m_Q introduces non-physical large logarithms, which negatively affects perturbative convergence.

Thus, we need an entirely new set of mass definitions, the so-called *threshold masses*, which are well behaved for observables below threshold in the low energy regime. These mass definitions are useful for heavy quark studies in the *non-relativistic* (NR) limit. Moreover, a threshold mass must be defined such that it avoids IR renormalons while also exhibiting well-behaved perturbative relations in the NR regime. Many threshold masses have been proposed and studied in a variety of NR process [56–60]. A few threshold-$\overline{\text{MS}}$ mass relations for the top quark have been determined to four-loop order in pure QCD [133], as depicted in Fig. 2.3. We will now introduce the threshold masses studied in the remainder of this thesis.

Kinetic Mass: The first threshold mass we will consider is known as the *kinetic mass*, $m_Q^{\text{kin}}(\mu_f)$, in the literature and was first introduce in Refs. [56, 154, 155]. The kinetic mass incorporates a new IR *factorisation scale*, μ_f, to subtract long-distance physics and avoid the renormalon ambiguity in its definition. The mass is defined by the heavy meson BE, $\bar{\Lambda}\mu_f$, and residual KE, $\mu_\pi^2(\mu_f)$,

$$m_Q = m_Q^{\text{kin}}(\mu_f) + \bar{\Lambda}(\mu_f) - \frac{\mu_\pi^2(\mu_f)}{2 m_Q^{\text{kin}}(\mu_f)} + \mathcal{O}(1/m_Q^2) \tag{2.92}$$

where m_Q denote quark pole mass. The energies are attainable perturbatively from the forward *scattering amplitude* of a heavy quark non-flavour changing external current in the *small quark velocity* (SV) limit [156]. By definition, in the factorisation limit $\mu_f \to 0$, $m_Q^{\rm kin}(\mu_f)$ is simply the pole mass while for $\Lambda_{\rm QCD} < \mu_f < m_Q$, the kinetic mass eliminates the IR renormalon ambiguity and is well-behaved in the heavy quark limit. The $\overline{\rm MS}$-kinetic mass relation has been determined to three loops in pure QCD [157], for the bottom quark the relation is given by,

$$\frac{m_b^{\rm kin}(\mu_f)}{\bar{m}_b} = 1 + \frac{4}{3}\frac{\bar{\alpha}_s}{\pi}\left[1 - \frac{4}{3}\frac{\mu_f}{\bar{m}_b} - \frac{\mu_f^2}{2\bar{m}_b^2}\right] + \left(\frac{\bar{\alpha}_s}{\pi}\right)^2\left[K - \frac{8}{3} + \frac{\mu_f}{\bar{m}_b}\left(\frac{8\beta_0}{9}X_1 + \frac{8\pi^2}{9} - \frac{52}{9}\right)\right.$$
$$\left. + \frac{\mu_f^2}{\bar{m}_b^2}\left(\frac{\beta_0}{3}X_2 + \frac{\pi^2}{3} - \frac{23}{18}\right)\right] + \mathcal{O}(\alpha_s^3, \mu_f^3/m_b^3), \tag{2.93}$$

up to NNLO [158], such that,

$$K = \frac{\beta_0}{2}\left(\frac{\pi^2}{6} + \frac{71}{48}\right) + \frac{665}{144} + \frac{\pi^2}{18}\left(2\ln 2 - \frac{19}{2}\right) - \frac{1}{6}\zeta_3,$$
$$X_1 = \ln\frac{2\mu_f}{\bar{m}_b} - \frac{8}{3}, \quad X_2 = \ln\frac{2\mu_f}{\bar{m}_b} - \frac{13}{6}. \tag{2.94}$$

The term ζ_n is the *Riemann zeta function*, and β_0 is the first QCD beta function coefficient.

Potential Subtracted Mass: Another important threshold mass used in heavy quark precision studies is known as *potential subtracted* (PS) mass [57]. As in the kinetic mass, the PS mass is dependent on energetic quantities determined from the dynamics of heavy physics. To define the PS mass, let us begin by considering the dynamics of a quark-antiquark (quarkonium) system, which is governed by the *Schrödinger equation*,

$$\left(-\frac{\nabla^2}{m_Q} - E + V(\boldsymbol{r})\right) G(\boldsymbol{r}, 0, E) = \delta^{(3)}(\boldsymbol{r}). \tag{2.95}$$

The binding energy of the system is given by $E = \sqrt{s} - 2m_Q$, and $V(\boldsymbol{r})$ is the Coulomb-like potential between the pair of heavy quarks, also known as the *static potential* [39, 159]. Thus, Eq. (2.95) incorporates the *total static energy* of a pair of heavy quarks in its description at some fixed distance, $\boldsymbol{r}$, given by,

$$E_{\rm stat}(\boldsymbol{r}) = 2m_Q + V(\boldsymbol{r}). \tag{2.96}$$

The total static energy is physical and always well-defined, meaning it can not exhibit non-physical renormalon ambiguities. The lack of ambiguities has been demonstrated in the context of QCD as the higher-order behaviour of $V(\boldsymbol{r})$ cancels that of the pole mass, implying the total static energy in Eq. (2.96) is well-defined.

We can explictly draw out this cancelation by expressing the pole mass in terms of the PS mass, which is defined as,

$$m_Q^{\rm PS}(\mu_f) = m_Q - \delta m(\mu_f) \tag{2.97}$$

such that,

$$\delta m = \int_{|\boldsymbol{q}|<\mu_f} \not{d}^3\boldsymbol{q}\tilde{V}(\boldsymbol{q}), \tag{2.98}$$

and $\tilde{V}(\boldsymbol{q})$ is the momentum space potential [159]. Note the inclusion again of an explicit factorisation scale to avoid the small $|\boldsymbol{q}|$ region in which the renormalon resides. Thus, to obtain this mass one needs to extract the Coulomb-like terms from quarkonium scattering in the heavy quark limit of the SM [160, 161]. In the case of pure QCD the PS mass has been determined to four loop orders [134], as is shown in Fig. 2.3. We present the PS-pole bottom mass relation for illustration, to one-loop order [57],

$$\frac{m_b^{\rm PS}(\mu_f)}{m_b} = 1 - C_F \frac{\alpha_s(\mu)}{\pi} \frac{\mu_f}{m_b} \left(1 + \frac{\alpha_s(\mu)}{4\pi} \left[a_1 - 2\beta_0 \left(\ln \frac{\mu_f}{\mu} - 1\right)\right]\right) + \mathcal{O}(\alpha_s^3, m_b^{-2}),$$
$$a_1 = \frac{31}{3} - \frac{20}{9} T_f n_f, \tag{2.99}$$

neglecting finite mass affects. The colour factors in QCD are given by $C_A = 3$, $C_F = 4/3$ and $T_f = 1/2$, also $n_f = 4$ in the case of the bottom quark while $n_f = 5$ when considering the top quark in QCD. One can then relate the PS mass directly to the $\overline{\rm MS}$-mass using the $\overline{\rm MS}$-pole mass relation. Again in the case of the PS mass, for $\mu_f < m_Q$ the pole mass and PS mass differ by $\mathcal{O}(E_Q)$ where $E_Q \sim m_Q \boldsymbol{v}^2$ which is useful for power counting.

1S Mass: Recall that the previous threshold mass definitions we introduced are dependent on an explicit IR factorisation scale, μ_f. This additional IR scale controls spurious non-perturbative behaviour arising from the IR regime in the pole mass definition. Although such scales are necessary for those definitions, they are free parameters and finding the best choice to minimise poor behaviour is not always trivial. There are, however, threshold mass definitions that require no factorisation scales to be introduced; the first discovered and most often employed definition is the so-called *1S mass* [59, 132].

The 1S mass is defined simply as one-half the energy of the 1S $q\bar{q}$ state calculated perturbatively. The perturbative point is crucial as this excludes non-perturbative effects automatically and it then lies firmly in the realms of short-distance mass definitions. The difficulty in the 1S mass, as has been shown in QCD, is that the renormalon cancellation is subtle and achieved with appropriate re-ordering of terms in perturbation theory. In the case of pure QCD the 1S mass is known to four loop orders [134], as depicted in Fig. 2.3. The 1S-pole bottom mass relation to one-loop order is [162],

$$\frac{m_b^{1S}(\mu_f)}{m_b} = 1 - \frac{(\alpha_s(\mu) C_F)^2}{8} \left(1 + \frac{\alpha_s(\mu)}{\pi} \left[\beta_0(l+1) + \frac{a_1}{2}\right]\right) + \mathcal{O}(\alpha_s^3, m_b^{-2}), \tag{2.100}$$

with $l \equiv \ln(\mu/(C_F m_b \alpha_s))$, and other parameters are as previously defined. In chapters 4 and 5 of this thesis we will be focusing on determining the leading EW corrections to the kinetic, PS and 1S masses, which appear at one-loop order in each case. We end by noting that we have by no means introduced all threshold mass definitions, for instance, there is the *renormalon subtracted* (RS) mass which is also illustrated in Fig. 2.3. For a review of more definitions not considered in this thesis we recommend Refs. [122].

2.4 Beyond The Standard Model Motivation

The SM has been incredibly successful in its description of fundamental interactions, and until now, there exists no direct detection of particles that lie beyond. Moreover, the SM exhibits a

very delicate structure that discounts many BSM theory proposals, as they have to be consistent with the plethora of confirmed data thus far. Direct detection aside, however, there is plenty of indirect evidence that the SM cannot describe, impelling the theory community to consider models beyond. This section will consider a few pieces of BSM evidence along with compelling models that describe their origin.

Before we begin, let us list for reference and perspective what exists beyond a reasonable doubt and is unexplained thus far: *neutrino mixing* and masses [163], *matter-antimatter asymmetry* [164], non-baryonic *cold dark matter* [165], acausal density perturbations consistent with a period of *inflation* in the early universe [166]. Moreover, there are many deep unexplained features of nature, for instance: Planckian scale physics, hierarchies of scale between the known constants of nature, the number of fermion families, the number of space-time dimensions, etcetera. As the primary focus of this thesis is heavy fields and EFTs, we will avoid cosmology in the examples considered next.

2.4.1 Flavour Puzzle

Recall that the SM Lagrangian in Eq. (2.59) includes 18 parameters in total: 6 quark masses, three lepton masses (SM has massless neutrinos), three angles plus a phase of the CKM matrix, three gauge coupling constants, two Higgs potential couplings. Aside from the gauge and Higgs potential couplings, the remaining 13 parameters lie in what is known as the *flavour sector* of the SM. The flavour sector exhibits many puzzles ripe for consideration, for instance, the hierarchy of scales between the fermion masses.

As measured, there is an enormous scale separation in mass among the SM fermions, whether taking them as a single group or separating into quarks and leptons, the hierarchy persists [167, 168]. Moreover, with regard to quarks and their CKM matrix an elusive pattern is present, which is more apparent in the *Wolfenstein basis* [169],

$$V \sim \begin{pmatrix} 1-\lambda^2/2 & \lambda & \lambda^3 \\ \lambda & 1-\lambda^2/2 & \lambda^2 \\ \lambda^3 & \lambda^2 & 1 \end{pmatrix}, \tag{2.101}$$

up to $\mathcal{O}(\lambda^4)$ with $\lambda = \sin\theta_{12} \sim 0.2$. Thus, in the flavour sector these hierarchies and patterns are not yet determined.

The answer to this mystery could lie in a *flavour symmetry breaking* mechanism, i.e. hierarchies in the SM arise from particles with flavour symmetry that experience symmetry breaking at some higher *grand unified theory* (GUT) scale. For instance, the *minimal supersymmetric Standard Model* (MSSM) is often cited as providing such a mechanism. In the MSSM, each SM fermion field has a bosonic super-partner and vice-versa, accompanied by their masses and couplings [170]. Alternatively, the apparent patterns may be based on a $U(1)$ *Froggatt-Nielsen* (FN) symmetry [171], combined with a discrete A_4 symmetry [172], which is apparent in SM extensions containing hypothetical fields known as *leptoquarks* [163]. Leptoquarks are particles that couple to both quarks and leptons and may be involved in lepton flavour violation and non-universality.

On the other hand, one can explain the smallness of the Yukawa couplings and CKM angles through RGE evolution in the IR. Unfortunately, Yukawa couplings exhibit little logarithmic

energy dependence, and thus RGE flow is insufficient to explain the hierarchy of scales even for strong coupling. Lastly, *conformal field theory* (CFT) offers a neat solution [173]. A CFT is defined as a local QFT invariant under conformal, or angle preserving, mappings. By extending the SM gauge group with a conformal sector, containing scale-invariant gauge couplings, the flavour hierarchy is then generated by *strong conformal dynamics* [174, 175].

The only way to confirm any of these model solutions in the flavour sector, aside from direct detection of new particles, is through anomalies in data. We are at an exciting time for flavour physics as several new such anomalies appear in various experiments. For instance, several measurements over the years of B-decay are hinting at deviations from the predictions of the SM alone. Such B-decay anomalies are now being accompanied by discrepancies in measurements of the muon's *anomalous magnetic moment* (AMM).

B-decay Anomalies: A large number of data discrepancies are appearing in analyses of various independent groups with regards to *flavour changing current* (FCC) transitions. Such anomalies have been detected in both neutral, $b \to s l^+ l^-$, and charged, $b \to c l^- \bar{\nu}_l$ transitions. We group and describe the confirmed results over the years into four distinct types:

- The *branching ratio* suppression in $b \to s\mu^+\mu^-$ transitions [176, 177]. In these studies, the dominant uncertainties are hadronic in nature [178, 179].
- Angular observable deviation from the SM in $B \to K^* s\mu^+\mu^-$ transitions [180]. In this case, the dominant uncertainties are also hadronic but less significant [181].
- Lepton universality deviation from the SM in $b \to s l^+ l^-$, $B \to K l^+ l^-$ and $B \to K^* l^+ l^-$, between electrons and muons (e-μ universality) [23]. On the theory side, the uncertainty is sufficiently small [182], but the experimental sensitivity is not sufficient as of yet.
- Lepton universality deviation in $b \to s l^- \bar{\nu}_l$ transitions, between all SM leptons [177, 183]. In this case, e-μ universality holds to high precision [120, 184]. Similar to the previous point, dominant uncertainties are experimental [185].

On the experimental front, the B-decay observables to test lepton-flavour universality violation in $b \to c$ are given by branching ratios. These ratios have been measured over time by various collaborations including LHCb [23, 177, 183], Belle [23, 184], and BaBar [183]. The discrepancy with the SM from combined measurements stand at $\sim 3\sigma$ [182, 185]; however, the latest and most precise Belle measurement of,

$$R_{D^*} = \frac{\int dq^2 d\mathrm{BR}(B \to D^* \tau \nu_\tau)/dq^2}{\int dq^2 d\mathrm{BR}(B \to D^* e \nu_e)/dq^2}, \tag{2.102}$$

has only shown a 1.2σ discrepancy. Therefore it may be that statistical fluctuations will eventually explain away these anomalies. Assuming, however, that these anomalies turn to discoveries and BSM physics is needed, there are various proposals [186].

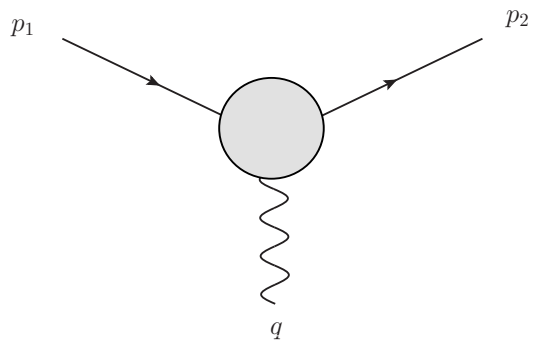

Figure 2.4: Diagrams of charged lepton AMM with initial momenta, p_i, and transfer momentum, $q = p_2 - p_1$. Shaded circle represents higher-loop virtual SM corrections.

AMM Anomalies: Quantum corrections to the AMM of a particle are important to determine as they are observables that can be measured to very high precision. Currently, the AMM of the electron is the most precisely determined observable in particle physics to date. The charged lepton AMM is given by the diagram illustrated in Fig. 2.4 which evaluates to,

$$A_l^{\rm SM} = -ie\bar{u}(p_2)\left[F_1(\frac{q^2}{m_l^2})\gamma^\mu + \frac{i\sigma^{\mu\nu}}{2m_l}q_\nu F_2(\frac{q^2}{m_l^2})\right]u(p_1), \tag{2.103}$$

with F_i known as form factors and are given to LO by $F_1 = 1$ and $F_2 = 0$. At NLO and beyond additional terms $\propto \alpha_e$ become apparent in F_2, which have the same structure as a *magnetic moment*. Thus, if at tree-level, $F_2 = 0$, then the magnetic moment is $g_l = 2$, as predicted by the Dirac equation. At NLO, the first quantum corrections start to appear, and for $q^2 \to 0$, the leading term in the momentum expansion is,

$$F_2(0) = \frac{\alpha_e(\mu)}{2\pi} \Rightarrow g_l = 2 + 2F_2(0) = 2 + \frac{\alpha_e(\mu)}{\pi}. \tag{2.104}$$

and the AMM is then conventionally defined as,

$$a_l = \frac{g_l - 2}{2}, \tag{2.105}$$

which corresponds to all deviations for $g_l = 2$ at LO for all leptons, $l = e, \mu, \tau$. It turns out that the theory predictions must incorporate all EW and hadronic contributions to attain the precision achieved thus far [187]. The latter of contributes the highest theoretical uncertainty and therefore requires further thorough study to match the low EW uncertainty [188–191].

Measurements have recently found curious anomalies concerning SM theory predictions for the muon AMM in particular. After adding uncertainties from theory and experiment in quadrature, there is a significant deviation of 4.1σ from the latest theory predictions [188, 189]. Curiously, however, at the same time, an extensive lattice QCD collaboration which performed a very precise computation of the hadronic vacuum polarisation (the sector with the most prominent theory uncertainty) agrees with experiment, and their results are consistent with the SM [190]. Of course, this is only one theory prediction, and it is in contradiction with a large body of knowledge, including EW data [191, 192], and previous lattice calculations [193]. Hence, further investigation is required on all fronts.

Assuming this anomaly persists and is indeed a discovery, various BSM models exhibit explicit breaking of lepton universality. For instance, models which introduce additional fields such as light scalars [194–196], or partners from supersymmetry (SUSY) extensions [197–199].

2.4.2 Strong CP Problem

Another mystery of the SM lies in the QCD sector of the SM, which includes only quarks and gluons. As described in Section 2.1, QCD arises from the local $SU(3)_C$ symmetry group being gauged. Furthermore, QCD is CP-symmetric, in contrast to the EW sector, which includes gauge fields coupled to chiral currents that violate Parity. In QCD, gluons only couple to vector currents and CP-symmetry in QCD has been confirmed by experiment beyond a reasonable doubt. Furthermore, if CP-violation does occur, it would be suppressed by a factor of 10^9 [200]. We thus arrive at the *strong CP problem*, which can be seen by the addition of the following term into the colour sector of the SM,

$$\mathcal{L}_{\text{SM}} \supset \theta \frac{g_s^2}{16\pi^2} G^a_{\mu\nu} \tilde{G}^{a,\mu\nu}, \tag{2.106}$$

with θ a constant parameter and dual tensor, $\tilde{G}^{a,\mu\nu} = \frac{1}{2}\epsilon^{\mu\nu\sigma\rho} G^a_{\sigma\rho}$. This additional term is permitted by the gauge symmetry and must be included in the SM, as there is no conservation law forbidding it.

The reason why Eq. (2.106) is not included in the original SM is that it can be written as a total derivative, and thus it does not contribute perturbatively. However, it is, in fact, non-zero non-perturbatively and therefore required in non-perturbative studies such as *lattice QCD* [201, 202]. More importantly, it imposes a big issue; the term is CP-violating, resulting in new contributions to the calculated *neutron electric dipole moment* (NEDM) [203]. Nevertheless, CP-symmetry holds, as has been measured consistently. More precisely, measured bounds in NEDM have placed the constraint of $\theta < 10^{-11}$ [204], which are very small relative to other SM couplings. The smallness of θ and the underlying reason is known as the strong CP problem.

The most well-known solution to this problem is known as *Peccei-Quinn* (PQ) theory [205]. The authors suggested introducing a new anomalous global $U(1)$ symmetry, now called $U(1)_{\text{PQ}}$, which exhibits SSB. After PQ symmetry breaking (PQSB) at some high PQ scale, the constant θ parameter gets exchanged for a dynamical field, $\bar{\theta}(x)$. If one minimises the vacuum energy, the field, $\bar{\theta}(x)$, naturally tends to zero, acting as a potential. This solution to the strong CP problem was later found to necessarily introduce an additional *pseudo-scalar* field known as the *axion* [206, 207]. The axion can be seen as a pseudo-Goldstone boson associated with the PQSB and the net effect in the Lagrangian is,

$$\mathcal{L}_{\text{axion}} = \frac{a(x)}{f_a} \frac{g_s^2}{16\pi^2} G^a_{\mu\nu} \tilde{G}^{a,\mu\nu}, \tag{2.107}$$

where $\bar{\theta}(x)$ is replaced by the dimensionless, $a(x)/f_a$, such that f_a is a PQSB order parameter and $a(x)$ is the axion field. The θ parameter in Eq. (2.106) has been effectively replaced with $\theta + a/f_a$ and it has a CP-preserving potential minimum at the point, $\theta + a/f_a = 0$. Then conveniently, the CP-violating angle is dynamically tuned to zero without further need for fine-tuning.

The PQ proposal solves the strong CP problem. It has the bonus of providing an excellent candidate for DM in the axion, which makes up $\sim 20\%$ of the energy density of the universe in

our cosmological era [165]. On the experimental side, axion direct detection in colliders is not feasible as the axion interaction is extremely weak. However, because the interaction is weak and much lower than typical star temperatures, axions must be emitted from stars [208]. Therefore the PQ order parameter, f_a, is bounded below stringently so as not to alter stellar evolution significantly. The most stringent such bound has been observed from supernova (SN)1987A and is given by $f_a > 4 \times 10^8$ GeV [209]. This bound is doubly important as it is axion model-independent, as long as the axion model solves the strong CP problem. Various experimental searches are being performed currently:

- Solar axions are emitted with energy $\sim$ keV from axion-photon conversion in the presence of the Sun's large magnetic field. The CAST collaboration has used *axion helioscopes* [210], to cover the parameter space for QCD axions with order parameter in the range, $f_a \sim 10^{7-8}$ GeV. IAXO is a collaboration for a future project which may push this range to 10^9 GeV [211, 212].

- DM axions in the galactic halos can be detected with *haloscopes* with a microwave cavity. Experiments detecting axion radio frequencies that correspond to the cold axion Compton wavelengths are being conducted. The ADMX collaboration has already excluded DM axions in a small mass range for $f_a \sim 10^{11}$ GeV [213]. Once these studies are completed, they are expected to map the largest parameter space yet, which are consistent with DM axions [214].

- Powerful lasers can be used to detect axions through the axion-photon-photon currents. These experiments let light through a wall under a magnetic field, some of which would pass through as axions. The ALPS collaboration has employed this method and already placed strict bounds, albeit much less strict than the CAST collaboration [215].

- As axions are incredibly light; their existence would mediate long-range macroscopic forces. As the axion is CP-odd, this results in a suppression of its interactions with macroscopic objects. Studies on monopole-dipole interactions have exploited this property and placed bounds on the axion-nucleon/electron couplings. Unfortunately, these current bounds are not near theoretical predictions [216].

In conclusion, the tightest bounds on the PQ order parameter and mass are attained from astrophysical arguments and observables. Future axion helioscope experiments could attain the requisite precision to detect QCD axions. Cavity experiments will also be able to detect DM axions for appropriate f_a values if they are the dominant components of DM. Moreover, there have been many experimental proposals to detect GUT-scale axions with $f_a > 10^{15}$ GeV [217].

Chapter 3

Effective Field Theories

An *effective field theory* (EFT) can be interpreted as a framework that one can employ to perform scale separation in a consistent way [218]. The need for such a framework arises in precision studies when attempting to identify deviations from the SM in observables. As a tool, EFTs are particularly useful as they cleanly glean unnecessary ambiguities and identify deviations in a global and model-independent fashion. The main requirement to define an EFT from a full theory is the existence of various widely separated scales. Moreover, EFTs are mathematically consistent by the *decoupling theorem* [219]. The theorem states that large degrees of freedom of a theory decouple at energies well below their mass, i.e. they are suppressed by inverse powers of their large mass scale.

From a more calculation-based perspective, an EFT is a tool that manifests scale separation explicitly. I.e. given some large energy scale, Λ, an EFT is defined by systematically expanding in powers of p/Λ at energies, $p \ll \Lambda$. The separation of scales is then further made explicit at the level of observables. Thus, given an EFT, calculations are simplified greatly, and contributions from different energetic regimes are kept track of systematically. The first step is defining an EFT; this can be done algorithmically,

1. Identify the low-energy scale of interest, p, and the degrees of freedom with masses or virtualities less than or near p^2.

2. Determine a complete set of Lagrangian operators, $\mathcal{O}_i$, consistent with the symmetries of the low-energy theory. The order in the (p/Λ)-expansion must be chosen as well, depending on uncertainty tolerance.

3. Matching is the final step to producing a well-defined EFT, given a general EFT Lagrangian, $\mathcal{L}_{\text{eff}} = \sum_i C_i \mathcal{O}_i$, the coefficients, C_i are known as *matching* (or *Wilson*) *coefficients* [61]. The determination of C_i is achieved by comparing Green's functions in the underlying theory to ones in the EFT, ensuring their equality in the (p/Λ)-expansion at each loop-order.

Once the EFT is defined, low-energy observables can be calculated with the EFT Lagrangian. Essentially, we may now reduce processes to ones with only the relevant degrees of freedom present. The effects of the remaining degrees of freedom are only present as factors in the matching coefficients. In EFT terminology, this is known as integrating out irrelevant degrees of freedom.

The EFT framework is helpful whether the underlying theory, known as the *full theory* in EFT terminology, is either known or yet to be determined. Thus, there are two EFT approaches to consider, the first being the top-down approach, in which the full (UV) theory is known, and we are solely interested in low-energy (IR) effects. Conversely, we have the bottom-up approach in which the full theory is unknown, or its low-energy description has not yet been formulated.

Top-Down Approach: In general, determining a low-energy EFT from a known UV theory is called a top-down EFT [61]. The advantage of using a top-down EFT to study low-energy observables is that the calculations become significantly simpler to perform. One of the main complicating factors in QFT calculations is when various scales are present in the model, any reduction in the number of which makes higher-order calculations simpler or even feasible in the first place [220]. In this approach, one can *integrate out* heavy fields of the full theory diagrammatically. Integrating out is achieved by first considering the amplitudes of a particular process in the full theory and perform an expansion in p/Λ. The same process is considered in the EFT, and the matching coefficient is defined by enforcing equality between the two amplitudes.

The procedure described can be further applied sequentially if there are various well separated scales in the full theory. Given a hierarchy of scales, $\Lambda_1 > \Lambda_2 > \ldots > \Lambda_N$, one can start at the largest scale, Λ_1, and evolve parameters to Λ_2 with RGE evolution. Upon integrating out the heavy field at Λ_1 via diagrammatic methods, one can further evolve the EFT with its RGE to the next threshold, Λ_3, and integrate out further heavy degrees of freedom above Λ_3. This procedure can be re-iterated down to the lowest scale, Λ_N of the underlying theory. The EFT at the smallest scale is *multiplicatively matched* to all the EFTs at higher scales.

As an elementary illustration of the top-down approach, we take the textbook example of a *multi-pole expansion* in classical electrodynamics. Consider the dynamics of a rigid body with charge distribution, $\rho(\boldsymbol{x})$, localised at small distance, $\boldsymbol{x} \sim 1/\Lambda$. If the EM field is slowly varying over large distances, $\boldsymbol{x} \sim 1/p$, we can describe the dynamics very accurately in terms of a small number of multi-pole moments. Higher-order terms in the multi-pole expansion are analogous to higher powers in p/Λ in the EFT formalism just described, and the moment factors are simply matching coefficients. In a more general sense, the quest of fundamental physics has revolved around transforming bottom-up EFTs to top-down EFTs as higher energy scales, and shorter distances are probed.

Bottom-Up Approach: A bottom-up EFT is one where the UV theory is unknown, or a low-energy description is not possible in the top-down approach. An example of the latter is QCD, in which low-energy interactions are non-perturbative. In this case, *chiral perturbation theory* is employed as an EFT for hadrons [220]. On the other hand, applying EFTs in cases where the UV theory is unknown is highly convenient as one is not tied to a specific model, and therefore assumptions are minimised. All that is assumed is what has been observed at the experimental scale of interest. In constructing a bottom-up EFT, it is instructive to glean insight from the previously defined top-down approach. We are then fully informed on what is needed to construct a bottom-up EFT: the symmetries and field content at the scale of interest and consistent *power counting* for our expansion in some large scale. In a bottom-up EFT, the high energy physics is encoded in a systematically expanded series of operators which solely contain

low-energy fields. We re-iterate that if the EFT is defined with these requirements alone, it is entirely model-independent up to the Wilson coefficients, which can be specified.

The field content of a bottom-up EFT is easily identified by the specific degrees of freedom propagating at the scale of interest. The second requirement of symmetry selection requires one of two assumptions: either the low energy symmetry continues to hold in the UV (usually the case for gauge symmetries), or a new physics sector is assumed to exist which breaks the symmetry. In the latter case, higher-order operators can violate low-energy symmetry at some scale, for instance, CP-symmetry violation as in the strong CP problem, discussed in Section 2.4. Power counting selection automatically indicates the expected size of the Wilson coefficient of a particular operator in the bottom-up EFT. There are two types of power countings one can specify, which depend on whether the EFTs are decoupling or non-decoupling.

In a *decoupling* EFT, the leading EFT Lagrangian is completely renormalisable, and thus, UV physics is suppressed by $1/\Lambda$. We usually take Λ as some large energy scale identified with the lowest-lying scale of new physics. Higher-order operators have larger mass dimension and are therefore suppressed further by higher powers of $1/\Lambda$; as in four dimensions, the product of the EFT operator and its coefficient must consistently have mass dimension four. On the other hand, in *non-decoupling* EFTs, the leading EFT Lagrangian contains mass dimension operators greater than four and is thus non-renormalisable already at LO. Thus, an expansion in mass dimension can not be achieved consistently. Instead, one must rely on the renormalisation procedure to instruct the expansion; counterterms not part of the LO Lagrangian will be included at NLO. Thus, the Lagrangian becomes renormalisable at each order in the loop expansion. In non-decoupling EFTs, the large cut-off scale, Λ, must be identified with a low-energy scale, $4\pi v$. This expansion places one-loop contributions of the LO Lagrangian at NLO tree-level terms, as $v^2/\Lambda^2 = 1/(16\pi^2)$. Thus, one can define consistent power counting in both decoupling and non-decoupling EFTs.

3.1 Standard Model Effective Field Theory

We will begin by briefly reviewing one example of a bottom-up EFT, for completeness, known as the *Standard Model effective field theory* (SMEFT) [63]. The idea behind SMEFT is to build a model-independent EFT based on the SM and current experimental observables. With such an EFT, one can search for anomalies that point to extensions of the SM without testing every proposed UV theory individually. Employing an EFT specifically for these studies is further justified by the lack of direct detection of new particles from experimental collaborations such as the LHC [167,168,221]. This lack of detection implies a large *mass gap* to the UV theory, which is ideal for employing an EFT approach as it is an essential ingredient of any EFT. Therefore, one can use the SM Lagrangian with parameters from current experimental observables as the leading-order Lagrangian of SMEFT. Our only assumption in constructing SMEFT is that the new physics is decoupling, as defined in the previous section.

Given the assumption of new physics decoupling and power counting given by mass dimensions of a higher-order operator, we can write the SMEFT Lagrangian as,

$$\mathcal{L}_{\text{SMEFT}} = \mathcal{L}_{\text{SM}}^{d=4} + \sum_{d=5}^{\infty} \sum_{i} (\frac{1}{\Lambda})^{d-4} C_i^{(d)} \mathcal{O}_i^{(d)}. \tag{3.1}$$

The sum over the index i is based on all possible Lorentz and gauge-invariant operators at each order in $1/\Lambda$. Note that any *approximate symmetries* (AS) respected by the SM can be violated by the higher-order operators. AS-violating operators can then be further suppressed by their coefficients depending on the assumptions enforced. Initially, the set of conceivable operators of a given mass dimension may be huge, which is the case beyond dimension five [222]. However, *Fierz transformations*, *integration-by-parts* (IBP) identities, and EOMs can all reduce this set to a minimal set of manageable size [223], known as an *operator basis*. The choice of basis is not unique, and some are more convenient for specific applications than others. For instance, a basis can be chosen, which reduces the number of operators with derivatives, as such operators complicate calculations [224]. Going to arbitrarily high dimensional order is complex as the number of operators per order increases dramatically; luckily, they are generally heavily suppressed by higher powers in $1/\Lambda$.

For example, consider dimension five operators, the next dimension above the SM in SMEFT. It turns out that at dimension five, as first noted by Weinberg [225], only a single operator structure is permitted [226, 227]. This operator is known as the *Weinberg operator* and is given by,

$$\mathcal{O}_{\nu\nu} = (\tilde{\varphi}^\dagger l_r)^T C(\tilde{\varphi}^\dagger l_s) + \text{h.c}, \tag{3.2}$$

and in the SMEFT Lagrangian, the matching coefficient of this operator, $\tilde{c}^{rs}_{\nu\nu}$ is a 3×3 matrix with twelve elements that parametrise the three lepton generations [228]. Interestingly, after SSB, $\mathcal{O}_{\nu\nu}$ generates masses for the left-handed neutrinos, $m^{rs}_\nu = \tilde{c}^{rs}_{\nu\nu} v^2/(2\Lambda)$, providing a reason for the lightness of neutrinos relative to other SM particles. A UV theory that produces this operator is given if one extends the SM by including heavy *right-handed neutrinos*. In this case, a Yukawa interaction is permitted as well as a *Majorana mass* term. If the Majorana term is large, right-handed neutrinos can then be integrated out in the low energy top-down EFT, which at first order contains the operator $\mathcal{O}_{\nu\nu}$ of SMEFT [229]. This mechanism is known in the literature as the see-saw mechanism and provides an elegant solution to the neutrino problem, and the heavy neutrino is a DM candidate [230].

Dimension six operators are suppressed by two powers of $1/\Lambda$ for large UV physics scale Λ and thus, one would expect heavy suppression. Curiously, however, they are expected to be less suppressed than the dimension five operators as there are operators at dimension six which do not violate approximate symmetries. Moreover, many BSM models, after being passed through the top-down EFT algorithm, contain dimension six operators [231]. The difficulty lies in the number of possible operators at higher dimensions [228]. For instance, in the *Warsaw basis* of dimension six [227], for three fermion generations that conserve baryon and lepton number, there exist 2499 independent parameters. Nonetheless, dimension six operators have been a crucial tool for LHC searches for BSM physics, and the LHC-HCC working group has performed a large amount of EFT analysis with dimension six operators [232].

3.2 Heavy Quark Effective Theory

The first example of a top-down EFT employed in this thesis is heavy quark effective theory (HQET) [64, 68, 71, 72, 156, 233]. HQET was originally conceived as a tool to separate the short- and long-distance physics related to heavy quark mass and QCD dynamics, respectively. As an EFT, HQET is a decoupling theory and its Lagrangian is given by the heavy mass, m_Q, limit of

a quark of interest. Corrections to this limit are suppressed by powers of $1/m_Q$ and the theory is renormalisable at each order in $1/m_Q$. The EFT Lagrangian can be written,

$$\mathcal{L}_{\text{eff}} = \mathcal{L}_{\text{heavy}} + \mathcal{L}_{\text{light}}, \tag{3.3}$$

where $\mathcal{L}_{\text{light}}$ is the standard QCD Lagrangian for gluons and n_f light quarks,

$$\mathcal{L}_{\text{light}} = \sum_i \bar{q}_i (i\not{D} - m_i) q_i - \frac{1}{4} G^a_{\mu\nu} G^{a,\mu\nu}, \tag{3.4}$$

and $\mathcal{L}_{\text{heavy}}$ corresponds to the EFT Lagrangian for the heavy quark of interest. There are two overarching frameworks which define $\mathcal{L}_{\text{heavy}}$, these are HQET, which we discuss in this section and NRQCD which is considered in Section 3.3.

HQET was originally devised as a framework to systematically perform calculations in the heavy quark limit, simplifying both the perturbative and power corrections [68, 156]. To construct HQET, one begins by splitting the heavy quark momentum into a sum of two parts: a large part which scales like the heavy quark mass, m_Q, and a small part, k, generally referred to as the residual momentum,

$$p_Q^\mu = m_Q v^\mu + k^\mu, \quad |k| \sim \Lambda_{\text{QCD}}. \tag{3.5}$$

In the splitting, we introduce a four-velocity v^μ of the heavy quark and mass scale, m_Q. The mass scale, m_Q, is not limited and to be interpreted as being of the same order as the meson mass subtracted by a term of $\mathcal{O}(\Lambda_{\text{QCD}})$. In general, one takes m_Q to be the heavy quark pole mass, but other choices are more well-behaved in the large mass limit [234], as previously discussed in Section 2.3.

By inspection of Eq. (3.5), in the limit, $m_Q \to \infty$, light degrees of freedom interactions only affect the residual k^μ and not v^μ, which is therefore conserved. As is the case with conserved quantities QFTs, one can naturally use them to label states. Thus, in the literature, heavy quark states are labelled by their four-velocity [64]. The HQET Lagrangian is now attainable after momentum and state substitution and applying EOMs in the limit $m_Q \to \infty$,

$$\mathcal{L}_{\text{heavy}} = \sum_{n=0}^{\infty} \mathcal{L}_n, \tag{3.6}$$

where $\mathcal{L}_n$ is of expansion order $1/m_Q^n$, and the zeroth order term is given by the often quoted

$$\mathcal{L}_0 = \bar{h}_v iD \cdot v h_v. \tag{3.7}$$

Here h_v is a heavy quark field labelled by its four-velocity, v, and a frame is generally chosen such that $v^2 = 1$. One can see that Eq. (3.7) is independent of mass scale and exhibits spin-flavour independence as well. Hence, at leading order in the EFT, the interactions of a heavy quark with light degrees of freedom is *spin-flavour symmetric*. These two symmetries provide elegant simplifications for calculations in HQET, for instance, in the study of decay and spectroscopy processes involving heavy fields [68, 71, 156].

Of course, one must go beyond leading EFT order for precision calculations, for instance the next-to-leading term is given by,

$$\mathcal{L}_1 = \frac{c_2(\mu)}{2m_Q} \bar{h}_v (iD)^2 h_v + \frac{c_{\text{F}}(\mu)}{4m_Q} \bar{h}_v \sigma^{\mu\nu} G_{\mu\nu} h_v, \tag{3.8}$$

with anti-commutators, $\sigma^{\mu\nu} = -\frac{i}{4}[\gamma^\mu, \gamma^\nu]$ and $G^{\mu\nu} = \frac{1}{ig_s}[D^\mu, D^\nu]$. The matching coefficients are given by, $c_2(\mu) = 1$, to all loop orders and $c_{\rm F}(\mu)$ has been determined to two-loop orders in QCD [235]. The HQET Lagrangian is currently studied to $1/m_Q^4$ [218, 236, 237], and the associated matching coefficients are being determined to N^{3}LO in QCD [238, 239]. In Chapter 6 we present the HQET Lagrangian to $1/m_Q^3$ order and determine the leading radiative EW corrections to the matching coefficients.

We end by noting that this framework is not limited to heavy spin-1/2 fermions; one can define such an EFT for heavy fermionic and bosonic fields of arbitrary spin [240–243]. This has been particularly useful in constructing top-down EFTs from BSM physics [241, 243], and bottom-up EFTs for black hole physics [242, 244]. For a review of the history, development and applications of HQET, we recommend Ref. [218].

3.3 Non-relativistic QCD

Let us now consider what may be interpreted as a re-formulation of the HQET framework in non-relativistic QCD (NRQCD) [73,74]. NRQCD was first conceived to deal with bound states of heavy *quarkonia*, or quark-antiquark systems in the NR limit. As both HQET and NRQCD are based on the expansion, $m_Q \to \infty$, the operators appearing in the two EFTs are identical [218]. The physics, however, of an NR bound state differs significantly from the physics of a lone heavy quark and its interactions with light degrees of freedom. From an EFT perspective, this difference lies in the power counting, i.e. the power counting of operators in NRQCD is what differentiates it from HQET.

In HQET, assuming light degrees of freedom are massless, there exist two scales of interest: the confinement scale, $\Lambda_{\rm QCD}$, and the heavy quark mass, m_Q. Whence, all HQET operators are distinguished by their order in a $\Lambda_{\rm QCD}/m_Q$ expansion. On the other hand, power counting in NRQCD is more complex as two more scales need to be taken into account: the heavy quark momentum and kinetic energy, $p_Q = m_Q v$ and $E_Q = \frac{1}{2} m_Q v^2$, respectively. Moreover, the four-velocity, v, in NRQCD has a different meaning; it is no longer the heavy quark velocity but the relative velocity of the two heavy quarks. Thus, with these other scales, one can no longer expand consistently in $1/m_Q$. This issue can be seen if one considers, for instance, E_Q/m_Q, which is the same order as p_Q^2/m_Q^2. The appropriate expansion parameter is instead the heavy quark velocity, v, and the appropriate scaling rules have been determined in Ref. [245].

The inspiration for a formulation of NRQCD came from the analogous EM version in NRQED, first proposed in Ref. [73]. With NRQED as a template, the first form of the heavy portion of the NRQCD Lagrangian was produced [74],

$$\mathcal{L}_{\rm heavy} = \sum_{n=0}^{\infty} \mathcal{L}_n, \tag{3.9}$$

such that the leading Lagrangian by NRQCD power counting is given by,

$$\mathcal{L}_0 = \phi^\dagger (iD_t + \frac{\boldsymbol{D}^2}{2m_Q})\phi. \tag{3.10}$$

Here the field, $\psi(x)$ is a two-component *Pauli spinor* and there exists an analogous term $\chi(x)$, not explicitly written for the anti-quark field. We see further, by comparison of Eqs. (3.7)

and (3.10), that the kinetic next-to-leading term of the HQET Lagrangian has shifted to being leading in NRQCD. The next-to-leading EFT Lagrangian are those terms suppressed by $\mathcal{O}(v^2)$ and are represented by terms of the form,

$$\mathcal{L}_1 = \frac{c_1}{8m_Q^3}\psi^\dagger(\boldsymbol{D}^2)^2\psi + g_s\frac{c_2}{8m_Q^2}\psi^\dagger(\boldsymbol{D}\cdot\boldsymbol{E} - \boldsymbol{E}\cdot\boldsymbol{D})\psi + g_s\frac{c_3}{2m_Q}\psi^\dagger(\boldsymbol{\sigma}\cdot\boldsymbol{B})\psi + \ldots, \tag{3.11}$$

with $\boldsymbol{E} = -\frac{i}{g_s}[D_t, \boldsymbol{D}]$, $\boldsymbol{\sigma}$ is a vector of Pauli spinors and $\boldsymbol{B}^i = \frac{i}{2g_s}\epsilon^{ijk}[\boldsymbol{D}_j, \boldsymbol{D}_k]$. As we will be re-introducing this Lagrangian in Chapter 6 and considering it in detail we refrain from expressing it fully in this section.

We conclude by re-expressing the importance of the kinetic term being a leading contribution to the NRQCD Lagrangian. This correct treatment of the kinetic terms has resulted in important findings for describing NR Coulomb exchange. When considering bound states near threshold, the power counting, $v \sim \alpha_s$, is appropriate; correspondingly, Coulomb exchange terms $\propto (\alpha_s/v)^m$ require all-order summation. Therefore, NRQCD is a helpful tool for studying NR dynamics and calculating relativistic corrections as it incorporates these in its higher order EFT operators. Moreover, there are various valid formulations of NRQCD that are useful for different purposes, for instance ones where the scales m, mv and mv^2 are explicitly separated [141, 246–251].

3.4 Soft-Collinear Effective Theory

The last EFT which is employed in this thesis is the soft-collinear EFT (SCET) [252]. The framework of SCET arose from a willingness to describe low invariant mass *jet* interactions in which the jets are highly boosted with respect to one another. This high energy, conventionally parametrised by Q, which boosts the particles, defines the SCET expansion. At leading order in the EFT expansion, a field redefinition is employed to decouple the *soft* and *collinear* degrees of freedom in the operator expansion. Soft and collinear fields can still interact with one another, and these are represented in the EFT currents by light-like *Wilson lines* [253]. The benefit of studying factorisation theorems within the SCET framework is precisely the manifest decoupling of soft and collinear pieces at the Lagrangian level [254–256]. Working with the full theory instead complicates the process immensely, and with SCET, power corrections in inverse boost energy can be studied systematically.

As in NRQCD there are a few formulations of SCET, we will employ the more modern so-called label SCET formulation in this thesis [257]. As with all top-down EFTs their construction is dependent on the underlying theory. To illustrate the EFT we will consider SCET for highly energetic quarks with energy, Q, interacting with collinear and soft gluons [255, 256, 258–263]. The reference frame to work from is that of the heavy fields, as in HQET, in which light degrees of freedom move along the *light-cone* (LC) direction n^μ. Hence, the dynamics of the light field can be decribed by LC coordinates $p = (p^+, p^-, p_\perp)$, such that $p^+ = n\cdot p$ and $p^- = \bar{n}\cdot p$. For convenience, one takes the direction of motion to be along the z-direction, in this case, $n^\mu = (1, 0, 0, -1)$ and $\bar{n}^\mu = (1, 0, 0, 1)$. For large energy, $p^- \sim Q$, and the remaining components are small. Defining a small parameter, $\lambda \sim p_\perp/p^-$, the momentum can be separated into,

$$p^\mu = \bar{n}\cdot p\frac{n^\mu}{2} + n\cdot p\frac{\bar{n}^\mu}{2} + p_\perp^\mu = \mathcal{O}(\lambda^0) + \mathcal{O}(\lambda^2) + \mathcal{O}(\lambda^1). \tag{3.12}$$

Collinear and soft gluons have LC-momenta that scale as $k_c \sim Q(\lambda^2, 1, \lambda)$ and $k_s \sim Q\lambda^2(1,1,1)$, respectively [256, 262].

As shown in Ref. [257], at a scale, $\mu \sim Q$, one can match QCD onto an EFT with collinear heavy and light quarks as well as collinear and soft gluons. Collinear quarks and their interactions with collinear and soft gluons are defined by the QCD Lagrangian expanded in small parameter, λ. To illustrate the expansion, consider the massless QCD Lagrangian,

$$\mathcal{L}_{\rm QCD}^{m_Q=0} = \bar{\psi} i \not{D} \psi - \frac{1}{4} G^a_{\mu\nu} G^{a,\mu\nu}, \tag{3.13}$$

we may proceed by eliminating large momenta from the EFT fields. This process is reminiscent of HQET as introduced in Section 3.2, however in this case it is more complex as there are three scales to take into account. Splitting the momenta into large and small parts,

$$p = \tilde{p} + k, \quad \tilde{p} \equiv \frac{1}{2}(\bar{n} \cdot p) n + p_\perp, \tag{3.14}$$

we see the large part, $\tilde{p}$, becomes the EFT label as in HQET while the residual part, k^μ, is dynamical. The large momenta, $\tilde{p}$, are eliminated by defining a new field, $\phi_{n,p}$, labelled by p, through,

$$\psi(x) = \sum_{\tilde{p}} e^{-i\tilde{p}\cdot x} \psi_{n,p}, \tag{3.15}$$

with implicit recognition that only $\bar{n} \cdot p$ and $p_\perp$ are true labels. For a particle moving along n-direction $\psi_{n,p}$ has two large and two small components, $\xi_{n,p}$ and $\xi_{\bar{n},p}$, respectively. The components are attainable with *projectors*,

$$\xi_{n,p} = \frac{\not{n}\bar{\not{n}}}{4} \psi_{n,p}, \quad \xi_{\bar{n},p} = \frac{\bar{\not{n}}\not{n}}{4} \psi_{n,p} \tag{3.16}$$

which satisfy identities,

$$\frac{\not{n}\bar{\not{n}}}{4} \xi_{n,p} = \xi_{n,p}, \quad \frac{\bar{\not{n}}\not{n}}{4} \xi_{\bar{n},p} = \xi_{\bar{n},p}, \quad \not{n} \xi_{n,p} = 0, \quad \bar{\not{n}} \xi_{\bar{n},p} = 0. \tag{3.17}$$

Upon this field replacement, the quark portion of Eq. (3.13) becomes,

$$\begin{aligned} \mathcal{L} = \sum_{\tilde{p},\tilde{p}'} \Bigg[& \bar{\xi}_{n,p'} \frac{\bar{\not{n}}}{2} (in \cdot D)\, \xi_{n,p} + \bar{\xi}_{\bar{n},p'} \frac{\not{n}}{2} (i\bar{n} \cdot D + \bar{n} \cdot p)\, \xi_{\bar{n},p} \\ & + \bar{\xi}_{n,p'} \left(\not{p}_\perp + i \not{D}_\perp \right) \xi_{\bar{n},p} + \bar{\xi}_{\bar{n},p'} \left(\not{p}_\perp + i \not{D}_\perp \right) \xi_{n,p} \Bigg]. \end{aligned} \tag{3.18}$$

As derivatives on fermionic fields lead to suppression of order λ^2, we may eliminate $\xi_{\bar{n},p}$ with its EOM,

$$(\bar{n} \cdot p + \bar{n} \cdot iD) \xi_{\bar{n},p} = (\not{p}_\perp + i \not{D}_\perp) \frac{\not{n}}{2} \xi_{n,p}. \tag{3.19}$$

Combining Eqs. (3.18) and (3.19) gives a Lagrangian of only $\xi_{n,p}$,

$$\mathcal{L} = \sum_{\tilde{p},\tilde{p}'} e^{-i(\tilde{p}-\tilde{p}')\cdot x} \bar{\xi}_{n,p'} \left[in \cdot D + (\not{p}_\perp + i \not{D}_\perp) \frac{1}{\bar{n} \cdot p + i\bar{n} \cdot D} (\not{p}_\perp + i \not{D}_\perp) \right] \frac{\bar{\not{n}}}{2} \xi_{n,p}, \tag{3.20}$$

in which the summation includes all copies of $\tilde{p}$ and $\tilde{p}'$ labelled fields.

What remains to be expanded are the gluons inside the covariant derivatives, D^μ, i.e. we need to split $A^\mu \to A_c^\mu + A_s^\mu$ into soft and collinear parts. A_c^μ and A_s^μ fluctuations scale as λ^2 and λ^4, respectively and when collinear gluons are acted on by derivatives, this results in $\lambda^0, 1$ contributions. One can make the power counting explicit through collinear gluons fields being labelled by large momentum components, $\tilde{q}$. This is done the same way as with fermionic fields, by extracting a *phase factor* containing large $\tilde{q}$ through field redefinition, $A_c(x) \to e^{-i\tilde{q}\cdot x} A_{n,q}(x)$. Inserting this into Eq. (3.20) and expanding in power of small scale λ, gives the $\mathcal{O}(\lambda^0)$ Lagrangian [259],

$$\begin{aligned}\mathcal{L} = \bar{\xi}_{n,p} \left[in\cdot D + \frac{p_\perp^2}{\bar{n}\cdot p} \right] \frac{\bar{\not{n}}}{2} \xi_{n,p} \\ + \bar{\xi}_{n,p+q} \left[gn\cdot A_{n,q} + g\not{A}_{n,q}^\perp \frac{\not{p}_\perp}{\bar{n}\cdot p} + \frac{\not{p}_\perp + g\not{q}_\perp}{\bar{n}\cdot(p+q)} \not{A}_{n,q}^\perp - \frac{\not{p}_\perp + g\not{q}_\perp}{\bar{n}\cdot(p+q)} \bar{n}\cdot A_{n,q} \frac{\not{p}_\perp}{\bar{n}\cdot p} \right] \frac{\bar{\not{n}}}{2} \xi_{n,p} \\ + \ldots + \mathcal{O}(\lambda). \end{aligned} \tag{3.21}$$

Here the label summation over $\tilde{p}, \tilde{q}$ is implicit, and the ellipsis corresponds to terms containing two or more collinear gluon fields. By inspection, the first term in Eq. (3.21) gives the collinear quark propagator. The soft gluon interaction arises from the covariant term, and collinear gluon interactions are label-changing, unlike soft gluons. Thus, we now have a leading SCET Lagrangian of the general type, which can be applied to particular processes of interest. We end this section by noting that as this is an extensive subject, the brief motivation we provide here is far from sufficient; instead, we point to Refs. [252] for a complete overview of the subject. Moreover, in Chapter 7 we re-introduce SCET and its necessary parts for our specific calculation.

Chapter 4

Heavy Quark Potential

In this Chapter we consider the static potential in theories exhibiting spontaneous symmetry breaking. We do so in both the *Wilson loop* and *scattering amplitude* approaches and discuss the limitations of the Wilson loop approach. We use our findings to calculate the static potential of the SM at electroweak one-loop order. As the field content of the SM is extensive, analogous results to ours in a large set of models are now achievable by varying the appropriate couplings and group theory factors. This Chapter is based on Ref. [264], reflecting the author's contribution.

4.1 Motivation

The *static potential* is a crucial quantity for QFTs, as it represents the interaction energy of a pair of heavy particles. The potential allows one to study the fundamental properties of a given theory in the NR limit. The most well-known static potentials are the *Coulomb potential* in QED and its non-Abelian analogue of QCD. The QCD static potential for a pair of heavy quarks is known to $\mathrm{N^3LO}$ order [41, 265] and valuable in the study of NR bound states, such as heavy quarkonia. It is of importance in many areas, such as quark mass definitions [57–60, 135] and quark pair production at *threshold* [235, 266]. The static potential has also been studied for heavy particles predicted in the context of BSM theories, such as the MSSM and $\mathcal{N} = 4$ *super Yang–Mills* (SYM) theory [267–269].

We begin by focusing on the QCD static potential, which is of leading importance to heavy-quark theory due to the dominance of the strong coupling in the SM. The original idea of describing a bound state of heavy coloured objects, in analogy to the hugely successful Hydrogen atom, was proposed by Susskind in his 1970 Les Houches lecture [270]. In order to demonstrate asymptotic freedom in *Yang–Mills* (YM) theory, he computed the one-loop pole terms using a Wilson loop formula for the potential and, in the process, re-derived the first coefficient of the renormalization group beta function. More recently, the two- and three-loop corrections were found and turned out to be numerically significant triggering several investigations in further contexts [40, 41, 265, 271, 272].

It is expected that the potential consists of two terms: a Coulomb-like short-distance term, which is perturbatively calculable; and a long-distance term responsible for the phenomenon of quark confinement [273]. Thus, a perturbative analysis will not provide the full potential and

may not hold the key to gaining a deeper understanding of confinement. However, the short-distance part may still be employed as a starting point for constructing potential models, which have been vastly successful in the description of heavy quarkonia [159]. Moreover, it provides an excellent description for very heavy systems, such as the $t\bar{t}$ system, to high accuracy. The potential in perturbative calculations is comparable with results from numerical calculations in lattice gauge theory.

The *Wilson loop approach*, first employed by Susskind, continues to be used to this day due to its computational simplicity. In this approach, the static potential in coordinate space, $V(\boldsymbol{r})$, is defined in terms of a Wilson loop, $W(\boldsymbol{r}, T)$, with small but finite spatial extension, $\boldsymbol{r}$, and infinite temporal extension, $T \to \infty$ [271]. In this limit, $W(\boldsymbol{r}, T) \sim \exp[-iTV(\boldsymbol{r})]$, and the potential in momentum space, $V(\boldsymbol{q})$, is simply its Fourier transform. However, there has always been discussion about whether the Wilson loop formula is well defined due to possible IR divergences at higher orders [274]. On the other hand, the scattering amplitude approach yields identical results, involves a computation of the on-shell quark-antiquark scattering amplitude, and directly yields the momentum space static potential in the NR, $\boldsymbol{q} \to \boldsymbol{0}$, limit.

In this paper, we consider extending the static potential to theories that exhibit SSB; in particular, we take on the case of the SM. The only case of a static potential in the context of a theory with SSB was in the seminal result by Maldacena for heavy W bosons in $\mathcal{N} = 4$ SYM [267]. Working off of his result, we attempted an analogous procedure to obtain a SM potential; however, limitations became apparent, which we discuss in detail. Whence, instead, we employed the scattering amplitude approach, which provided us with the full SM static potential to one-loop order. Furthermore, due to the richness of the SM field content, it becomes simple to compute static potentials in other theories by a replacement of the appropriate couplings and group theory factors.

We then demonstrate applications of our result to beyond-QCD corrections in heavy-quark EFTs and threshold mass schemes [57, 59, 60], in particular, the popular PS [57] and 1S [59] mass definitions. We found that, as is to be expected from previous results on EW corrections to short-distance heavy-quark mass definitions [51,145,148,149,151], the EW regime contributes to the static potential at the same order as NNLO pure QCD contributions. Therefore, it stands to reason that they must be incorporated into high-precision heavy-quark-antiquark threshold calculations [235, 266].

4.2 Wilson Loop Approach

Let us consider a system with an arbitrary field, $\psi(x)$, defined by an action, $S_0[\psi] = \int d^d x \mathcal{L}(\psi)$, in the presence of external sources, $J(x)$. One can express the ground state energy of this system in quantum field theory as [159]

$$-\lim_{T\to\infty} \frac{1}{T} \ln \frac{\int \mathcal{D}\{\psi\} \exp\left\{-\int d^d x \left[\mathcal{L}(\psi) + J(x)\psi(x)\right]\right\}}{\int \mathcal{D}\{\psi\} \exp\left[-\int d^d x \mathcal{L}(\psi)\right]}, \tag{4.1}$$

where the sources are switched off outside the time interval $[-T/2, T/2]$. This formula in perturbation theory has been proven exactly for the case of a linear local coupling between the field

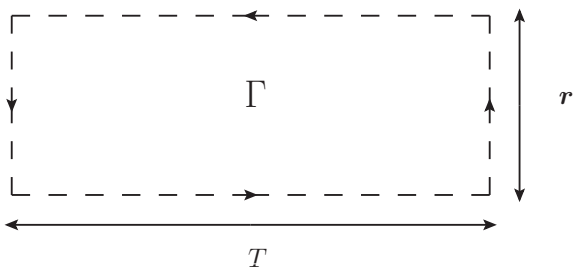

Figure 4.1: Rectangular Wilson loop to be integrated over.

and the external source [275]. We generalise this by assuming that, in all cases, the vacuum-to-vacuum transition amplitude is given by

$$\langle 0^+|0^-\rangle_J = \frac{\int \mathcal{D}\{\psi\} \exp\{-S_0[\psi] + S_{\rm int}[\psi, J]\}}{\int \mathcal{D}\{\psi\} \exp\{-S_0[\psi]\}}, \tag{4.2}$$

where $S_{\rm int}[\psi, J]$ is the source-dependent part of the action. Then, inserting a complete set of energy eigenstates, we may write

$$\langle 0^+|0^-\rangle_J = \langle 0|\, e^{-HT}\, |0\rangle = \sum_n \langle 0|\, e^{-HT}\, |n\rangle \langle n|0\rangle = \sum_n |\langle 0|n\rangle|^2\, e^{-E_n T}, \tag{4.3}$$

where the smallest-energy eigenvalue, E_0, corresponds to the ground state, which dominates the sum in the limit $T \to \infty$. Whence taking the logarithm and dividing by $(-T)$ provides one with the ground state energy, in Eq. (4.1), as is well known [273].

We may now be more specific in our discussion and take a gauge field theory, QED for instance, where the energy we calculate corresponds to a system of photons interacting with two pointlike static electric charges (with identical magnitudes, but opposite signs),

$$-\lim_{T\to\infty} \frac{1}{T} \ln \frac{\int \mathcal{D}\{\psi\} \exp\left\{-\int d^d x \left[-\frac{1}{4}F_{\mu\nu}^2 + \frac{1}{2\eta}(\partial_\mu A_\mu)^2 + J_\mu(x) A^\mu(x)\right]\right\}}{\int \mathcal{D}\{\psi\} \exp\left\{-\int d^d x \left[-\frac{1}{4}F_{\mu\nu}^2 + \frac{1}{2\eta}(\partial_\mu A_\mu)^2\right]\right\}}, \tag{4.4}$$

where

$$J_\mu(x) = g\delta_{\mu 0}[\delta(\boldsymbol{x}) - \delta(\boldsymbol{x} - \boldsymbol{r})]\theta\left(\frac{T^2}{4} - x_0^2\right). \tag{4.5}$$

We may then rewrite the numerator of Eq. (4.4) as the expectation value

$$\left\langle \mathcal{T} \exp\left\{ g \int dt [A_0(t, \boldsymbol{r}) - A_0(t, \boldsymbol{0})] \right\} \right\rangle, \tag{4.6}$$

where $\mathcal{T}$ stands for time ordering. This Green's function is manifestly gauge invariant, which one can see by considering the gauge invariant operator $\mathcal{P} \exp\left(g \oint_\Gamma dx^\mu A_\mu\right)$, where $\mathcal{P}$ denotes path ordering and Γ is the rectangular loop of spatial and time extent, $\boldsymbol{r}$ and T, respectively, as illustrated in Fig. 4.1. In the limit $T \to \infty$, the spatial components, $\boldsymbol{A}(T/2, \xi)$ and $\boldsymbol{A}(-T/2, \xi)$, reduce to pure gauge terms, as the field strength tensor $F_{\mu\nu} = 0$ at infinity and thus is gauge equivalent to $\boldsymbol{A} = \boldsymbol{0}$. Therefore, the operator $\mathcal{T} \exp\left\{g \int dt [A_0(t, \boldsymbol{r}) - A_0(t, \boldsymbol{0})]\right\}$ is gauge invariant and so is the ground state energy (or static potential), which is equal to

$$V(\boldsymbol{r}) = -\lim_{T\to\infty} \frac{1}{T} \ln \frac{\left\langle \mathcal{T} \exp\left\{g \int dt [A_0(t, \boldsymbol{r}) - A_0(t, \boldsymbol{0})]\right\}\right\rangle}{\langle \boldsymbol{1} \rangle}. \tag{4.7}$$

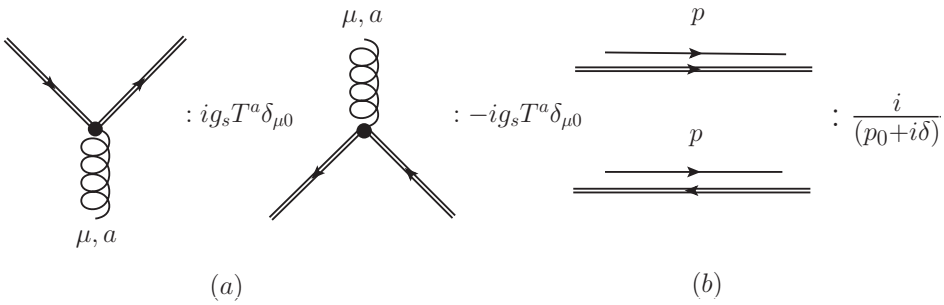

Figure 4.2: Feynman rules for (anti-)source propagator and (anti-)source-gluon vertices.

This approach has been employed in QED, where only the LO term contributes to all orders [39], and the non-Abelian case of QCD has been studied through the three-loop order [41, 265]. We begin by re-evaluating the QCD case and then extend this approach to theories with SSB, as in the case of the SM and beyond.

4.2.1 QED and QCD

Let us begin by considering the static potential in QCD [271], which corresponds to the interaction energy of an infinitely massive $Q\overline{Q}$ pair separated by a fixed distance, $\boldsymbol{r}$, interacting by exchanging virtual gluons. Using the definition

$$V(\boldsymbol{r}) = -\lim_{T\to\infty} \frac{1}{T} \ln \langle \mathcal{W}[\Gamma] \rangle \tag{4.8a}$$

$$= -\lim_{T\to\infty} \frac{1}{T} \ln \left\langle \overline{\mathrm{tr}} \mathcal{P} \exp\left(ig \oint_\Gamma d^4x J^\mu A_\mu \right) \right\rangle, \tag{4.8b}$$

where $\mathcal{W}[\Gamma]$ denotes the Wilson loop, $\mathcal{P}$ path ordering, $\overline{\mathrm{tr}}$ the normalised color trace, $\overline{\mathrm{tr}}(...) \equiv \mathrm{tr}(...)/\mathrm{tr}(\mathbf{1})$, and $A_\mu(x) = T^a_{ij} A^a_\mu(x)$ the gauge potential. Γ is the rectangular Wilson loop as shown in Fig. 4.1, and

$$\langle \mathcal{O}(A) \rangle \equiv \frac{\int \mathcal{D}A \exp(-S) \mathcal{O}(A)}{\int \mathcal{D}A \exp(-S)}. \tag{4.9}$$

The desired properties of the static color charge are dictated by

$$J^\mu(x) = v^\mu [\delta(\boldsymbol{x}) - \delta(\boldsymbol{x} - \boldsymbol{r})] \theta\left(\frac{T^2}{4} - x_0^2 \right), \tag{4.10}$$

where $v^\mu \equiv \delta^{\mu 0}$. After Fourier transforming to momentum space, we get the Feynman rules for our static potential [271]. The QCD Feynman rules remain unaltered besides those illustrated in Fig. 4.2.

To illustrate the computation of the Wilson loop, we consider the tree amplitude illustrated in Fig. 4.3, where $|\boldsymbol{p}| = |\boldsymbol{p'}|$ and $E = \sqrt{m^2 + \boldsymbol{p}^2}$. From this tree diagram, one obtains the following amplitude

$$i\mathcal{M} = i \frac{4\pi\alpha_s}{|\boldsymbol{k} - \boldsymbol{k'}|^2} T^a_{c'_1 c_1} T^a_{c'_2 c_2} \equiv i \frac{4\pi\alpha_s}{\boldsymbol{q}^2} \left(\delta_{c_1 c_2} \delta_{c'_1 c'_2} - \frac{1}{N_c} \delta_{c_1 c'_1} \delta_{c_2 c'_2} \right), \tag{4.11}$$

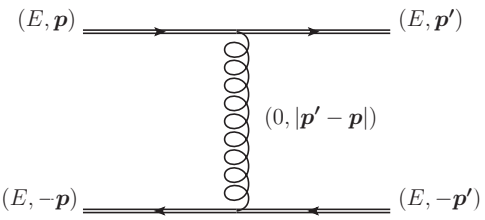

Figure 4.3: Tree-level diagram for the QCD static potential.

where $\boldsymbol{q}=\boldsymbol{k}-\boldsymbol{k}'$, and $c_{1(2)}$ and $c'_{1(2)}$ denote colors of initial and final states, respectively. The color singlet case, with $c_1=c_2$ and $c'_{1(2)}$ summed over, gives $V_s(\boldsymbol{q})=-C_F\alpha_s/\boldsymbol{q}^2$, while the *color octet* case, with $c_1=c'_1, c_2=c'_2$ and no summation, gives $V_o(\boldsymbol{q})=\alpha_s/(2C_A\boldsymbol{q}^2)$, where $C_A=N_c$ and $C_F=(N_c^2-1)/(2N_c)$ are color factors.

At one-loop in QCD, we have the amplitudes illustrated in Fig. 4.4. Upon reduction, in Feynman gauge, only amplitudes (a)–(d) are non-zero, since the remaining ones are scaleless. We recalculate the one-loop result in the $\overline{\text{MS}}$ scheme and find the well-known quantity [159]. A suggestive way of writing the final result in momentum space is

$$V(\boldsymbol{q}^2)=-C_F\frac{4\pi\alpha_V(\boldsymbol{q}^2)}{\boldsymbol{q}^2}, \tag{4.12a}$$

$$\alpha_V(\boldsymbol{q}^2)=\alpha_s(\mu^2)\sum_{n=0}^{\infty}\tilde{a}_n\left(\frac{\mu^2}{\boldsymbol{q}^2}\right)\left(\frac{\alpha_s(\mu^2)}{4\pi}\right)^n=\alpha_s(\boldsymbol{q}^2)\sum_{n=0}^{\infty}a_n\left(\frac{\alpha_s(\boldsymbol{q}^2)}{4\pi}\right)^n, \tag{4.12b}$$

where $a_0=\tilde{a}_0=1$,

$$a_1=\frac{31}{9}C_A-\frac{20}{9}T_Fn_f,\qquad \tilde{a}_1=a_1-\beta_0L_{\boldsymbol{q}}, \tag{4.13}$$

with $L_A\equiv\ln(A^2/\mu^2)$, $T_F=1/2$, n_f being the number of light quark flavors, and $\beta_0=11C_A/3-4T_Fn_f/3$ being the first coefficient of the QCD beta function. Here, α_s denotes the strong-coupling constant in the $\overline{\text{MS}}$ scheme and α_V represents the effective coupling constant which incorporates all radiative corrections into its definition. This provides a new scheme, the V scheme [276, 277], which defines the strong-coupling constant in terms of a potential. With the QCD result at hand, one expects to be able to extend this approach to the SM and other theories exhibiting SSB.

4.2.2 $\mathcal{N}=4$ SYM

The only case of a static potential calculated for a spontaneously broken theory with a Higgs-like field is in $(3+1)$-dimensional $\mathcal{N}=4$ SYM, which has been done with the Wilson loop approach [267]. The static potential in this theory is given by

$$V(\boldsymbol{r})=-\lim_{T\to\infty}\frac{1}{T}\ln\left\langle\overline{\text{tr}}\mathcal{P}\exp i\left(\oint_\Gamma ds\dot{x}^\mu A_\mu+\Phi_i\theta_i|\dot{x}|\right)\right\rangle, \tag{4.14}$$

where $A_\mu=A_\mu^aT^a$ is the gauge field, Φ_i $(i=1,\ldots,6)$ are the six scalar fields in this theory, $x^\mu(s)$ parameterizes the rectangular Wilson loop Γ to be integrated over, as previously shown in Fig. 4.1, and $\theta_i(s)$ is a six-vector to be defined below.

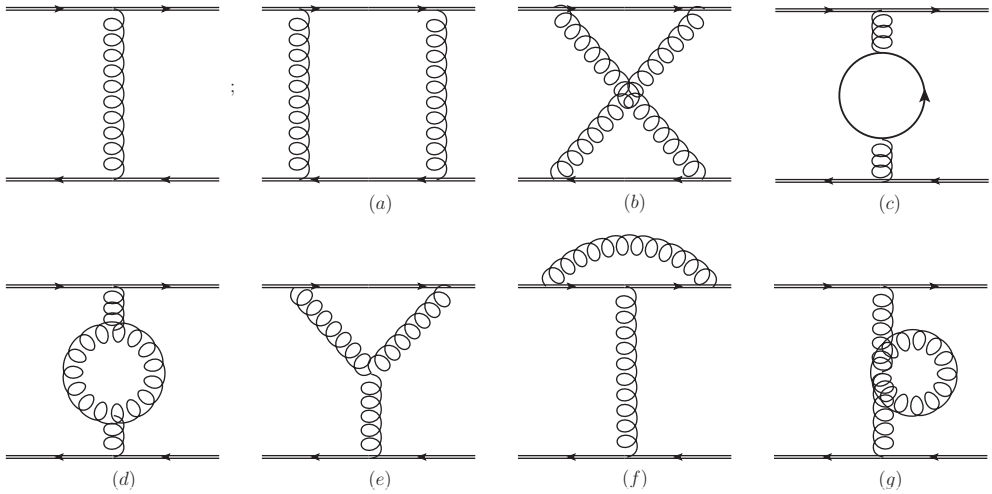

Figure 4.4: Feynman diagrams that contribute to the QCD static potential at one-loop. The arrowed circle represents light-quark and ghost loops.

We now summarise the derivation of this potential. Let us consider SSB according to $U(N+1) \to U(N) \times U(1)$ giving some expectation value, $\langle \mathbf{\Phi} \rangle = \boldsymbol{v}$, to a Higgs-like field. Then the massive W bosons have a mass proportional to $|\boldsymbol{v}|$ and transform in the fundamental representation of $U(N)$. In the limit $|\boldsymbol{v}| \to \infty$, they so provide the very massive "quarks" necessary to compute Wilson loops in the $U(N)$ theory. The physics of interest is related to energy scales much lower than $|\boldsymbol{v}|$, where the $U(N)$ theory is effectively decoupled from the $U(1)$ theory.

Let us then consider the equation of motion for the massive W boson. Extracting the leading time dependence as $W = e^{-i|\boldsymbol{v}|t}\tilde{W}$, we obtain an equation of motion from the Lagrangian for $\tilde{W}$, which to leading order in large $|\boldsymbol{v}|$ reads

$$(\partial_0 - iA_0 - i\theta_i \Phi_i)\tilde{W} = 0, \tag{4.15}$$

where we have defined $\theta_i \equiv v_i/|\boldsymbol{v}|$. Notice that A_0 and Φ_i are matrices in the adjoint representation of $U(N)$. This implies that, if we consider this massive W boson describing a closed loop, Γ, its interaction with the $U(N)$ gauge field leads to the insertion of the Wilson loop operator

$$\mathcal{W}(\Gamma) = \overline{\mathrm{tr}} \mathcal{P} \exp i \left(\oint_\Gamma ds \dot{x}^\mu A_\mu + \Phi_i \theta_i |\dot{x}| \right). \tag{4.16}$$

This operator is determined by the contour Γ, parametrised by $x^\mu(s)$, as well as a function, $\theta_i(s)$, which is a unit six-vector, with $|\boldsymbol{\theta}| = 1$. From this Wilson loop, one obtains the static potential by taking the expectation value and $T \to \infty$ limit,

$$V(\boldsymbol{r}) = -\lim_{T\to\infty} \frac{1}{T} \ln \langle \mathcal{W}[\Gamma] \rangle. \tag{4.17}$$

This potential has been evaluated in detail, and limits have been mapped to classical D-string solutions [267]. More recently, this very potential has been computed in the *weak-coupling limit* to NLO using EFT methods inspired by potential NRQCD (pNRQCD) [278].

Following this case, we may apply the same procedure to the equation of motion of heavy quarks in the SM obtained from the SM Lagrangian. The leading time dependence is exhibited analogously for the heavy quarks, $Q = e^{-im_Q t}\tilde{Q}$, where $m_Q = yv$, with y being the

quark Yukawa coupling and v the Higgs VEV. We can then consider the analogous limit, $v \sim m_Q, M_W, M_Z, M_H \gg |\boldsymbol{q}|$, where $|\boldsymbol{q}|$ is the momentum exchange between the *static sources*.

4.2.3 SM

Since the Wilson loop approach is technically simpler, we apply it to heavy quarks in the SM, inspired by the $\mathcal{N} = 4$ SYM derivation. For the sake of illustration, we omit couplings to the W, Z, and Goldstone bosons, as we will see later that they cannot be taken into account in this approach. The quark field, $\psi(x)$, then has the equation of motion

$$\left[i\not{D} - m_Q - yH(x)\right]\psi(x) = 0, \tag{4.18}$$

where $\not{D} = \gamma_\mu[\partial^\mu - i\tilde{A}^\mu(x)]$ with $\tilde{A}^\mu = g_s A_g^{\mu,a} T_{ij}^a - eA_e^\mu$ represents the covariant derivative involving the couplings to the massless gauge fields, $H(x)$ corresponds to a gauge singlet scalar field that models Higgs exchange in the SM, y is the quark Yukawa coupling, and $m_Q = yv$ with v being the Higgs VEV [84]. Expanding Eq. (4.18) component-wise gives

$$\left\{i\gamma^0\partial_0 - i\boldsymbol{\gamma}\cdot\boldsymbol{\partial} + \gamma^0\tilde{A}_0(x) - \boldsymbol{\gamma}\cdot\tilde{\boldsymbol{A}}(x) - y[H(x)+v]\right\}\psi(x) = 0. \tag{4.19}$$

We can reduce this further by solving the Schrödinger equation for the heavy-quark field, providing us with the leading time dependence,

$$\psi = e^{-im_Q t}\tilde{\psi}. \tag{4.20}$$

Plugging this back into Eq. (4.19) gives

$$\left[(\gamma_0 - 1)yv - i\boldsymbol{\gamma}\cdot\boldsymbol{\partial} + \gamma^0\tilde{A}_0(x) - \boldsymbol{\gamma}\cdot\tilde{\boldsymbol{A}}(x) - yH(x)\right]\tilde{\psi}(x) = 0. \tag{4.21}$$

Taking the limit $v \to \infty$ of this expression, we attain the *bi-spinor* constraint $(1-\gamma_0)\tilde{\psi} = 0$, which forces the first component to be zero, $\tilde{\psi} = (0, \chi)$. Therefore, all terms acted on by the matrices $\boldsymbol{\gamma}$ and γ_5 do not contribute, restricting the naive inclusion of W, Z, and Goldstone couplings, as they are chiral and flavor changing. We are then left with the equation of motion

$$\left(\partial_t - i\tilde{A}_0 + iyH\right)\chi(x) = 0. \tag{4.22}$$

Thus, if we consider the heavy quark describing a closed loop, Γ, its interaction with the Higgs and gauge fields leads to the insertion of the Wilson loop operator

$$\mathcal{W}(\Gamma) = \overline{\mathrm{tr}}\mathcal{P}\exp i\left[\oint_\Gamma d\tau\left(\dot{x}^\mu\tilde{A}_\mu(x) - yH(x)|\dot{x}|\right)\right], \tag{4.23}$$

and the static potential is then given by Eq. (4.17) in the large-v limit. The interaction with the static sources, ψ and χ, is given by the static Lagrangian,

$$\mathcal{L}_{stat} = \psi^\dagger(i\partial_0 - \tilde{A}_0 + yH)\psi + \chi_c^\dagger(i\partial_0 + \tilde{A}_0 + yH)\chi_c \tag{4.24}$$

We may also consider the large-y limit. In this case, the simplification of the bi-spinor to one large component ceases to occur. Instead, spatio-temporal mixing in spinor components happens resulting in the loss of gauge invariance.

Otherwise, in the large-v limit, we have a potential allowing for interactions between the static source and the bosons g, γ, and H. Evaluating this potential in momentum space to one-loop order in the $\overline{\text{MS}}$ scheme gives the following extension of the pure QCD result:

$$V(\boldsymbol{q}) = V^{\text{QCD}}(\boldsymbol{q}) - \frac{4\pi\alpha}{\boldsymbol{q}^2} Q_i Q_j \left(1 - \frac{\alpha}{4\pi}\frac{4N_s}{3}\left(\frac{5}{3} - L_{\boldsymbol{q}}\right)\right), \tag{4.25}$$

where $N_s = (N_c[Q_u^2 n_u + Q_d^2 n_d] + n_l)$ such that N_c is the number of colours, $Q_{i,j}$ represents the heavy quark charges, $Q_{u,d}$ and $n_{u,d}$ are the charges and numbers of light up-type and down-type quark flavors, respectively, and n_l is the number of charged-lepton flavors. Note there is no contribution from the Yukawa coupling at NLO as they either cancel or are eliminated by *wave-function renormalisation* (WFR), which is known in literature [153]. Although corrections can occur at NNLO as is the case for theories with scalars [271, 279].

We note that taking the large-vacuum-expectation-value limit, as is done here, can also be applied to BSM theories with Higgs-like fields and higher symmetry breaking scales. On the other hand, if we choose to include all interactions of the SM consistently in the static limit, $|\boldsymbol{q}| \ll m_Q, M_W, M_Z, M_H$, then the more computationally intensive scattering amplitude approach seems to be the safest path. We look at this next.

4.3 Scattering Amplitude Approach

Although we derived the QCD static potential in the Wilson loop approach, it is worthwhile cross-checking this with the original, *scattering amplitude approach* [280]. In this way, one can compute the potential directly in momentum space from the *on-shell* (OS) quark-antiquark scattering amplitude in the static limit. Although this is a textbook result in QED [281], we recalculate this here in QCD to verify that it matches the Wilson loop result.

The idea of the calculation is to study the QCD scattering amplitude of the process

$$Q(p) + \bar{Q}'(p') \to Q(p-q) + \bar{Q}'(p'+q), \tag{4.26}$$

where $q^\mu = (0, \boldsymbol{q})$, in the limit of NR scattering, $m_Q \gg |\boldsymbol{q}|$. There are various ways to parametrise the four-momenta. We choose to minimise the algebra by employing light-cone coordinates. We take the initial particles to be moving along the z axis and introduce two light-cone vectors, $n_\pm^\mu = (1, 0, 0, \mp 1)$. Then any momentum is expressible as

$$k^\mu = \frac{1}{2}\left(n_-^\mu k_+ + n_+^\mu k_-\right) + k_T^\mu, \tag{4.27}$$

where k_T^μ represents the remaining transverse components. This choice of coordinates leads to useful identities,

$$n_+ \cdot n_- = 2, \quad n_\pm^2 = 0, \quad n_\pm \cdot k_T = 0, \quad k_\pm = k \cdot n_\pm = k_0 \pm k_3, \tag{4.28}$$

and the scalar product can be rewritten as

$$k \cdot q = \frac{1}{2}(k_+ \cdot q_- + k_- \cdot q_+) - \boldsymbol{k}_T \cdot \boldsymbol{q}_T, \qquad k^2 = k_+ \cdot k_- - \boldsymbol{k}_T^2. \tag{4.29}$$

In our case, we have four-vectors, p and p', which satisfy

$$p_+ \cdot p_- = m_Q^2, \quad p'_\pm = p_\mp, \quad p_\pm = \sqrt{m_Q^2 + p^2} \pm |\boldsymbol{p}|. \tag{4.30}$$

Assuming that we know the transverse part of the momentum transfer, $\boldsymbol{q}_T$, we may fix q^+ and q^- in such a way that outgoing-particle momenta are on shell,

$$\begin{cases} (p-q)^2 = m_Q^2 \\ (p'+q)^2 = m_Q^2 \end{cases} \Rightarrow \begin{cases} (p_+ - q_+)\cdot(p_- - q_-) - \boldsymbol{q}_T^2 = m_Q^2 \\ (p_- + q_+)\cdot(p_+ + q_-) - \boldsymbol{q}_T^2 = m_Q^2 \end{cases} \tag{4.31}$$

Solving this system of equations and substituting the explicit expressions for $p_\pm$, we obtain

$$q_+ = -q_- = \mathcal{P} - \bar{\mathcal{P}}, \tag{4.32}$$

where

$$\mathcal{P} = |\boldsymbol{p}|, \quad \bar{\mathcal{P}} = \sqrt{\boldsymbol{p}^2 - \boldsymbol{q}_T^2}, \tag{4.33}$$

so that $\boldsymbol{q}_T^2 = \mathcal{P}^2 - \bar{\mathcal{P}}^2$. This implies that we may express everything in terms of $\mathcal{P}$ and $\bar{\mathcal{P}}$. As these parameters are independent of m_Q, we infer that $\mathcal{P}, \bar{\mathcal{P}} \ll m_Q$, which allows for the leading power dependence of the amplitude to be safely taken in the limit $m_Q \to \infty$. To proceed, we need to express all scalar products in terms of our new parameters,

$$\begin{aligned} q^2 &= q_+\cdot q_- - \boldsymbol{q}_T^2 = 2\mathcal{P}(\bar{\mathcal{P}} - \mathcal{P}), \\ p\cdot q &= \frac{1}{2}(p_+\cdot q_- + p_-\cdot q_+) = \mathcal{P}(\bar{\mathcal{P}} - \mathcal{P}), \\ p'\cdot q &= \frac{1}{2}(p_-\cdot q_- + p_+\cdot q_+) = -\mathcal{P}(\bar{\mathcal{P}} - \mathcal{P}), \\ p\cdot p' &= \frac{1}{2}(p_+^2 + p_-^2) = m_Q^2 + 2\mathcal{P}^2. \end{aligned}$$

With this set of coordinate redefinitions, we may now proceed and calculate the static potential in QCD.

4.3.1 QCD

In the pure QCD case, the one-loop bare amplitude is proportional to the *Born amplitude* and both ultraviolet (UV) and IR finite. The expression for the scattering amplitude in perturbation theory through NLO in the *Fourier-transformed* potential, $U(\boldsymbol{q})$, reads [281],

$$f(\boldsymbol{k},\boldsymbol{k}') = -\frac{m_*}{2\pi\hbar^2}\left[U(\boldsymbol{k}-\boldsymbol{k}') + \frac{2m_*}{\hbar^2}\int\frac{d^3\boldsymbol{l}}{(2\pi)^3}\,\frac{U(\boldsymbol{k}'-\boldsymbol{l})U(\boldsymbol{l}-\boldsymbol{k})}{\boldsymbol{k}^2-\boldsymbol{l}^2+i0} + O(U^3)\right], \tag{4.34}$$

where $\boldsymbol{k} = \boldsymbol{p}$, $\boldsymbol{k}' = \boldsymbol{p} - \boldsymbol{q}$, and $m_* = m_Q/2$ is the effective mass of the scattering particles. For the Coulomb potential, the integral is IR divergent, but we can calculate this in dimensional regularization. The terms we obtain from this procedure should match the corresponding terms in the Wilson loop approach. The UV divergences are removed by the renormalization of the coupling and the mass in the $\overline{\text{MS}}$ scheme, while the IR divergence in the NR limit is known to come exclusively from the long-range Coulomb interaction and is removed by on-shell WFR.

The QCD scattering amplitudes contributing at NLO are represented in Fig. 4.5. We calculate them and take the NR limit. More specifically, we expand the Dirac spinor chains in terms of Pauli matrices and Pauli spinors, taking the $\boldsymbol{q}^2 \to 0$ limit. Next, we pick out the terms that are of $\mathcal{O}(1/\boldsymbol{q}^2)$ and contain only Pauli spinors, dropping terms with insertions of Pauli matrices,

i.e., *spin-dependent* terms, as these contribute at $\mathcal{O}(\boldsymbol{q}^2/m_Q^2)$. This leads us to to the following renormalized *color singlet* potential in the $\overline{\text{MS}}$ scheme:

$$V(\boldsymbol{q}) \;=\; -\frac{4\pi\alpha_s}{\boldsymbol{q}^2}\left\{1+\frac{\alpha_s}{4\pi}\left[\left(2\pi i C_F\frac{m_Q}{\mathcal{P}}-\beta_0\right)L_{\boldsymbol{q}}+\frac{31}{9}C_A-\frac{20}{9}n_f\right]\right\}, \tag{4.35}$$

where the imaginary term proportional to $(-2\pi i)$ is the so-called Coulomb contribution, which is known to appear [280]. The real part is exactly the QCD static potential at one-loop order, which is identical to the result one obtains with the Wilson loop approach, as required.

4.3.2 SM

We may now extend this approach from QED and QCD to the SM, expanding the scattering amplitudes illustrated in Fig. 4.5 in the NR limit and taking the real part of the expression to be the static potential. As in the QCD case, we investigate the following process at one-loop:

$$Q_1(p)+\bar{Q}_2(p')\to Q_1(p-q)+\bar{Q}_2(p'+q), \tag{4.36}$$

where $q^\mu=(0,\boldsymbol{q})$ is the momentum transfer. The limit of NR scattering in the SM is given by $|\boldsymbol{q}|\ll m_1,m_2,M_W,M_Z,M_H$, where the subindices 1 and 2 are to provide the possibility of working with different particles, having different masses. Therefore, we have three cases to consider,

$$V_{ij}^{\text{SM}}=V^{\text{QCD}}+V^{\text{QED}}+\delta V_{(i,j)}^{\text{SM}}, \tag{4.37}$$

where $\delta V_{(i,j)}^{\text{SM}}$ is the one-loop correction from contributions outside pure QCD, the leading of which may be written as,

$$\delta V_{(i,j)}^{\text{SM}}\equiv\frac{\alpha\alpha_s}{\boldsymbol{q}^2}c_{(i,j)}+\frac{\alpha^2}{\boldsymbol{q}^2}\left(d_{(i,j)}+e_{(i,j)}L_{\boldsymbol{q}}\right). \tag{4.38}$$

We note that flavor changing is permitted in the SM, so we take the internal quark masses to be non-zero to maintain consistency. To present our large expression for $\delta V_{(i,j)}^{\text{SM}}$ concisely, we consider the limit $m_1\gg M_W,M_Z,M_H\gg m_2\gg|\boldsymbol{q}|$, which is valid for top and bottom quarks, i.e., $m_1=m_t$ and $m_2=m_b$. Other limits, including the more physical limit $m_1\sim M_W,M_Z,M_H\gg m_2\gg|\boldsymbol{q}|$, can be considered from the full expressions presented in an arXiv ancillary file of Ref. [264]. In the regime examined, we have the following leading terms:

$$\begin{aligned}
\delta V_{(1,1)}^{\text{SM}}=\frac{\alpha\alpha_s}{\boldsymbol{q}^2}\frac{C_F}{s^2}\Bigg[&\left(r_{1,w}^2-\frac{1}{4}-\frac{21r_{h,z}^2}{16c^2}\right)L_{z,h}+\left(\frac{7s^2}{36}+r_{1,w}^2+\frac{16s^2}{9}-\frac{7}{36c^2}-\frac{21\tilde{r}_{h,z}^2}{16c^2}\right)L_{1,z}\\
&+\frac{\tilde{r}_{h,z}^2}{2c_w^2}-\frac{1}{4}-\frac{1}{2c^2}+3\pi\frac{r_{1,w}r_{h,w}}{2}+\frac{1}{4}L_{h,w}\Bigg]+\frac{\alpha^2}{\boldsymbol{q}^2}\Bigg[\frac{4N_s}{3}Q_1^2\left(\frac{5}{3}-L_{\boldsymbol{q}}\right)-\frac{8}{27}+\frac{2}{9s^2}\\
&+\frac{1}{96s^4}+2\pi\frac{r_{1,w}r_{h,w}}{3s^2}-\frac{37}{144c^2s^2}+\frac{2r_{h,z}^2}{9c^2s^2}+\frac{25}{864c^4}+\frac{28}{9}L_w-\left(\frac{5}{18s^2}+\frac{r_{1,w}^2}{6s^2}\right)L_{h,w}\\
&+\left(\frac{5}{288c^2s^2}+\frac{5}{144\tilde{r}_{h,z}^2c^2s^2}+\frac{5r_{1,w}^2}{18s^2}-\frac{1}{192s^4}-\frac{1}{96\tilde{r}_{h,z}^2s^4}-\frac{7r_{h,z}^2}{12c^2s^2}-\frac{25}{1728c^4}\right.\\
&\left.-\frac{25}{864\tilde{r}_{h,z}^2c^4}\right)L_{z,h}-\frac{5}{18s^2}+\left(\frac{64}{81}-\frac{13}{162s^2}+\frac{5r_{1,w}^2}{18s^2}-\frac{7}{81c^2s^2}-\frac{7r_{h,z}^2}{12c^2s^2}\right)L_{1,z}\Bigg],
\end{aligned} \tag{4.39}$$

$$\delta V^{\rm SM}_{(1,2)} = \frac{\alpha\alpha_s}{\boldsymbol{q}^2}\frac{C_F}{s^2}\left[\left(\frac{1}{9}+\frac{10s^2}{9}+\frac{5}{36c^2}\right)L_{h,z}+\left(\frac{5}{36c^2}-\frac{5r_{h,z}^2}{4c^2}+\frac{10s^2}{9}+\frac{r_{1,w}^2}{2}-\frac{5}{36}\right)L_{1,h}\right.$$
$$\left.-\frac{5r_{h,z}^2}{16c^2}L_{2,w}+\frac{1}{4}L_{h,w}-\frac{5r_{h,z}^2}{16c^2}L_w-\frac{1}{4}+\frac{r_{h,z}^2}{2c^2}-\frac{1}{2c^2}-3\pi\frac{r_{1,z}r_{h,z}}{4s}+3\pi\frac{r_{1,w}r_{h,w}}{4s^3}\right]$$
$$+\frac{\alpha^2}{\boldsymbol{q}^2}\left[\frac{4N_s}{3}Q_1Q_2\left(\frac{5}{3}-L_{\boldsymbol{q}}\right)+\frac{4}{27}-\frac{7}{36s^2}-\frac{1}{96s^4}+\pi\frac{r_{1,w}r_{h,w}}{6\tilde{r}_{h,z}^2s^5}+\pi\frac{r_{1,z}r_{h,z}^3}{6\tilde{r}_{h,z}^2s^3}\right.$$
$$+\frac{19}{144c^2s^2}-\frac{r_{h,z}^2}{9c^2s^2}-\frac{5}{864c^4}-\pi\frac{r_{1,w}r_{h,w}r_{h,z}^2}{6\tilde{r}_{h,z}^2s^3}+\left(\frac{5}{864c^4\tilde{r}_{h,z}^2}+\frac{5}{1728c^4}-\frac{1}{\tilde{r}_{h,z}^2c^2s^2}\right.$$
$$+\frac{53}{2592c^2s^2}+\frac{1}{96\tilde{r}_{h,z}^2s^4}+\frac{1}{192s^4}+\frac{2}{81s^2}+\frac{20}{81}\Big)L_{z,h}+\left(\frac{5\tilde{r}_{h,z}^2}{768c^4}+\frac{53r_{h,z}^2}{1152c^2s^2}\right.$$
$$+\frac{3}{128c^2s^2}+\frac{3r_{h,z}^2}{256s^4}-\frac{3}{256s^4}\Big)L_{2,w}+\left(\frac{5\tilde{r}_{h,z}^2}{768c^4}+\frac{53r_{h,z}^2}{1152c^2s^2}+\frac{3}{128c^2s^2}+\frac{3\tilde{r}_{h,z}^2}{256s^4}\right.$$
$$-\frac{14}{9}\Big)L_w+\left(\frac{r_{1,2}^2r_{1,z}^2}{12c^2}-\frac{r_{1,w}^2}{8s^2}+\frac{13}{72s^2}\right)L_{h,w}+\left(\frac{r_{1,2}^2r_{1,z}^2}{12c^2}-\frac{17r_{1,w}^2}{72s^2}+\frac{101}{648s^2}\right.$$
$$\left.\left.-\frac{20}{81}+\frac{5r_{h,z}^2}{18c^2s^2}-\frac{5}{162c^2s^2}\right)L_{1,h}\right], \tag{4.40}$$

$$\delta V^{\rm SM}_{(2,2)} = \frac{\alpha\alpha_s}{\boldsymbol{q}^2}\frac{C_F}{s^2}\left[\left(\frac{7}{4}-\frac{17r_{h,z}^2}{16c^2}\right)L_{z,h}+\left(\frac{4s^2}{9}+\frac{55}{36}-\frac{85}{144c^2}-\frac{17\tilde{r}_{h,z}^2}{16c^2}\right)L_{2,z}+\frac{\tilde{r}_{h,z}^2}{2c_w^2}-\frac{3}{4}\right.$$
$$\left.-L_{1,h}+\frac{3}{4}L_{h,w}\right]+\frac{\alpha^2}{\boldsymbol{q}^2}\left[\frac{4N_s}{3}Q_2^2\left(\frac{5}{3}-L_{\boldsymbol{q}}\right)+\frac{1}{12s^2}+\frac{1}{96s^4}-\frac{1}{144c^2s^2}+\frac{\tilde{r}_{h,z}^2}{18c^2s^2}\right.$$
$$+\frac{1}{864c^4}+\frac{2}{27}+\frac{7}{9}L_w-\frac{1}{9s^2}L_{1,h}+\left(\frac{4}{81}-\frac{17\tilde{r}_{h,z}^2}{144c^2s^2}-\frac{85}{1296c^2s^2}+\frac{7}{81s^2}\right)L_{2,z}$$
$$+\left(\frac{1}{9s^2}-\frac{1}{192s^4}-\frac{1}{96\tilde{r}_{h,z}^2}-\frac{11}{96c^2s^2}+\frac{1}{144\tilde{r}_{h,z}^2c^2s^2}-\frac{17\tilde{r}_{h,z}^2}{144c^2s^2}-\frac{1}{864\tilde{r}_{h,z}^2c^4}\right.$$
$$\left.\left.-\frac{1}{1728c^4}\right)L_{z,h}\right], \tag{4.41}$$

where $L_A \equiv \log(A^2/\mu^2)$, $L_{A,B} \equiv L_A - L_B$, $r_{i,j} \equiv m_i/m_j$, $\tilde{r}_{i,j} \equiv \sqrt{r_{i,j}^2-1}$, $c \equiv \cos\theta_w = M_W/M_Z$, $s \equiv \sin\theta_w$, θ_w is the weak mixing angle, and the notation introduced for Eq. (4.25) has been used. Of course, we have $\delta V^{SM}_{(1,2)} = \delta V^{SM}_{(2,1)}$. The results presented in Eqs. (4.39)–(4.41) represent color singlet contributions. Their color octet counterparts emerge via the simple replacement $C_F \to -1/(2C_A)$. Thus, we have now fully expressed the SM static potential to one-loop order.

4.4 Applications

The static potential represents a fundamental concept in its own right, not only giving rise to potential models, which have been astonishingly successful in the description of heavy quarkonia, but also provides a deeper understanding of confinement. From a more phenomenological standpoint, however, the primary interest resides in heavy-quark pair production at threshold [235,

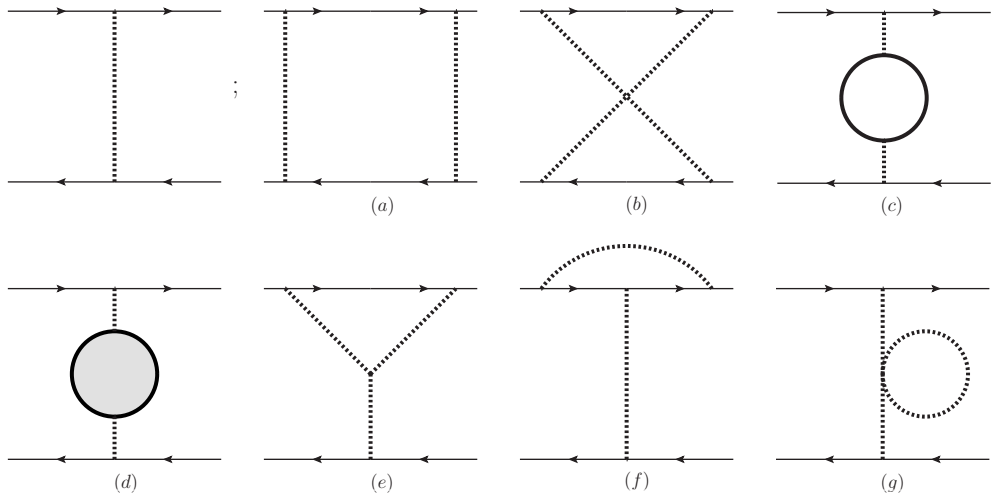

Figure 4.5: Feynman diagrams that contribute to the static potential at one-loop order. The dotted lines represent possible bosonic propagators, the shaded circles light-fermion and ghost loops insertions, and the hollow circles boson loop insersions.

251,266]. The static potential enters heavy-quark EFTs, for instance pNRQCD [251,282], where both the color singlet and octet potentials appear as Wilson coefficients of the theory. Moreover, there has been significant interest in designing high-precision quark mass definitions appropriate for processes occurring at production threshold, the most popular of which are the PS [57] and 1S [59] masses. In the following, we summarise these two applications and comment on the effects of incorporating the SM static potential, or EW corrections to the QCD static potential, in these results.

4.4.1 Potential NRQCD

The pNRQCD EFT is an often employed extension of NRQCD. The difference between these two theories is that pNRQCD takes further advantage of the hierarchy of scales that appear in a particular process. The hierarchy under consideration is taken to be $m_Q \gg |\boldsymbol{p}| \sim m_Q v \gg E \sim m_Q v^2$, where pNRQCD takes into account the ultrasoft (US) scale, $E \sim m_Q v^2$, which is neglected in NRQCD [282]. To take into account the US scale, one alters the Lagrangian of NRQCD by including the following terms:

$$\mathcal{L}_{\text{pNRQCD}} = \mathcal{L}^{\text{US}}_{\text{NRQCD}} + \mathcal{L}_{\text{pot}}, \tag{4.42}$$

where $\mathcal{L}^{\text{US}}_{\text{NRQCD}}$ is identical to $\mathcal{L}_{\text{NRQCD}}$ with all gluons taken to be in the US regime. The second term, $\mathcal{L}_{\text{pot}}$, is of particular interest to us. It arises from the Schrödinger equation as

$$\mathcal{L}_{\text{pot}} = -\int d^3\boldsymbol{x}_1 d^3\boldsymbol{x}_2 \psi^\dagger(t,\boldsymbol{x}_1)\chi(t,\boldsymbol{x}_2)V(\boldsymbol{r})\chi^\dagger(t,\boldsymbol{x}_2)\psi(t,\boldsymbol{x}_1), \tag{4.43}$$

where $\boldsymbol{p}_j = -i\boldsymbol{\nabla}_j$ and $\boldsymbol{S}_j = \boldsymbol{\sigma}_j/2$ with $j = 1,2$ act on the fermion and antifermion, respectively. Moreover, the fermion and antifermion spin indices are contracted with the indices of $V(\boldsymbol{r})$, which are not explicitly displayed. The potential in this expression, $V(\boldsymbol{r})$, is precisely the QCD static potential. There are implicitly two terms in this Lagrangian, depending on if the wave functions

are color singlet or octet with corresponding singlet and octet potentials, respectively. By inspection, the potential $V_{s,o}(\boldsymbol{r})$ contains both the expansion parameter and Wilson coefficients of this EFT. Conversely, this EFT can be seen as defining the static potential, i.e., any term matching to the EFT is the static potential. Whence, when employing this EFT, one should include the EW corrections to the QCD static potential at NLO as they are comparable to NNLO QCD corrections.

4.4.2 Threshold Masses

It is well known that, contrary to intuition, the notion of quark pole mass is, in fact, inadequate for accurate calculations of heavy-quark cross sections near threshold. The loss of accuracy is due to the existence of IR renormalons, which have been studied in various contexts [47]. The PS and 1S masses are by far the most frequently used threshold mass definitions that evade the renormalon problem by employing the static potential. The PS mass is slightly more involved phenomenologically, as it introduces a new factorisation scale, μ_F, in its definition. Before introducing these mass definitions, we must first examine the Fourier transform of our static potential.

4.4.2.1 Fourier Transform

We are now able to compute the SM analogue of the well-known Coulomb potential, i.e., the SM static potential in position space. From this, we may obtain the corrections to the PS mass and compare them with the pure QCD result. In order to simplify our expressions, it is convenient to introduce the notation [40]

$$\mathcal{F}(\boldsymbol{r},\mu,u)=\mu^{2u}\int \not{d}^3\boldsymbol{q}\frac{e^{i\boldsymbol{q}\cdot\boldsymbol{r}}}{(\boldsymbol{q}^2)^{1+u}}, \tag{4.44}$$

for the Fourier transform of a general power of $1/\boldsymbol{q}^2$. We then employ a *Schwinger parameter*,

$$\frac{1}{(\boldsymbol{q}^2)^{1+u}}=\frac{1}{\Gamma(1+u)}\int_0^\infty dx\, x^u e^{-x\boldsymbol{q}^2}, \tag{4.45}$$

where $\Gamma(x)$ is Euler's *gamma function*. There are various representations of $\mathcal{F}$. The ones which are useful to us are

$$\mathcal{F}(|\boldsymbol{r}|,\mu,u)=\frac{(\mu|\boldsymbol{r}|)^{2u}}{4\pi^2|\boldsymbol{r}|}\frac{\Gamma(1/2+u)\Gamma(1/2-u)}{\Gamma(1+2u)} \tag{4.46}$$

$$=\frac{(\mu|\boldsymbol{r}|e^{\gamma_E})^{2u}}{4\pi|\boldsymbol{r}|}\exp\left\{\sum_{n=2}^{\infty}\frac{\zeta(n)u^n}{n}\left[2^n-1-(-1)^n\right]\right\}, \tag{4.47}$$

where the first and second formulas are applicable if $-1<u<1/2$ and $|u|<1/2$, respectively. By inspection of the static potential, we need the Fourier transform of $\ln^m(\mu^2/\boldsymbol{q}^2)$, which is easily attainable from $\mathcal{F}$, since

$$\ln^m\frac{\mu^2}{\boldsymbol{q}^2}=\left[\frac{\partial^m}{\partial u^m}\frac{\mu^2}{\boldsymbol{q}^2}\right]_{u=0}, \tag{4.48}$$

and, therefore,

$$\int \not{d}^3 q\frac{e^{i\boldsymbol{q}\cdot\boldsymbol{r}}}{\boldsymbol{q}^2}\ln^m\frac{\mu^2}{\boldsymbol{q}^2}=\left[\frac{\partial^m}{\partial u^m}\mathcal{F}(r,\mu,u)\right]_{u=0}. \tag{4.49}$$

Whence the color singlet potential (in the $\overline{\text{MS}}$ scheme) in position space is

$$\begin{aligned} V^{\text{SM}}_{(i,j)}(\boldsymbol{r}) &= -\frac{\alpha_s}{|\boldsymbol{r}|}C_F\left\{1+\frac{\alpha_s}{4\pi}\left[2\beta_0\ln(\mu r')+a_1\right]\right\} \\ &\quad -\frac{\alpha}{|\boldsymbol{r}|}\left\{Q_iQ_j+\frac{\alpha_s}{4\pi}c_{(i,j)}+\frac{\alpha}{4\pi}\left[d_{(i,j)}+2e_{(i,j)}\ln(\mu r')\right]\right\}, \end{aligned} \tag{4.50}$$

where Q_i are the electric charges of the incoming and outgoing heavy quarks. In our calculation, we take $Q_1 = 2/3$, $Q_2 = -1/3$, and $r' = |\boldsymbol{r}|e^{\gamma_E}$. The result as it stands is possibly plagued by large logarithms. To remedy this problem, it is useful to select a renormalisation scale, μ, that reduces the higher-order corrections. Choices of μ most frequently employed in the literature include $\mu = 1/|\boldsymbol{r}|$ or $\mu = 1/r'$. Other choices of μ are tuned so that the first-order pure QCD coefficient is removed entirely or so that all n_f dependencies are removed from the coefficients [283]. With the Fourier-transformed potential at hand, we may now consider the PS mass.

4.4.2.2 PS Mass

It is well-known that the coordinate space static potential is more sensitive to long distances than its counterpart in momentum space and that its leading power correction is linear in $\Lambda_{\text{QCD}}|\boldsymbol{r}|$ [57]. The implication is that the expansion of the QCD coordinate space static potential in $\alpha_s(e^{-\gamma_E}|\boldsymbol{r}|)$ diverges as

$$\sum_n r_n\alpha_s^{n+1}(e^{-\gamma_E}|\boldsymbol{r}|) \sim \sum_n(-2\beta_0)^n n!\, n^b\alpha_s\left(\frac{e^{-\gamma_E}}{|\boldsymbol{r}|}\right), \tag{4.51}$$

which is much faster than the expansion of the static potential in momentum space. This divergent behavior has been studied in previous works [284, 285]. It is clear that the rapid divergence originates only from the Fourier transform to coordinate space and is not present in momentum space. Knowing this, one can subtract the leading long-distance contribution and the LO divergent behaviour completely by restricting the Fourier integral with the cut $|\boldsymbol{q}|> \mu_f$, where μ_f is a new factorisation scale, which is viewed as an IR regulator. The result is called the *subtracted potential*, $V(\boldsymbol{r},\mu_f)$. The subtraction terms can be evaluated order by order in the coupling once $V(\boldsymbol{q})$ is given to that order. More precisely,

$$V(\boldsymbol{r},\mu_f) = V(\boldsymbol{r}) + 2\delta m(\mu_f), \tag{4.52}$$

where

$$\delta m(\mu_f) = -\frac{1}{2}\int_{|\boldsymbol{q}|<\mu_f} \not{d}^3\boldsymbol{q}V(\boldsymbol{q}). \tag{4.53}$$

To subtract the leading long-distance contribution of order Λ_{QCD}, it is reasonable to replace the factor $e^{i\boldsymbol{q}\cdot\boldsymbol{r}}$ in the Fourier transform by unity, and this is used as the definition of the subtraction term in the PS mass definition,

$$m_{\text{PS}}(\mu_f) \equiv m_{\text{pole}} - \delta m(\mu_f). \tag{4.54}$$

Of course, with this procedure, one has only swept the large loop corrections from $\delta m(\mu_f)$ to $m_{\text{PS}}(\mu_f)$. However, when m_{pole} is expressed in terms of a short-distance mass parameter, such as the $\overline{\text{MS}}$ mass through a perturbative series, this series will also contain large loop corrections [286]. Conveniently, these perturbative corrections cancel with large perturbative

corrections to the pole mass in $\delta m(\mu_f)$. In this way, one may determine the $\overline{\text{MS}}$ mass from threshold cross sections with better accuracy than the pole mass, the use of which implicitly contains the non-subtracted potential. Let us now compute $\delta m(\mu_f)$ from the definition in Eq. (4.53). We so obtain

$$\begin{aligned}\delta m_{(i)}^{\text{SM}}(\mu_f) = C_F \frac{\alpha_s}{\pi}\mu_f \left\{1 + \frac{\alpha_s}{4\pi}\left[a_1 + 2\beta_0\left(\ln\frac{\mu}{\mu_f} + 1\right)\right]\right\} \\ + \frac{\alpha}{\pi}\mu_f \left\{Q_i^2 + \frac{\alpha_s}{4\pi}c_{(i,i)} + \frac{\alpha}{4\pi}\left[d_{(i,i)} + 2e_{(i,i)}\left(\ln\frac{\mu}{\mu_f} + 1\right)\right]\right\},\end{aligned} \tag{4.55}$$

where, as in Section 4.3.2, the cases $i = 1, 2$ apply to the top and bottom quarks, respectively. For completeness, we avoid taking limits and employ the complete result to get a numerical estimate of the one-loop SM PS mass. One usually picks $\mu_f = 3$ GeV, a typical scale for heavy quarks, and $\mu = M_Z$ to avoid large logarithms in the coefficients $c_{(i,j)}$ and $d_{(i,j)}$. Moreover, we choose $m_1 = m_t(M_Z)$, $m_2 = m_b(M_Z)$, $n_u = n_d = 2$, $n_l = 3$, and adopt the residual parameters from Ref. [168]. We thus obtain

$$\delta m_{(t)}^{SM}(\mu_f) = C_F \frac{\alpha_s}{\pi}\mu_f \left(1 + 79.5\frac{\alpha_s}{4\pi}\right) + \frac{\alpha}{\pi}\mu_f \left(0.44 + 89.9\frac{\alpha_s}{4\pi} + 30.9\frac{\alpha}{4\pi}\right), \tag{4.56}$$

$$\delta m_{(b)}^{SM}(\mu_f) = C_F \frac{\alpha_s}{\pi}\mu_f \left(1 + 79.5\frac{\alpha_s}{4\pi}\right) + \frac{\alpha}{\pi}\mu_f \left(0.11 + 16.4\frac{\alpha_s}{4\pi} - 2.42\frac{\alpha}{4\pi}\right). \tag{4.57}$$

We conclude that, albeit the additional SM contributions are significantly smaller than the pure QCD and QED ones at NLO, they are comparable to the QCD corrections at NNLO and beyond. Thus, they have an appreciable impact on high-precision determinations of the PS mass and must, therefore, be taken into account.

4.4.2.3 1S Mass

The PS mass along with other threshold mass definitions, such as the the kinetic mass [56, 287], are defined by introducing a new explicit IR factorisation scale, μ_f, to remove the IR ambiguity of the pole mass. By contrast, the 1S mass [59], m_{1S}, achieves a similar goal without introducing a new factorisation scale. The 1S mass is defined as one half of the perturbative energy of the 1S heavy $q\bar{q}$ bound state,

$$m_{1S}(\mu) = \frac{1}{2}(m_{1S}^{q\bar{q}})_{\text{pert}} \equiv m_{\text{pole}}(1 - \delta m(\mu)). \tag{4.58}$$

The ground state energy calculated from the Schrödinger equation of elementary quantum mechanics is exactly $(m_{1S}^{q\bar{q}})_{\text{pert}}$. At leading order in the expansion in the relative velocity of the (anti)quark in the $q\bar{q}$ rest frame (threshold region), the dynamics of the $q\bar{q}$ pair is governed by the Hamiltonian [288]

$$H = -\frac{\boldsymbol{\nabla}^2}{m_Q} + V(\boldsymbol{r}) + U(\boldsymbol{q}, \boldsymbol{r}), \tag{4.59}$$

where m_Q is the quark pole mass, $V(\boldsymbol{r})$ is the static potential, the analogue of the Coulomb potential, and $U(\boldsymbol{q}, \boldsymbol{r})$ encodes higher-order corrections in the small-velocity expansion and is the SM analogue of the Breit potential [280]. The leading contributions at threshold come from the static potential, so that we may omit $U(\boldsymbol{q}, \boldsymbol{r})$ from our calculation. Solving for the S-wave Green's function, we have

$$G(E) = \langle 0|\, \hat{G}(E)\, |0\rangle = \langle 0|\, \frac{1}{H - E - i\delta}\, |0\rangle\,, \tag{4.60}$$

where $\langle 0|$ denotes a position eigenstate with eigenvalue $|\boldsymbol{r}|= 0$, and the Green's function has single poles at the exact S-wave energy levels, $E = E_n$,

$$G(E) \overset{E\to E_n}{=} \frac{|\psi_n(0)|^2}{E_n - E - i\delta}. \tag{4.61}$$

From this expression, one gets $(m_{1S}^{q\bar{q}})_{\text{pert}} = E_1$, and expanding $E_1/2$ in small SM couplings gives the 1S mass, which is the SM analogue of the well-known Bohr potential of quantum mechanics. We may then find the leading EW corrections at one-loop to the 1S mass with our SM potential, as only the QCD corrections are known, and they have been found to N^{3}LO [289]. At one-loop through third order in the SM couplings, α and α_s, we have

$$\delta m_{(i)}^{\text{SM}}(\mu) = \frac{(\alpha Q_i^2 + \alpha_s C_F)}{16\pi}\left[\alpha^2 B_i + \alpha(\alpha_s c_{(i,i)} + 2\pi Q_i^2) + \alpha_s C_F(\alpha_s A_i + 2\pi)\right], \tag{4.62}$$

with

$$A_i = 2\beta_0(l_i + 1) + a_1, \quad B_i = 2e_{(i,i)}(l_i + 1) + d_{(i,i)}, \tag{4.63}$$

where m_i is the pole mass of heavy quark i and $l_i \equiv \ln[\mu/(C_F\alpha_s(\mu)m_i)]$. We further note that the IR renormalon cancellation is more subtle in the 1S mass definition, as the latter is a well-behaved parameter only if the orders of terms in perturbation theory are re-interpreted [59]. To see how the leading EW corrections at one-loop alter the 1S mass, we obtain a numerical estimate in a similar fashion as for the PS mass and compare the $\mathcal{O}(\alpha\alpha_s, \alpha^2)$ terms to the $\mathcal{O}(\alpha_s^2)$ ones. Choosing the same input parameters and renormalisation scale as in the PS mass case, we obtain the following results:

$$\delta m_{(t)}^{\text{SM}} = 0.22\alpha_s^2 + 1.51\alpha_s^3 + 0.02\alpha^2 + 0.71\alpha^3 + 0.15\alpha_s\alpha - 2.89\alpha_s^2\alpha + 2.93\alpha_s\alpha^2, \tag{4.64}$$

$$\delta m_{(b)}^{\text{SM}} = 0.22\alpha_s^2 + 3.61\alpha_s^3 + 0.002\alpha^2 + 0.04\alpha^3 + 0.04\alpha_s\alpha + 0.74\alpha_s^2\alpha + 0.48\alpha_s\alpha^2. \tag{4.65}$$

It is apparent that the additional SM contributions are significantly smaller than the pure QCD and QED ones at NLO, esspecially in the case of the bottom quark. However, they are comparable in size to the QCD corrections at NLO and beyond, so that it is necessary to include them in high-precision determinations of the 1S mass, similarly to the case of the PS mass in Section 4.4.2.2.

4.4.3 Further Applications

We now briefly address possible applications of our results to popular BSM scenarios. The number of viable dark-matter candidates is rapidly being constrained by precise collider and cosmological experiments. For example, self-interacting theories have been practically ruled out recently by galactic observations [290]. We may thus focus on computing the static potential of the most viable DM candidates, the *lightest Kaluza-Klein particle* (LKP) and right-handed neutrinos. As is well understood, SUSY [291] and extra-dimensional theories [292] are two strong proponents to an array of issues that cannot be explained by the SM. Dark matter is known to exist. While it is missing in the SM, both SUSY and *Kaluza-Klein* (KK) theories posit viable dark matter candidates, the properties of which can be understood better in the NR regime due to their large predicted masses.

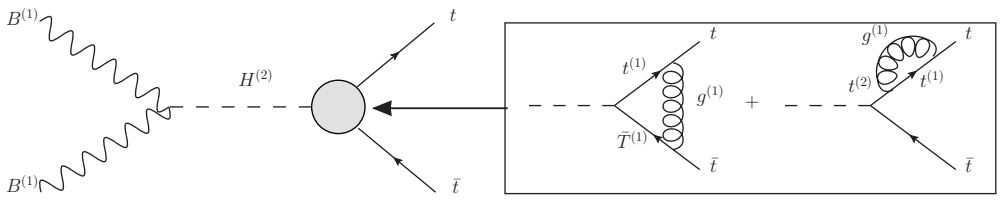

Figure 4.6: Resonant annihilation process of LKP dark matter, $B^{(1)}$, through s-channel $H^{(2)}$ exchange.

A recent static-potential calculation for *higgsino-wino* DM found the $SU(2)\times U(1)$ EW static potential between a fermionic triplet in the broken phase of the SM at one-loop order [269]. The NLO terms provided the leading NR correction to the large resonances (or *Sommerfeld effect*) in the annihilation cross-section of wino or wino-like dark-matter particles, χ_0. The authors found sizeable modifications from the LO prediction of the $\chi_0\chi_0$ annihilation cross section and determined the shifts of the resonance locations due to the loop correction to the wino potential. Although these results seem promising for future detections, such resonances would also occur in KK theory for the LKP coupling [293] to the second excitation of the Higgs as shown in Fig. 4.6. This will inevitably also be true for right-handed (or sterile) neutrinos due to their possible large mass [294–296], and thus their potential for producing heavy $t\bar{t}$ pairs through s-channel Higgs-boson exchange in the SM. Neutrinos are the only matter particles in the SM that have been observed with solely left-handed chirality to date. If right-handed neutrinos exist, they could be responsible for several phenomena that have no explanation within the SM, including neutrino oscillations, the baryon asymmetry of the universe, dark matter, and dark radiation [297]. These particles provide us with a test bed case of our ability to deal with static potentials in theories with SSB, as these massive neutrinos solely couple to gravity and the SM Higgs field.

4.5 Technical Details

Our calculations of the one-loop correction to the SM static potential were performed using standard tools. The Feynman diagrams of the type as in Fig. 4.5 were reduced to calculating a set of *master integrals*, which were found analytically, since all one-loop master integrals are known. For the scattering amplitude approach, we achieved this with the help of the algebraic manipulation program `Mathematica` accompanied by the program package `FeynCalc` [298] to compute the necessary amplitudes and to deal with the algebra. We employed further subpackages of `FeynCalc`, such as `FeynHelpers` [299], which reduces and provides explicit expressions for one-loop scalar integrals by connecting the reduction package `fire` [300] with the analytic scalar-integral package `Package-X` [301]. Lastly, we employed the `FeynOnium` [302] subpackage, which comes equipped with functions for dealing with amplitudes in the NR limit. For the Wilson loop approach, we employed the program package `QGRAF` [303] to generate the Feynman diagrams and the programming language `FORM` [304] to deal with the algebra. We also used the `Mathematica` package `LiteRed` [305] to reduce our integrals and again `Package-X` [301] for the analytic one-loop scalar integrals.

4.6 Summary

In this Chapter, we proposed a novel way of studying static potentials in theories that exhibit SSB. We discussed the limitations of the Wilson loop approach for the SM and the need to derive the static potentials directly from the scattering amplitudes. We also pointed out how these techniques could be extended to BSM theories, mentioning examples that would satisfy the criteria to be treated in the Wilson loop fashion. We then presented the static potential for the full SM and considered the regimes of applicability. In particular, we showed how our EW corrections to the static potential modify two frequently-employed short-distance definitions of heavy-quark mass, the PS and 1S ones. Moreover, we rounded off each discussion by comparing the size of the terms arising from generalizing the static potential from QCD to the SM with the familiar QCD results. In doing so, we found the contributions from the EW regime to be significant and comparable to pure QCD contributions of NNLO. Therefore, we recommend that the SM potential be employed in future high-precision heavy-quark studies. The theoretical framework elaborated here can now be usefully applied to investigate the static potential of further models, in particular BSM theories with higher symmetry breaking scales, to better understand the NR regime and explore implications for measurable observables. Our full results are contained in the ancillary file submitted along with Ref. [264] on the arXiv.

Chapter 5

Threshold Mass Definitions

This chapter deals more explicitly with the leading EW corrections to the short-distance heavy quark mass definitions. We achieve this with the static potential determined in the previous chapter, along with similar expressions for a heavy meson's binding and residual kinetic energy. These energies form the building blocks of the majority of short-distance mass definitions. We explain how attaining the EW contributions to these energies leads to analogous corrections to the masses. We find that the leading EW corrections are of the same strength as their next-to-leading pure QCD counterparts and, therefore, must be included for a precise determination of heavy quark mass. This chapter is based on Ref. [306], reflecting the author's contribution.

5.1 Motivation

A precise determination of quark masses is coveted due to them being fundamental SM Lagrangian parameters. In particular, the attainment of heavy quark (top, bottom and charm) masses provides a gamut of phenomenological insights. We are primarily interested in the top quark mass, m_t, which a precise determination of not only serves as consistency checks for the SM [48–50] but also is the dominant uncertainty when weighing the stability of the electroweak vacuum [33, 51, 52]. We are also concerned with the bottom quark, the next heaviest quark in the same generation. This parameter plays a role in B-meson and Higgs boson decays as they contain high power factors of m_b, the bottom quark mass [53–55]. These instances and many more call for precise theoretical predictions for these heaviest quark masses to relate to the advent of precise experimental observations. Defining a well-behaved perturbative quark mass presents unique challenges not found when considering theories such as QED and the electron mass. Many successful proposals have been considered and studied to very high precision in pure QCD. However, quarks also interact with the EW sector of the SM and thus, in this chapter, we will focus on determining the leading EW corrections to heavy quark mass schemes.

The SM is a perturbative quantum field theory, and in such theories, mass parameters are defined as the location of the single-particle pole in the two-point function. In the quark case, the pole or on-shell (OS) mass, m_Q, is given by requiring that the inverse of the heavy quark propagator with a momentum, p_Q, is a pole at the point $p_Q^2 = m_Q^2$ in momentum-space. Thus, the renormalisation scheme is fixed in this way, which is necessary for quantum corrections in perturbation theory. Although this definition is natural, it suffers when applied to quarks in QCD. At high energies, the pole mass includes large logarithms, which cause spurious

divergences. Moreover, due to the phenomenon of quark confinement, the non-perturbative regime of QCD does not have the requisite pole in the propagator. This leads to a confinement scale ambiguity in the OS definition for quark mass $m_Q \sim \Lambda_{\rm QCD}$, which is known as the $\mathcal{O}(\Lambda_{\rm QCD})$ renormalon problem [130, 286]. One, therefore, needs an alternative, a so-called running mass, $m_Q(\mu)$, where one absorbs said misbehaving non-perturbative contributions and is finite after renormalisation. Schemes that do not exhibit these IR divergences make up a family of short-distance mass definitions dependent on an additional scale, μ_f, which acts as a regulator for the spurious IR behaviour.

5.2 $\overline{\rm MS}$-scheme Electroweak Corrections

The primary short-distance mass candidate is the minimal subtracted ($\overline{\rm MS}$) mass, $\overline{m}(\mu)$, which is defined by regulating the field theory in dimensional regularisation and subtracting the UV divergences in the $\overline{\rm MS}$ renormalisation scheme. The t'Hooft mass from dimensional regularisation, μ, is generally chosen to be of the order of the characteristic energy scale of the process, Q, as perturbative calculations lead to large factors of $\ln^n(\mu/Q)$. One can then use RGE flow from a quark mass at one scale to that at another scale. In general, one can always write short-distance mass definitions in terms of the familiar OS mass by relating the bare mass, m^0. Explicitly, the $\overline{\rm MS}$-OS relation is given by comparing the two quantities,

$$m^0 = Z_m^{\rm OS} m, \quad m^0 = Z_m^{\overline{\rm MS}} \overline{m}, \tag{5.1}$$

which are finite by construction and related to the quark OS self-energy [142, 144, 145]. Thus, the ratio of the two quantities in Eq. (5.1), gives the $\overline{\rm MS}$-OS relation, which is a perturbative series in the QCD and EW couplings $\alpha_s(\mu)$ and $\alpha(\mu)$, respectively. The required renormalisation constants, $Z_m^{\overline{\rm MS}}$ and $Z_m^{\rm OS}$, have been determined to four-loops in pure QCD [133, 135, 143, 307, 307–310], and two-loop orders in the full SM [51, 145, 147–149].

We are primarily interested in leading EW effects as these have been scarcely considered, although in general, they contribute in the same order as their next-to-leading QCD counterparts. As described in Ref. [115], to determine the pole mass, m, of a fermion in the SM, we start with the propagator for a fermion of mass bare mass, m_0, and momentum, p,

$$S^{-1}(\not{p}) = \not{p} - m_0 - \Sigma(\not{p}), \tag{5.2}$$

where the self-energy function, $\Sigma(\not{p})$, is given by the sum of all one-particle-irreducible Feynman diagrams that contribute to the two-point function. A further subtlety in EW theory is the parity violation of the left- and right-handed quark fields, which causes them to propagate differently. Moreover, CP violation is avoided by taking the unit CKM matrix.

One can then decompose the self-energy as [311],

$$\Sigma(\not{p}) = P_L \not{p} A_L(p^2) + P_R \not{p} A_R(p^2) + m_0 B(p^2), \tag{5.3}$$

such that $P_{L/R} = (1 \mp \gamma_5)/2$ are the left- and right-handed projectors, respectively, $A_{L/R}$ and B are dimensionless scalar functions of p^2 dependent on SM parameters. The poles of $S(\not{p})$ have left- and right-handed components that coincide and are given by the solution to the equation at $p^2 = m^2$,

$$p^2[1 - A_L(p^2)][1 - A_R(p^2)] - m_0^2[1 + B(p^2)]^2 = 0, \tag{5.4}$$

which is solvable perturbatively as an expansion,

$$m = m_0(1 + X_1 + X_2 + \ldots), \tag{5.5}$$

where the X_k are given in Ref. [148] and the index k refers to the order in the couplings. One can then simply convert from the OS scheme to the $\overline{\text{MS}}$ scheme by keeping terms proportional to $\Delta = 1/\epsilon - \gamma_E + \ln 4\pi$, where γ_E is the Euler-Mascharoni constant.

Whence, we determine the ratio, eliminating m_0 from Eq. (5.1), providing us with the $\overline{\text{MS}}$-OS relation,

$$\overline{m} = m(1 - \overline{\delta}), \quad \overline{\delta} = \overline{\delta}^{\text{QCD}} + \overline{\delta}^{\text{QED}} + \overline{\delta}^{\text{W}}, \tag{5.6}$$

and in the case of leptons, the QCD contribution would not arise. To one-loop order we have [145],

$$\overline{\delta}_i^{\text{QCD}}(\mu) = C_F \frac{\alpha_s}{4\pi} (4 - 3L_i) \,. \tag{5.7}$$

wih quark labelling, i, and $L_A \equiv \ln(A^2/\mu^2)$ and $\overline{\delta}_f^{\text{QED}}$ is obtained from Eq. (5.7) by substituting $Q_f^2\alpha$ for $C_F\alpha_s$. In the large m_t limit, one can concisely express the EW contributions for top and bottom quarks as,

$$\overline{\delta}_t^{\text{W}} = \frac{G_F m_t^2}{8\pi^2\sqrt{2}} \left[2\pi r_{h,t} - \frac{N_c}{2} - 4 + \left(N_c + \frac{3}{2} \right) L_t \right], \tag{5.8a}$$

$$\overline{\delta}_b^{\text{W}} = \frac{G_F}{8\pi^2\sqrt{2}} \left\{ m_t^2 \left[\frac{5}{4} - \left(\frac{3}{2} - N_c \right) L_t - \frac{N_c}{2} \right] - \frac{M_H^2}{4} \right\}, \tag{5.8b}$$

where G_F is the Fermi constant, which is $G_F^{(0)} = \pi\alpha/(\sqrt{2}M_W^2 s^2)$ at tree-level. The remaining parameters are, $r_{i,j} \equiv m_i/m_j$, $c = \cos\theta_w = M_W/M_Z$, $s = \sin\theta_w$ such that θ_w is the weak mixing angle, M_H and $M_{W,Z}$ are the masses of the and weak and Higgs bosons, respectively. The expressions for the two-loop EW contributions at $\mathcal{O}(\alpha\alpha_s, \alpha^2)$ are given in Ref. [148].

We now have a valid short-distance mass definition that side-steps the IR ambiguities. Note that the $\overline{\text{MS}}$ mass is defined in the full theory where the heavy quark of interest is fully dynamical. This treatment and definition are valid for running the mass between some large scale, $\mu = Q$, down to the quark mass or so-called threshold scale [152], $\mu = m$. However, from an effective theory perspective [153], once one runs below to the low energy regime, $\mu < m$, the appropriate EFT is HQET [64, 72], in which the pole mass is no longer dynamical.

As is described in Ref. [56, 154], if one insists on renormalising $m(\mu)$ in the $\mu < m$ regime, non-physical large logarithms start to appear, which no longer improve the convergence of the higher-order quantum corrections. One requires new mass definitions, which both avoid the IR renormalon while being well-behaved near-threshold and below. We note that in this low-energy regime, the physics being described is that of NR heavy quarks in which one can employ effective theories to study physical phenomena such as HQET and NRQCD [72–74]. These effective theories and out-shoots have been thoroughly considered in pure QCD. Still, as we are primarily interested in EW effects, we refer the reader to Ref. [161] for recent consideration of the EW effects in said theories.

When dealing with NR heavy quarks, as introduced in Chapter 2.3, a range of successful mass definitions have been proposed and studied in the context of QCD. They are collectively referred to as the threshold masses [152], and fulfil both requirements: independence from the IR

renormalon and a well-behaved perturbative series below threshold energies. We will be exploring some of the more practical and popular masses; in particular, we will be explicitly considering the following definitions: the potential subtracted (PS) mass [57], the 1S mass [59,132], and the kinetic mass [56]. The PS and 1S mass depend on the perturbative potential, $V(\boldsymbol{r})$, of a heavy NR quark-antiquark pair (meson) system at fixed separation $\boldsymbol{r}$. The kinetic mass depends on said heavy meson's perturbative binding and residual kinetic energies, $\bar{\Lambda}$ and μ_π^2, respectively. Thus, our job is to begin by determining these energy parameters and procuring their leading EW corrections, as they are already known to three- and four-loop order in pure QCD [133,134,157].

5.3 Static Potential

As we thoroughly discuss evaluating the heavy quark potential in Chapter 4, we will only outline technical details in this section. The focus will be on elucidating the calculation further and focusing on the specific cases of top and bottom quarks in the SM. The heavy quark or static potential, as it is called, is a well-known parameter in QED. Moreover, it has been shown not to exhibit higher-order quantum corrections and instead is elegantly given by the standard Coulomb potential for two static point charges in electromagnetism [39]. However, in QCD, as it is a non-Abelian theory, quantum corrections do indeed arise, and these have been determined in the literature to three-loop orders [159, 265, 271, 274]. At one-loop in QCD the momentum-space potential with parameters renormalised in the $\overline{\text{MS}}$ scheme is given by [271],

$$V(\boldsymbol{q}^2) = -C_F \frac{4\pi\alpha_V(\boldsymbol{q}^2)}{\boldsymbol{q}^2}, \tag{5.9a}$$

$$\alpha_V(\boldsymbol{q}^2) = \alpha_s(\mu^2) \sum_{n=0}^{\infty} \tilde{a}_n \left(\frac{\boldsymbol{q}^2}{\mu^2}\right) \left(\frac{\alpha_s(\mu^2)}{4\pi}\right)^n \tag{5.9b}$$

where $\boldsymbol{q}$ is the transfer momentum between the scattered particles and,

$$\tilde{a}_1 = a_1 - \beta_0 L_{\boldsymbol{q}}, \qquad a_1 = \frac{31}{9} C_A - \frac{20}{9} T_f n_f \tag{5.10}$$

where $a_0 = \tilde{a}_0 = 1$. The colour factors, $C_F = (N_c^2 - 1)/(2N_c)$, $C_A = N_c$ and $T_f = 1/2$ arise from the colour gauge group, $\text{SU}(N_c)$, where N_c is the number of colours and in QCD $N_c = 3$. The number of light quarks which factor the light quark loops is given by n_f and $\beta_0 = 11C_A/3 - 4T_F n_f/3$ is the first coefficient of the QCD beta function. The strong-coupling constant renormalised in the $\overline{\text{MS}}$ scheme is denoted by α_s and the effective coupling, α_V, includes all higher order corrections in its definition. This coupling leads to a new coupling renormalisation scheme, the so-called V scheme [277], which defines the strong-coupling constant in terms of a potential.

The static potential is practically attained by considering the static limit of the vacuum transition amplitude, the so-called Wilson loop approach [159]. The limit is defined in coordinate-space by fixing the two heavy quark and antiquark to be stationary point sources a fixed distance apart. Employing this limit leads to source and anti-source vertices and propagators corresponding to the heavy quarks and antiquarks. Although the Wilson loop approach is technically simpler, we determined, in Chapter 4 that it is lacking when dealing with chiral gauge theories such as the SM. We found that one must employ the original scattering amplitude approach to attain the potential [160]. In this way, one computes the potential directly from the relativistic OS quark-antiquark scattering amplitude and taking the static or large quark mass and small

velocity limit. Although this is a textbook calculation in QED [281], we employed this approach in QCD to verify that it matches the Wilson loop result [271]. The upshot of the calculation is to determine the scattering amplitude of the process,

$$Q_1(p) + \bar{Q}_2(p') \to Q_1'(p-q) + \bar{Q}_2'(p'+q), \tag{5.11}$$

which to all orders results in an amplitude,

$$\mathcal{M} = (\bar{u}_1'\gamma^\mu u_1) D_{\mu\nu}(q) (\bar{v}_2\gamma^\nu v_2') \tag{5.12}$$

where $q^\mu = (0, \boldsymbol{q})$ is the transfer momentum and $i = 1, 2$ labels the masses. For instance, The QCD scattering amplitudes contributing up to NLO are represented in Fig. 4.4. After performing dimensional regularisation, the one-loop UV and IR divergences are removed by parameter renormalization in the $\overline{\text{MS}}$ scheme and on-shell WFR. Next, one takes the NR scattering limit, in which one expands in $|\boldsymbol{q}| \ll m_i$ and performs the NR expansion of four-component bi-spinors from the solution free-field NR Dirac equation for a particle with momentum p^μ and mass m_i,

$$u_i(p) \mapsto \sqrt{2m_i} \begin{bmatrix} \xi_i \\ \frac{\boldsymbol{\sigma}\cdot\boldsymbol{p}}{2m_i}\xi_i \end{bmatrix}, \quad v_i(p) \mapsto \sqrt{2m_i} \begin{bmatrix} \frac{\boldsymbol{\sigma}\cdot\boldsymbol{p}}{2m_i}\xi_i \\ \xi_i \end{bmatrix}. \tag{5.13}$$

where $\boldsymbol{\sigma}$ are the Pauli matrices and ξ_i are two-component spinors. After the amplitude is evaluated and renormalised, one may then expand the Dirac spinor chains that arise in terms of Pauli matrices and two-component spinors. Taking the $\boldsymbol{q}^2 \to 0$ limit leaves one with the following amplitude,

$$\mathcal{M} = -2m_1 m_2 \left(\xi_1^\dagger \xi_2^\dagger U(\boldsymbol{q}, \boldsymbol{p}, \boldsymbol{p'}) \xi_1 \xi_2 \right) \tag{5.14}$$

where the potential is of the form,

$$U(\boldsymbol{q}, \boldsymbol{p}, \boldsymbol{p'}) = V(\boldsymbol{q}) + \mathcal{O}(\boldsymbol{q}^0) + \mathcal{O}(\boldsymbol{q}^2, \text{spin-dep.}), \tag{5.15}$$

such that $V(\boldsymbol{q})$ is precisely the Coulomb-like term of $\mathcal{O}(1/\boldsymbol{q}^2)$ and thus picking this out from the full expression gives the momentum-space static potential. At leading order, we may drop contact terms, $\mathcal{O}(\boldsymbol{q}^0)$, and contributions from insertions of Pauli matrices, i.e., spin-dependent terms, as these contribute at $\mathcal{O}(\boldsymbol{q}^2)$. Extending this approach to the full SM is analogous, expanding the scattering amplitudes illustrated in Fig. 4.5 with all possible QCD and EW interactions. After renormalising all parameters in the $\overline{\text{MS}}$ scheme and applying WFR in the OS scheme, one then commits to the NR limit, $m_i \gg |\boldsymbol{q}|$, where labels i grant the possibility of working with quarks of different masses. Whence, one has three cases to consider,

$$V_{ij}^{\text{SM}} = V^{\text{QCD}} + V^{\text{QED}} + \delta V_{(i,j)}^{\text{SM}}, \tag{5.16}$$

as $\delta V_{(i,j)}^{\text{SM}}$ is the one-loop EW contribution, the leading of which is of $\mathcal{O}(\alpha\alpha_s, \alpha^2)$. The full expressions for $\delta V_{(i,j)}^{\text{SM}}$ are given in an arXiv ancillary file of Ref. [264], and to one-loop order have the general form,

$$\delta V_{(i,j)}^{\text{SM}} = \frac{\alpha\alpha_s}{\boldsymbol{q}^2} c_{(i,j)} + \frac{\alpha^2}{\boldsymbol{q}^2} \left(d_{(i,j)} + e_{(i,j)} L_{\boldsymbol{q}} \right). \tag{5.17}$$

We present the limit $m_t \gg M_{\rm EW}, m_b \gg |\boldsymbol{q}|$, for top and bottom quarks. Further limits, including the more physical limit $m_t \sim M_{\rm EW} \gg m_b \gg |\boldsymbol{q}|$, can be considered from the full expressions. The useful quantities for threshold masses are $\delta V^{\rm SM}_{(i,i)}$ and have the following leading terms,

$$\begin{aligned}\delta V^{\rm SM}_{(t,t)} = \frac{\alpha\alpha_s}{\boldsymbol{q}^2}\frac{C_F}{s^2}\Bigg[&\left(r_{t,w}^2 - \frac{1}{4} - \frac{21r_{h,z}^2}{16c^2}\right)L_{z,h} + \left(\frac{7s^2}{36} + r_{t,w}^2 + \frac{16s^2}{9} - \frac{7}{36c^2} - \frac{21\tilde{r}_{h,z}^2}{16c^2}\right)L_{t,z} \\ &+ \frac{\tilde{r}_{h,z}^2}{2c_w^2} - \frac{1}{4} - \frac{1}{2c^2} + 3\pi\frac{r_{t,w}r_{h,w}}{2} + \frac{1}{4}L_{h,w}\Bigg] + \frac{\alpha^2}{\boldsymbol{q}^2}\Bigg[\frac{4N_s}{3}Q_t^2\left(\frac{5}{3} - L_{\boldsymbol{q}}\right) - \frac{8}{27} + \frac{2}{9s^2} \\ &+ \frac{1}{96s^4} + 2\pi\frac{r_{t,w}r_{h,w}}{3s^2} - \frac{37}{144c^2s^2} + \frac{2r_{h,z}^2}{9c^2s^2} + \frac{25}{864c^4} + \frac{28}{9}L_w - \left(\frac{5}{18s^2} + \frac{r_{t,w}^2}{6s^2}\right)L_{h,w} \\ &+ \left(\frac{5}{288c^2s^2} + \frac{5}{144\tilde{r}_{h,z}^2c^2s^2} + \frac{5r_{t,w}^2}{18s^2} - \frac{5}{18s^2} - \frac{1}{192s^4} - \frac{1}{96\tilde{r}_{h,z}^2s^4} - \frac{7r_{h,z}^2}{12c^2s^2}\right. \\ &\left. - \frac{25}{1728c^4} - \frac{25}{864\tilde{r}_{h,z}^2c^4}\right)L_{z,h} + \left(\frac{64}{81} - \frac{13}{162s^2} + \frac{5r_{t,w}^2}{18s^2} - \frac{7}{81c^2s^2} - \frac{7r_{h,z}^2}{12c^2s^2}\right)L_{t,z}\Bigg],\end{aligned} \tag{5.18}$$

$$\begin{aligned}\delta V^{\rm SM}_{(b,b)} = \frac{\alpha\alpha_s}{\boldsymbol{q}^2}\frac{C_F}{s^2}\Bigg[&\left(\frac{7}{4} - \frac{17r_{h,z}^2}{16c^2}\right)L_{z,h} + \left(\frac{4s^2}{9} + \frac{55}{36} - \frac{85}{144c^2} - \frac{17\tilde{r}_{h,z}^2}{16c^2}\right)L_{b,z} + \frac{\tilde{r}_{h,z}^2}{2c_w^2} - \frac{3}{4} \\ &- L_{t,h} + \frac{3}{4}L_{h,w}\Bigg] + \frac{\alpha^2}{\boldsymbol{q}^2}\Bigg[\frac{4N_s}{3}Q_b^2\left(\frac{5}{3} - L_{\boldsymbol{q}}\right) + \frac{1}{12s^2} + \frac{1}{96s^4} - \frac{1}{144c^2s^2} + \frac{\tilde{r}_{h,z}^2}{18c^2s^2} \\ &+ \frac{1}{864c^4} + \frac{2}{27} + \frac{7}{9}L_w - \frac{1}{9s^2}L_{t,h} + \left(\frac{4}{81} - \frac{17\tilde{r}_{h,z}^2}{144c^2s^2} - \frac{85}{1296c^2s^2} + \frac{7}{81s^2}\right)L_{b,z} \\ &+ \left(\frac{1}{9s^2} - \frac{1}{192s^4} - \frac{1}{96\tilde{r}_{h,z}^2} - \frac{11}{96c^2s^2} + \frac{1}{144\tilde{r}_{h,z}^2c^2s^2} - \frac{17\tilde{r}_{h,z}^2}{144c^2s^2} - \frac{1}{864\tilde{r}_{h,z}^2c^4}\right. \\ &\left. - \frac{1}{1728c^4}\right)L_{z,h}\Bigg],\end{aligned} \tag{5.19}$$

such that $N_l = (N_c[Q_u^2 n_u + Q_d^2 n_d] + n_g)$ correspond to light fermion loop factors, where n_u and n_d are the number of up- and down-like light quarks, respectively, and analagously for the electro-magnetic charges, Q_u and Q_d. N_c is the number of light quark colours and n_g are the number of lepton generations. The logarithms are represented as previously shown in Eq. (5.1) and $L_{A,B} \equiv L_A - L_B$. We note that Eqs. (5.18) and (5.19) represent color singlet contributions to the potential. Their color octet counterparts emerge via the simple replacement $C_F \to -1/(2C_A)$.

5.4 Binding and residual kinetic energy

With the potential at hand, what remains to determine are the heavy meson BE and residual KE parameters, $\bar{\Lambda}(\mu_f)$ and $\mu_\pi^2(\mu_f)$. The energies are attainable perturbatively from the forward scattering amplitude of an arbitrary non-flavour changing external current, J, and heavy quark, Q, as shown in Fig. 5.1. The amplitude can be written in momentum-space as,

$$T(q) = \frac{i}{2m}\int d^4x e^{-iq\cdot x}\left\langle Q\right|\mathcal{T}J(x)J^\dagger(0)\left|Q\right\rangle, \tag{5.20}$$

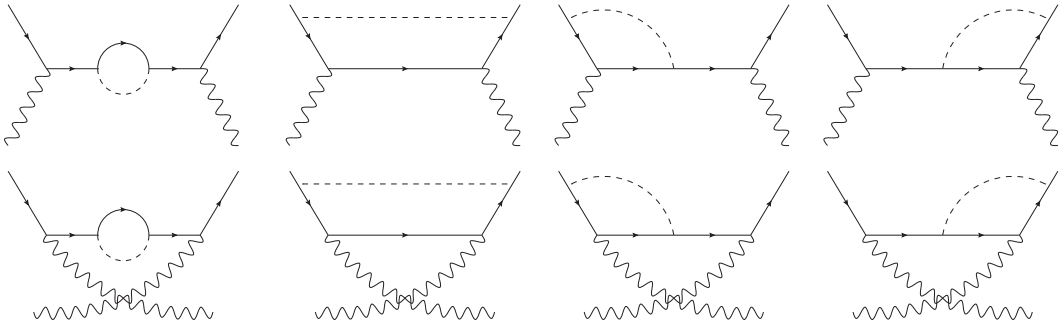

Figure 5.1: One-loop Feynman diagrams for scattering of an external current (wavy line) and a heavy quark (solid line). The dotted lines represent boson propagators.

where $\mathcal{T}$ is the usual time-ordering and q is an external momentum. The heavy quark is on-shell with momentum, $p^\mu = (0, m)$, and thus, $p^2 = m^2$ and $s = (p+q)^2$. From this amplitude one can then obtain the perturbative BE and KE from the following integrals,

$$\bar{\Lambda}(\mu_f) = \frac{2}{\boldsymbol{v}^2} \frac{\int_0^{\mu_f} d\omega W(\omega, \boldsymbol{v})\omega}{\int_0^{\mu} d\omega W(\omega, \boldsymbol{v})}\bigg|_{\boldsymbol{v}\to 0, m\to\infty} \tag{5.21}$$

$$\mu_\pi^2(\mu_f) = \frac{3}{\boldsymbol{v}^2} \frac{\int_0^{\mu_f} d\omega W(\omega, \boldsymbol{v})\omega^2}{\int_0^{\mu} d\omega W(\omega, \boldsymbol{v})}\bigg|_{\boldsymbol{v}\to 0, m\to\infty}, \tag{5.22}$$

where $\boldsymbol{q} = \boldsymbol{v}/m$, the structure function $W(q) = 2\mathrm{Im}[T(q)]$ and the large m-limit is always taken firstly as otherwise terms that contribute will be dropped. We then re-express our amplitude in terms of the excitation energy of the system [286],

$$\omega \equiv q_0 - q_0^{\min} = q_0 - \frac{m\boldsymbol{v}^2}{2} + \mathcal{O}(\boldsymbol{v}^4), \tag{5.23}$$

and velocity, $\boldsymbol{v}$. The threshold value at $s = m^2$ is given at,

$$q_0^{\min} \equiv \sqrt{\boldsymbol{q}^2 + m^2} - m = \frac{m\boldsymbol{v}^2}{2} + \mathcal{O}(\boldsymbol{v}^4), \tag{5.24}$$

where for smaller values of s, the structure function and energy parameters of interest vanish. Practically when determining the amplitude, it is convenient to first express the NR parameters, ω and $\boldsymbol{v}$, in terms of Lorentz invariant quantities,

$$y \equiv m^2 - s = -m\omega(2 + \boldsymbol{v}^2) + \mathcal{O}(\boldsymbol{v}^4, \omega^2) \leq 0 \tag{5.25}$$

$$, q^2 \equiv m^2 - s = -m\boldsymbol{v}^2(m - \omega) + \mathcal{O}(\boldsymbol{v}^4, \omega^2) \leq 0 \tag{5.26}$$

in doing so one simplifies the computation and upon extracting the imaginary part to determine the structure function, one can then do the expansion in terms of original NR parameters to perform the integrals in Eq. (5.22). We also note that the structure function is IR finite and that at the one-loop order, which we are considering, the renormalisation of SM parameters as well as WFR for the external quarks are not necessary as they do not contribute to the imaginary part of the forward scattering amplitude [157, 286].

5.5 Potential subtracted and 1S mass

With the above quantities at hand we may tackle the PS mass which arises from the NR limit of heavy quark-antiquark systems. As introduced in Chapters 3 and 4, the PS is determined in general by the Schrödinger equation,

$$\left(-\frac{\nabla^2}{m}+V(\boldsymbol{r})-E\right)G(\boldsymbol{r},0,E)=\delta^{(3)}(\boldsymbol{r}), \tag{5.27}$$

such that $V(\boldsymbol{r})$ is the NR or static potential and $E=\sqrt{s}-2m$ is the binding energy. Thus, one can write the total static energy of two heavy quarks separated by a fixed distance, $\boldsymbol{r}$, as [57,59]

$$E_{\rm stat}(\boldsymbol{r})=2m+V(\boldsymbol{r}). \tag{5.28}$$

As Eq. (5.28) is a well-defined physical quantity, it has been shown not to suffer from IR divergences in higher-order quantum corrections. Moreover, the IR ambiguities in the pole mass definition have been shown to cancel with the IR ambiguities of the static potential. This convenient cancellation is the impetus for defining the PS mass and is made explicit when considering the coordinate-space potential,

$$V(\boldsymbol{r})=\int \not{d}^3\boldsymbol{q}e^{i\boldsymbol{q}\cdot\boldsymbol{r}}V(\boldsymbol{q}). \tag{5.29}$$

It is known that the coordinate-space potential is sensitive to IR physics while the momentum-space potential is not [57]. This sensitivity is due to the contribution in the Fourier transform integral from regions of small $|\boldsymbol{q}|$, which results in the leading renormalon behaviour of $V(\boldsymbol{r})$. One can then define a subtracted potential,

$$V(\boldsymbol{r},\mu_f)=V(\boldsymbol{r})+2\delta^{\rm PS}(\mu_f), \tag{5.30}$$

for a newly introduced IR-cut off scale, μ_f and isolate the renormalon contribution through a mass definition,

$$m^{\rm PS}(\mu_f)=m-\delta^{\rm PS}(\mu_f), \tag{5.31}$$

such that the PS mass counter-term is given by,

$$\delta^{\rm PS}(\mu_f)=-\frac{1}{2}\int_{|\boldsymbol{q}|<\mu_f}\not{d}^3\boldsymbol{q}V(\boldsymbol{q}). \tag{5.32}$$

Thus, employing the PS mass and subtracted potential in Eq. (5.27) results in quark mass without leading non-perturbative ambiguities.

Of course, with this procedure, one has only swept the large loop corrections from $\delta m(\mu_f)$ to $m_{\rm PS}(\mu_f)$. However, when $m_{\rm pole}$ is expressed in terms of a short-distance mass parameter, such as the $\overline{\rm MS}$ mass through a perturbative series, this series will also contain large loop corrections [56]. Conveniently, these perturbative corrections cancel with large perturbative corrections to the pole mass in $\delta^{\rm PS}$. In this way, one may determine the $\overline{\rm MS}$ mass from threshold cross sections with better accuracy than the pole mass, the use of which implicitly contains the non-subtracted potential. Let us now compute $\delta m(\mu_f)$ from the definition in Eq. (4.53). We then obtain

$$\begin{aligned}\delta_i^{\rm PS}(\mu_f)=&C_F\frac{\alpha_s}{\pi}\mu_f\left(1+\frac{\alpha_s}{4\pi}\left[a_1+2\beta_0\left(\ln\frac{\mu}{\mu_f}+1\right)\right]\right)+\\&\frac{\alpha}{\pi}\mu_f\left(Q_i^2+\frac{\alpha_s}{4\pi}c_{(i,i)}+\frac{\alpha}{4\pi}\left[d_{(i,i)}+2e_{(i,i)}\left(\ln\frac{\mu}{\mu_f}+1\right)\right]\right),\end{aligned} \tag{5.33}$$

The PS mass and kinetic mass, are defined by introducing a new explicit IR factorization scale, μ_f, to remove the leading IR ambiguity of the pole mass. By contrast, the 1S mass [59], $m^{\rm 1S}$, achieves a similar goal without introducing a new factorization scale. The 1S mass is defined as one-half of the perturbative energy of the 1S heavy $q\bar{q}$ bound state,

$$m^{\rm 1S}(\mu) = \frac{1}{2}(m^{\rm 1S}_{q\bar{q}})_{\rm pert} \equiv m(1-\delta^{\rm 1S}(\mu)). \tag{5.34}$$

The ground state energy calculated from the Schrödinger equation of quantum mechanics is exactly $(m^{\rm 1S}_{q\bar{q}})_{\rm pert}$. At leading order in the expansion in the relative velocity of the (anti)quark in the $q\bar{q}$ rest frame (threshold region), the dynamics of the $q\bar{q}$ pair is governed by the Hamiltonian [288],

$$H = -\frac{\boldsymbol{\nabla}^2}{m_Q} + V(\boldsymbol{r}) + U(\boldsymbol{q},\boldsymbol{r}), \tag{5.35}$$

where m_Q is the quark pole mass, $V(\boldsymbol{r})$ is the static potential, the analogue of the Coulomb potential, and $U(\boldsymbol{q},\boldsymbol{r})$ encodes higher-order corrections in the small-velocity expansion and is the SM analogue of the Breit potential [160]. The leading contributions at threshold come from the static potential, so that we may omit $U(\boldsymbol{q},\boldsymbol{r})$ from our calculation. Solving for the S-wave Green's function, we have

$$G(E) = \langle 0|\,\hat{G}(E)\,|0\rangle = \langle 0|\,\frac{1}{H-E-i\delta}\,|0\rangle\,, \tag{5.36}$$

where $\langle 0|$ denotes a position eigenstate with eigenvalue $|\boldsymbol{r}|= 0$, and the Green's function has single poles at the exact S-wave energy levels, $E = E_n$,

$$G(E) \overset{E\to E_n}{=} \frac{|\psi_n(0)|^2}{E_n - E - i\delta}. \tag{5.37}$$

From this expression, one gets $(m^{\rm 1S}_{q\bar{q}})_{\rm pert} = E_1$, and expanding $E_1/2$ in small SM couplings gives the 1S mass, which is the SM analogue of the well-known Bohr potential of quantum mechanics. We may then find the leading EW corrections at one-loop to the 1S mass with our SM potential, as only the QCD corrections are known, and they have been found to N^{3}LO [289]. At one-loop through third order in the SM couplings, α and α_s, we have

$$\begin{aligned}
\delta_i^{\rm 1S} =& \frac{(\alpha Q_i^2 + \alpha_s C_F)}{16\pi}\left\{\alpha^2 B_i + \alpha(\alpha_s c_{(i,i)} + 2\pi Q_i^2)\right. \\
&\left. +\alpha_s C_F(\alpha_s A_i + 2\pi)\right\}, \\
A_i =& 2\beta_0(l_i+1) + a_1, \\
B_i =& 2e_{(i,i)}(l_i+1) + d_{(i,i)},
\end{aligned} \tag{5.38}$$

where m_i is the pole mass of heavy quark i and $l_i \equiv \ln[\mu/(C_F\alpha_s(\mu)m_i)]$. We further note that the IR renormalon cancellation is more subtle in the 1S mass definition, as the latter is a well-behaved parameter only if the orders of terms in perturbation theory are re-interpreted [59].

5.6 Kinetic Mass

On the other hand, the kinetic mass is defined directly by the heavy quark BE and residual KE, as shown by its relation to the pole mass,

$$m^{\rm kin}(\mu_f) = m\left(1 - \delta^{\rm kin}(\mu_f)\right) \tag{5.39}$$

$$\delta^{\rm kin}(\mu_f) = \frac{\bar{\Lambda}(\mu_f)}{m} + \frac{\mu_\pi^2(\mu_f)}{2m_{\rm kin}m} \tag{5.40}$$

The leading EW corrections may then be determined at one-loop with the BE and residual KE by evaluating Eq. (5.22). The QCD corrections are known, and they have been found to N^{3}LO [157]. At one-loop we have the following relation with both QCD and EW contributions in the large quark mass limit,

$$\delta_t^{\rm kin}(\tilde{\mu}) = \tilde{\mu}\left\{\frac{4}{3}\frac{C_F\alpha_s}{\pi} + \frac{\alpha}{\pi}\left(\frac{4}{3}Q_t^2 - \frac{1}{16}\frac{r_{t,w}^2}{s^2} - \frac{1}{4}\frac{1}{s^2}\right)\right\}, \tag{5.41}$$

$$\delta_b^{\rm kin}(\tilde{\mu}) = \tilde{\mu}\left\{\frac{4}{3}\frac{C_F\alpha_s}{\pi} + \frac{\alpha}{\pi}\left(\frac{4}{3}Q_b^2 - \frac{1}{24}\frac{r_{b,w}^2}{s^2} - \frac{1}{6}\frac{1}{s^2} - \frac{1}{24}\frac{r_{t,w}^2}{s^2}\right)\right\} \tag{5.42}$$

such that $\tilde{\mu} \equiv \frac{\mu_f}{m} + \frac{3}{8}\frac{\mu_f^2}{m^2}$, m_i is the pole mass of heavy quark i and the scale μ_f labels the usual IR Wilsonian cut-off. Using the $\overline{\rm MS}$-OS relations in Eq. (5.6), we may express the kinetic mass in terms of the $\overline{\rm MS}$ mass to one-loop order,

$$m_i^{\rm kin}(\bar{m}_i) = \bar{m}_i\left(1 + \overline{\delta}_i(\bar{m}_i) - \delta_i^{\rm kin}(\bar{m}_i)\right). \tag{5.43}$$

The relation is given by Eq. (5.43) with the direct replacement of the pole mass with $\bar{m}$ dropping higher-order terms in small coupling expansion contributing past NLO.

5.7 Numerical Estimates

We are now able to provide numerical estimates to our heavy quark short-distance mass relations at the standard scale $\mu = M_Z$ from Ref. [167]. In the case of the PS and kinetic masses we select the IR cut-off scale to be, $\mu_f = 3$ GeV, a typical scale for heavy quarks. Moreover, we take $n_f = 4$, $n_u = n_d = 2$ and $n_l = 3$ and run the strong and EW couplings to the Z-boson mass scale. We then obtain the contributions up to one-loop order for the mass definitions studied here,

$$\overline{\delta}_t = 0.015\alpha_s + 2.01\alpha, \quad \overline{\delta}_b = 0.015\alpha_s + 0.65\alpha. \tag{5.44a}$$

$$\delta_t^{\rm kin} = 0.010\alpha_s - 0.018\alpha, \quad \delta_b^{\rm kin} = 0.427\alpha_s - 0.701\alpha, \tag{5.44b}$$

$$\delta_t^{\rm PS} = \alpha_s(1.27 + 8.06\alpha_s + 6.83\alpha) + \alpha(0.42 + 2.34\alpha), \tag{5.44c}$$

$$\delta_b^{\rm PS} = \alpha_s(1.27 + 8.06\alpha_s + 1.25\alpha) + \alpha(0.11 - 0.18\alpha), \tag{5.44d}$$

$$\delta_t^{\rm 1S} = 0.22\alpha_s^2 + 1.51\alpha_s^3 + 0.02\alpha^2 + 0.71\alpha^3 + 0.15\alpha_s\alpha - 2.89\alpha_s^2\alpha + 2.93\alpha_s\alpha^2, \tag{5.44e}$$

$$\delta_b^{\rm 1S} = 0.22\alpha_s^2 + 3.61\alpha_s^3 + 0.002\alpha^2 + 0.04\alpha^3 + 0.04\alpha_s\alpha + 0.74\alpha_s^2\alpha + 0.48\alpha_s\alpha^2. \tag{5.44f}$$

Therefore, we can conclude that although the novel EW contributions are significantly smaller than the pure QCD contributions at NLO, they are comparable to QCD corrections at NNLO and

beyond. Whence, for high-precision determination of short-distance mass definitions, the EW corrections must be taken into account. At this point, we briefly mention that the definitions we studied, although often employed, do not represent an exhaustive list. For instance, there are the RS [131] and RGI [312] masses as well as the more recently proposed MRS mass [60]. Moreover, there are ways to refine studies when converting between short-distance mass definitions [313]. In this scheme, one takes the IR factorisation scale, μ_f, to be a continuous parameter and studying the RG flow in μ_f of the masses, one can avoid large logarithms of cut-off scales, $\ln(\mu_f'/\mu_f)$.

5.8 Technical Details

Our calculations of the one-loop corrections to the heavy quark masses were performed using standard tools. The Feynman amplitudes were reduced to a few master integrals, which were found analytically since all one-loop master integrals are known. We achieved this with the help of the algebraic manipulation program `Mathematica` accompanied by the program package `FeynCalc` [298] to compute the necessary amplitudes and to deal with the algebra. We employed further sub-packages of `FeynCalc`, such as `FeynHelpers` [299], which reduces and provides explicit expressions for one-loop scalar integrals by connecting the reduction package `fire` [300] with the analytic scalar-integral package `Package-X` [301]. Lastly, we employed the `FeynOnium` [302] subpackage, which comes equipped with functions for dealing with amplitudes in the NR limit.

5.9 Summary

In this chapter, we determined the EW corrections to heavy-quark energy parameters up to NLO. By mapping these parameters accordingly, we illustrated how they modify a range of often-employed short-distance mass definitions. Moreover, we provided numerical estimates for comparing the EW corrections at NLO versus pure QCD contributions in the same order. The contributions from the EW regime were significant and comparable to pure QCD contributions at NNLO. The groundwork laid here may be incorporated and expanded on in future high precision studies. For instance, to match the $\mathrm{N^3LO}$ precision in QCD, it is necessary to determine the NNLO EW corrections in the mass definitions studied here and others mentioned. Moreover, the theoretical framework we introduce can help study the NR regime of theories beyond the SM.

Chapter 6

Matching the Standard Model to HQET and NRQCD

In this Chapter we determine the leading electroweak corrections to the HQET/NRQCD Lagrangian. These corrections appear in the Wilson coefficients of the two- and four-quark operators and are considered here up to $\mathcal{O}(1/m^3)$ at EW one-loop order. The two-quark operators up to this order will include new parity-violating terms, which we derived analogously to the parity-preserving QCD result at one-loop order. This Chapter is based on Ref. [161], reflecting the author's contribution.

6.1 Motivation

This Chapter is mainly concerned with extending the framework of HQET and NRQCD from pure QCD to the full SM. As we only briefly motivated these two EFTs in Chapter 3, we will re-introduce them here and delve deeper into their properties. Originally, HQET and NRQCD were developed to take advantage of the fact that the masses of the heavy quarks are much larger than the remaining dynamical scales being considered.

More specifically, HQET has mainly been employed to study systems with a single heavy quark [71, 72, 314]. In these studies, when considering heavy-light systems, the authors reduce the problem down to one with two dynamical scales; the heavy quark mass, m_Q, and the rest which is chosen to be the quark confinement scale, Λ_{QCD}, the scale of all processes in pure QCD - i.e. independent of quark mass. One then constructs the HQET Lagrangian as a power series in the inverse heavy quark pole mass. One can then estimate the size of each term by assigning the scale Λ_{QCD} to every parameter present other than the heavy quark mass. One is then left with operators exhibiting two distinct structures; terms containing light degrees of freedom describing gluons and light quarks; or terms that are bi-linear in the heavy quark fields.

On the other hand, we have NRQCD which is mostly employed to study systems with a heavy quark and antiquark, $Q\bar{Q}$, bound state [73, 74]. In NRQCD one usually takes into account two additional dynamical scales, the relative momentum, $\boldsymbol{q} \sim mv \sim \Lambda_{\text{QCD}}$, such that v is the relative velocity of the $Q\bar{Q}$ combination, and binding energy, $E \sim mv^2$, of the $Q\bar{Q}$ bound state. These extra scales add increased complexity to the power counting rules. Thus the size of each term in the NRQCD Lagrangian is no longer unique but dependent on the system under consideration. One can, however, still provide reasonable estimates of each term with velocity counting rules [74, 315]. The difference between HQET and NRQCD is immediately clear by

considering the first two bi-linear terms in the effective Lagrangian,

$$\mathcal{L} = \bar{Q}\left(iD^0 + \frac{\boldsymbol{D}^2}{2m}\right)Q. \tag{6.1}$$

To compare the two theories, one can note that the first term and second term are $\mathcal{O}(\Lambda_{\rm QCD})$ and $\mathcal{O}(\Lambda^2_{\rm QCD}/m)$, respectively, in HQET while both terms are of order $mv^2 \sim \mathcal{O}(\Lambda^2_{\rm QCD}/m)$ in NRQCD. Thus one can immediately note that the heavy quark propagator in HQET is $i/(k^0+i\epsilon)$ while in NRQCD the propagator is $i/(k^0 - \boldsymbol{k}^2/2m + i\epsilon)$. The NRQCD Lagrangian mimics the HQET Lagrangian in that it consists of terms in a power series expansion in heavy quark mass. It contains two and four fermion operators, i.e. terms bi-linear in the heavy (anti)quark fields and terms bi-linear in both heavy quark and antiquark fields, respectively.

Our work is focused on calculating the primary building block of an effective theory, the EFT Lagrangian and its matching to the full theory Lagrangian. The matching process is achievable by ensuring that the full and effective theory S-matrix elements are equal. Both the NRQCD and HQET matching conditions are computed in the same way, and the Lagrangians are thus identical [218]. The parameters that are modified by the matching procedure are called the matching (or Wilson) coefficients, which factor each operator in the EFT. The matching in NRQCD is then achieved order by order in the strong coupling, α_s, and inverse heavy quark mass [316].

This study will focus on extending the NRQCD Lagrangian and considering the leading EW corrections to one-loop order with terms up to and including $\mathcal{O}(\alpha\alpha_s/m^3, \alpha^2/m^2)$, for the two and four fermion operators of NRQCD. Although the Wilson coefficients are known in the EFT up to $\mathcal{O}(\alpha_s^2/m^4)$, the EW corrections have not yet been considered. They must be incorporated since at leading order they start altering the matching coefficients at the same order as the higher-order QCD terms. Whence, we study the effect at leading order of incorporating the EW contributions and noticing how the matching coefficients are improved.

Moreover, the Lagrangian itself must be extended to include parity-violating operators for the matching procedure to hold with the SM. The utility of our efforts lies in the prolific use of heavy quark effective theories for high precision observable predictions at threshold energies which would be the primary purpose of a future collider [317]. For instance, with regards to the top quark mass determination, which is crucial for understanding the stability of the EW vacuum [33]. Many so-called threshold quark mass definitions [57, 131, 133] have arisen from the HQ EFT frameworks and we know that the EW sector plays a crucial role in determining the $\overline{\rm MS}$ mass of the top quark [146, 147] thus it stands to reason that the same is true for the threshold mass definitions.

6.2 The Lagrangian

The continuum NRQCD Lagrangian up to the same order we are considering have previously been computed [218, 316] using dimensional regularisation for the IR and UV divergences taking the external states to be on shell. To express the NRQCD effective Lagrangian, one must consider heavy fermions and antifermions coupled to non-Abelian gauge fields, enforcing *Hermicity*, *parity*, *time-reversal* and *rotational invariance* [236]. One can further perform heavy field re-definitions to eliminate time derivatives acting on the heavy fermions at higher orders in $1/m$, this is known as the *canonical form* of the heavy particle Lagrangian [318]. Note that when employing the NRQCD Lagrangian which we define below, NRQCD has a UV cut-off, $\nu_{\rm NR} = \{\nu_p, \nu_s\}$, where $mv \ll \nu_{\rm NR} \ll m$, which corresponds to integrating out the hard modes of QCD to obtain NRQCD [319]. More specifically, ν_p is the UV cut-off of the relative three

momentum between the heavy quark and antiquark while ν_s is the UV cut-off of the three-momentum of the gluons and light quarks. The NRQCD Lagrangian including light fermions reads (up to field redefinitions) is [73, 233, 251],

$$\mathcal{L} = (\mathcal{L}_\psi + \mathcal{L}_\chi + \mathcal{L}_{\psi\chi}) + \mathcal{L}_g + \mathcal{L}_l, \tag{6.2}$$

such that ψ and χ are the Pauli spinors that annihilate a fermion and create an anti-fermion, respectively. We are mainly interested in the bracketed parts of the Lagrangian as these terms will attain the leading EW corrections to their matching coefficients. More explicitly, the Lagrangian for heavy quarks of masses $m_{1,2} \gg \Lambda_{\rm QCD}$ and velocity, v, in a frame where $v = (1, \mathbf{0})$ has bi-linear terms (up to the order we are considering) [73, 218, 320],

$$\begin{aligned}\mathcal{L}_{\psi,\chi} = \psi^\dagger \Bigg\{ & ic_0 D_t + c_2 \frac{\boldsymbol{D}^2}{2m} + c_4 \frac{\boldsymbol{D}^4}{8m^3} + c_{\rm F} g_s \frac{\boldsymbol{\sigma}\cdot\boldsymbol{B}}{2m} + c_{\rm D} g_s \frac{[\boldsymbol{D}\cdot\boldsymbol{E}]}{8m^2} + ic_{\rm S} g_s \frac{\boldsymbol{\sigma}\cdot(\boldsymbol{D}\times\boldsymbol{E} - \boldsymbol{E}\times\boldsymbol{D})}{8m^2} \\ & + c_{{\rm W}_1} g_s \frac{\{\boldsymbol{D}^2, \boldsymbol{\sigma}\cdot\boldsymbol{B}\}}{8m^3} - 2c_{{\rm W}_2} g_s \frac{\boldsymbol{D}_i \boldsymbol{\sigma}\cdot\boldsymbol{B}\boldsymbol{D}_i}{8m^3} + c_q g_s \frac{\boldsymbol{\sigma}\cdot\boldsymbol{D}\boldsymbol{B}\cdot\boldsymbol{D} + \boldsymbol{D}\cdot\boldsymbol{B}\boldsymbol{\sigma}\cdot\boldsymbol{D}}{8m^3} \\ & + ic_{\rm M} g_s \frac{\boldsymbol{D}\cdot[\boldsymbol{D}\times\boldsymbol{B}] + [\boldsymbol{D}\times\boldsymbol{B}]\cdot\boldsymbol{D}}{8m^3} \Bigg\} \psi + ({\rm h.c},\, \psi \leftrightarrow \chi) + \mathcal{O}(1/m^4, g_s^2/m^3),\end{aligned} \tag{6.3}$$

and four quark operators given by [321],

$$\begin{aligned}\mathcal{L}_{\psi\chi} = & \frac{d_{ss}}{m_1 m_2} \psi_1^\dagger \psi_1 \chi_2^\dagger \chi_2 + \frac{d_{sv}}{m_1 m_2} \psi_1^\dagger \boldsymbol{\sigma} \psi_1 \chi_2^\dagger \boldsymbol{\sigma} \chi_2 \\ & + \frac{d_{vs}}{m_1 m_2} \psi_1^\dagger T^a \psi_1 \chi_2^\dagger T^a \chi_2 + \frac{d_{vv}}{m_1 m_2} \psi_1^\dagger T^a \boldsymbol{\sigma} \psi_1 \chi_2^\dagger T^a \boldsymbol{\sigma} \chi_2,\end{aligned} \tag{6.4}$$

The terms in this Lagrangian require some unpacking; the covariant derivative is $D^\mu = \partial^\mu + ig_s A_a^\mu T^a \equiv (D^0, -\boldsymbol{D})$ defined in the usual way, $iD_t = i\partial_t - g_s A_0$ and $i\boldsymbol{D} = i\boldsymbol{\partial} + g_s \boldsymbol{A}$, with combinations thereof, $\boldsymbol{B}^i = \frac{i}{2g_s}\epsilon_{ijk}[\boldsymbol{D}_j, \boldsymbol{D}_k]$ and $\boldsymbol{E} = -\frac{i}{g_s}[D_t, \boldsymbol{D}]$. Moreover, covariant derivatives in square brackets act only on the fields within the brackets. The subscripts F,S and D on the Wilson coefficients stand for *Fermi*, *spin-orbit* and *Darwin*, respectively. We use the common summation convention, $X^i Y^i \equiv \sum_{i=1}^3 X^i Y^i$, and define $[X, Y] \equiv XY - YX$, $\{X, Y\} \equiv XY + YX$ to denote commutators and anti-commutators, respectively. The QCD analogues of the electric and magnetic fields are defined as usual by $\boldsymbol{E} = -[\partial_t \boldsymbol{A}] - [\boldsymbol{\partial} A^0]$ and $\boldsymbol{B} = [\boldsymbol{\partial} \times \boldsymbol{A}]$. The most general term we obtained in Eqs. (6.3) and (6.4) are constructed from all possible rotationally invariant, Hermitian combinations of iD_t, $\boldsymbol{D}$, $\boldsymbol{E}$, $i\boldsymbol{B}$, $i\boldsymbol{\sigma}$, with parity requiring even numbers of factors of $\boldsymbol{D}$ and $\boldsymbol{E}$.

On the other hand, the four quark operators in the Lagrangian represented by 6.4 have sub-indices, $\{1, 2\}$, which distinguishes for the case of distinct heavy quarks with unequal masses. Moreover, one can re-write these terms by applying a Fiertz transformation,

$$\begin{aligned}\mathcal{L}_{\psi\chi} = & \frac{d^c_{ss}}{m_1 m_2} \psi_1^\dagger \chi_2 \chi_2^\dagger \psi_1 + \frac{d^c_{sv}}{m_1 m_2} \psi_1^\dagger \boldsymbol{\sigma} \chi_2 \chi_2^\dagger \boldsymbol{\sigma} \psi_1 \\ & + \frac{d^c_{vs}}{m_1 m_2} \psi_1^\dagger T^a \chi_2 \chi_2^\dagger T^a \psi_1 + \frac{d^c_{vs}}{m_1 m_2} \psi_1^\dagger T^a \boldsymbol{\sigma} \chi_2 \chi_2^\dagger T^a \boldsymbol{\sigma} \psi_1,\end{aligned} \tag{6.5}$$

where one can transform between the two bases with the relations,

$$d_{ss} = -\frac{d^c_{ss}}{2N_c} - \frac{3d^c_{sv}}{2N_c} - \frac{N_c^2-1}{4N_c^2}d^c_{vs} - 3\frac{N_c^2-1}{4N_c^2}d^c_{vv}, \tag{6.6}$$

$$d_{sv} = -\frac{d^c_{ss}}{2N_c} + \frac{d^c_{sv}}{2N_c} - \frac{N_c^2-1}{4N_c^2}d^c_{vs} + \frac{N_c^2-1}{4N_c^2}d^c_{vv}, \tag{6.7}$$

$$d_{vs} = -d^c_{ss} - 3d^c_{sv} + \frac{d^c_{vs}}{2N_c} + \frac{3d^c_{vv}}{2N_c}, \tag{6.8}$$

$$d_{vv} = -d^c_{ss} + d^c_{sv} + \frac{d^c_{cs}}{2N_c} - \frac{d^c_{vv}}{2N_c}. \tag{6.9}$$

Both versions of $\mathcal{L}_{\psi\chi}$ are employed, the Lagrangian in (6.5) is more convenient for matching, when one is studying the equal mass case with annihilation processes. On the other hand, (6.4) is preferable when considering a bound state calculation. We employ (6.4) for matching in the unequal mass case.

6.3 Form Factors and Matching

Any loop diagram in an integrable QFT can be written as a function, $F(\{p\},\{m\},\mu,\epsilon)$, such that $\{p\}$ are the external momenta, $\{m\}$, the external and internal masses, μ the scale parameter in dimensional regularisation where the calculation is done in $d = 4-2\epsilon$ dimensions. Let us then consider, for instance, the radiative corrections to the quark-gluon three point vertex. This vertex can be expressed fully in terms of two form factors in QCD, $F_{1,2}(q^2)$, defined by the irreducible three point function,

$$\Gamma_3^{\rm QCD} = -ig_s T^a \bar{u}(p')\left[F_1(q^2)\gamma^\mu + iF_2(q^2)\frac{\sigma^{\mu\nu}q_\nu}{2m}\right]A^a_\mu(q)u(p), \tag{6.10}$$

where $q = p'-p$, m is the mass of the heavy quark, $\sigma^{\mu\nu} = -\frac{i}{4}[\gamma^\mu,\gamma^\nu]$. We only have two form factors as $\{\gamma_\mu,\sigma^{\mu\nu}q_\nu\}$ are the only Lorentz structures that appear in QCD due to the non-chiral nature of the theory. On the other hand, if one considers Γ_3 in the full SM, two additional chiral Lorentz structures emerge, and their corresponding form factors have the following form,

$$\Gamma_3^{\rm SM} = \Gamma_3^{\rm QCD} - ig_s T^a \bar{u}(p')\left[F_3(q^2)\gamma^\mu\gamma_5 + F_4(q^2)\frac{q^\mu\gamma_5}{2m}\right]A^a_\mu(q)u(p) \tag{6.11}$$

Employing dimensional regularisation on the diagrams one finds that the form factors $F_{1,3}(q^2)$ are UV and IR divergent [218]. We can always expand our two form factors, $F_i(q^2/m^2,\mu/m,\epsilon)$, as a power series in q^2/m^2 at fixed ϵ, then take the limit $\epsilon\to 0$ to obtain an expression of the form,

$$\begin{aligned} F_i = F_i(0)\left(\frac{A_0}{\epsilon_{\rm UV}} + \frac{B_0}{\epsilon_{\rm IR}} + (A_0+B_0)\ln\frac{\mu}{m} + D_0\right) + \\ q^2\partial_{q^2}F_i(0)\left(\frac{A_1}{\epsilon_{\rm UV}} + \frac{B_1}{\epsilon_{\rm IR}} + (A_1+B_1)\ln\frac{\mu}{m} + D_1\right), \end{aligned} \tag{6.12}$$

Conventionally, we label ϵ with the subscripts, $\epsilon_{\rm UV}$ and $\epsilon_{\rm IR}$ to indicate whether the divergence is ultraviolet or infrared, respectively. UV divergences are cancelled by renormalisation counter-terms while IR divergences cancel when a physical observable is considered. The coefficients of the effective Lagrangian are determinable from the difference between the form factors in the full theory versus the effective theory of interest. More specifically, the non-analytic terms in the

form factors cancel in the difference while the analytic ones determine the Wilson coefficients of the Lagrangian. By inspection of the terms in the effective Lagrangian in Eq. (6.3), all terms contain at least one power of A^μ, the gauge field. Thus all form factors at one-loop are attainable by computing the three-point on-shell scattering amplitude, which have been previously calculated [322].

To find the relationship between the full theory form factors and the Wilson coefficients for a low-momentum heavy quark scattering off a background vector potential, we expand Eq. (6.11) in the NR limit and multiply by a factor of $\sqrt{m/E}$ for both the incoming and outgoing quark. If we take $\boldsymbol{p}$ and $\boldsymbol{p'}$ to be the three-momentum of the incoming and outgoing quark, respectively, then $\boldsymbol{q} = \boldsymbol{p'} - \boldsymbol{p}$ is the transfer momentum of the background vector potential. We are then left with the following effective interaction operator,

$$-ig_s T^a u^\dagger_{\rm NR}(\boldsymbol{p'})[A^a_0 j^0 - \boldsymbol{A}^a \cdot \boldsymbol{j}] u_{\rm NR}(\boldsymbol{p}), \tag{6.13}$$

which can then be compared to the scattering amplitude in the effective theory Lagrangian to relate the Wilson coefficients to the form factors. We re-computed the NR expansion of Eq. (6.13) in QCD and confirmed the previous result [218, 320], i.e. we found for the time component of the current,

$$j^0 = F_1(q^2)\left\{1 - \frac{1}{8m^2}\boldsymbol{q}^2 + \frac{i}{4m^2}\boldsymbol{\sigma}\cdot(\boldsymbol{p'}\times\boldsymbol{p})\right\} + F_2(q^2)\left\{-\frac{1}{4m^2}\boldsymbol{q}^2 + \frac{1}{2m^2}\boldsymbol{\sigma}\cdot(\boldsymbol{p'}\times\boldsymbol{p})\right\} \tag{6.14}$$

and the spatial component of the current,

$$\begin{aligned}
\boldsymbol{j} = F_1(q^2)\Bigg\{&\frac{1}{2m}(\boldsymbol{p}+\boldsymbol{p'}) + \frac{i}{2m}\boldsymbol{\sigma}\times\boldsymbol{q} - \frac{i}{8m^3}(\boldsymbol{p}^2+\boldsymbol{p'}^2)\boldsymbol{\sigma}\times\boldsymbol{q} - \frac{1}{16m^3}(\boldsymbol{p'}^2-\boldsymbol{p}^2)\boldsymbol{q} \\
&-\frac{i}{16m^3}(\boldsymbol{p}^2-\boldsymbol{p'}^2)\boldsymbol{\sigma}\times(\boldsymbol{p}+\boldsymbol{p'}) - \frac{1}{8m^3}(\boldsymbol{p'}^2+\boldsymbol{p}^2)(\boldsymbol{p'}+\boldsymbol{p})\Bigg\} \\
&+ F_2(q^2)\Bigg\{\frac{i}{2m}\boldsymbol{\sigma}\times\boldsymbol{q} - \frac{i}{16m^3}\boldsymbol{q}^2\boldsymbol{\sigma}\times\boldsymbol{q} - \frac{1}{16m^3}\boldsymbol{q}^2(\boldsymbol{p}+\boldsymbol{p'}) - \frac{1}{16m^3}(\boldsymbol{p'}^2-\boldsymbol{p}^2)\boldsymbol{q} \\
&-\frac{i}{8m^3}(\boldsymbol{p'}^2-\boldsymbol{p}^2)\boldsymbol{\sigma}\times(\boldsymbol{p'}+\boldsymbol{p}) + \frac{i}{8m^3}\boldsymbol{\sigma}(\boldsymbol{p'}+\boldsymbol{p})(\boldsymbol{p'}\times\boldsymbol{p})\Bigg\}.
\end{aligned} \tag{6.15}$$

This can then be compared to the relevant subset of the Hamiltonian of Eq. (6.3),

$$\begin{aligned}
\mathcal{H}_{\psi,\chi} \supset \psi^\dagger\Bigg\{&g_s A^0 - c_2\frac{g_s}{2m}\boldsymbol{A}\cdot(\boldsymbol{p'}+\boldsymbol{p}) - ic_{\rm F}\frac{g_s}{2m}\boldsymbol{A}\cdot(\boldsymbol{\sigma}\times\boldsymbol{q}) - c_{\rm D}\frac{g_s}{16m^3}\boldsymbol{q}\cdot\boldsymbol{A} \\
&+ic_{\rm S}\frac{g_s}{4m^2}\boldsymbol{\sigma}\cdot(\boldsymbol{p'}\times\boldsymbol{p})A^0 + ic_{\rm S}\frac{g_s}{16m^3}(\boldsymbol{p'}^2-\boldsymbol{p}^2)\boldsymbol{A}\cdot\boldsymbol{\sigma}\times(\boldsymbol{p'}+\boldsymbol{p}) \\
&+i(c_{\rm W_1}-c_{\rm W_2})\frac{g_s}{8m^3}(\boldsymbol{p'}^2+\boldsymbol{p}^2)\boldsymbol{A}\cdot(\boldsymbol{\sigma}\times\boldsymbol{q}) + ic_{\rm W_2}\frac{g_s}{8m^3}\boldsymbol{q}^2\boldsymbol{A}\cdot(\boldsymbol{\sigma}\times\boldsymbol{q}) \\
&-ic_q\frac{g_s}{8m^3}\boldsymbol{\sigma}\cdot(\boldsymbol{p'}+\boldsymbol{p})\boldsymbol{A}\cdot(\boldsymbol{p'}\times\boldsymbol{p}) - c_{\rm M}\frac{g_s}{8m^3}(\boldsymbol{p'}^2-\boldsymbol{p}^2)\boldsymbol{A}\cdot\boldsymbol{q} \\
&+c_{\rm M}\frac{g_s}{8m^3}\boldsymbol{q}^2\boldsymbol{A}\cdot(\boldsymbol{p'}+\boldsymbol{p})\Bigg\}\psi + (\text{h.c},\ \psi\leftrightarrow\chi)
\end{aligned} \tag{6.16}$$

$$\equiv g_s\psi^\dagger\{A^0 j^0 - \boldsymbol{A}\cdot\boldsymbol{j}\}\psi + (\text{h.c},\ \psi\leftrightarrow\chi) \tag{6.17}$$

and matching the Lorentz structures provides one with the following relations between the

Wilson coefficients and form factors,

$$c_0 = c_2 = c_4 = F_1, \tag{6.18}$$
$$c_{\mathrm{F}} = F_1 + F_2, \tag{6.19}$$
$$c_{\mathrm{D}} = F_1 + 2F_2 + 8F_1', \tag{6.20}$$
$$c_{\mathrm{S}} = F_1 + 2F_2, \tag{6.21}$$
$$c_{\mathrm{W}_1} = F_1 + \frac{1}{2}F_2 + 4F_1' + 4F_2', \tag{6.22}$$
$$c_{\mathrm{W}_2} = \frac{1}{2}F_2 + 4F_1' + 4F_2', \tag{6.23}$$
$$c_{\mathrm{q}} = F_2, \tag{6.24}$$
$$c_{\mathrm{M}} = \frac{1}{2}F_2 + 4F_1', \tag{6.25}$$

such that,

$$F_i = F_i(0), \quad F_i' = \left.\frac{dF_i}{d(q^2/m^2)}\right|_{q^2=0}. \tag{6.26}$$

These relations between the form factors and Wilson coefficients remain unchanged by the allowance of further interactions from the standard model. This can be seen by taking the NR limit of Eq. (6.11), the 4-current $j \mapsto j + j'$ where j' includes the new form factors and their expanded Lorentz structures, for the time component of the current one obtains,

$$\begin{aligned} j'^0 = {} & F_3(q^2)\left\{\frac{1}{2m}\boldsymbol{\sigma}\cdot(\boldsymbol{p'}+\boldsymbol{p}) - \frac{1}{8m^3}(\boldsymbol{\sigma}\cdot\boldsymbol{p'}\boldsymbol{p'}^2 + \boldsymbol{\sigma}\cdot\boldsymbol{p}\boldsymbol{p}^2) - \frac{1}{16m^3}\boldsymbol{\sigma}\cdot(\boldsymbol{p'}+\boldsymbol{p})(\boldsymbol{p'}^2+\boldsymbol{p}^2)\right\} \\ & + F_4(q^2)\left\{-\frac{1}{4m^3}\boldsymbol{\sigma}\cdot\boldsymbol{q}(\boldsymbol{p'}^2 - \boldsymbol{p}^2)\right\} \end{aligned} \tag{6.27}$$

and the spatial component of the current,

$$\begin{aligned} \boldsymbol{j'} = {} & F_3(q^2)\left\{\boldsymbol{\sigma} - \frac{1}{4m^2}\boldsymbol{\sigma}(\boldsymbol{p'}^2+\boldsymbol{p}^2) + \frac{1}{8m^2}\boldsymbol{\sigma}\boldsymbol{q}^2 + \frac{1}{4m^2}(\boldsymbol{\sigma}\cdot\boldsymbol{p}\boldsymbol{p'} + \boldsymbol{\sigma}\cdot\boldsymbol{p'}\boldsymbol{p}) - \frac{i}{4m^2}\boldsymbol{p'}\times\boldsymbol{p}\right\} \\ & + F_4(q^2)\left\{-\frac{1}{4m^2}\boldsymbol{q}\boldsymbol{\sigma}\cdot\boldsymbol{q}\right\}. \end{aligned} \tag{6.28}$$

By comparison, one can see that $F_{3,4}$ are factors of entirely different Lorentz structures. In fact, one can count nine independent structures and thus one requires nine new linearly independent terms in the effective Lagrangian that result in the same Lorentz structures upon inspection of the Hamiltonian. Due to the fact that the SM is chiral and exhibits less symmetry than QCD there is more freedom in selecting the possible terms to include in the effective Lagrangian, we thus select a set that provides us with the correct Lorentz structures without claiming uniqueness,

$$\begin{aligned} \mathcal{L}_{\mathrm{Ch}} = {} & \psi^\dagger(p')\left\{b_0 i\boldsymbol{\sigma}\cdot\boldsymbol{D} - ib_1\frac{g_s}{2m}\boldsymbol{\sigma}\cdot\tilde{\boldsymbol{E}} + ib_2\frac{g_s}{8m^2}(\boldsymbol{D}\cdot\boldsymbol{B} + \boldsymbol{B}\cdot\boldsymbol{D})\right. \\ & + b_3\frac{g_s}{8m^2}\boldsymbol{\sigma}\cdot(\boldsymbol{D}\times\boldsymbol{B} + \boldsymbol{B}\times\boldsymbol{D}) + ib_4\frac{1}{2m^2}\{\boldsymbol{\sigma}\cdot\boldsymbol{\partial}, \boldsymbol{D}^2\} + ib_5\frac{1}{4m^2}[\boldsymbol{D}^2\boldsymbol{\sigma}\cdot\boldsymbol{D}] \\ & + b_6\frac{g_s}{2m^2}[D_t, \boldsymbol{\sigma}\cdot\boldsymbol{E}] + ib_7\frac{g_s}{16m^3}\{\boldsymbol{D}^2, \boldsymbol{\sigma}\cdot\tilde{\boldsymbol{E}}\} + ib_8\frac{g_s}{8m^3}\boldsymbol{D}_i\boldsymbol{\sigma}\cdot\tilde{\boldsymbol{E}}\boldsymbol{D}_i \\ & \left. + ib_9\frac{g_s}{8m^3}(\boldsymbol{\sigma}\cdot\boldsymbol{D}\tilde{\boldsymbol{E}}\cdot\boldsymbol{D} + \boldsymbol{D}\cdot\tilde{\boldsymbol{E}}\boldsymbol{\sigma}\cdot\boldsymbol{D})\right\}\psi(p) + (\text{h.c},\, \psi\leftrightarrow\chi) + \mathcal{O}(1/m^4, g_s^2/m^3), \end{aligned} \tag{6.29}$$

with the operator, $\tilde{\boldsymbol{E}} = -\frac{i}{g_s}\{D_t, \boldsymbol{D}\}$. Upon employing the free field Schrodinger equation (up to $\mathcal{O}(1/m)$), the following replacement holds,

$$i\frac{\partial\psi}{\partial t} + \frac{\nabla^2\psi}{2m} = 0, \quad \psi(t,\boldsymbol{x}) = e^{ip\cdot x} \Rightarrow \{\partial_t\psi = -ip^0\psi, \boldsymbol{\partial}\psi = i\boldsymbol{p}\psi\}, \tag{6.30}$$

and analogously for the vector field, $A(x^\mu)$. Therefore, after Legendre transforming the Lagrangian in Eq. (6.29) to its Hamiltonian one can then match the relevant terms by inspection of Lorentz structures. This can then be compared to the chiral Hamiltonian and the Lorentz structures matched to provide the following relations between the new Wilson coefficients and form factors,

$$b_0 = b_1 = b_2 = b_4 = b_9 = -F_3, \tag{6.31}$$
$$b_3 = F_3 + 2F_4, \tag{6.32}$$
$$b_5 = 4F_3' + F_4, \tag{6.33}$$
$$b_6 = -F_4, \tag{6.34}$$
$$b_7 = 8F_3', \tag{6.35}$$
$$b_8 = F_3 - 8F_3'. \tag{6.36}$$

Note that we have written HQET Lagrangians in the special frame, $v = (1, \mathbf{0})$, and the notation of [320] was employed. However, one can re-write Eq. (6.3) to the same order in $1/m$ in an arbitrary frame as follows,

$$\begin{aligned}\mathcal{L}_v = \bar{Q}_v \Bigg\{ & c_0 iD\cdot v - c_2\frac{D_\perp^2}{2m} + c_4\frac{D_\perp^4}{8m^3} - g_s c_{\rm F}\frac{\sigma_{\mu\nu}G^{\mu\nu}}{4m} - g_s c_{\rm D}\frac{v^\mu[D_\perp^\nu G_{\mu\nu}]}{8m^2} \\ & + ig_s c_{\rm S}\frac{v_\lambda\sigma_{\mu\nu}\{D_\perp^\mu, G^{\nu\lambda}\}}{8m^2} + g_s c_{\rm W_1}\frac{\{D_\perp^2, \sigma_{\mu\nu}G^{\mu\nu}\}}{16m^3} - g_s c_{\rm W_2}\frac{D_\perp^\lambda\sigma_{\mu\nu}G^{\mu\nu}D_{\perp\lambda}}{8m^3} \\ & + g_s c_{\rm q}\frac{\sigma^{\mu\nu}(D_\perp^\lambda G_{\lambda\mu}D_{\perp\nu} + D_{\perp\nu}G_{\lambda\mu}D_\perp^\lambda - D_\perp^\lambda G_{\mu\nu}D_{\perp\lambda})}{8m^3} \\ & - ig_s c_{\rm M}\frac{D_{\perp\mu}[D_{\perp\nu}G^{\mu\nu}] + [D_{\perp\nu}G^{\mu\nu}]D_{\perp\mu}}{8m^3}\Bigg\} Q_v,\end{aligned} \tag{6.37}$$

such that,

$$D_\perp^\mu = D^\mu - v^\mu v\cdot D, \tag{6.38}$$

and $\sigma^{\mu\nu} = -\frac{i}{4}[\gamma^\mu, \gamma^\nu]$ and $G^{\mu\nu} = \frac{1}{ig_s}[D^\mu, D^\nu]$. We can also write the chiral Lagrangian in Eq. (6.29) in the same covariant form,

$$\begin{aligned}\mathcal{L}_v^{\rm Ch} = \bar{Q}_v \Bigg\{ & -2b_0\gamma_5 v^\mu\sigma_{\mu\nu}D^\nu + ib_1\frac{1}{m}\gamma_5\{v^\mu D_\mu, v^\nu\sigma_{\nu\lambda}D^\lambda\} - b_2\frac{g_s}{4m^2}\gamma_5 v_\mu\sigma^{\mu\nu}[D^\lambda, G_{\nu\lambda}] \\ & - b_3\frac{g_s}{16m^2}\gamma_5\{\sigma_{\mu\nu}, \gamma_\lambda\}\{D^\mu, G^{\nu\lambda}\} + b_4\frac{1}{m^2}\gamma_5\{v^\mu\sigma_{\mu\nu}\partial^\nu, D_\perp^2\} \\ & + b_5\frac{1}{2m^2}\gamma_5[v^\mu\sigma_{\mu\nu}D^\nu D_\perp^2] + ib_6\frac{g_s}{2m^2}\gamma_5[v^\mu D_\mu, \sigma_{\nu\lambda}G^{\nu\lambda}] \\ & + ib_7\frac{1}{8m^3}\gamma_5\{D_\perp^2, \{v^\mu D_\mu, v^\nu\sigma_{\nu\lambda}D^\lambda\}\} + ib_8\frac{1}{4m^3}\gamma_5 D_\perp^\alpha\{v^\mu D_\mu, v^\nu\sigma_{\nu\lambda}D^\lambda\}D_{\perp\alpha} \\ & + ib_9\frac{1}{4m^3}\gamma_5(v^\mu\sigma_{\mu\nu}D^\nu\{v^\lambda D_\lambda, D_\perp^\alpha\}D_{\perp\alpha} + D_{\perp\alpha}\{v^\lambda D_\lambda, D_\perp^\alpha\}v^\mu\sigma_{\mu\nu}D^\nu)\Bigg\} Q_v,\end{aligned} \tag{6.39}$$

in which the chirality is made explicit by the appearance of γ_5 factoring each term.

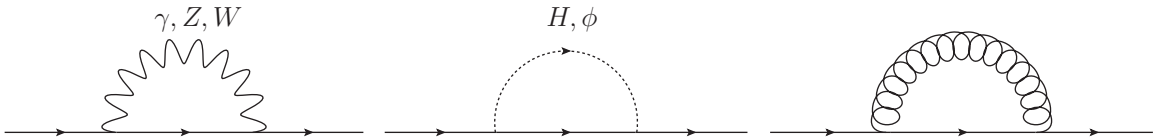

Figure 6.1: Self-energy diagrams contributing to the one-loop WFRC.

6.4 Two Quark Matching

The self energy contributions which contribute to the wave function renormalisation (WFR), represented in Fig. 6.1, can be split into left/right and scalar components, respectively,

$$\Sigma(p) = \Sigma_L + \Sigma_R - \Sigma_S/2 \tag{6.40}$$
$$= P_L\omega_L + P_R\omega_R - \Sigma_S/2, \tag{6.41}$$

such that $P_{R/L} = \frac{1}{2}(1 \pm \gamma_5)$ are the usual left/right chiral projection operators, from this expression one can obtain the on-shell WFR correction,

$$\delta Z = \delta Z_L + \delta Z_R, \tag{6.42}$$

such that,

$$\delta Z_{L/R} = -\left\{\Sigma_{L/R} + m^2(\Sigma'_L + \Sigma'_R - 2\Sigma'_S)\right\}|_{q^2=m^2}, \tag{6.43}$$

and therefore,

$$\delta Z = -\left\{[\omega_L + \omega_R + 2m^2(\omega'_L + \omega'_R + \Sigma'_S)] - \gamma_5[\omega_R - \omega_L + 2m^2(\omega'_R - \omega'_L)]\right\}|_{q^2=m^2} \tag{6.44}$$
$$= \delta Z_1 + \gamma_5\delta Z_3. \tag{6.45}$$

The total on-shell form factors at one-loop can then be calculated from the amplitudes present in Fig. 6.2. We present the result in the large external on-shell quark mass, $m \equiv m_1$, limit and small new internal mass appearing from flavour changing, m_2, along with small transfer momentum, q,

$$\begin{aligned} F_1 = 1 - \delta Z_1 + F_1^{(a)} + F_1^{(b)} = 1 &+ \frac{\alpha_s}{\pi}\frac{q^2}{m_1^2}\left[\left(-\frac{1}{8} + \frac{1}{6}L_1\right)C_F + \left(-\frac{1}{16} + \frac{5}{48}L_1\right)C_A\right] \\ &+ \frac{\alpha}{\pi}\frac{q^2}{m_1^2}\left[\frac{2}{27}L_z + \frac{1}{c^2}\left(-\frac{13}{288} + \frac{17}{432}L_{1,z}\right) + \frac{1}{s^2}\left(-\frac{5}{96} + \frac{3}{64}\pi r_{1,w}r_{h,w} - \frac{1}{192}r_{1,w}^2\right.\right. \\ &\left.\left. + \frac{1}{192}r_{h,w}^2 - \frac{1}{16}r_{h,w}^2L_{1,h} + \frac{1}{48}r_{1,w}^2L_{2,h} + \frac{1}{24}L_{2,1} + \frac{1}{48}L_{2,z} - \frac{i\pi}{48}\left(1 + \frac{1}{3}r_{1,w}^2\right)\right)\right], \end{aligned} \tag{6.46}$$

$$\begin{aligned} F_2 = F_2^{(a)} + F_2^{(b)} = &\frac{\alpha_s}{\pi}\left[\frac{1}{2}C_F + \left(\frac{1}{2} - \frac{1}{4}L_1\right)C_F\right] + \frac{\alpha_s}{\pi}\frac{q^2}{m_1^2}\left[\frac{1}{12}C_F + \left(\frac{1}{12} - \frac{1}{4}L_1\right)C_A\right] \\ &+ \frac{\alpha}{\pi}\left[\left(\frac{35}{144} - \frac{1}{16}L_{1,z}\right)\frac{1}{c^2} + \left(\frac{7}{16} + \frac{1}{16}r_{1,w}^2 - \frac{1}{8}\pi r_{1,w}r_{h,w} - \frac{3}{16}r_{h,w}^2L_{1,h} - \frac{1}{16}L_{1,z}\right)\frac{1}{s^2}\right] \\ &+ \frac{\alpha}{\pi}\frac{q^2}{m_1^2}\left[\frac{1}{c^2}\frac{13}{432} + \frac{1}{s^2}\left(\frac{1}{48}\left(1 - i\pi r_{1,w}^2\right) + \frac{1}{96}r_{1,w}^2 - \frac{r_{h,w}}{32}\left(\pi r_{h,w} + r_{1,w}\right) + \frac{1}{48}r_{1,w}^2L_{1,2}\right.\right. \\ &\left.\left. + \frac{1}{16}r_{h,w}^2L_{1,h}\right)\right], \end{aligned} \tag{6.47}$$

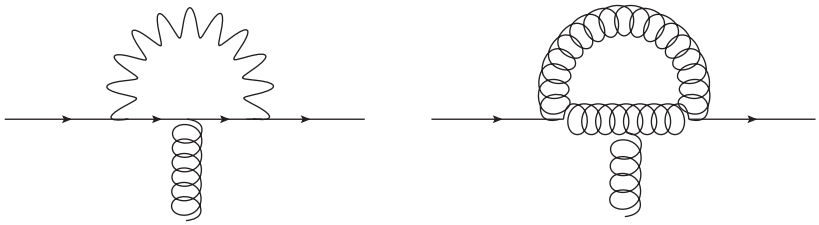

Figure 6.2: Diagrams that contribute to three-point matching coefficients in the SM. The Abelian and non-Abelian contributions are given by diagrams (a) and (b), respectively.

$$
\begin{aligned}
F_3 = & -\delta Z_3 + F_3^{(a)} + F_3^{(b)} = \frac{\alpha}{\pi}\left[\left(\frac{5}{16} - \frac{5}{48}L_{1,z}\right)\frac{1}{c^2} + \left(-\frac{7}{16} + \frac{1}{16}r_{1,w}^2 + \frac{1}{8}L_{1,w}\right.\right. \\
& \left.\left. + \frac{1}{16}L_{1,z} - \frac{i\pi}{8}\right)\frac{1}{s^2}\right] + \frac{\alpha}{\pi}\frac{q^2}{m_1^2}\left[\left(-\frac{35}{576} + \frac{5}{96}L_{1,z}\right)\frac{1}{c^2} + \left(\frac{9}{64} + \frac{1}{64}r_{1,w}^2 - \frac{1}{48}r_{1,w}^2 L_{1,2}\right.\right. \\
& \left.\left. - \frac{1}{48}L_{2,1} - \frac{1}{32}L_{1,z} - \frac{i\pi}{48}(1 - r_{1,w}^2)\right)\frac{1}{s^2}\right],
\end{aligned} \tag{6.48}
$$

$$
\begin{aligned}
F_4 = F_4^{(a)} + F_4^{(b)} = & \frac{\alpha}{\pi}\left[\left(-\frac{35}{144} + \frac{5}{24}L_{1,z}\right)\frac{1}{c^2} + \left(\frac{9}{16} + \frac{1}{16}r_{1,w}^2 - \frac{1}{12}r_{1,w}^2 L_{1,z} - \frac{1}{6}L_{2,z}\right.\right. \\
& \left.\left. - \frac{1}{24}L_{1,z} - \frac{i\pi}{12}(1 - r_{1,w}^2)\right)\frac{1}{s^2}\right] + \frac{\alpha}{\pi}\frac{q^2}{m_1^2}\left[\left(-\frac{7}{96} + \frac{5}{144}L_{1,z}\right)\frac{1}{c^2} + \left(\frac{17}{96} - \frac{1}{60}r_{1,w}^2 r_{1,2}^2\right.\right. \\
& \left.\left. + \frac{19}{480}r_{1,w}^2 + \frac{1}{60}r_{w,2}^2 + \frac{1}{60}r_{1,2}^2 - \frac{7}{240}r_{1,w}^2 L_{1,2} - \frac{1}{48}L_{1,z} - \frac{1}{20}L_{1,2} + \frac{i\pi}{20} + \frac{7i\pi}{240}r_{1,w}^2\right)\frac{1}{s^2}\right],
\end{aligned} \tag{6.49}
$$

where $L_A \equiv \ln A^2/\mu^2$, $L_{A,B} \equiv L_A - L_B$ and $r_{i,j} = m_i/m_j$, we fix the Yukawa coupling to the EW coupling, α, and quark masses in the standard way [115]. We also define the mixing angles, $c = \cos\theta_w = M_W/M_Z$ and $s = \sin\theta_w$. Moreover, we leave out IR divergences, $\epsilon_{\rm IR}$, to reduce the size of the expressions and they are conventionally not included in the matching coefficients. Although the form factors in the limit presented above provide an adequate approximation for $m_1 \gg M_{W,Z}, M_H \gg m_2, q^2$, in the SM the correct limit is $m_1 \sim M_{W,Z}, M_H \gg m_2, q^2$ and thus we recommend the latter for precision calculations. We leave a limit comparison to future numerical studies and the full expression with no approximations is included with an arXiv ancillary file of Ref. [161].

6.5 Four Quark Matching

To achieve the matching we follow the procedure originally outlined in [316] reproducing there results and extending them. One begins by expanding the dimensionally regulated matrix elements about zero residual momentum. This expansion is done to zeroth order since there are no derivative terms in the four fermion portion of our effective Lagrangian, by inspection of Eq. (6.4) and Eq. (6.5) - i.e. we solely require the matrix elements for the four heavy quarks at rest. Diagrammatically, this means the amputated legs in a given diagram can be multiplied by a projector, P_+ and P_-, to the particle and anti-particle sub-spaces, respectively. The kinematic factor which relates the relativistic and non-relativistic expansions, $\sqrt{m/E}$ may also be set to unity without loss of generality.

The calculation of such matrix elements in QCD and HQET has been achieved in previous studies [316, 323, 324]. In the S-matrix elements of such heavy-heavy systems, one can see a unique IR behaviour appearing, which gives rise to the Coulomb pole and hence to the standard NR weakly coupled bound states. This behaviour in the IR appears expectantly in both the effective and full theory. Expanding the dimensionally regulated matrix elements of QCD about the residual momentum, one would expect an IR singularity - reflecting the Coulomb pole - to emerge. This odd power-like IR divergence is set to zero in dimensional regularisation; the EFT has identical IR behaviour which is consistently put to zero by dimensional regularisation. Crucially, we are taking into account all the non-analytic behaviour in the heavy quark masses coming from high momenta such as in QCD logarithms, for instance.

The $\overline{\text{MS}}$ scheme is employed throughout for both UV and IR divergences. As was done previously, we avoid on-shell WFR and stick to $\overline{\text{MS}}$ [316]. The scheme is followed to avoid identifying the UV divergences in the on-shell (OS) scheme which correspond to a WFR constant and subtracting them accordingly, this is less straightforward than employing $\overline{\text{MS}}$ throughout. The price to be paid for this choice is that the heavy quark fields cease to be adequately normalised - hence one requires the proper WFR factor, Z, to be included when calculating the on-shell matrix elements, for instance, in QCD one has,

$$Z^{\text{QCD}} = 1 + C_F \frac{\alpha_s}{\pi}\left(\frac{3}{4}L_m - 1\right) + \mathcal{O}(\alpha_s^2), \quad Z^{\text{NRQCD}} = 1. \tag{6.50}$$

To be clear, Z only contribute at one-loop order in the equal mass case, the amplitudes of which are illustrated in Fig. 6.4. Lastly, we note that in our calculation, the Wilson coefficients in Eqs. (6.4) and (6.5) are invariant under local field re-definitions as discussed in detail previously [218].

6.5.1 Unequal Mass Case

In the unequal fermion mass case, annihilation diagrams do not contribute, and thus we are left with the box diagrams present in Fig. 6.3. The aforementioned Coulomb singularity and the mechanism by which it vanishes is identifiable. The upshot is that a suitable dimensionful parameter - the relative momentum of the heavy quarks - is not present in the calculation. Thus dimensional regularisation has no way to reproduce the Coulomb pole which was pointed out and discussed in detail in Refs. [316, 323].

We re-calculate the following known QCD matching coefficients in the large $m_{1,2}$ limit and confirm the result of [316],

$$d_{ss} = -C_F\left(\frac{C_A}{2} - C_F\right)\frac{\alpha_s^2}{m_1^2 - m_2^2}\left\{m_1^2\left(L_2 + \frac{1}{3}\right) - m_2^2\left(L_1 + \frac{1}{3}\right)\right\}, \tag{6.51}$$

$$d_{sv} = C_F\left(\frac{C_A}{2} - C_F\right)\frac{\alpha_s^2}{m_1^2 - m_2^2} m_1 m_2 L_{1,2}, \tag{6.52}$$

$$\begin{aligned} d_{vs} = &\left(\frac{3}{4}C_A - 2C_F\right)\frac{\alpha_s^2}{m_1^2 - m_2^2}\left\{m_1^2\left(L_2 + \frac{1}{3}\right) - m_2^2\left(L_1 + \frac{1}{3}\right)\right\} \\ &+ \frac{C_A\alpha_s^2}{4(m_1^2 - m_2^2)m_1 m_2}\left\{m_1^4\left(L_2 + \frac{10}{3}\right) - m_2^4\left(L_1 + \frac{10}{3}\right)\right\}, \end{aligned} \tag{6.53}$$

$$d_{vv} = \frac{2C_F\alpha_s^2}{m_1^2 - m_2^2} m_1 m_2 L_{1,2} + \frac{C_A\alpha_s^2}{4(m_1^2 - m_2^2)}\left\{m_1^2\left(L_2 + \frac{10}{3}\right) - m_2^2\left(L_1 + 3\right) - 3m_1 m_2 L_{1,2}\right\}. \tag{6.54}$$

Note that imaginary parts appear in Wilson coefficients, this occurs often and are qualitatively related to the inelastic cross sections which are unattainable with NR theory alone. Moreover, the decay width of heavy quarkonium states into light hardons are also implicated in the imaginary

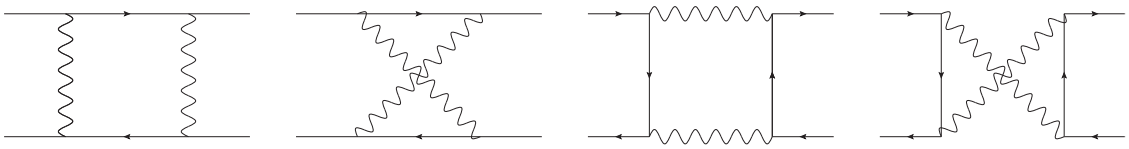

Figure 6.3: Relevant diagrams for the matching of the four-fermion operators at one-loop order and $\mathcal{O}(1/m^2)$ in the unequal mass case. The incoming and outcoming particles are on-shell and exactly at rest.

parts, which has been previously calculated [73], which agrees with our results. The $\mathcal{O}(\alpha\alpha_s)$ real EW corrections, which we define as d'_{ij}, to these coefficients will be presented in the limit, $m_1 \gg m_2, M_{\rm EW}$, where $M_{\rm EW}$ labels bosonic masses in the EW sector. We choose this limit for compactness mainly but the full result up to $\mathcal{O}(\alpha^2)$ in the analogous limit to the QCD result is included as an arXiv ancillary file of Ref. [161]. We note that at $\mathcal{O}(\alpha\alpha_s)$, $d'_{ss} = d'_{sv} = 0$, and what remains to display are the following coefficients,

$$\begin{aligned} d'_{vs} = \alpha\alpha_s \Bigg\{ \frac{1}{24} \Bigg(& 1 + 3L_2 + 12i\pi - 4r_{1,2} i\pi - 3r_{1,w} r_{2,w} \left[3L_1 + 7L_2 + \frac{25}{3} - 9i\pi \right] \\ & - 12 r_{2,w}^2 \left[\frac{9}{2} + i\pi \right] - \frac{1}{2} r_{1,w}^2 i\pi \Bigg) \frac{1}{s^2} + \frac{15}{216} \left[L_2 + \frac{1}{3} \right] \frac{1}{c^2} \Bigg\}, \end{aligned} \tag{6.55}$$

$$\begin{aligned} d'_{vv} = \alpha\alpha_s \Bigg\{ \frac{1}{72} \Bigg(& 55 + 15L_2 + 6r_{h,w}^2 \left[L_2 + \frac{11}{3} \right] + 36 r_{2,w}^2 L_{1,2} \Bigg) \frac{1}{s^2} \\ & + \left(\frac{5}{24} L_2 + \frac{55}{72} \right) \frac{1}{c^2} \Bigg\}, \end{aligned} \tag{6.56}$$

where the EW parameters present in this expression mimic the definitions present in Section 6.4.

6.5.2 Equal Mass Case

When considering the equal particle case more amplitudes are involved since annihilation processes are now allowed and must be taken into account (see Fig. 6.4). The inclusion of annihilation processes, most significantly, includes, at leading order, the tree level contributions. We confirm the previously calculated matching coefficients in pure QCD,

$$d^c_{ss} = \alpha_s^2 C_F \left(\frac{C_A}{2} - C_F \right) (2 - 2l_2 + i\pi), \tag{6.57}$$

$$d^c_{sv} = 0, \tag{6.58}$$

$$d^c_{vs} = \frac{\alpha_s^2}{2} \left(-\frac{3}{2} C_A + 4C_F \right) (2 - 2l_2 + i\pi), \tag{6.59}$$

$$\begin{aligned} d^c_{vv} = (-\pi\alpha_s) \Bigg\{ & 1 + \frac{\alpha_s}{\pi} \left[\frac{N_f}{6} \left(L_1 + 2l_2 - \frac{5}{3} \right) - \frac{8}{9} + \frac{1}{3} L_1 \right] \\ & + C_A \left[-\frac{11}{12} L_1 + \frac{109}{36} \right] - 4C_F \Bigg\}, \end{aligned} \tag{6.60}$$

where $l_2 \equiv \ln(2)$. The $\mathcal{O}(\alpha, \alpha\alpha_s)$ EW corrections to these coefficients, defined as $d^{c\prime}_{ij}$, will be presented in the following limit, $m_1 \gg M_{\rm EW} \gg m_2$. This limit is again chosen for compactness

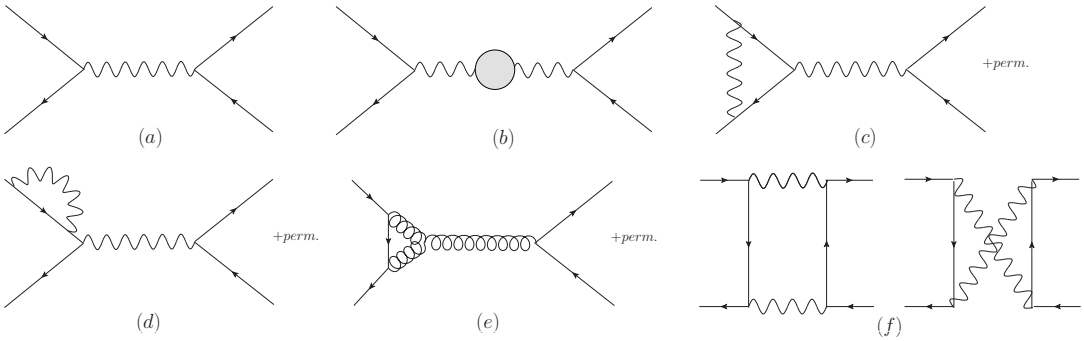

Figure 6.4: Relevant diagrams to the matching for four-fermion operators at one-loop order and $\mathcal{O}(1/m^2)$ in the equal mass case. The incoming and outgoing particles are on-shell and exactly at rest.

but the full result up to $\mathcal{O}(\alpha^2)$ is included as an arXiv ancillary file of Ref. [161],

$$d_{ss}^{c'} = \alpha\left\{-\frac{1}{4s^2}\pi r_{1,w}^2 + \alpha_s C_F\left(\frac{3}{32}L_1 - \frac{1}{8}\right)\frac{1}{c^2} + \alpha_s C_F\left(-\frac{1}{8} + \frac{3}{32}L_1 - 4r_{1,w}^2 + \frac{25}{8}r_{1,w}^2 L_1\right)\frac{1}{s^2}\right\}, \quad (6.61)$$

$$d_{sv}^{c'} = \alpha\alpha_s C_F\left\{\left(\frac{1}{8} + \frac{3}{32}L_1\right)\frac{1}{s^2} + \left(\frac{25}{72} + \frac{25}{96}L_1\right)\frac{1}{c^2}\right\}, \quad (6.62)$$

$$\begin{aligned} d_{vs}^{c'} = \alpha\Bigg\{&\left(-\frac{\pi}{16} + \alpha_s\left[\frac{1}{4} - \frac{15}{16}C_F + \frac{19}{32}C_F L_1 - \frac{1}{4}l_2 - \frac{1}{8}i\pi\right]\right)\frac{1}{s^2} \\ &+\left(-\frac{25\pi}{144} + \alpha_s\left[\frac{25}{36} - \frac{125}{48}C_F + \frac{475}{288}C_F L_1 - \frac{25}{36}l_2 - \frac{25}{72}i\pi\right]\right)\frac{1}{c^2} + \frac{16}{9}i\pi\alpha_s\Bigg\}, \end{aligned} \quad (6.63)$$

$$\begin{aligned} d_{vv}^{c'} = \alpha\alpha_s\Bigg\{&\left(\frac{88}{9} + \frac{44}{9}L_1 - \frac{76}{9}L_{1,z} + \frac{8\pi}{9}r_{1,z} - \frac{2\pi}{9}r_{1,w}r_{z,w}\right) + \frac{1}{c^2}\left(\frac{89}{72}L_{1,z} - \frac{361}{72}\right) \\ &+\frac{1}{s^2}\left(\frac{1}{4}L_{w,z} - \frac{23}{24} - \frac{9}{8}L_{1,z} - \frac{7}{24}r_{1,w}^2 + \frac{7}{8}r_{h,w}^2 - \frac{19}{48}\pi r_{1,w}r_{h,w} - \frac{1}{2}\pi r_{1,h}^2 r_{1,w}^2 + \frac{1}{3}\left(l_2 - \frac{7}{4}i\pi\right)\right. \\ &\left.-\frac{1}{3}r_{1,w}^2\left(l_2 + 2i\pi\right) + \frac{1}{12}r_{h,w}^2\left(l_2 + 2i\pi\right) + \frac{1}{16}r_{1,w}^2 L_1 + \frac{1}{2}r_{1,w}^2 L_{h,z} + \frac{1}{4}r_{1,w}^2 L_{1,z} + \frac{25\pi}{24c}r_{1,w}\right)\Bigg\}. \end{aligned} \quad (6.64)$$

6.6 Discussion

To underline our discussion the full set of EW corrections to the two and four quark matching coefficients is presented in Tables 6.1 and 6.2, respectively. We avoid taking any limits and plug in the latest SM parameters to compare with the known QCD result. The reason we choose the full expression up to the order we are considering is to maximise accuracy and we focus on comparing the real parts of the Wilson coefficients. For our comparison we choose for our renormalisation scale, $\mu = M_Z$, $m_1 = m_t(M_Z)$, $m_2 = m_b(M_Z)$ and the coupling, $\alpha_s = \alpha_s(M_Z)$ and the parameters were taken from the latest PDG review [167]. We will begin by considering the b_i and c_i Wilson coefficients factoring the two quark operators. By inspection of Table 6.1, at the renormalisation scale we are inspecting, it is clear that the EW corrections alter the Wilson coefficients significantly. Moreover, the size of these corrections varies widely depending on the coefficient under consideration and this provides further credence to the lack of reliability of naive order of magnitude estimates. As for the new parity-violating operators, they come equipped with non-negligible matching coefficients of similar order of magnitude to the ones

Coeff.	$c_{0,2,4}$	c_{F}	c_{D}	c_{S}	c_{W_1}	c_{W_2}	c_q	c_{M}
QCD	1	1.04	1.192	1.08	0.996	-0.004	0.04	0.076
EW corr.	0	0.0006	-0.1012	0.0012	-0.0639	-0.0629	0.0006	-0.0509

Coeff.	$b_{0,1,2}$	b_3	b_4	b_5	b_6	b_7	b_8	b_9
EW corr.	-0.002	0.024	-0.002	-0.04	0.02	-0.04	0.042	-0.002

Table 6.1: Three-point matching coefficients with $\mu = M_Z$ and SM parameters taken from PDG.

Coeff.	d_{ss}	d_{sv}	d_{vs}	d_{vv}	d^c_{ss}	d^c_{sv}	d^c_{vs}	d^c_{vv}
QCD	0.02	0.0004	-2.269	-0.038	0.0018	0	0.003	-0.366
EW corr.	0.093	-0.077	-0.2734	2.145	-0.134	0.002	-0.014	-0.034

Table 6.2: Four-point matching coefficients with the equal and unequal mass cases distinguished by the superscript, c, with $\mu = M_Z$ and SM parameters taken from PDG.

factoring the parity-preserving operators. On the other hand, the matching coefficients of the four quark operators vary even more strongly in both the QCD and EW sectors. If we now consider Table 6.2, we may focus on the largest Wilson coefficients in QCD which are d_{vs} and d^c_{vv} in the unequal and equal mass cases, respectively. The EW corrections to these coefficients are an order of magnitude smaller which align well with naive estimates, i.e. $\mathcal{O}(\alpha\alpha_s)$. However, the largest EW contributions which arise in d_{vv} and d^c_{ss} are of the same order as the largest QCD coefficients and further justify the necessity of including them in precision calculations. We end by noting that these results were achieved with the help of `Mathematica` accompanied by the package, `FeynCalc` [298], to compute the necessary amplitudes and deal with the algebra. We employed further sub-packages of `FeynCalc` such as `FeynHelpers` [299] which reduces and provides explicit expressions for one-loop scalar integrals by connecting the reduction package, `fire` [300], with the analytic scalar integrals program, `Package-X` [301]. Lastly, we employed the `FeynOnium` sub-package, for dealing with calculations in the NR limit [302].

6.7 Summary

The matching coefficients of the NRQCD Lagrangian have been computed at one-loop up to and including terms of order $\mathcal{O}(1/m_Q^3)$ with QCD as the full theory, confirming previous results. The Lagrangian was then extended to include the leading QCD+EW and EW corrections at one-loop, of which various limits were presented and discussed. New parity-violating operators were found to be necessary for the two quark terms in the effective Lagrangian, and we showed them to be frame independent. The new terms arose due to the SM being parity-violating and new Lorentz structures emerged that are not present in the NR limit of QCD; thus, the matching coefficients accompanying said terms exhibited EW corrections purely. When studying the four quark operators, we considered both the equal and unequal external heavy quark mass cases. We rounded off by comparing all the matching coefficients for a particular renormalisation scale with and without EW corrections and found the contributions from the EW regime to be relevant. Therefore, we recommend their inclusion in future heavy quark precision studies. Our full results are contained in the ancillary file submitted along with Ref. [161] on the arXiv.

Chapter 7

Two-loop Electroweak Form Factor Corrections

In this chapter we compute the massive gauge and scalar corrections to *form factors* up to and including two-loop orders. The corrections are calculated for processes involving two external fermions and scalars in the spontaneously broken $SU(N)$-Higgs model, examining a range of *composite operators*. The formalism we deploy is applied in both the *Sudakov* and *threshold* energetic regimes. We further discuss how our form factors can be mapped from our model to the Standard Model and beyond. This Chapter is based on Ref. [325], reflecting the author's contribution.

7.1 Motivation

The often addressed *form factor* is a crucial building block in the perturbative analysis of scattering processes occurring at the LHC and future colliders [326, 327]. It is also the simplest amplitude which can be used to study the IR structure of the Standard Model and beyond. For reference, the QCD form factors of massless quarks have been evaluated through to the three-loop level [328] and even recently towards four loop orders [329–338]. On the other hand for massive quarks in QCD three-loop results are available thus far [339–341]. In our study, we consider massive gauge and Higgs corrections to the form factor for scalar, fermion and mixed external particles on a range of operators, checking and extending the results of [76] to two-loop orders. Furthermore, unlike previous work which focus solely on the *Sudakov regime* relevant for LHC studies, we also consider the *threshold regime* appropriate for future high precision colliders [218, 341, 342]. When the COM energy of a process is large compared to predicted masses in our theory, this is known as the Sudakov energetic regime. For instance, with regards to the SM, LHC partonic processes lie in this regime as the COM energy is $\sqrt{s} \sim 14$ TeV, which is an order of magnitude above the largest SM masses. Radiative corrections of both exclusive and inclusive scattering processes include terms with up to two powers of large logarithms, $\ln(s/M^2_{W/Z})$, known as *electroweak Sudakov logarithms* [343]. Such logarithms cause a break-down of fixed-order perturbation theory and thus, resummation is necessary at all orders. Thus far, the literature on EW Sudakov effects in most cases focuses on employing IR evolution equations to deal with computations [75, 344–351].

One can see the so-called Sudakov logarithm as an IR logarithm in EW theory, as it diverges in the small EW mass limit. Naturally, this calls for the use of EFT, in which the IR logarithms of the full theory are convertible to UV logarithms in the EFT, and then summable using standard RG techniques. In this regime, the appropriate effective theories are SCET and *heavy particle*

effective theory (HPET) for both fermions and scalars [259, 260], which have been previously used to study high energy EW Sudakov corrections [76, 352], and to perform resummation. This paper studies high energy EW Sudakov corrections in the EFT formalism, expanding on previous work [76,352,353]. With regards to studies in the high energy (Sudakov) regime, many observables have been found to a high level of accuracy. For instance, inclusive top quark pair production cross-section uncertainties, now are at around $3-5\%$ for a fixed top quark mass of $m_t = 172.5$ GeV [354]. Moreover, although precision measurements are crucial for testing SM predictions, BSM physics can hide as anomalies within the uncertainties. Thus, to discover or rule out signs of BSM physics, further precision is necessary than what can be provided by the LHC, and indeed, a future high precision collider which operates at threshold energies along with theoretical studies can achieve that [355, 356]. In the threshold regime, the processes we consider have a COM energy, $\sqrt{s}$, near equal to the sum of the on-shell masses of the particles produced. Radiative corrections to scattering processes at threshold depend on the large on-shell external particle masses, as well as EW masses which are significant and, again, must be taken into account. We note further that in the threshold case, we take the gauge and Higgs masses to be IR as in the Sudakov case. Although there is extensive literature on QCD corrections at threshold, there is much more that needs to be achieved when considering EW and even BSM physics. The effective theory we employ at threshold is HPET along with standard RG techniques to perform logarithmic resummation.

In this work, we generalise previous results in a gauge-invariant fashion to massive scalars and fermions, incorporating the Higgs sector. Moreover, we study the threshold regime, as in previous works only the Sudakov regime was considered. We take the EFT analysis to two-loop orders to match the highest precision IR evolution results keeping the EW gauge boson and Higgs masses non-degenerate [75, 348]. We choose to study form factors instead of specific collider processes since they form the building blocks for a vast array of processes. In particular, they can be employed to study di-jet, $\bar{t}t$, squark pair, and DM production in various models [353, 357–359]. Previous and future results on processes are attainable from our results by external particle pair summation. Group-theoretic factor replacements are necessary as well since the model we study, $SU(N)$-Higgs theory with SSB, is selected for generality. Moreover, the various set of *composite operators*, we look into allows future studies to be derived from our results. To illustrate such derivations, we apply our formalism to EW corrections in the SM for the case of light quarks, leptons and the top quark as external particles.

7.2 Full and Effective Theory Formalism

7.2.1 $SU(N)$-Higgs Theory and the Standard Model

Our calculation is set in a spontaneously broken $SU(2)$ gauge model, however we keep our results quite general, i.e. not substituting numerical colour factors and sticking with composite operators so that our results are more conveniently mapped to more specific models for pheonmenological studies. In particular, with regards to the SM, the mapping of our model to the SM has been studied in detail previously [75, 76, 353]. Our model lacks solely in representing mass eigen-state γ-Z mixing, this occurs in the SM when the left-handed fermion $SU(2)$ isospin group mixes with the $U(1)$ hypercharge gauge group.

In our model the EW fields, $W^{\pm}$ and Z, are replaced with equal mass neutral $SU(2)$ gauge bosons, $W^a : a = \{1, 2, 3\}$. We label the $SU(N)$ generators by $T^a : a = \{1, \dots, N^2 - 1\}$ in the fundamental representation. The Lie algebra provides structure constants f^{abc} with Casimir operators for the adjoint and fundamental representations given by, $C_A = N$ and $C_F = (N^2 - 1)/2N$, respectively. Moreover, we take the convention, $\mathrm{tr}(T^a T^b) = T_F \delta^{ab}$, and

even in the specific case of $N = 2$ for $SU(2)$, we remain with the general symbols rather than the specific values, which makes our results easily convertible for specific models. For instance, in the SM which includes the $U(1)$ hypercharge gauge group. For $SU(2)$, the generators are $T^a = \sigma^a/2 : a = \{1, 2, 3\}$ with Pauli matrices, σ^a, and $f^{abc} = \epsilon^{abc}$. With the above specifications we may now state the $SU(2)$-Higgs Lagrangian in the *t'Hooft-Feynman gauge*,

$$\mathcal{L} = \mathcal{L}_\psi + \mathcal{L}_\chi + \mathcal{L}_{\rm YM} + \mathcal{L}_{\rm GF} + \mathcal{L}_{\rm gh} + \mathcal{L}_{\rm Higgs} + \mathcal{L}_{\rm Yuk}. \tag{7.1}$$

The Lagrangian is split into a few parts; $\mathcal{L}_\psi$ and $\mathcal{L}_\chi$ which describe the fermions and scalars (external particles), respectively; $\mathcal{L}_{\rm YM}$ and $\mathcal{L}_{\rm GF}$ corresponds to the massive *Yang–Mills* (YM) and *gauge–fixing* (GF) terms, respectively; $\mathcal{L}_{\rm gh}$ describes the *Faddeev-Poppov* (FP) ghost fields; $\mathcal{L}_{\rm Higgs}$ corresponds to the free Higgs Lagrangian which induces SSB and lastly, $\mathcal{L}_{\rm Yuk}$ entails the *Yukawa interaction* terms which provide mass to the external fermions and scalars.

Fermions/Scalars Let $\psi_i(x)$ and $\chi_i(x)$ correspond to Fermions and scalar fields with subscripts labelling fields as we consider different incoming outgoing external states for generality. The Dirac and scalar Lagrangians then have the following form,

$$\mathcal{L}_\psi = \bar{\psi}_i i \not{D} \psi_i, \quad \mathcal{L}_\chi = D_\mu \chi_i^\dagger D^\mu \chi_i, \tag{7.2}$$

where $D_\mu = \partial_\mu - igW_\mu^a T^a$, $W^a(x)$ is the gauge field as previously defined and g corresponds to the $SU(N)_W$ gauge coupling.

YM and Gauge-Fixing The Yang-Mills and gauge-fixing Lagrangians have the usual form,

$$\mathcal{L}_{\rm YM} = -\frac{1}{4} F^a_{\mu\nu} F^{\mu\nu,a}, \quad \mathcal{L}_{\rm GF} = -\frac{1}{2\xi_W} F_W^2, \tag{7.3}$$

such that $F^a_{\mu\nu} = \partial_\mu W^a_\nu - \partial_\nu W^a_\mu + g f^{abc} W^b_\mu W^c_\nu$ and $F_W = (\partial^\mu W^a_\mu - \xi_W M_W \phi^a) T^a$ where ϕ^a is the Goldstone boson field and ξ_W the linear t'Hooft gauge fixing parameter.

FP-ghosts In order to compensate for the effects of the unphysical components of the gauge fields in $\mathcal{L}_{\rm GF}$, one introduces the Lagrangian,

$$\mathcal{L}_{\rm gh} = -i(\partial^\mu \bar{c}^a) D^{ab}_\mu c^b - \xi_W M_W^2 \bar{c}^a c^a, \tag{7.4}$$

with FP-ghosts, $c^a(x), \bar{c}^a(x)$, and $D^{ab}_\mu = \partial_\mu \delta^{ab} + g f^{abc} W^c_\mu$.

Higgs and Yukawa The Higgs sector is defined by a complex scalar field, $\Phi(x)$, coupled to the gauge fields in the minimal Higgs Lagrangian,

$$L_H = (D_\mu \Phi)^\dagger D^\mu \Phi - V(|\Phi|^2), \tag{7.5}$$

with a potential, $V(|\Phi|^2) = \frac{\lambda}{2}(|\Phi|^2 - v^2/2)^2$. The Higgs potential is defined such that it gives rise to spontaneous symmetry breaking. Meaning the parameters, λ and v, are chosen in such a way that the potential minimum occurs for a non-vanishing Higgs field. More specifically, the scalar field ground state is non-zero,

$$|\langle \Phi \rangle|^2 = \frac{v^2}{2} \neq 0. \tag{7.6}$$

In perturbation theory one has to expand around the ground state and the Higgs field is written as

$$\Phi = \frac{1}{\sqrt{2}}\left((H+v) + i\phi^a T^a\right), \tag{7.7}$$

where H and ϕ^a have zero vacuum expectation value and are real. The physical Higgs field is labelled H and the Goldstone bosons which encode non-physical degrees of freedom are labelled ϕ^a. Inserting Eq. (7.7) back into the full Lagrangian, $\mathcal{L}$, provides mass to the Higgs field and W-boson,

$$M_H = \sqrt{\frac{\lambda}{2}}v \quad \text{and} \quad M_W = \frac{gv}{2}, \tag{7.8}$$

respectively. As for fermion and scalar masses, these arise from the Yukawa-like interactions,

$$\mathcal{L}_{\text{Yuk}} = -y_{f,i}\bar{\psi}_i\Phi\psi_i - y_{s,i}\chi_i^\dagger\Phi\chi_i + h.c., \tag{7.9}$$

where $y_{f,i}$ and $y_{s,i}$ are the Yukawa couplings for the fermions and scalars, respectively. After spontaneous symmetry breaking, i.e. inserting Eq. (7.7) back into Eq. (7.9), results in mass terms for said fermions and scalars,

$$\mathcal{L}_{\text{Yuk}} = -\sqrt{2}(y_{f,i}\bar{\psi}_i\psi_i + y_{s,i}\chi_i^\dagger\chi_i)(H+v), \tag{7.10}$$

therefore we can re-write,

$$m_\psi = \sqrt{2}vy_f \Rightarrow y_f = \frac{g}{2\sqrt{2}}\frac{m_\psi}{M_W} \equiv \frac{g}{2\sqrt{2}}Y_f, \tag{7.11a}$$

$$m_\chi^2 = \sqrt{2}vy_s \Rightarrow y_s = \frac{g}{2\sqrt{2}}\frac{m_\chi^2}{M_W} \equiv \frac{g}{2\sqrt{2}}Y_s, \tag{7.11b}$$

and in this notation the Lagrangian becomes,

$$\mathcal{L}_{\text{Yuk}} = -m_{\psi_i}\bar{\psi}_i\psi_i - m_{\chi_i}^2\chi_i^\dagger\chi_i - \frac{g}{2}Y_{f,i}H\bar{\psi}_i\psi_i - \frac{g}{2}Y_{s,i}H\chi_i^\dagger\chi_i, \tag{7.12}$$

where $h_{\psi,\chi}$ is conventionally used in Feynman rules, as given in Appendix A, which we attain by expanding each term in the full Lagrangian.

7.2.2 Heavy Particle Effective Theory

In the case of fermions we deploy HQET, which we describe briefly in this section but refer to other works for more detail [64, 153, 360]. HQET is useful when considering a bound state of a heavy quark with mass $m \gg \Lambda_{\text{QCD}}$, and light quarks with mass smaller than the colour confinement scale, Λ_{QCD}. The heavy quark interacts with the light degrees of freedom at an energy scale of order Λ_{QCD}. Whence, one can perform a system momentum decomposition,

$$p^\mu = mv^\mu + k^\mu, \tag{7.13}$$

such that the velocity of the heavy quark, v, is usually normalised with $v^2 = 1$, and the residual momentum, k, is small and labels light quark interactions. The first part of Eq. (7.13) is approximately conserved in processes and represents the energy of the heavy quark. The second part parameterises the remaining momentum due light and heavy-light quark interaction, such that,

$$|k| \sim \mathcal{O}(\Lambda_{\text{QCD}}) \quad \text{and} \quad m \gg \Lambda_{\text{QCD}}. \tag{7.14}$$

Therefore, we have a scale hierarchy which is a requirement for an EFT and upon which HQET was founded.

We now derive the HQET Lagrangian for a quark coupled to our $SU(N)$ gauge and Higgs fields, the full theory Lagrangian is given by,

$$\mathcal{L} = \bar{\psi}(i\not{D} - m)\psi - \frac{g}{2}Y_f H\bar{\psi}\psi, \tag{7.15}$$

such that $D^\mu = \partial^\mu - igW^\mu$ and Y_f is the Yukawa coupling as previously defined. By introducing the projection operators [84],

$$P_\pm = \frac{1 \pm \not{v}}{2}, \tag{7.16}$$

and two eigen-functions of these operators,

$$h_f = e^{imv\cdot x}P_+\psi, \tag{7.17a}$$

$$H_f = e^{imv\cdot x}P_-\psi, \tag{7.17b}$$

we then perform a spinor decomposition,

$$\psi = \frac{1+\not{v}}{2}\psi + \frac{1-\not{v}}{2}\psi = e^{-imv\cdot x}(h_f + H_f), \tag{7.18}$$

where the field and anti-field are given by H_f and h_f, respectively. These fields satisfy the relations, $\not{v}h_f = h_f$ and $\not{v}H_f = -H_f$ and heavy field external states are explained in Ref. [153]. Now, substituting Eq. (7.18) into Eq. (7.16), employing identities and using the anti-field, H_f, equation of motion to integrate it out, the HQET Lagrangian is arrived at,

$$\mathcal{L}_{\text{HQET}} = \bar{h}_f iv\cdot D h_f - \frac{g}{2}Y_f H\bar{h}_f h_f + \mathcal{O}(1/m), \tag{7.19}$$

where we neglect terms of $\mathcal{O}(1/m)$ in our derivation as they are heavily suppressed. The heavy quark propagator is thus,

$$S(k) = \frac{1}{k\cdot v + i\delta}\frac{1+\not{v}}{2}, \tag{7.20}$$

with residual momentum, k, and the vertex couplings are given in Appendix A.

To derive the heavy-field limit of a real scalar, or spin-0, field, it is very similar to the fermionic, or spin-1/2, derivation. One takes the full theory Lagrangian to be that of a complex scalar field, χ, with mass, m, coupled once again to to our $SU(N)$ gauge and Higgs fields,

$$\mathcal{L} = D_\mu\chi^\dagger D^\mu\chi - m^2\chi^\dagger\chi - \frac{g}{2}Y_s H\chi^\dagger\chi \tag{7.21}$$

Motivated by earlier studies [361–363], we then decompose the scalar field in the following way,

$$\chi = \frac{e^{-imv\cdot x}}{\sqrt{2}}\left(h_s + H_s\right), \tag{7.22}$$

where again, H_s is the anti-field containing the heavy modes, which needs to be integrated out. More specifically,

$$h_s = \frac{e^{imv\cdot x}}{\sqrt{2m}}\left(iv\cdot\partial + m\right)\chi \tag{7.23a}$$

$$H_s = \frac{e^{imv\cdot x}}{\sqrt{2m}}\left(-iv\cdot\partial + m\right)\chi, \tag{7.23b}$$

and plugging Eq. (7.23) into Eq. (7.22) gives,

$$iv\cdot\partial H_s = (2m + iv\cdot\partial)h_s. \tag{7.24}$$

Hence, substituting Eq. (7.22) and Eq. (7.24) into the Lagrangian given by Eq. (7.21), and using the equation of motion, one obtains the *heavy scalar effective theory* (HSET) Lagrangian in our model,

$$\mathcal{L}_{\text{HSET}} = h_s^\dagger iv \cdot D h_s - \frac{g}{2} Y_s H h_s^\dagger h_s + \mathcal{O}(1/m). \tag{7.25}$$

We again neglect terms of $\mathcal{O}(1/m)$ in our derivation as they are heavily suppressed. The heavy scalar propagator is thus,

$$S(k) = \frac{1}{k \cdot v + i\delta}, \tag{7.26}$$

where k is again the residual momentum and the vertex coupling is also given in Appendix A. Moreover, the HSET Feynman rules are directly attainable from the full theory rules through Eq. (7.13) and division by $2m$.

7.2.3 Soft-collinear effective theory

The appropriate effective theory for high-energy particles is SCET, which is defined by some energy of $\mathcal{O}(Q)$, where Q is a large characteristic scale of the process under consideration. SCET preserves the modes of the full theory with small invariant mass in comparison with Q^2. To describe fields in SCET, null vectors, n and $\bar{n}$, are necessary where $n = (1, \boldsymbol{n})$ and $\bar{n} = (1, -\boldsymbol{n})$. The three-vector, $\boldsymbol{n}$, is chosen to be a unit vector, thus, $\bar{n} \cdot n = 2$.

When calculating the Sudakov form factor, we choose the Breit frame where n and $\bar{n}$ to be along the p_2 and p_1 directions, respectively. The momentum transfer is labelled by, $q = p_2 - p_1$, and has zero time-component. We work with light-cone components, which for a four-vector, p, are defined by $p^+ \equiv n \cdot p$ and $p^- \equiv \bar{n} \cdot p$. In our problem, $p_1^- = p_{1\perp} = p_2^+ = p_{2\perp} = 0$, and $Q^2 = p_1^+ p_2^-$, which is reflected in our Feynman rules, see Appendix A. When a field is moving approximately along n, it is describable by an n-collinear field, $\xi_{n,p}(x)$, in SCET where p labels momentum, with components $\bar{n} \cdot p$ and $p_\perp$ [259, 260]. Kinematically, the field, $\xi_{n,p}(x)$, describes a particle with $p^2 \ll Q^2$. We can now define power counting in SCET,

$$p^- \sim Q, \quad p^+ \sim Q^2\lambda, \quad p_\perp \sim Q\lambda, \tag{7.27}$$

with small expansion parameter, λ, useful for power counting. The SCET field, $\xi_{n,p}(x)$, has momentum $p + k$, where as in HPET, k is the residual momentum, except in this effective theory, k is of order $Q\lambda^2$.

On the other hand, the gauge fields in SCET are, $W_{n,p}(x)$, $W_{\bar{n},p}(x)$ and $W(x)$ which correspond to n-collinear, $\bar{n}$-collinear and *ultrasoft* (US) fields. The US fields in SCET are the same as those present in other well-known effective theories [141, 364]. The n-collinear fields scale in momentum as,

$$p^- \sim Q, \quad p^+ \sim Q^2\lambda, \quad p_\perp \sim Q\lambda, \tag{7.28}$$

whereas the scaling of $\bar{n}$-collinear fields is given by,

$$p^+ \sim Q, \quad p^- \sim Q^2\lambda, \quad p_\perp \sim Q\lambda. \tag{7.29}$$

The US fields scale simply as $p^+ \sim p^- \sim p_\perp \sim Q\lambda^2$. The SCET fermion Lagrangian at leading order is given by [259],

$$\mathcal{L}_{\xi\xi} = \bar{\xi}_{n,p} \frac{\bar{n}}{4} \left(in \cdot D + \frac{p_\perp^2}{2\bar{n} \cdot p} \right) \xi_{n,p} \frac{\bar{n}}{4} \tag{7.30}$$

such that $iD^\mu = i\partial^\mu + gW^\mu$ is the US covariant derivative. The associated fermionic SCET propagator is then given by,

$$S(p) = \frac{\not{\bar{n}}}{2} \frac{\bar{n} \cdot p}{p^2}. \tag{7.31}$$

At this stage we define the projection operators for fermions in SCET,

$$P_n = \frac{n\bar{n}}{4}, \quad P_{\bar{n}} = \frac{\bar{n}n}{4}, \quad P_{\bar{n}} + P_n = 1, \tag{7.32}$$

where $P_n \xi_{n,p} = \xi_{n,p}$, $P_{\bar{n}} \xi_{,p} = 0$ and the converse holds for $\xi_{\bar{n},p}$. We further note that the large scale Q is not integrated out completely in SCET. The scale is implicit in the field labels and Q may appear in the anomalous dimension, however Q^2, which appears in the full theory, may not.

We also require SCET analogues for scalar fields. Let $\Phi_{n,p}$ be the scalar analogue of $\xi_{n,p}$, which describes a scalar particle moving approximately along n. One normalises the SCET field, $\Phi_{n,p}$, in the same way as the full theory field, ϕ, producing scalar particles with unit amplitude. The scalar field kinetic energy term in the Lagrangian then becomes,

$$D_\mu \phi^\dagger D^\mu \phi \to \Phi^\dagger_{n,p} \left((\bar{n} \cdot p)(in \cdot D) + p_\perp^2 \right) \Phi_{n,p} \tag{7.33}$$

in SCET. It is also convenient to re-define the scalar field as follows,

$$\phi_{n,p} = \sqrt{\bar{n} \cdot p} \Phi_{n,p} \tag{7.34}$$

in terms of which the kinetic term becomes,

$$\mathcal{L}_{\phi\phi} = \phi^\dagger_{n,p} \left(in \cdot D + \frac{p_\perp^2}{(\bar{n} \cdot p)} \right) \phi_{n,p} \tag{7.35}$$

with identical normalisation as Eq. (7.30). The re-scaled scalar propagator is given by,

$$\frac{1}{p^2} \to \frac{\bar{n} \cdot p}{p^2}. \tag{7.36}$$

Hence, $\phi_{n,p}$ as defined, creates n-collinear scalar fields with amplitude, $\sqrt{\bar{n} \cdot p}$.

7.3 The Form Factor

In this work we consider the Euclidean form factor given by the on-shell scattering amplitude, $F_E(Q^2) = \langle p_2 | \mathcal{O} | p_1 \rangle$. The external particles have momentum, $p_i^2 = m_i^2$, and are scattered by a set of operators $\mathcal{O}$, with transfer momentum, $Q^2 = -(p_2 - p_1)^2 > 0$. The time-like form factor is given by analytically continuing, $F(s) = F_E(-s - i0^+)$, implying $\ln Q^2/\mu^2 \to \ln s/\mu^2 - i\pi$. We are interested in $F_E(Q^2)$ for scattering of fermions, $\mathcal{O}^{(j)} = \{\bar{\psi}\gamma^\mu\psi, \bar{\psi}\psi, \bar{\psi}\sigma^{\mu\nu}\psi\} : j = \{1, 2, 3\}$, scattering of scalars, $\mathcal{O}^{(j)} = \{\chi^\dagger\chi, i(D^\mu\chi^\dagger\chi - \chi^\dagger D^\mu\chi)\} : j = \{4, 5\}$, and mixed scattering with, $\mathcal{O}^{(j)} = \{\bar{\psi}\chi, \chi^\dagger\psi\} : j = \{6, 7\}$. We consider gauge singlets operators as in previous studies [76, 352]. Thus, the external particles have the same gauge quantum numbers, but differing mass. We then compute the form factor, $F_E(Q^2)$, in the EFT approach with a set of theories, each appropriate at a particular scale.

To illustrate the matching, consider the Sudakov regime. At scales higher than Q^2, the model is the original (or full) Higgs-gauge theory. As one shifts to scales below $\mathcal{O}(Q^2)$, one transitions to the EFT (SCET) with $\mathcal{O}(Q^2)$ degrees of freedom integrated out. The IR behaviour of the full and EFT are identical but the UV behaviour differs. One must further introduce a so-called multiplicative matching coefficient to the EFT operator to ensure that the full and EFT operators produce identical OS matrix elements. More precisely, when matching the full theory onto SCET at the scale, $\mu \sim Q$, one attains,

$$\langle p_2 | \mathcal{O}(\mu) | p_1 \rangle = \exp\left[C(\mu)\right] \langle p_2 | \tilde{\mathcal{O}}(\mu) | p_1 \rangle , \tag{7.37}$$

where the matching coefficient, $\exp[C(\mu)]$, at $\mu \sim Q$ appears explicitly and can be computed perturbatively. The coefficient is indpendent of IR physics and presented in exponential form for later convenience. The operator, $\tilde{\mathcal{O}}(\mu)$ is the effective theory version of the operator in the full theory, $\mathcal{O}(\mu)$. More generally, a full theory operator, $\mathcal{O}$, may need to be matched to a more than one operator, $\tilde{\mathcal{O}}_i$, with identical quantum numbers in the EFT [365, 366]. Note that $C(\mu)$ will contain logarithms, $\ln \mu^2/Q^2$, and do not produce large contributions when $\mu \sim Q$. Although we choose $\mu = Q$, any value of $\mathcal{O}(Q)$ may be chosen as well, and all physical observables do not depend on the renormalisation scale, μ. The convention we follow is to pick the coefficient, $c(\mu)$, of $\mathcal{O}$ in the full theory, to be unity at $\mu = Q$. Our choice then provides the normalisation for $F_E(Q^2)$, and $c(Q) = \exp[C(Q)]$ is the SCET operator coefficient at $\mu = Q$. Moreover, to do RGE for $c(\mu)$ between scales we use the usual relation,

$$\mu \frac{dc(\mu)}{d\mu} = \gamma(\mu)c(\mu), \tag{7.38}$$

with anomalous dimension, $\gamma(\mu)$, of the EFT operator, $\tilde{\mathcal{O}}$. We then repeat these steps of matching and RGE as we shift between well-separated energy scales, integrating out the appropriate degrees of freedom along the way. The EFT approach is superior to IR evolution as it divides a multi-scale calculation into multiple single-scale pieces which are simpler to work with. One can then trivially identify so-called universal quantities which exhibit scale independence.

For reference, our notation mirrors previous work [76, 352], and is as follows, we use $a(\mu) \equiv \alpha(\mu)/(4\pi)$, and for applications to the SM, $a_i(\mu) \equiv \alpha_i(\mu)/(4\pi)$ such that $i = \{s, 2, 1\}$ represents the couplings for QCD, $SU(2)$ and $U(1)$ interactions. Hypercharge is taken to be normalised such that $Q = T_3 + Y$. We further employ the abbreviated notation, $L_A \equiv \ln A^2/\mu^2$, for logarithms present.

7.4 Renormalisation

7.4.1 Field Renormalisation

The OS renormalization of the external scalar/fermion fields in our form factor expansions is done when the vertex contributions are multiplicatively renormalised. The renormalisation factor, Z, is known as the scalar/fermion wave function renormalization (WFR) constant. The OS self-energy corrections, Σ, at $p^2 = m^2$ define the WFR constant as we will describe. The external fields we study are, $\{\psi, \chi, h_f, h_s, \xi_{n,p}, \phi_{n,p}\}$, and letting $\{I, J\}$ denote these fields such that V_{IJ} and $Z_{IJ} = \sqrt{Z_I Z_J}$ correspond to the vertex and wave-function contributions, we have the perturbative expansion,

$$V_{IJ} = 1 + aV_{IJ}^{(1)} + a^2 V_{IJ}^{(2)} + \mathcal{O}(a^3), \tag{7.39}$$

$$Z_I = 1 + a\delta Z_I^{(1)} + a^2 \delta Z_I^{(2)} + \mathcal{O}(a^3). \tag{7.40}$$

Therefore, the WFR is given by,

$$Z_{IJ} = 1 + \frac{a}{2}\left(\delta Z_I^{(1)} + \delta Z_J^{(1)}\right) + \frac{a^2}{2}\left(\delta Z_I^{(2)} + \delta Z_J^{(2)} + \frac{1}{2}\delta Z_I^{(1)}\delta Z_J^{(1)} - \frac{1}{4}(\delta Z_I^{(1)})^2 - \frac{1}{4}(\delta Z_J^{(1)})^2\right).$$

Whence, the total form factor, $F_{IJ} = V_{IJ}Z_{IJ}$, up to order α^2, can be written as follows,

$$\begin{aligned} F_{IJ} =& 1 + a\left\{V_{IJ}^{(1)} + \frac{1}{2}\left(\delta Z_I^{(1)} + \delta Z_J^{(1)}\right)\right\} + a^2\left\{V_{IJ}^{(2)} + \frac{1}{2}\left(\delta Z_I^{(2)} + \delta Z_J^{(2)}\right)\right. \\ &\left. + \frac{1}{2}\left(\delta Z_I^{(1)} + \delta Z_J^{(1)}\right)V_{IJ}^{(1)} + \frac{1}{4}\delta Z_I^{(1)}\delta Z_J^{(1)} - \frac{1}{8}(\delta Z_I^{(1)})^2 - \frac{1}{8}(\delta Z_J^{(1)})^2\right\}. \end{aligned} \tag{7.41}$$

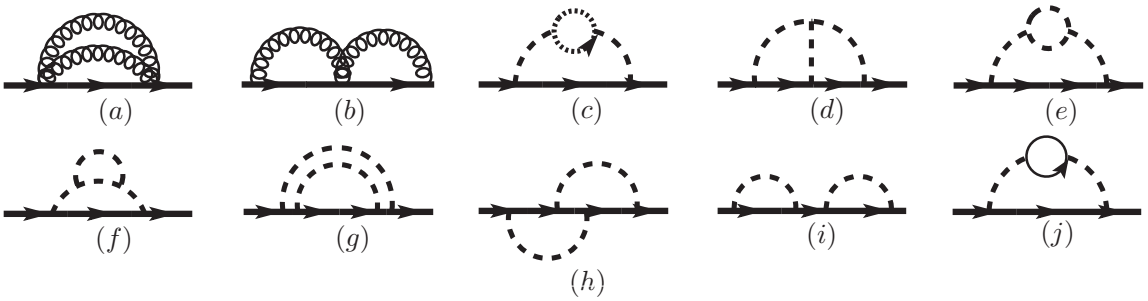

Figure 7.1: Two-loop self-energy graphs, arrowed lines represent all incoming-outgoing particles, dashed lines correspond to bosonic propagators. $(a), (b)$ are seagull terms and only occur with scalar propagators, (h)-(j) and (c)-(g) represent Abelian and non-Abelian corrections, respectively.

With the above notation we may now discuss how to obtain the WFR constant, Z_I, for the spin-$\{0, 1/2\}$ fields we study. In all cases, the WFR contributions are garnered from self-energy amplitudes, $\tilde{\Sigma}_I$ [84, 115].

Before determining WFR contributions for our fields of interest, we note that collinear SCET and full theory field WFR contributions are identical [76, 259]. Whence, we only need to outline how to obtain the wave-function contributions to the form factors for the full theory and HPET fields.

Scalar field: For massive scalars of momentum, p, and mass, m, the self-energy amplitudes, as shown in Fig. 7.1 are of the form,

$$\tilde{\Sigma}_\chi = -i\Sigma_\chi(p^2)\mathbf{1}. \tag{7.42}$$

From this we may extract the WFR contributions in the following way,

$$\delta Z_\chi = \frac{i}{4}\mathrm{tr}(\partial_{p^2}\tilde{\Sigma}_\chi|_{p^2=m^2}). \tag{7.43}$$

The massless case is identical except one takes $p^2 = 0$ instead.

Fermion field: In the case of fermions of momentum, p, and mass, m, the self-energy amplitudes are of the form,

$$\tilde{\Sigma}_\psi = -i\left(\Sigma^V_\psi(p^2)\not{p} + \Sigma^S_\psi(p^2)m\right)\mathbf{1}, \tag{7.44}$$

where the super-scripts, V and S, denote vector and scalar contributions, respectively. From this we may extract the WFR contributions,

$$\delta Z_\psi = \left\{\Sigma^V_\psi(m^2) + 2m^2\partial_{p^2}\left(\Sigma^V_\psi(p^2) + \Sigma^S_\psi(p^2)\right)|_{p^2=m^2}\right\}. \tag{7.45}$$

The massless case simplifies as $p^2 = 0$ instead and the terms proportional to m^2 vanish.

Heavy fields: Lastly, for heavy scalars and fermions, h, of momentum, p, and velocity, v, the self-energy amplitudes are of the form,

$$\tilde{\Sigma}_h = -i\left\{\Sigma^F_h(v\cdot p) + \Sigma^R_h(M_B)\right\}\mathbf{1}, \tag{7.46}$$

Field	m	M	$\delta Z^{(1)}$	$\delta Z^{(2)}$
ψ	0	0	$\left(\frac{C_F}{2}+\frac{Y_f^2}{16}\right)\left\{\frac{2}{\epsilon_{\rm IR}}-\frac{2}{\epsilon_{\rm UV}}\right\}$	$F_\psi^{(0,0)}$
ψ	0	M	$\frac{C_F}{2}\left(\frac{2}{-\epsilon_{\rm UV}}+1+2L_{M_W}\right)+\frac{Y_f^2}{16}\left(-\frac{2}{\epsilon_{\rm UV}}-1+2L_{M_H}\right)$	$F_\psi^{(0,M)}$
ψ	m	0	$\frac{C_F}{2}\left(-\frac{2}{\epsilon_{\rm UV}}-\frac{4}{\epsilon_{\rm IR}}-4+3L_m\right)+\frac{Y_f^2}{16}\left(-\frac{2}{\epsilon_{\rm UV}}+\frac{8}{\epsilon_{\rm IR}}+14-6L_m\right)$	$F_\psi^{(m,0)}$
ψ	m	M	$\frac{C_F}{2}\left(-\frac{2}{\epsilon_{\rm UV}}-8+2L_{M_W}-P\right)+\frac{Y_f^2}{16}\left(-\frac{2}{\epsilon_{\rm UV}}+14+2L_{M_H}-P'\right)$	$F_\psi^{(m,M)}$
χ	0	0	$\frac{C_F}{2}\left\{\frac{4}{\epsilon_{\rm UV}}-\frac{4}{\epsilon_{\rm IR}}\right\}$	$F_\chi^{(0,0)}$
χ	0	M	$-\frac{Y_s^2}{8M_H^2}+\frac{C_F}{2}\left(\frac{4}{\epsilon_{\rm UV}}+3-4L_{M_W}\right)$	$F_\chi^{(m,0)}$
χ	m	0	$\frac{C_F}{2}\left(\frac{4}{\epsilon_{\rm UV}}-\frac{4}{\epsilon_{\rm IR}}\right)+\frac{Y_s^2}{4m^2}\left(\frac{1}{2\epsilon_{\rm IR}}+1-L_m\right)$	$F_\chi^{(0,M)}$
χ	m	M	$-\frac{Y_s^2}{4M_H^2}S'+\frac{C_F}{2}\left(\frac{4}{\epsilon_{\rm UV}}-4L_{M_W}+S\right)$	$F_\chi^{(m,M)}$
$h_{f,s}$	-	0	$\frac{C_F}{2}\left(\frac{4}{\epsilon_{\rm UV}}-\frac{4}{\epsilon_{\rm IR}}\right)+\frac{Y_s^2}{4}\left(-\frac{2}{\epsilon_{\rm UV}}+\frac{2}{\epsilon_{\rm IR}}\right)$	$F_h^{(0)}$
$h_{f,s}$	-	M	$\frac{C_F}{2}\left(\frac{4}{\epsilon_{\rm UV}}-4L_{M_W}\right)+\frac{Y_s^2}{4}\left(-\frac{2}{\epsilon_{\rm UV}}+2L_{M_H}\right)$	$F_h^{(M)}$

Table 7.1: On-shell wave-function renormalisation contributions. Exchanged boson masses are $M = M_{W,H}$ where $L_M = \ln M^2/\mu^2$, and the external particle (scalar or fermion) mass is m. The two-loop wave-function corrections, $F_I^{(i,j)}$, and the parametric integral functions, $P, P^{'}$ and $S, S^{'}$, shown in Appendix B.8.

for bosons of mass, M, coupling to the heavy fields, as in our case. We thus obtain a heavy field residual mass term, δm, along with the usual wave function contribution,

$$\delta Z_h = i\partial_{v\cdot p}\tilde{\Sigma}_h|_{v\cdot p=0} \tag{7.47}$$

$$\delta m_I = -i\tilde{\Sigma}_h(v\cdot p=0). \tag{7.48}$$

The residual shift in the heavy particle mass, δm, occur as a result of divergent loop integrals with odd-powered loop momenta, l, and δm is not analytic in M^2. Residual shifts of his kind are known to occur in mass corrections to particles with $l\cdot v$ propagators [367,368]. Integrals such as these are finite but not analytic upon dimensional regularisation. In the HPET Lagrangian there is both m_0 and δm which are not independent of each other. Thus, one can pick $m_0 \to m_0+\Delta m$, $\delta m \to \delta m - \Delta m$, and for convenience, define m_0 such that δm is not longer present. This choice is known as the pole mass [286], and as in previous work we stick with this convention.

7.4.2 Mass and Coupling Renormalisation

Our loop calculations up to two-loop order are done with the bare (unrenormalised) Lagrangian and thus Feynman rules. We thus have to multiplicatively renormalise the bare mass and couplings with their respective constants. Although this does not alter the bare two-loop results at $\mathcal{O}(\alpha^2)$, the one-loop bare parameters must be replaced by the renormalised ones as terms will appear which contribute at two-loop order. In our work we employ the $\overline{\rm MS}$ scheme for the coupling renormalisation and the OS scheme for mass renormalisation. With the OS scheme, one defines the (physical) renormalised mass squared as the real part of the propagator's pole.

In the case of coupling renormalisation the replacement can be applied naively as shown below. However, in the case of mass renormalisation, say given a mass M, with replacement (we denote the bare quantities with index, 0),

$$M_0^2 = M^2 + \delta M^2 + \mathcal{O}(\alpha^2), \tag{7.49}$$

in which δM^2 corresponds to the mass contribution, the masses to be renormalisaed often appear in terms of the form $(\mu^2/M^2)^\epsilon$ or in powers of logarithms. Thus the substitutions at one-loop are,

$$\left(\frac{M^2}{\mu^2}\right)^\epsilon \to \left(\frac{M^2}{\mu^2}\right)^\epsilon \left(1+\epsilon\frac{\delta M^2}{M^2}\right) + \mathcal{O}(\alpha^2), \tag{7.50}$$

$$L_M^n = L_M^n + nL_M^{n-1}\frac{\delta M^2}{M^2} + \mathcal{O}(\alpha^2), \tag{7.51}$$

which, when applied provides corrections of $\mathcal{O}(\alpha^2)$. For the particles we are considering below, the renormalized quantities and renormalization constants are defined as follows,

$$\alpha_0 = (1+\delta Z_\alpha)\alpha \tag{7.52a}$$

$$M_{W,0}^2 = M_W^2 + \delta M_W^2 \tag{7.52b}$$

$$M_{H,0}^2 = M_H^2 + \delta M_H^2 \tag{7.52c}$$

$$m_{\chi,0}^2 = m_\chi^2 + \delta m_\chi^2 \tag{7.52d}$$

$$m_{\psi,0} = m_\psi + \delta m_\psi, \tag{7.52e}$$

where the subscripts ψ and χ indicate that the masses belong to fermion and scalar fields, respectively, that appear externally in the form factor.

7.4.2.1 Coupling Renormalisation

In the $\overline{\text{MS}}$ scheme, the bare coupling α_0 is renormalised to the physical coupling α with the following relation,

$$\alpha_0 = (1+\delta Z_\alpha)\alpha = \alpha\left(1 - \frac{\alpha}{4\pi}\frac{\beta_0}{\epsilon_{\text{UV}}}\right) + \mathcal{O}(\alpha^3), \tag{7.53}$$

such that β_0 is the leading (one-loop) renormalisation group beta function coefficient. We note that β_0 has the following form,

$$\beta_0 = \frac{11}{3}C_A - \frac{4}{3}T_f n_f - \frac{1}{6}, \tag{7.54}$$

where the terms proportional to C_A and n_f correspond to the non-Abelian and fermionic contributions, respectively, while the last term corresponds to a Higgs contribution. Thus by applying the substitution in Eq. (7.53) to our one-loop form factors, we get terms which contribute at $\mathcal{O}(\alpha^2)$.

7.4.2.2 Gauge Mass Renormalisation

As this is the first case of mass renormalisation we consider we will discuss this in detail, at the amplitude level. The bare mass, $M_{W,0}$, is related to the renormalized mass, M_W, by the self-energy corrections of the gauge boson, given by,

$$\tilde{\Pi}^{\mu\nu,ab}(p) = i\delta^{ab}g^{\mu\nu}p^2\Pi(p^2)\mathbf{1} + \text{terms} \propto p^\mu p^\nu. \tag{7.55}$$

After extracting $\Pi(p^2)$ from the amplitudes with the help of the projection operator, $P_{\mu\nu} = g_{\mu\nu} - \frac{p_\mu p_\nu}{p^2}$, the renormalised mass is given by setting $\delta M_W^2 = -M_W^2\Pi(M_W^2)$, and we may check various contributions at one-loop, up to $\mathcal{O}(\epsilon)$, where ϵ are UV divergences. The results up to

$\mathcal{O}(\epsilon^2)$, needed for mass renormalisation contributing at two-loop orders is provided in an arXiv ancillary file of Ref. [325]. We begin with the self-energy contributions from the fermion loop,

$$\Pi(M_W^2)_{n_f} = -\frac{4a}{9} T_f n_f \left\{ 5 + 3i\pi + \frac{3}{\epsilon} - 3L_{M_W} \right\} + \mathcal{O}(\epsilon), \tag{7.56}$$

where as we stated before, $a(\mu) = \alpha(\mu)/4\pi$. Next, we have contributions from the non-Abelian gauge boson and ghost field loops,

$$\Pi(M_W^2)_{WW,cc} = \frac{a}{9} C_A \left\{ 82 - 12\sqrt{2}\pi + \frac{51}{\epsilon} - 51 L_{M_W} \right\} + \mathcal{O}(\epsilon), \tag{7.57}$$

from the loop with gauge and Higgs boson,

$$\Pi(M_W^2)_{WH} = a \left\{ -2 - \frac{1}{\epsilon} + L_{M_W} + \frac{sr}{M_W} \ln w + r^2 \ln r \right\} + \mathcal{O}(\epsilon), \tag{7.58}$$

where we define $r = M_H/M_W$, $s = \sqrt{M_H^2 - 4M_W^2}$ and $w = \frac{2M_W}{M_H + s}$, and finally a contribution from the loops with Higgs and Goldstone bosons,

$$\Pi(M_W^2)_{\phi\phi} = \frac{a}{72} C_A \left\{ 34 - 3\sqrt{3} + \frac{15}{\epsilon} - 15 L_{M_W} \right\} + \mathcal{O}(\epsilon), \tag{7.59}$$

$$\begin{aligned} \Pi(M_W^2)_{H\phi} = a \Bigg\{ & \frac{1}{18} \left(5 + \frac{3}{\epsilon} - 3L_{M_W} \right) + \frac{r^2}{2} \left(\ln r + \frac{3}{2} + \frac{1}{2\epsilon} - \frac{1}{3} L_{M_H} \right) \\ & - \frac{r^4}{12} - \frac{r^4}{2} \ln r + \frac{r^5 s}{12 M_W} \ln w - \frac{r^3 s}{3 M_W} \ln w + \frac{r^6}{12} \ln r \Bigg\} + \mathcal{O}(\epsilon). \end{aligned} \tag{7.60}$$

Thus combining all terms provides one with the gauge boson mass correction in the replacement rules. Moreover, we omit tadpole diagram contributions in the self-energy amplitude as they are momentum-independent and cancel with the associated vertex and WFR tadpole contributions, which are excluded as well.

7.4.2.3 Higgs Mass Renormalisation

As we were explicit in the previous section and broke down each contribution we will be brief now as the above still applies and we simply state the correction. The bare Higgs mass, M_{H_0}, and the renormalized mass, M_H, are related by the Higgs self-energy corrections, $\tilde{\Sigma}(p^2) = i\Sigma(p^2)\mathbf{1}$. Extracting $\Sigma(p^2)$ gives the renormalized mass by setting $\delta M_H^2 = \Sigma(M_H^2)$, which has the following form after combining all contributions,

$$\begin{aligned} \delta M_H^2 = a C_A C_F \frac{M_W}{64 r} \Bigg\{ & -2 M_W r (r^4 - 16 r^2 + 36) + M_W r (r^4 - 16 r^2 + 48) \left(L_{M_W} - \frac{1}{\epsilon} \right) \\ & - s (r^4 - 16 r^2 + 56) \ln \left(\frac{r(s - M_H)}{2 M_W} + 1 \right) \Bigg\} - a r^4 \frac{9 M_W^2}{32} \Bigg\{ 2 - \frac{\pi}{\sqrt{3}} + \frac{1}{\epsilon} - L_{M_W} \\ & - \ln r \Bigg\} + \mathcal{O}(\epsilon), \end{aligned} \tag{7.61}$$

up to $\mathcal{O}(\epsilon)$, where ϵ are UV divergences. The results up to $\mathcal{O}(\epsilon^2)$, needed for mass renormalisation contributing at two-loop orders is provided an arXiv ancillary file of Ref. [325]. Whence the above provide us with the Higgs mass correction at two-loop order. Moreover, we note that the self-energy diagrams with tadpoles have been omitted for the same reason previously described.

7.4.2.4 Fermion and Scalar Mass Renormalisation

Lastly we discuss the mass renormalisation of the massive external fermion and scalar fields we consider. These masses appear and the corrections contribute at two-loop order in the threshold regime. Due to expression size we show the example of the case where the Higgs and gauge masses are taken to be IR and vanishing. We begin with the scalar contributions; the relation between the bare scalar mass, m_{χ_0}, and the renormalised mass, m_χ, is determined by the scalar self-energy corrections, $\tilde{\Sigma}(p^2) = i\Sigma(p^2)\mathbf{1}$. Extracting $\Sigma(p^2)$ gives the renormalised mass by setting $\delta m_\chi^2 = \Sigma(m_\chi^2)$, which has the following form after combining all contributions,

$$\delta m_\chi^2 = a e^{\gamma_E \epsilon} \left(\frac{\mu^2}{m_\chi^2}\right)^\epsilon \left\{ C_F m_\chi^2 \frac{(2\epsilon-3)\Gamma(\epsilon-1)}{2\epsilon-1} + Y_s^2 \frac{\Gamma(\epsilon)}{4-8\epsilon} \right\}, \tag{7.62}$$

where ϵ are UV divergences. Note that the first and second term have the same dimensions by definition of Y_s in Eq. (7.11).

Next, the bare fermion mass, m_{ψ_0}, and the renormalised mass, m_ψ, are related by fermion field self-energy corrections,

$$\tilde{\Sigma}(p^2) = i\left(\Sigma^V(p^2)\not{p} + \Sigma^S(p^2) m_\psi\right)\mathbf{1}, \tag{7.63}$$

where the superscripts, S and V, label the scalar and vector contributions. Extracting $\Sigma^{S,V}(p^2)$ gives the renormalized mass by setting $\delta m_\psi = m_\psi \left(\Sigma^V(m_\psi^2) + \Sigma^S(m_\psi^2)\right)$, which has the following form after combining all contributions,

$$\delta m_\psi = a e^{\gamma_E \epsilon} \left(\frac{\mu^2}{m_\psi^2}\right)^\epsilon \left\{ C_F \frac{(2\epsilon-3)\Gamma(\epsilon)}{2\epsilon-1} - \frac{Y_f^2}{8}\left(\Gamma(\epsilon-1) + \frac{4\Gamma(\epsilon)}{1-2\epsilon}\right) \right\}, \tag{7.64}$$

where again ϵ are UV divergences. In this case dimensions hold since Y_f is dimensionless as shown in Eq. (7.11). Note that the expansions up to $\mathcal{O}(\epsilon)^3$ are needed for mass renormalisation. Now we have all the one-loop terms that arise in our problem which, when replacement rules are applied, contribute at the two-loop level.

7.4.3 Operator Renormalisation

Composite operators like ours require both WFR and subsequent subtractions [153]. This holds for both full and effective theory operators, to illustrate, let us take, for instance, the bare heavy-light fermion operator from HPET,

$$\mathcal{O}^{(0)} = \bar{\psi}^{(0)} \Gamma h_f^{(0)} = \sqrt{Z_f Z_h}\, \bar{\psi} \Gamma h_f, \tag{7.65}$$

with Γ being a Dirac matrix of interest. The renormalised composite operator is then,

$$\begin{aligned} \mathcal{O} = Z_{\mathcal{O}}^{-1} \mathcal{O}^{(0)} =& \frac{\sqrt{Z_f Z_h}}{Z_{\mathcal{O}}} \bar{\psi} \Gamma h_f \\ &= \bar{\psi} \Gamma h_f + \text{counter term}, \end{aligned} \tag{7.66}$$

such that the additional operator, $Z_{\mathcal{O}}$, is found by calculating an operator-inserted Green's function. Therefore, $Z_{\mathcal{O}}$ can be found from the one particle irreducible Green's function of $\bar{\psi}$, h_f and $\mathcal{O}$, where the counter term in Eq. (7.66) contributes,

$$\left(\frac{\sqrt{Z_f Z_h}}{Z_{\mathcal{O}}} - 1\right)\Gamma, \tag{7.67}$$

to this time-ordered product. Thus, the counter term given by Eq. (7.66), must eliminate the UV divergences present in the vertex contribution. Hence, Eq. (7.66) must be finite as $\epsilon_{\rm UV} \to 0$. Plugging in the wave function contributions, $\sqrt{Z_f Z_h}$ then gives $Z_{\mathcal{O}}$ by the finiteness requirement. The anomalous dimension of the composite operator,

$$\gamma_{\mathcal{O}} = \frac{\mu}{Z_{\mathcal{O}}} \left(\frac{dZ_{\mathcal{O}}}{d\mu} \right), \tag{7.68}$$

is then obtained from the renormalisation constant,

$$Z_{\mathcal{O}} = 1 + \delta Z_{\mathcal{O}} = 1 - \frac{1}{\epsilon_{\rm UV}} \gamma_{\mathcal{O}} \tag{7.69}$$

Note in this case the independence of the renormalisation of $\mathcal{O}$ from our gamma matrix, Γ, in the composite operator. This is due to heavy and light fermion spin and chiral symmetry, respectively. In fact, this independence holds for all our effective operators in the threshold regime as they include operators with heavy/light fermions/scalars [153]. On the other hand, in the full theory as well as SCET the gamma matrix plays a role and $Z_{\mathcal{O}}$ varies for different operators. In particular, in the full theory for both scalars and fermions, the scalar and tensor currents require renormalisation while the vector currents, at all orders, do not, meaning $\delta Z_{\mathcal{O}}$ is zero [84].

7.5 Radiative Corrections in Sudakov Limit

We may now determine the form factor, $\ln F_E(Q^2)$, in the large Q^2, or Sudakov, limit. We perform calculations up to two-loop order, extending previous studies and refraining from including computational details which have been presented in other works [75, 76].

7.5.1 Massless External Particles

Let us consider the case of massless external particles in a fair amount of detail to begin with. The limit we consider is thus, $Q^2 \gg M^2 \gg m^2$, where M and m denote the bosonic and external masses, respectively. Schematically, in this case, the matching and running steps can be illustrated as follows,

$$\mathcal{O} \xleftrightarrow[m,M=0]{\mu \sim Q} e^C \tilde{\mathcal{O}}_1 \xrightarrow{\gamma_1} e^C \tilde{\mathcal{O}}_1 \xleftrightarrow[m=0]{\mu \sim M} e^{C+D} \tilde{\mathcal{O}}_2,$$

where C and D are multiplicative matching coefficients, γ_1 the effective theory anomalous dimension and $\tilde{\mathcal{O}}_{1,2}$ the effective theory operators at each scale. At scale, $\mu > Q$, we use the full theory, and at scale, $\mu < Q$, we match down to SCET with the Wilson coefficient, $c(\mu)$. The RGE of $c(\mu)$ is given by,

$$\mu \frac{dc(\mu)}{d\mu} = \gamma_F(a(\mu)) c(\mu), \tag{7.70}$$

where $\gamma_F(\mu)$ is the anomalous dimension for a full theory composite operator, $\mathcal{O}$. The full theory is matched onto SCET at a scale $\mu \sim Q$.

On the other hand, the EFT has off-shell modes of $\mathcal{O}(Q)$ integrated out. The matching coefficient thus depends on L_Q, and these logarithms are not large if $\mu \sim Q$. The full theory

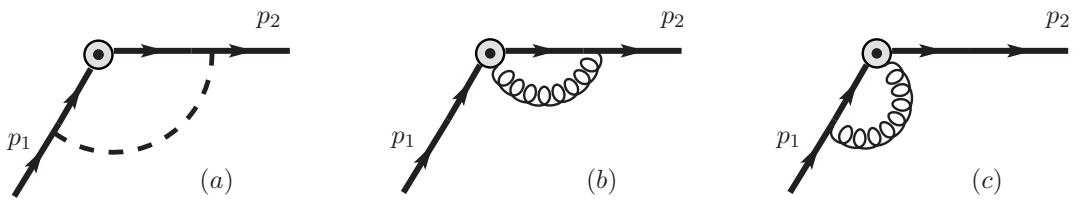

Figure 7.2: One-loop vertex corrections, bulls-eye represents composite operator, arrowed lines represent all incoming-outgoing particles we consider, dashed lines correspond to bosonic propagators. $(b), (c)$ only exists with the operator, $\mathcal{O} = i\phi^\dagger \overleftrightarrow{D}_\mu \phi$, and EFT equivalents, $\tilde{\mathcal{O}}$.

operator, $\mathcal{O}$ matches to the SCET operator, $\tilde{\mathcal{O}}$. More specifically,

$$\bar{\psi}\Gamma\psi \to e^C(\bar{\xi}_{n,p_2}W_n)\Gamma(W_{\bar{n}}^\dagger \xi_{\bar{n},p_1}), \tag{7.71a}$$

$$\chi^\dagger\chi \to e^C(\Phi_{n,p_2}^\dagger W_n)(W_{\bar{n}}^\dagger \Phi_{\bar{n},p_1}), \tag{7.71b}$$

$$i\chi^\dagger \overleftrightarrow{D}_\mu \chi \to e^C(\Phi_{n,p_2}^\dagger W_n)[i\mathcal{D}_1 + i\mathcal{D}_2]_\mu (W_{\bar{n}}^\dagger \Phi_{\bar{n},p_1}), \tag{7.71c}$$

$$\bar{\psi}\chi \to e^C(\bar{\xi}_{n,p_2}W_n)(W_{\bar{n}}^\dagger \Phi_{\bar{n},p_1}), \tag{7.71d}$$

where $i\mathcal{D}_1 = \mathcal{P} + g\,(n\cdot A_{\bar{n},q})\,\frac{\bar{n}}{2}$, $i\mathcal{D}_2 = \mathcal{P}^\dagger + g\,(\bar{n}\cdot A_{n,-q})\,\frac{n}{2}$, $\mathcal{P}$ are label operators in SCET and W_n is a Wilson line with n-collinear gauge fields [259]. Of course $C(\mu)$ is indeed $C_j(\mu) : j = \{1,\ldots,7\}$ as it differs for each operator. We have also written the multiplicative matching coefficient as $\exp[C(\mu)]$ rather than $C(\mu)$ for convenience. Upon computing the OS full theory matrix element with all IR scales set to zero, the matching coefficient is found by extracting the finite part [218, 369, 370].

To illustrate the computation, let us consider the one-loop result. The full and EFT diagrams to be determined are those in Fig. 7.2, except in SCET the external lines are both taken to be collinear and graphs (b) and (c) are no longer identical. After combining the vertex graphs with the wave-function and tree-level graphs, one obtains the value of the full and effective theory matrix elements, $\langle p_2|\,\mathcal{O}\,|p_1\rangle$ and $\langle p_2|\,\tilde{\mathcal{O}}\,|p_1\rangle$, respectively. The IR scales to be set to zero are the internal and external particle masses, resulting in scaleless integrals for the EFT and wave-function contributions. One then combines the vertex and wave-function contributions as prescribed in Eq. (7.41) to obtain the one and two-loop order results. Moreover, as the masses are zero there are no two-loop contributions from mass renormalisation, only coupling renormalisation contributes.

The EFT matrix element has no radiative corrections as scaleless integrals are null in dimensional regularization. Thus, both full and effective theory operators are then normalised to have the same values at tree-level [218],

$$\exp[C(\mu)] = \frac{\langle p_2|\,\mathcal{O}\,|p_1\rangle}{\langle p_2|\,\mathcal{O}\,|p_1\rangle_{tree}}. \tag{7.72}$$

When computing the one-loop graphs for $\mathcal{O}$, $\exp[C(\mu)]$ is given by the on-shell full theory matrix element, normalised by its tree-level value. The particle masses are all much smaller than Q^2, resulting in contributions, M^2/Q^2 (where M corresponds to the gauge and Higgs masses), which are negligible.

At one-loop order, one can determine $C(\mu)$ for the other operators in a similar fashion, and these are presented in Table 7.2, where in the loop expansion, $C(\mu) = aC^{(1)}(\mu) + a^2C^{(1)}(\mu) + \mathcal{O}(a^3)$. Large logarithms are not apparent if $\mu \sim Q$, in this work we choose $\mu = Q$ and the RGE

$\mathcal{O}$	$\gamma_F^{(1)}$	$C^{(1)}$	$C^{(2)}$
$\bar{\psi}\psi$	$-3C_F + \frac{Y_f^2}{8}$	$\frac{C_F}{6}\left\{-6L_Q^2 + \pi^2 - 12\right\} + \frac{Y_f^2}{4}\left\{L_Q - 2\right\}$	$V_1^{(Q)} + \Delta C_1$
$\bar{\psi}\gamma^\mu\psi$	$-\frac{Y_f^2}{4}$	$\frac{C_F}{6}\left\{\pi^2 - 6L_Q\left(L_Q - 3\right)L_Q - 48\right\} - \frac{Y_f^2}{8}\left\{L_Q - 1\right\}$	$V_2^{(Q)} + \Delta C_2$
$\bar{\psi}\sigma^{\mu\nu}\psi$	$C_F - \frac{Y_f^2}{8}$	$\frac{C_F}{6}\left\{-6L_Q\left(L_Q - 4\right)L_Q + \pi^2 - 48\right\} + \frac{Y_f^2}{4}$	$V_3^{(Q)} + \Delta C_3$
$\chi^\dagger\chi$	$-3C_F$	$\frac{C_F}{6}\left\{-6L_Q\left(L_Q - 1\right)L_Q + \pi^2 - 12\right\}$	$V_4^{(Q)} + \Delta C_4$
$i\chi^\dagger \overleftrightarrow{D}_\mu \chi$	0	$\frac{C_F}{6}\left\{-6L_Q\left(L_Q - 4\right)L_Q + \pi^2 - 48\right\}$	$V_5^{(Q)} + \Delta C_5$
$\bar{\psi}\chi,\ \chi^\dagger\psi$	$-\frac{3}{2}C_F - \frac{Y_f^2}{16}$	$\frac{C_F}{6}\left\{-6L_Q\left(L_Q - 3\right)L_Q + \pi^2 - 36\right\}$	$V_6^{(Q)} + \Delta C_6$

Table 7.2: Matching corrections, $C(\mu)$, to the Sudakov form factor at $\mu \sim Q$. $V_i^{(Q)}$ are two-loop vertex corrections. $\Delta C(\mu)$ is the coupling corrections to matching at $\mu \sim Q$. Both are given in Appendix B.1. γ_F is the one-loop full theory anomalous dimension.

of $c(\mu)$ in the EFT is described by, γ_1, the anomalous dimension of $\tilde{O}$ in SCET. The full thoery anomalous dimension, γ_F, of $\tilde{O}$ is also given in Table 7.2, we avoid presenting the two-loop result as this has been previously found for a number of operators [371].

On the other hand, γ_1 in SCET is used to evolve $c(\mu)$ from $\mu = Q \to M$. As previously defined, the UV counter terms for the SCET graphs are precisely the anomalous dimension, and can depend on Q, the largest scale. UV divergences are independent of IR properties and γ_1 is linear in $\ln \mu^2/Q^2$ to all order [370, 372], so one can always write,

$$\gamma_1(\mu) = A(\alpha(\mu)) \ln \frac{\mu^2}{Q^2} + B(\alpha(\mu)). \tag{7.73}$$

The anomalous dimension can be written in a loop expansion, $\gamma_1 = a\gamma_1^{(1)} + a^2\gamma_2^{(2)} + \mathcal{O}(a^3)$, and is presented for each operator in Table 7.2. By inspection, γ_1 varies solely based on the operator's external fields, meaning it is equal for the three fermion and two scalar operators, respectively, and the average of the two field's result for the mixed operator. The reason being that the EFT anomalous dimension is dependent on the full theory IR divergences, which do not appear in the vertex factors.

The next matching step occurs at the lower scale, $\mu \sim M$, where the massive bosons are integrated out. The matching is done from SCET with massive bosons ($\mu > M$), to SCET without massive bosons ($\mu < M$). In our model, this is a free theory, so there is no need for propagating bosonic modes below M. The matching coefficient at $\mu \sim M$ is given by $d(\mu) = \exp\left[D(\mu)\right]$ in Table 7.3 and is found from the SCET vertex and wave-function corrections. More specifically, one matches in the following way,

$$e^C(\bar{\xi}_{n,p_2} W_n)\Gamma(W_{\bar{n}}^\dagger \xi_{\bar{n},p_1}) \to e^{C+D}\bar{\xi}_{n,p_2}\Gamma\xi_{\bar{n},p_1}, \tag{7.74a}$$

$$e^C(\Phi_{n,p_2}^\dagger W_n)(W_{\bar{n}}^\dagger \Phi_{\bar{n},p_1}) \to e^{C+D}\Phi_{n,p_2}^\dagger \Phi_{\bar{n},p_1}, \tag{7.74b}$$

$$e^C(\Phi_{n,p_2}^\dagger W_n)[i\mathcal{D}_1 + i\mathcal{D}_2]_\mu(W_{\bar{n}}^\dagger \Phi_{\bar{n},p_1}) \to e^{C+D}\Phi_{n,p_2}^\dagger i(\mathcal{P}^\dagger + \mathcal{P})_\mu \Phi_{\bar{n},p_1}, \tag{7.74c}$$

$$e^C(\bar{\xi}_{n,p_2} W_n)(W_{\bar{n}}^\dagger \Phi_{\bar{n},p_1}) \to e^{C+D}\bar{\xi}_{n,p_2}\Phi_{\bar{n},p_1}. \tag{7.74d}$$

As for the results, although we calculate up to two-loops fully for $c(\mu)$, we have not yet determined the bare two-loop vertex contribution of $d(\mu)$ due to the complexity of massive SCET integrals. As for mass and coupling renormalisation, we present these $\mathcal{O}(a^2)$ contributions for both $c(\mu)$ and $d(\mu)$ in Appendices B.1 and B.2. Moreover, the collinear particle propagator corrections are the same as in the full theory and the US corrections vanish [259]. Thus, the WFR

$\mathcal{O}$	$\gamma_1^{(1)}/C_F$	$D^{(1)}/C_F$	$\Delta D^{(2)}$
$\bar{\psi}\Gamma\psi$	$4L_Q - 6$	$-L_{M_W}^2 + 2L_{M_W}L_Q - 3L_{M_W} + \frac{9}{2} - \frac{5}{6}\pi^2$	ΔD_1
$\chi^\dagger\chi$, $i\chi^\dagger \overset{\leftrightarrow}{D}_\mu \chi$	$4L_Q - 8$	$-L_{M_W}^2 + 2L_{M_W}L_Q - 4L_{M_W} + \frac{7}{2} - \frac{5}{6}\pi^2$	ΔD_2
$\bar{\psi}\chi$, $\chi^\dagger\psi$	$4L_Q - 7$	$-L_{M_W}^2 + 2L_{M_W}L_Q - \frac{7}{2}L_{M_W} + 4 - \frac{5}{6}\pi^2$	ΔD_2

Table 7.3: SCET form factor contributions at $\mu \sim M$, with one-loop matching, $D^{(1)}(\mu)$, and two-loop mass and coupling renormalisation correction, $\Delta D^{(2)}(\mu)$. The latter is given in Appendix B.2. γ_1 is the one-loop SCET anomalous dimension.

corrections are the same as in the full theory and we have these up to two-loops. For a more detailed description on the specific one-loop SCET integrals, we point to previous work [76,252]. What remains to calculate is the bare two-loop SCET vertex contributions to have a complete account at this order, we will leave this to future work.

The above matching steps are identical at each order, and the two-loop vertex and wave-function graphs we calculated are shown in Figs. 7.3 and 7.1. Furthermore, we note that both in the massive and massless external particle cases of SCET, there is no Higgs contributions in the vertex corrections. This is because the fermion Yukawa vertex vanishes, as by construction,

$$\bar{\xi}_{n,p}\xi_{n,p} = \bar{\xi}_{n,p}\frac{\bar{n}\!\!\!/ n\!\!\!/}{4}\frac{n\!\!\!/ \bar{n}\!\!\!/}{4}\xi_{n,p} = 0, \tag{7.75}$$

since $n\!\!\!/ n\!\!\!/ = n^2 = 0$. Moreover, couplings of three scalars have dimension of mass, and scalar operators have Higgs exchange corrections with sub-leading factors of Y_s/Q which we drop. This is easily seen when using the re-scaled, $\phi_{n,p}$, with a propagator of identical form to those of fermions. The Yukawa coupling is then given by,

$$Y_s H\chi^\dagger\chi \to Y_s H\Phi_{n,p}^\dagger\Phi_{n,p} = \frac{Y_s}{\bar{n}\cdot p}H\phi_{n,p}^\dagger\phi_{n,p}, \tag{7.76}$$

which is $\mathcal{O}(1/Q)$ as $\bar{n}\cdot p$ is of order $\mathcal{O}(Q)$ which suppresses any graph at each tri-scalar coupling. Thus, scalar full theory graphs only contribute at $\mu \sim Q$ in the matching, as well as scalar effective theory contributions to the wave-function renormalisation.

7.5.2 Massive External Particles

In this section, we consider the Sudakov regime for massive external particles, extending previous results. We are primarily interested in the limits, $Q \gg m_{1,2} \gg M$, although we will discuss other cases that can be studied as well, in particular one that can be applied for LHC studies of the top quark.

There are two cases to consider, $Q \gg m_2 \gg m_1 \gg M$ and $Q \gg m_2 \sim m_1 \gg M$, we begin with the former. Again, the Sudakov form factor can be determined with an EFT at each well-separated scale [373]. One begins as in the massless external particle case by matching the full theory onto SCET with a single massive particle at the scale, $\mu \sim Q$. The same operators are matched to as in Eq. (7.71), except now in SCET, ξ_{n,p_2}, is taken to have mass, m_2. Again, IR scales in the matching are those much smaller than Q and as usual are not present in $\exp[C(\mu)]$, as shown in Table 7.2. Next, one runs the operator from the scale Q to m_2, which can be done with γ_1, given in 7.2, as the anomalous dimension is also IR scale-independent. The matching steps that follow lie at scales $\mu = m_2$, $\mu = m_1$ and $\mu = M$. Schematically, the matching and running steps can be illustrated as follows,

$$e^C\tilde{\mathcal{O}}_1 \xleftarrow[m_1,M=0]{\mu\sim m_2} e^{C+R}\tilde{\mathcal{O}}_2 \xrightarrow{\gamma_2} e^{C+R}\tilde{\mathcal{O}}_2 \xleftarrow[M=0]{\mu\sim m_1} e^{C+R+T}\tilde{\mathcal{O}}_3 \xrightarrow{\gamma_3} e^{C+R+T}\tilde{\mathcal{O}}_3 \xleftarrow[M\neq 0]{\mu\sim M} e^{C+R+T+U}\tilde{\mathcal{O}}_4,$$

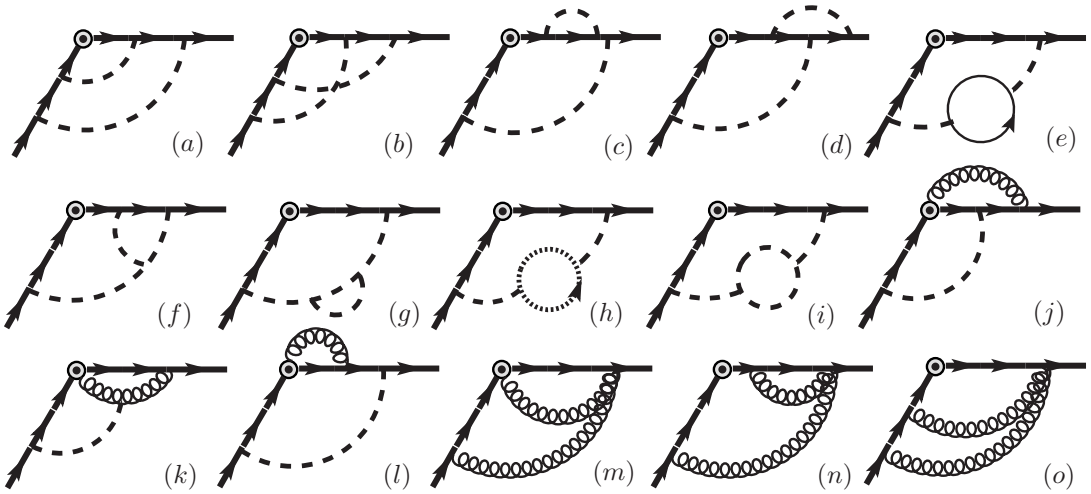

Figure 7.3: Two-loop vertex correction graphs, (a)-(d) are Abelian corrections; (f)-(i) are non-Abelian, (j)-(m) only exists with the operator, $\mathcal{O} = i\phi^\dagger \overset{\leftrightarrow}{D}_\mu \phi$ and EFT equivalents, (m)-(o) are seagull terms and occur only for scalar fields.

$\mathcal{O}$	$R^{(1)}/C_F$	$\gamma_2^{(1)}/C_F$	$T^{(1)}/C_F$
$\bar{\psi}_2 \Gamma \psi_1$	$\frac{1}{2}L_{m_2}^2 - \frac{1}{2}L_{m_2} + \frac{\pi^2}{12} + 2$	$4L_Q - 2L_{m_2} - 5$	$\frac{1}{2}L_{m_1}^2 - \frac{1}{2}L_{m_1} + \frac{\pi^2}{12} + 2$
$\chi_2^\dagger \chi_1$, $i\chi_2^\dagger \overset{\leftrightarrow}{D}_\mu \chi_1$	$\frac{1}{2}L_{m_2}^2 - L_{m_2} + \frac{\pi^2}{12} + 2$	$4L_Q - 2L_{m_2} - 6$	$\frac{1}{2}L_{m_1}^2 - L_{m_1} + \frac{\pi^2}{12} + 2$
$\bar{\psi}_2 \chi_1$	$\frac{1}{2}L_{m_2}^2 - \frac{1}{2}L_{m_2} + \frac{\pi^2}{12} + 2$	$4L_Q - 2L_{m_2} - 6$	$\frac{1}{2}L_{m_1}^2 - L_{m_1} + \frac{\pi^2}{12} + 2$
$\chi_2^\dagger \psi_1$	$\frac{1}{2}L_{m_2}^2 - L_{m_2} + \frac{\pi^2}{12} + 2$	$4L_Q - 2L_{m_2} - 5$	$\frac{1}{2}L_{m_1}^2 - \frac{1}{2}L_{m_1} + \frac{\pi^2}{12} + 2$

Table 7.4: Matching and running results for $Q \gg m_2 \gg m_1 \gg M$. R is the matching at $\mu \sim m_2$ and T the matching at $\mu \sim m_1$. The anomalous dimensions for running from m_2 to m_1 are γ_2. R and T are only dependent on the spin of the light particle.

where the exponents are multiplicative matching coefficients, γ_i the effective theory anomalous dimensions and $\tilde{\mathcal{O}}_i$ the effective theory operators at each scale.

Firstly, at $\mu = m_2$, one matches SCET to an EFT with the massive particle described by a heavy field [153], $h_{f,s}$, with a velocity, v_2, such that $v_2^2 = 1$. Whereas, the other particle remaining massless continues to be described by the SCET field, $\xi_{\bar{n},p_1}$. The fermionic operators, for instance, are then given by $\bar{h}_{f,2} \Gamma W_{\bar{n}}^\dagger \xi_{\bar{n},p_1}$, and similarly for other operators [374]. The matching correction at $\mu = m_2$ can be calculated from the vertex diagrams in Figs. 7.2 and 7.3, for the corresponding external particles in the effective theories above and below m_2. More specifically, in the fermion example, the difference between graphs where ξ_{n,p_2} and $h_{f,2}$, for the particle with mass, m_2. Note that in the theory below m_2 there are no graphs which contain collinear Wilson lines associated with $h_{f,s}$ and thus such corrections do not appear. Above m_2, the graphs in this theory are evaluated with bosonic masses set to zero, as $m_2 \gg M$, and on-shell at $p_2^2 = m_2^2$. Below m_2 the graphs in the EFT are evaluated at $M = 0$ as well, at the on-shell point, $k_2 \cdot v_2 = 0$ where k_2 is the heavy particle's residual momentum. As for the wave-function graphs, the $\xi_{\bar{n},p1}$ and HQET graphs both vanish on-shell. Hence, the vertex correction and the on-shell wave-function graph for ξ_{n,p_2} provide the matching [76], and results are shown in Tables 7.4 and 7.1, respectively.

We proceed then with the next matching step with the coefficient, $\exp[T(\mu)]$, at the scale,

$\mathcal{O}$	$\gamma_3^{(1)}/C_F$	$U^{(1)}(\mu)$	$U^{(2)}(\mu)$
$\bar{\psi}\Gamma\psi$	$4\,(wh(w)-1)$	$2C_F(wh(w)-1)L_{M_W} - \frac{Y_f^2}{4}\,(h(w)-1)\,L_{M_H}$	$U_1^{(2)}$
$\chi^\dagger\chi$, $i\chi^\dagger\overset{\leftrightarrow}{D}_\mu\chi$	$4\,(wh(w)-1)$	$2C_F(wh(w)-1)L_{M_W} - \frac{Y_s^2}{4}\,(h(w)-1)\,L_{M_H}$	$U_2^{(2)}$
$\chi^\dagger\psi$, $\bar{\psi}\chi$	$4\,(wh(w)-1)$	$2C_F(wh(w)-1)L_{M_W} - \left(\frac{Y_fY_s}{4}h(w) - \frac{1}{8}(Y_f^2+Y_s^2)\right)L_{M_H}$	$U_3^{(2)}$

Table 7.5: One- and two-loop matching contributions, $U^{(1,2)}$, at $\mu \sim M$. The latter is given in Appendix B.3. The anomalous dimensions for running m_1 to M are given by γ_3 and are operator independent.

$\mu \sim m_1$. At this scale, the theory above m_1 is SCET with heavy field for particle with mass, m_2, and the theory below m_1, the $\bar{n}$-collinear SCET field, $\xi_{\bar{n},p_1}$ becomes a heavy field, $h_{f,s}$, with velocity, v_1, such that $v_1^2 = 1$ and $v_1 \cdot v_2 = w$. The fermionic operators, for example, are then given by $\bar{h}_{f,2}\Gamma h_{f,1}$ instead of $\bar{h}_{f,2}\Gamma W_{\bar{n}}^\dagger \xi_{\bar{n},p_1}$. In the theory below m_1 vertex corrections due to collinear Wilson lines do not occur, as there are no collinear Wilson lines, W, associated with heavy fields. The matching is determined by the vertex and wave-function graphs in the theories above minus the theories below m_1, setting all scales less than m_1 to zero. Note that in the theory below m_1 only scaleless integrals appear which are trivial and thus, the sole non-zero contributions come from vertex contributions above m_1 and the $\bar{n}$-collinear WFR diagram. Conveniently, the matching at m_2 is determined by identical graphs, so T is given by R with $m_2 \to m_1$, and is presented in Table 7.4.

The anomalous dimension, γ_3, remains to be computed for the running between m_1 and M, as well as the matching coefficient, $\exp[U(\mu)]$, at $\mu \sim M$. These are determined by on-shell HPET graphs, with non-zero bosonic masses, M, as they are no longer IR scales. The one-loop contributions are presented in the last column of Table 7.5, and by inspection we see they are operator-independent and only differ in appropriate Yukawa coupling. The function,

$$h(w) = \frac{\ln\left(w + \sqrt{w^2-1}\right)}{\sqrt{w^2-1}}, \tag{7.77}$$

is well-known and appears as a factor in the HQET anomalous dimension [153]. Note further that in the Sudakov regime, the Higgs contribution in $\exp U$ is sub-leading as, $Q^2 \sim m_1 m_2 w$, and in this limit,

$$h(w) \sim \frac{\ln w}{w}, \tag{7.78}$$

thus the gauge contribution dominates in the Sudakov regime. Later we will see that in the threshold regime, the Higgs and gauge contributions turn out to be on equal footing. We also present the two-loop contribution to the matching contribution, $\exp[U(\mu)]$, in Appendix B.3. As for remaining two-loop contributions, we present the mass and coupling renormalisation, which contribute at two-loop order for each matching coefficient in an arXiv ancillary file of Ref. [325].

We have a similar situation in the case $Q \gg m_2 \sim m_1 \gg M$, which is why we left this for last. Evolving down to $m_1 \sim m_2$ is the same as for the case where $m_i = 0$. The matching is simply given by the sum of R and T at m_2 and m_1, respectively [76]. Below $m_1 \sim m_2$ the matching and running is identical to the previous case with anomalous dimension, γ_3, and matching coefficient, $\exp[U(\mu)]$. Lastly, if $m_2 = m_1$, then the case is identical to $m_2 \sim m_1$, except one sets $m_2 = m_1$ in all matching and running contributions.

Further Cases: We note finally, as considered in previous work [76], that there are other cases one can compare for complete generality, in particular, one case resonates with regard to heavy SM particles in the high energy regime. The Sudakov limit being, $Q \gg m_1 \sim m_2 \sim M$,

which involves one running step with γ_1 and two matching steps. At $\mu \sim Q$ the matching coefficient is represented by the usual, $\exp[C(\mu)]$. On the other hand, at one-loop the matching at $\mu \sim m_{1,2} \sim M$ mimics the massless case. However, the matching condition, $\exp[D(\mu)]$, is determined with massive collinear propagators, which modifies the matching in the following way,

$$D(m_i, M) = D(0,0) + (f_2(z_2) - \tilde{f}_2(z_2)/2) + (f_1(z_1) - \tilde{f}_1(z_1)/2), \tag{7.79}$$

where $z_i = m_i/M_W$, $f_{1,2}$ corresponds to the massive collinear contributions,

$$f_i(z_i) \equiv I_n(m_i) - I_n(0), \tag{7.80}$$

where I_n is the collinear vertex contribution and,

$$\tilde{f}_i(z_i) \equiv \delta Z_i(m_i, M) - \delta Z_i(0, M), \tag{7.81}$$

is the difference between the wave-function contribution with all mass scales non-zero and the external mass scales set to zero from Table 7.1. Both the vertex and wave-function contributions depend solely on whether the corresponding particle is a fermion or a scalar. More specifically, $f_i(z_i)$ maps to $f_F(z_i)$ and $f_S(z_i)$ in the case of fermions and scalars, respectively, and are given by,

$$f_F(z) = 2 + \left(\frac{1}{z^2} - 2\right)\ln z^2 + \frac{2\tilde{z}}{z^2}\tanh^{-1}\tilde{z} + \frac{1}{2}\ln^2(z^2) - 2(\tanh^{-1}\tilde{z})^2, \tag{7.82a}$$

$$f_S(z) = 1 - \left(1 - \frac{1}{2z^2}\right)\ln z^2 + \frac{\tilde{z}}{z^2}\tanh^{-1}\tilde{z} + \frac{1}{2}\ln^2(z^2) - 2(\tanh^{-1}\tilde{z})^2, \tag{7.82b}$$

where $\tilde{z} = \sqrt{1-4z^2}$, as was also found in [76]. The one-loop renormalisation corrections to $D(m_i, M)$ that contribute at two-loop order are given analagously to the previous cases. As for bare contributions at two-loop order, the WFR are given by $F^{(m,M)}_{\psi,\chi}$ in Appendix B.7, and the bare vertex contributions are still to be determined. Thus, now that we have considered cases of interest in the Sudakov limit, we can shift to studying counterparts in the threshold limit.

7.6 Radiative Corrections in Threshold Limit

In this section, we calculate the form factor $\ln F_E(m^2)$, in the opposite limit, i.e. small Q^2 and large m^2, or threshold regime. Evidently, at threshold, the external particle masses are then taken to be the largest scale, and we consider the following three cases: $m_2 \gg m_1 \gg M \gg Q$, $m_1 \sim m_2 \gg M \gg Q$ and $m_1 \sim m_2 \sim M \gg Q$. We provide the form factor up to and including two-loop order, which is computed using a sequence of effective field theories.

We begin by noting that at scales higher than m^2, the theory is the original gauge-Higgs theory, or so-called full theory. Moving to scales below m^2, we transition to HPET where degrees of freedom of off-shellness on the order m^2 are integrated out. More specifically, let us commence with the case, $m_1 \sim m_2 \gg M \gg Q$, where $m_{1,2}$ and M denote the external particle and bosonic masses, respectively. Schematically, we then have the following matching and running steps, illustrated as follows,

$$\mathcal{O} \xleftrightarrow[Q,M=0]{\mu\sim m_{1,2}} e^B\tilde{\mathcal{O}}_1 \xrightarrow{\gamma_3} e^B\tilde{\mathcal{O}}_1 \xleftrightarrow[Q=0]{\mu\sim M} e^{B+U}\tilde{\mathcal{O}}_2,$$

where B and U are multiplicative matching coefficients, γ_3, is the effective theory anomalous dimension, and $\tilde{\mathcal{O}}_{1,2}$ the effective theory operators at each scale. At the scale $\mu > m_{1,2}$, we

employ the full theory graphs and below, at $\mu < m_{1,2}$, we match down to HPET with the matching coefficient, $b(\mu)$, and RGE given by,

$$\mu \frac{db(\mu)}{d\mu} = \gamma_F(a(\mu))b(\mu), \tag{7.83}$$

where γ_F is the anomalous dimension of the operator, $\mathcal{O}$, in the full theory and is independent of energetic regime as given in Table 7.2.

The full theory is then matched onto HPET at $\mu \sim m_{1,2}$. The matching coefficient then depends on logarithms, $L_{m_{1,2}}$, which are not divergent if $\mu \sim m_{1,2}$. The matching is done between full and effective theory operators as follows,

$$\bar{\psi}_2 \Gamma \psi_1 \to e^B \bar{h}_{f,2} \Gamma h_{f,1}, \tag{7.84a}$$

$$\chi_2^\dagger \chi_1 \to e^B h_{s,2}^\dagger h_{s,1}, \tag{7.84b}$$

$$i\chi_2^\dagger \overset{\leftrightarrow}{D}_\mu \chi_1 \to e^B h_{s,2}^\dagger [v_1 + v_2]_\mu h_{s,1}, \tag{7.84c}$$

$$\bar{\psi}_2 \chi_1 \to e^B \bar{h}_{f,2} h_{s,1}, \quad \chi_2^\dagger \psi_1 \to e^B h_{s,2}^\dagger h_{s,1}. \tag{7.84d}$$

We can then calculate the matching coefficient, $\exp[B(\mu)]$, as the full theory vertex and wave-function corrections with IR scales, M and Q, set to zero. The results of which at one- and two-loop order are given in Appendix B.4. Note that for the two-loop results, since $m_1 \sim m_2$ and we want to evaluate the *master integrals* (MIs) analytically, this can only be achieved with MIs at a single scale, whence, we expand the bare two-loop contributions about the difference, $\Delta_m = m_1 - m_2$, to NLO. This is an accurate representation as the scale we are considering is where $m_1 \sim m_2$ and although we chose to expand to first order as is conventionally done one can expand to any order and perform the single-scale two-loop MIs as they are independent of the expansion order. As for the remaining two-loop contributions, we present the mass and coupling renormalisation contributions at two-loop order in Appendix B.4.

What remains is the anomalous dimension, γ_3, between $m_{1,2}$ and M, and the matching coefficient, $\exp[U(\mu)]$, at $\mu \sim M$. Again, these contributions are found by computing graphs in Figs. 7.3 and 7.1, evaluated on-shell, with bosonic masses, M, included and external lines taken to be heavy with incoming and outgoing velocities, v_1 and v_2, reespectively. The difference here being that in the threshold limit,

$$w \sim \frac{m_1^2 + m_2^2}{2m_1 m_2} \sim \mathcal{O}(1), \tag{7.85}$$

since we take $m_1 \sim m_2$, and thus, $h(w) \sim \mathcal{O}(1)$, by inspection of Eq. (7.77). Whence, the sub-leading Higgs contribution which was sub-leading in the Sudakov regime becomes of the same order as the gauge contribution in the threshold regime.

Finally, we consider the slightly more involved, $m_2 \gg m_1 \gg M \gg Q$ case, where $m_{1,2}$ and M denote the external particle and bosonic masses, respectively. Schematically, we then have following matching and running steps, illustrated as follows,

$$\mathcal{O} \xleftrightarrow[Q,M,m_1=0]{\mu\sim m_2} e^{\tilde{B}} \tilde{\mathcal{O}}_1 \xrightarrow{\tilde{\gamma}_3} e^{\tilde{B}} \xleftrightarrow[Q,M=0]{\mu\sim m_1} e^{\tilde{B}+G} \tilde{\mathcal{O}}_2 \xrightarrow{\gamma_3} e^{\tilde{B}+G} \tilde{\mathcal{O}}_2 \xleftrightarrow[Q=0]{\mu\sim M} e^{\tilde{B}+G+U} \tilde{\mathcal{O}}_3,$$

where $\tilde{B}$, G and U are multiplicative matching coefficients, γ_3 and $\tilde{\gamma}_3$, are the effective theory anomalous dimensions, and $\tilde{\mathcal{O}}_{1,2,3}$ the effective theory operators at each scale. At the scale $\mu > m_2$, we employ the full theory graphs and below, at $\mu < m_2$, we match down to an effective theory with a single heavy field of mass, m_2. Thus, the effective theory operator is given by

$\mathcal{O}$	$\tilde{B}^{(1)}(\mu)$	$\tilde{\gamma}_3^{(1)}(\mu)$	$\tilde{B}^{(2)}(\mu)$
$\bar{\psi}_2\psi_1$	$-\frac{1}{48}\left(3L_{m_2}\left(8C_FL_{m_2}+8C_F+5Y_f^2\right)+4\left(24+\pi^2\right)C_F+9Y_f^2\right)$	$-5C_F+\frac{Y_f^2}{8}$	$\tilde{B}_1^{(2)}$
$\bar{\psi}_2\gamma^\mu\psi_1$	$\frac{1}{48}\left(-3L_{m_2}\left(8C_FL_{m_2}-40C_F+11Y_f^2\right)-4\left(60+\pi^2\right)C_F+27Y_f^2\right)$	$-2C_F-\frac{Y_f^2}{4}$	$\tilde{B}_2^{(2)}$
$\bar{\psi}_2\sigma^{\mu\nu}\psi_1$	$\frac{1}{48}\left(-3L_{m_2}\left(8C_FL_{m_2}-56C_F+9Y_f^2\right)-4\left(48+\pi^2\right)C_F+15Y_f^2\right)$	$-C_F-\frac{Y_f^2}{8}$	$\tilde{B}_3^{(2)}$
$\chi_2^\dagger\chi_1$	$-\frac{1}{12}C_F\left(6(L_{m_2}-2)L_{m_2}+\pi^2-12\right)+\frac{1}{96m_2^2}Y_s^2\left(-12L_{m_2}+6L_{m_2}^2+\pi^2+12\right)$	C_F	$\tilde{B}_4^{(2)}$
$i\chi_2^\dagger\overleftrightarrow{D}_\mu\chi_1$	$-\frac{1}{12}C_F\left(6(L_{m_2}-8)L_{m_2}+\pi^2+51\right)+\frac{Y_s^2}{96m_2^2}\left(6(L_{m_2}-4)L_{m_2}+\pi^2+12\right)$	$4C_F$	$\tilde{B}_5^{(2)}$
$\chi_2^\dagger\psi_1$	$-\frac{1}{12}C_F\left(6(L_{m_2}-2)L_{m_2}+\pi^2-24\right)-\frac{Y_s^2}{8m_2^2}(L_{m_2}-1)+\frac{Y_fY_s}{48m_2}\left(6L_{m_2}^2+\pi^2-12\right)$	C_F	$\tilde{B}_6^{(2)}$
$\bar{\psi}_2\chi_1$	$-\frac{1}{12}C_F\left(6(L_{m_2}-5)L_{m_2}+\pi^2+48\right)-\frac{Y_fY_s}{4m_2}-\frac{9}{16}Y_f^2(L_{m_2}-1)$	C_F	$\tilde{B}_7^{(2)}$

Table 7.6: Matching and running, $\tilde{B}(\mu)$ and $\tilde{\gamma}_3(\mu)$, to the threshold form factor for $m_2 \gg m_1 \gg M \gg Q$ at $\mu \sim m_2$. The two-loop contributions are given in Appendix B.5.

$\mathcal{O}$	$G^{(1)}(\mu)$	$G^{(2)}(\mu)$
$\bar{\psi}_2\Gamma\psi_1$	$\frac{1}{16}\left(L_{m_1}\left(16C_F-7Y_f^2\right)-16C_F+5Y_f^2\right)$	$G_1^{(2)}$
$\chi_2^\dagger\chi_1$	$\frac{1}{24}C_F\left(6L_{m_1}^2+\pi^2+48\right)-\frac{Y_s^2}{8m_1^2}(L_{m_1}-1)$	$G_2^{(2)}$
$i\chi_2^\dagger\overleftrightarrow{D}_\mu\chi_1$	$\frac{1}{12}C_F\left\{6(L_{m_1}-2)L_{m_1}+\pi^2+48\right\}-\frac{Y_s^2}{8m_1^2}(L_{m_1}-1)$	$G_3^{(2)}$
$\chi_2^\dagger\psi_1$	$\frac{1}{16}\left\{L_{m_1}\left(16C_F+Y_f(2Y_s-9Y_f)\right)-16C_F+Y_f(9Y_f-4Y_s)\right\}$	$G_4^{(2)}$
$\bar{\psi}_2\chi_1$	$\frac{1}{24m_1^2}\left\{6m_1^2C_FL_{m_1}^2+\left(48+\pi^2\right)m_1^2C_F-3Y_s^2(L_{m_1}-1)\right\}$	$G_5^{(2)}$

Table 7.7: Matching corrections, $G(\mu)$, to the threshold form factor for $m_2 \gg m_1 \gg M \gg Q$ at $\mu \sim m_1$. The two-loop contributions are given in Appendix B.6.

the full theory operators with particle 2 represented by a heavy field, $h_{f,s}$, for instance in the fermionic case we have, $\bar{h}_{f,2}\Gamma\psi_1$, and similarly for the other operators.

We can then calculate the matching coefficient, $\exp\left[\tilde{B}(\mu)\right]$, as the full theory vertex and wave-function corrections with IR scales, m_1, M and Q, set to zero. The results of the vertex and wave-function contributions, $\exp\tilde{B}(\mu)$, as well as the anomalous dimension, $\tilde{\gamma}_3$, between m_2 and m_1 are given in Table 7.6 and Appendix B.5. Moreover, the coupling and mass renormalisation corrections that contribute at two-loop order are also given, in Appendix B.5. What remains then is to evaluate the matching at $\mu \sim m_1$ as the final matching and running, $\exp\left[U(\mu)\right]$ and γ_3, at M is identical to the previous case. The theory above, $\mu > m_1$, is the effective theory with particle 2 taken to be a heavy field and the theory below, $\mu < m_1$, is heavy particle effective theory where both particles 1 and 2 are taken to be heavy and the IR scale being the bosonic masses are set to zero. The theory below m_1 is scaleless and thus does not contribute to the matching but the theory above m_1 is one of two scales, m_1 and $w' = p_1 \cdot v_2$. However, w' is integrated out at leading order in the threshold limit as,

$$w' = p_1 \cdot v_2 = \frac{m_1^2 + m_2^2 - Q^2}{2m_2} \sim \frac{m_2}{2}, \tag{7.86}$$

and thus, we obtained the matching and wave-function contributions, $\exp\left[G(\mu)\right]$, with logarithms of a single scale, m_1, and these are presented up to two-loops in Table 7.7 and Appendix B.6. As for the coupling and mass renormalisation corrections that also contribute at two-loop order, we present these results in Appendix B.6.

Lastly, we account for the case, $m_1 \sim m_2 \sim M \gg Q$, which applies to heavy fermions and scalars in the SM. Schematically, the matching is given by

$$\mathcal{O} \xleftarrow[Q,M=0]{\mu\sim m_{1,2}\sim M} e^{\tilde{D}}\tilde{\mathcal{O}}_1,$$

where $\tilde{D}$ is the multiplicative matching contribution and $\tilde{\mathcal{O}}_1$ the effective theory operators at $\mu \sim m_{1,2} \sim M$. Above μ, we employ the full theory graphs and below, we match down to HPET with the matching coefficient dependent on logarithms, $L_{m_{1,2}}$ and L_M. These logarithms are not large if $\mu \sim m_{1,2}, M$. The full and effective theory operators are as given in Eq. (7.84). We can then calculate the matching coefficient,

$$\tilde{D}(\mu) = a\tilde{D}(\mu)^{(1)} + a^2(\tilde{D}^{(2)}(\mu) + \Delta\tilde{D}^{(2)}(\mu)), \tag{7.87}$$

as the full theory vertex and wave-function corrections with IR scale, Q, set to zero. Due to the size of the expression, the result is attached in an arXiv ancillary file of Ref. [325]. Note again in this case, that for the two-loop results, since $m_1 \sim m_2 \sim M$ for analytical scalar integral evaluation, we expand the bare two-loop contributions about the difference of $\Delta_m = m_1 - m_2$, $\Delta_M = M_H - M_W$ and $\Delta_{m,M} = M_W - m_1$ to NLO. This is an accurate representation as the scale we are considering is where $m_1 \sim m_2 \sim M$.

With the above results, due to their generality one can map them to operators in models that are similar to the $SU(N)$-Higgs model we discuss here, including those with spontaneous symmetry breaking at a certain scale.

7.7 Application to the Standard Model

So far we have studied the $SU(N)$-Higgs model which can be used to compute results for the SM as discussed in Ref. [76]. We illustrate the mapping of our radiative corrections from our to other models of a similar type, which may exhibit SSB. When considering the SM, one must select the correct coupling constants with care, since, it is a chiral gauge theory, and our model is vector-like. Results for greater than two external particles are then attainable through appropriate combinations of form factors. We now focus on charged fermion production by quark and lepton currents, $\bar{Q}_i\gamma_\mu P_L Q_i$ and $\bar{L}\gamma_\mu P_L L$, respectively, where Q_i is the quark doublet with generation index, $i = u, c, t$, with only the top quark mass, m_t, taken to be a non-zero fermion mass.

7.7.1 Light Quarks

Let us begin by considering the representation of light quarks in the SM [84]. The first generation of the quark doublet is given by,

$$Q_u = \begin{bmatrix} u \\ d' \end{bmatrix} = \begin{bmatrix} u \\ V_{ud}d + V_{us}s + V_{ub}b \end{bmatrix}, \tag{7.88}$$

At the scale, $Q \gg m_q$, in the full EW theory, we assume the operator coefficient is unity. In performing the matching at $\mu \sim Q$ all masses and in turn Yukawa factors are IR and thus taken to be zero. Thus, the EFT operator may be written as,

$$\bar{Q}_u\gamma_\mu P_L Q_u \to c(Q)\left[\bar{\xi}^{(Q_u)}_{n,p_2} W_n\right]\gamma_\mu P_L\left[W^\dagger_{\bar{n}}\xi^{(Q_u)}_{\bar{n},p_1}\right], \tag{7.89}$$

with the quark doublet of Eq. (7.88) labelled by $\xi^{(Q_u)}$ in SCET. Thus, the matching condition, $c(\mu)$ at the scale $\mu = Q$ with $L_Q = 0$ is,

$$\ln c(Q) = a_{EW}(Q)\ln c^{(1)}(Q) + a_{EW}(Q)^2 \ln c^{(2)}(Q) + \mathcal{O}(a^3_{EW}), \tag{7.90}$$

where,

$$a_{EW}(\mu) = \left(\frac{\alpha_s(\mu)}{4\pi}\frac{4}{3} + \frac{\alpha_2(\mu)}{4\pi}\frac{3}{4} + \frac{\alpha_1(\mu)}{4\pi}\frac{1}{36}\right). \tag{7.91}$$

The couplings now include the appropriate SM gauge factors, C_F, which are 4/3 for an $SU(3)$ triplet, 3/4 for an $SU(2)$ doublet, and 1/36 for $Y = 1/6$. Renormalising the EW couplings at $\mu = M_Z$ gives the following [115],

$$\alpha_1(M_Z) = \frac{\alpha_{em}(M_Z)}{\cos^2\theta_W},$$
$$\alpha_2(M_Z) = \frac{\alpha_{em}(M_Z)}{\sin^2\theta_W}. \tag{7.92}$$

The SM beta functions can be used to run these couplings from M_Z to $\mu \sim Q$. The theory below Q is SCET with $SU(3) \times SU(2) \times U(1)$ symmetry. In this regime, the SCET current in Eq. (7.89) is multiplicatively renormalised with the anomalous dimension,

$$\ln\gamma(\mu) = a_{EW}(\mu)\gamma_1^{(1)}(\mu) + a_{EW}(\mu)^2\gamma_1^{(2)}(\mu) + \mathcal{O}(a_{EW}^3). \tag{7.93}$$

One can employ $\gamma(\mu)$ to run $c(\mu)$ down to the mass of exchanged bosons. The integrating out may be done sequentially, i.e. first the Z-boson and then the W-boson at their respective mass scales. This is not a good choice to use for the SM, as M_W/M_Z is not negligible, and terms with powers of M_W/M_Z are more dominant than terms with powers of $\alpha \ln M_W/M_Z$. It is preferable to integrate out both bosons at a common scale, say $\mu = M_Z$, in doing so the matching is done from $SU(3)\times SU(2)\times U(1)$ onto $SU(3)\times U(1)_{\rm EM}$, a theory with only massless gauge bosons. Moreover, the Higgs corrections for light particles are sub-leading as the Yukawa coupling is proportional to the light mass and thus, are suppressed. At $\mu = M_Z$, integrating out the massive gauge bosons leads to the following matching,

$$\left[\bar{\xi}^{(Q_u)}_{n,p_2}W_n\right]\gamma_\mu P_L\left[W^\dagger_{\bar{n}}\xi^{(Q_u)}_{\bar{n},p_1}\right] \to d^{(u)}\left[\bar{\xi}^{(u)}_{n,p_2}W_n\right]\gamma_\mu P_L\left[W^\dagger_{\bar{n}}\xi^{(u)}_{\bar{n},p_1}\right] + d^{(d')}\left[\bar{\xi}^{(d')}_{n,p_2}W_n\right]\gamma_\mu P_L\left[W^\dagger_{\bar{n}}\xi^{(d')}_{\bar{n},p_1}\right]. \tag{7.94}$$

Note that the u and d' parts have differing matching corrections due EW symmetry being broken. The matching corrections are as follows,

$$\begin{aligned}\ln d^{(u)}(M_Z) =& a_1 \ln d^{(1)}(M_W) + a_1^2 \ln d^{(2)}(M_W) + \mathcal{O}(a_1^3)\\ &+ a_2 \ln d^{(1)}(M_Z) + a_2^2 \ln d^{(2)}(M_Z) + \mathcal{O}(a_2^3)\end{aligned} \tag{7.95}$$

where the terms proportional to a_1 and a_2 correspond the Z and W contributions, respectively, and,

$$a_1 = \frac{\alpha_{em}}{4\pi\sin^2\theta_W\cos^2\theta_W}\left(\frac{1}{2} - \frac{2}{3}\sin^2\theta_W\right)^2 \tag{7.96}$$

$$a_2 = \frac{\alpha_{em}}{4\pi\sin^2\theta_W\cos^2\theta_W}\left(\frac{1}{2}\right)^2. \tag{7.97}$$

We multiplicatively renormalise operators of Eq. (7.88) below M_Z, using anomalous dimensions,

$$\gamma^{(u)}(\mu) = \tilde{a}_1(\mu)\gamma_1^{(1)}(\mu) + \tilde{a}_1(\mu)^2\gamma_1^{(2)}(\mu) + \mathcal{O}(\tilde{a}_1^3), \tag{7.98}$$

$$\gamma^{(d')}(\mu) = \tilde{a}_2(\mu)\gamma_1^{(1)}(\mu) + \tilde{a}_2(\mu)^2\gamma_1^{(2)}(\mu) + \mathcal{O}(\tilde{a}_2^3) \tag{7.99}$$

such that

$$\tilde{a}_1(\mu) = \left\{\frac{\alpha_s(\mu)}{4\pi}\frac{4}{3} + \frac{\alpha_{em}(\mu)}{4\pi}\frac{4}{9}\right\} \quad \text{and} \quad \tilde{a}_2(\mu) = \left\{\frac{\alpha_s(\mu)}{4\pi}\frac{4}{3} + \frac{\alpha_{em}(\mu)}{4\pi}\frac{1}{9}\right\}, \tag{7.100}$$

All-combined, the low-scale operator is then,

$$\left[\bar{\xi}^{(Q_u)}_{n,p_2}W_n\right]\gamma_\mu P_L\left[W^\dagger_{\bar{n}}\xi^{(Q_u)}_{\bar{n},p_1}\right] \to c^{(u)}\left[\bar{\xi}^{(u)}_{n,p_2}W_n\right]\gamma_\mu P_L\left[W^\dagger_{\bar{n}}\xi^{(u)}_{\bar{n},p_1}\right] + c^{(d')}\left[\bar{\xi}^{(d')}_{n,p_2}W_n\right]\gamma_\mu P_L\left[W^\dagger_{\bar{n}}\xi^{(d')}_{\bar{n},p_1}\right], \tag{7.101}$$

with

$$\ln c^{u,d'}(\mu) = \ln c(Q) + \int_Q^{M_Z}\frac{d\mu}{\mu}\gamma(\mu) + \ln d^{(u,d')}(M_Z) + \int_{M_Z}^{\mu}\frac{d\mu}{\mu}\gamma^{(u,d')}(\mu). \tag{7.102}$$

The EFT operator in Eq. (7.101) is usable now for studying specific LHC processes with SCET [375]. For instance, if one considers jet production it is important to choose the renormalisation scale to be at or near the LHC jet invariant mass.

7.7.2 Leptons

We now perform the analgous study for the lepton current, $\bar{L}\gamma_\mu P_L L$, where L is the lepton doublet,

$$L = \begin{pmatrix}\nu\\ l\end{pmatrix}, \tag{7.103}$$

and is identical to that for the quark doublet, aside from a few replacements. At the low scale, μ, the operator in the full theory is,

$$\bar{L}\gamma_\mu P_L L \to c^{(\nu)}\left[\bar{\xi}^{(\nu)}_{n,p_2}W_n\right]\gamma_\mu P_L\left[W^\dagger_{\bar{n}}\xi^{(\nu)}_{\bar{n},p_1}\right] + c^{(l)}\left[\bar{\xi}^{(l)}_{n,p_2}W_n\right]\gamma_\mu P_L\left[W^\dagger_{\bar{n}}\xi^{(l)}_{\bar{n},p_1}\right], \tag{7.104}$$

with Eq. (7.102) and replacements $u \to \nu$, $d' \to l$, along with different gauge theory factors which implies the following coupling replacements,

$$a_{EW}(\mu) \to a'_{EW}(\mu) = \left(\frac{\alpha_2(\mu)}{4\pi}\frac{3}{4} + \frac{\alpha_1(\mu)}{4\pi}\frac{1}{4}\right), \tag{7.105}$$

$$a_1 \to a'_1 = \frac{\alpha_{em}}{4\pi\sin^2\theta_W\cos^2\theta_W}\left(\frac{1}{2}\right)^2, \tag{7.106}$$

$$a_2 \to a'_2 = \frac{\alpha_{em}}{4\pi\sin^2\theta_W\cos^2\theta_W}\left(-\frac{1}{2}+\sin^2\theta_W\right)^2, \tag{7.107}$$

$$\tilde{a}_1(\mu) \to \tilde{a}'_1(\mu) = 0, \tag{7.108}$$

$$\tilde{a}_2(\mu) \to \tilde{a}'_2(\mu) = \frac{\alpha_{em}(\mu)}{4\pi}, \tag{7.109}$$

which provides us with the leptonic equivalent of the previous result.

7.7.3 Top Quarks

We now study the specific process of $t\bar{t}$-production by a vector current $\bar{Q}_t\gamma_\mu P_L Q_t$, where Q_t is the left-handed quark doublet in the SM. We may write the quark doublet as follows,

$$Q_t = \begin{pmatrix}t\\ b'\end{pmatrix} = \begin{bmatrix}t\\ V_{td}d + V_{ts}s + V_{tb}b\end{bmatrix}, \tag{7.110}$$

We will neglect all quark masses other than m_t. This example demonstrates how our model handles non-zero fermion mass as well as Higgs exchange. We will examine both the Sudakov and threshold regimes in this case as they are both available to us in this example.

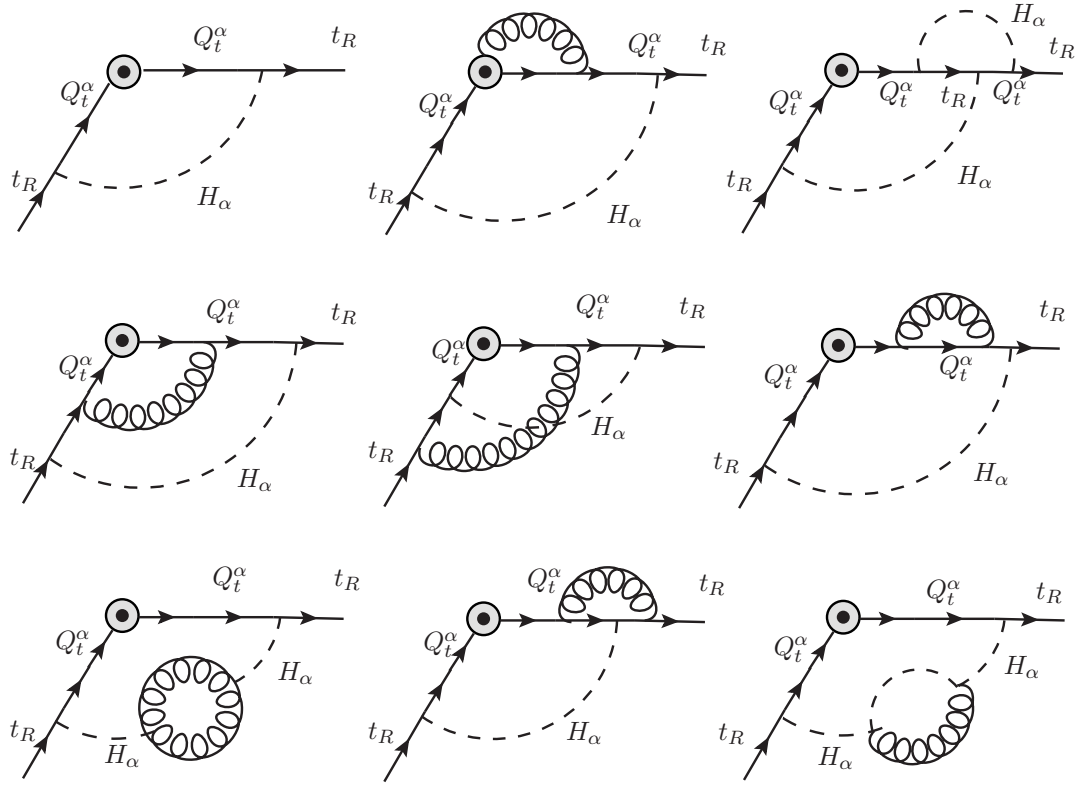

Figure 7.4: Vertex contributions to matching coefficient, $c_R(\mu)$, at one and two-loop order. Higgs exchanges cause $\bar{Q}_t\gamma_\mu P_L Q_t$ to mix with $\bar{t}_R\gamma_\mu P_R t$ and the index, α, is the fundamental $SU(2)$ and index and is summed over.

7.7.3.1 Sudakov Regime

In the Sudakov regime, the SCET operator at $\mu \sim Q$, can be written,

$$\begin{aligned}\bar{Q}_t\gamma_\mu P_L Q_t \to & c_L(Q)\left[\bar{\xi}^{(Q_t)}_{n,p_2}W_n\right]\gamma_\mu P_L\left[W^\dagger_{\bar{n}}\xi^{(Q_t)}_{\bar{n},p_1}\right] + \\ & c_R(Q)\left[\bar{\xi}^{(t)}_{n,p_2}W_n\right]\gamma_\mu P_R\left[W^\dagger_{\bar{n}}\xi^{(t)}_{\bar{n},p_1}\right],\end{aligned} \tag{7.111}$$

where $\xi^{(Q_t)}$ and $\xi^{(t)}$ represent the left-handed and right-handed t-quark doublet, Eq. (7.110), and singlet, t_R, respectively, in SCET with gauge indices suppressed. The reason t_R appears in this case is that Higgs exchange diagrams are chiral in the SM, and have been computed in our model value which is a vector-like theory, thus when mapping to the SM we must plaster on the fact that the Yukawa coupling switches the chirality of the fermion. Practically, the Higgs exchange causes Q_L and t_R *operator mixing*. The matching at $\mu = Q$ is then given by $c_{L/R}(Q)$, where one splits the left and right handed contributions of $c(Q)$ which now has non-zero Yukawa coupings. Hence, $c_R(Q)$ includes all terms which are due to Higgs exchange diagrams of type illustrated in Fig. 7.4; and the remaining graphs contribute to $c_L(Q)$. Note further that one must include appropriate factors of two for terms in $c_{L/R}$ arising from summing over each closed $SU(2)$ index loop, i.e. because both the Higgs and Q_t are doublets in $SU(2)$. As for the wave-function correction, the t_L and t_R field renormalisation contributions which include Higgs exchange must also include appropriate factors of two from loops with $SU(2)$ index summation.

The theory below Q is SCET with $SU(3)\times SU(2)\times U(1)$ symmetry. In this regime the two

operators in Eq. (7.111) are multiplicatively renormalised with anomalous dimensions (again splitting chiral contributions in the same way as for matching),

$$\frac{dc_L(\mu)}{d\mu} = \gamma_L(\mu)c_L \quad \text{and} \quad \frac{dc_R(\mu)}{d\mu} = \gamma_R(\mu)c_R. \tag{7.112}$$

At this scale, the Higgs vertex graph, which causes c_L/c_R mixing, is $1/Q^2$ suppressed. We may use γ to run c_L and c_R down to a scale of order m_t. At $\mu \sim m_t$ there are several different methods one can use. Since $\{m_t, M_{W,Z}, M_H\}$ are relatively close, it is best to integrate all of them out at $\mu \sim m_t$. Thus, we go from $SU(3) \times SU(2) \times U(1)$ to $SU(3) \times U(1)_{\rm EM}$ gauge theory, with broken $SU(2) \times U(1)$ symmetry and no massive degrees of freedom. At $\mu = m_t$ we replace the top quark SCET by the heavy quark field t_v, whereas the b' quark in the SCET field $\xi^{(Q_t)}$ remains a SCET field, $\xi^{(b')}$. Matching is then given by,

$$\left[\bar{\xi}^{(Q_t)}_{n,p_2} W_n\right] \gamma_\mu P_L \left[W^\dagger_{\bar{n}} \xi^{(Q_t)}_{\bar{n},p_1}\right] \to \frac{1}{2} a_1 \bar{t}_{v_2} t_{v_1} a_2 \left[\bar{\xi}^{(b')}_{n,p_2} W_n\right] \gamma_\mu P_L \left[W^\dagger_{\bar{n}} \xi^{(b')}_{\bar{n},p_1}\right] \tag{7.113}$$

$$\left[\bar{\xi}^{(t)}_{n,p_2} W_n\right] \gamma_\mu P_R \left[W^\dagger_{\bar{n}} \xi^{(t)}_{\bar{n},p_1}\right] \to \frac{1}{2} a_3 \bar{t}_{v_2} t_{v_1}, \tag{7.114}$$

using the results from Section 7.5.2 to obtain the coefficients, a_i. Moreover, we renormalise couplings at $\mu = m_t$, including contributions from W/Z, g, γ and $H, h^{0,+}$, where $h^{0,+}$ are the SM goldstone bosons. Lastly, below $\mu = m_t$, the anomalous dimension of $\bar{t}_{v_2} t_{v_1}$ is given by,

$$\gamma_3 = a\gamma_3^{(1)} + a^2\gamma_3^{(2)} + \mathcal{O}(a^3), \quad a = \left(\frac{4}{3}\frac{\alpha_s}{4\pi} + \frac{4}{9}\frac{\alpha_{em}}{4\pi}\right) \tag{7.115}$$

from the fourth column of Table 7.4, with the given group theory factor replacements. These $\bar{t}t$ results may be used in decay studies as has been done in pure QCD [374]. We have here the additional EW contributions including Higgs up to two-loop order.

7.7.3.2 Threshold Regime

In the threshold regime at $\mu \sim m_t$, m_t is the largest scale in the problem. As the scales, $\{m_t, M_{W,Z}, M_H\}$, are not far apart, integrating them all out together as in the Sudakov regime is the way forward. As before, one can first integrate out the top quark as $m_t \sim 172$ GeV and $m_t > m_H > M_{W,Z} \gg m_b$, which leads to an effective theory that breaks $SU(2) \times U(1)$ invariance as the b' quark remains along with dynamical W/Z bosons. From which one integrates out the Higgs first [376], as $M_H \sim 125$ GeV, and then the W/Z bosons at a common scale, $M_Z \sim 81$ GeV. Otherwise if one wants to avoid breaking $SU(2) \times U(1)$ invariance, as the scales are not widely separated it is most natural to integrate H, W/Z and t at a common scale, say $\mu \sim M_Z$. We consider the latter here. Moreover, we note that for treatment at the scale $\mu \sim m_b$ one needs a further matching and running step and the heavy-light current we consider applies in this case.

Integrating out at the common scale $\mu \sim M_Z$, below M_Z the top quark fields are replaced by their heavy quark counterparts t_v and the bottom quark in the doublet remains a full theory field. The operator matching is then,

$$\bar{Q}_t \gamma_\mu P_L Q_t \to \frac{1}{2} a_1^L \bar{t}_{v_2} t_{v_1} + a_2^L \bar{b}' \gamma_\mu P_L b' \quad \text{and} \quad \bar{t}_R \gamma_\mu P_R t_R \to \frac{1}{2} a_3^R \bar{t}_{v_2} t_{v_1}, \tag{7.116}$$

where the matching coefficients, $a_i^{L/R}$, are obtained using the matching coefficient, $\tilde{d}(\mu)$, from Section 7.6 with the appropriate graphs and group theory factors. Thus, we go from $SU(3) \times SU(2) \times U(1)$ theory to $SU(3) \times U(1)_{\rm EM}$, with broken $SU(2) \times U(1)$ symmetry and only light degrees of freedom. As in the Sudakov case, the renormalisation of the SM couplings is done at $\mu = m_Z$.

7.8 Technical Calculation

We produce the Feynman diagrams with `QGRAF` [303], process the output with `FORM` [304], obtaining amplitudes as a linear combination of scalar integrals. We then proceed in the standard way by reducing scalar integrals to a smaller set of so-called MIs using integration-by-parts identities (IBPs) [377], with the help of `LiteRed` [378] and home-grown tools. Our two-loop MIs in some cases are dependent on two mass scales taken to be not widely separated, either the external particle masses or the exchange boson masses, respectively. One can perform these integrals numerically but to obtain analytic results we expand such amplitudes in the mass difference to NLO in said difference, leading to single scale integrals. Once the integrals are maximally reduced, what remains is to evaluate the MIs. As these procedures are well-known, we refrain from delving into too much detail.

We focus here on the calculation of MIs of the two-loop vertex and wave-function contributions. The full theory integrals have been computed analytically and we present the MIs appearing in our calculation here [341]. We evaluate effective theory MIs which are not known analytically using the differential equations method [78, 82]. As evaluating HPET integrals of this type is involved, the calculation will instead be presented in Chapter 8.

We classify the MIs in relation to their *topology*. We begin by distinguishing between the vertex topologies for external full theory fields displayed in Figs. 7.5 (a)-(c). The MIs for each topology are expressible with an integral family which can be written as,

$$J^{(s)}_{\{\nu_1^{(m)}\cdots\nu_7^{(m)}\}} = \left[(4\pi)^{2-\epsilon}e^{\gamma_E\epsilon}\right]^2 \int \not{l}^D l_1 \not{l}^D l_2 \frac{1}{D_1^{\nu_1}(m)\cdots D_7^{\nu_7}(m)}, \tag{7.117}$$

where $l_i : i = 1, 2$ are the loop momenta, s is the scale in the EFT formalism at which the MIs play a role, and,

$$\begin{aligned} &D_1(m) = l_1^2 - m^2, \quad D_2(m) = l_2^2 - m^2, \quad D_3(m) = (l_1 + l_2)^2 - m^2, \\ &D_4(m) = (l_1 - p_1)^2 - m^2, \quad D_5(m) = (l_2 - q)^2 - m^2, \end{aligned} \tag{7.118}$$

$$D_6(m) = (l_1 + q)^2 - m^2, \quad D_7(m) = (l_1 + l_2 - q - p_1)^2 - m^2. \tag{7.119}$$

Here the on-shell external momenta are labelled by $p_i : i = 1, 2$, such that $(p_i^2 = m_i^2)$ and $q = p_2 - p_1$ is the usual transfer momentum. We therefore label the MIs by their associated denominator exponents, $\nu_1 \ldots \nu_7$. Note the single mass scale in our denominators, this arises from the fact that for integrals involving two mass scales or more, we expand our results in the difference of mass scales up to NLO. For instance, for graphs that include propagators of both W and Higgs bosons, we expand about $\Delta M = M_W - M_H$, assuming them to be not widely separated. This is done so we can work analytically as any number of scales can be handled numerically. Moreover, our choice to expand to NLO is for presentability as there is no issue in expanding the amplitudes to higher orders in ΔM computationally.

In the Sudakov regime the bare two-loop vertex matching contributions, $V_i^{(Q)}$, at the scale $\mu \sim Q$, has all mass scales set to zero as they are taken to be IR, and thus $m = 0$ in cases below, in which case we have MIs with topology given by Fig. 7.5 (a). Post-reduction one is left with the following MIs to the appropriate order in ϵ,

$$\begin{aligned} J^{(Q)}_{1010100} = Q^2 \left(\frac{Q^2}{\mu^2}\right)^{-2\epsilon} \Bigg(&\frac{5971\epsilon^3}{64} + \frac{865\epsilon^2}{32} + \frac{115\epsilon}{16} + \frac{1}{4\epsilon} - \frac{115\epsilon^3\zeta_2}{16} - \frac{13\epsilon^2\zeta_2}{8} - \frac{\epsilon\zeta_2}{4} - \frac{52\epsilon^3\zeta_3}{3} \\ &- \frac{8\epsilon^2\zeta_3}{3} - \frac{57\epsilon^3\zeta_4}{16} + \frac{13}{8} + \mathcal{O}(\epsilon^4)\Bigg), \end{aligned} \tag{7.120a}$$

$$J^{(Q)}_{1100110} = \left(\frac{Q^2}{\mu^2}\right)^{-2\epsilon} \Bigg(-192\epsilon^3 - 80\epsilon^2 - 32\epsilon - \frac{4}{\epsilon} - \frac{1}{\epsilon^2} + 32\epsilon^3\zeta_2 + 12\epsilon^2\zeta_2 + 4\epsilon\zeta_2 - \frac{14}{3}\epsilon^3\zeta_2\zeta_3$$

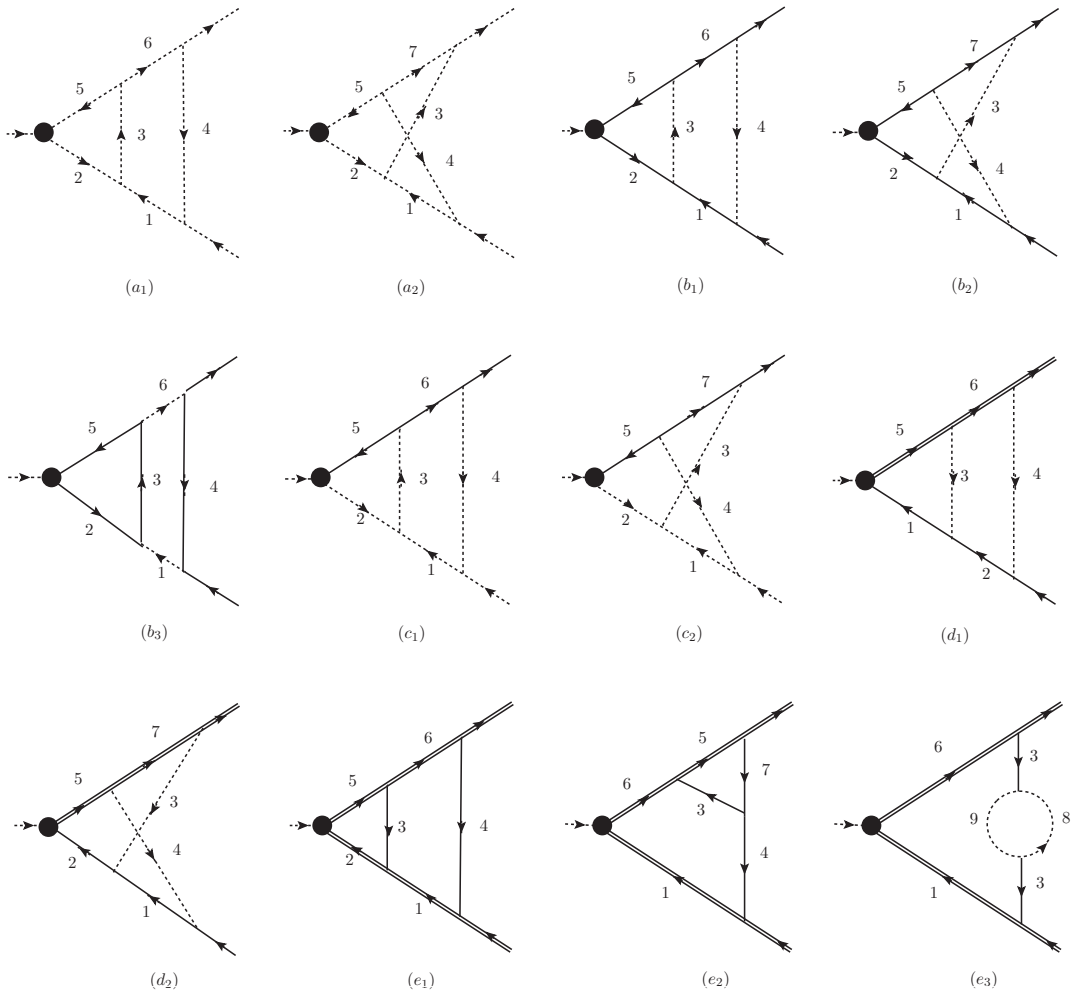

Figure 7.5: Two-loop form factor topologies. Massive fields are represented by solid lines, double lines represent heavy particles, massless propagators are shown as dashed lines. Arrows represent direction of momentum. (a_i) represent topologies of MIs at $\mu \sim Q$ (Sudakov), (b_i) represent topologies of MIs at $\mu \sim m_{1,2}$ (threshold), (c_i) represent topologies of MIs at $\mu \sim m_2$ (threshold), (d_i) represent topologies of MIs at $\mu \sim m_1$ (threshold) and (e_i) represent topologies of MIs at $\mu \sim M$ (Sudakov/threshold).

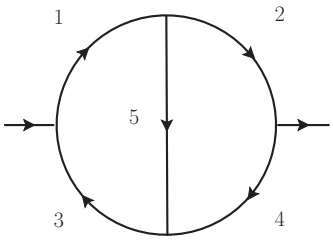

Figure 7.6: Full theory self-energy topology. Arrows represent momentum direction. The MIs associated to other topologies are subsets of the MIs required for this topology.

$$+\zeta_2+56\epsilon^3\zeta_3+\frac{56\epsilon^2\zeta_3}{3}+\frac{14\epsilon\zeta_3}{3}+21\epsilon^3\zeta_4+\frac{21\epsilon^2\zeta_4}{4}+\frac{62\epsilon^3\zeta_5}{5}-12+\mathcal{O}(\epsilon^4)\Bigg), \tag{7.120b}$$

$$\begin{aligned}J^{(Q)}_{1100101}=&\left(\frac{Q^2}{\mu^2}\right)^{-2\epsilon}\Bigg(-\frac{665\epsilon^3}{2}-\frac{211\epsilon^2}{2}-\frac{65\epsilon}{2}-\frac{5}{2\epsilon}-\frac{1}{2\epsilon^2}+\frac{65\epsilon^3\zeta_2}{2}+\frac{19\epsilon^2\zeta_2}{2}+\frac{5\epsilon\zeta_2}{2}\\&-\frac{16}{3}\epsilon^3\zeta_2\zeta_3+\frac{\zeta_2}{2}+\frac{304\epsilon^3\zeta_3}{3}+\frac{80\epsilon^2\zeta_3}{3}+\frac{16\epsilon\zeta_3}{3}+\frac{285\epsilon^3\zeta_4}{8}+\frac{57\epsilon^2\zeta_4}{8}+\frac{136\epsilon^3\zeta_5}{5}\\&-\frac{19}{2}+\mathcal{O}(\epsilon^4)\Bigg),\end{aligned} \tag{7.120c}$$

$$J^{(Q)}_{1111101}=\frac{1}{Q^2}\left(\frac{Q^2}{\mu^2}\right)^{-2\epsilon}\left(\frac{\pi^2}{\epsilon^2}-\frac{1}{\epsilon^4}+\frac{83\zeta_3}{3\epsilon}+\frac{59\pi^4}{120}+\mathcal{O}(\epsilon)\right), \tag{7.120d}$$

where ζ_s denotes the Riemann ζ-function,

$$\zeta_s=\sum_{k=1}^{\infty}\frac{1}{k^s},\quad s\geq 2:s\in\mathbb{N}, \tag{7.121}$$

and these integrals have been verified from previous work [379]. On the other hand, in the threshold regime, the full theory MIs have topologies represented by Figs. 7.5 (b,c). Due to the threshold limit, $Q\to 0$, the MIs are further reduced down to two-loop self-energy topologies, as shown in Fig. 7.6, and analytic expressions are known [380]. The MIs can therefore be expressed in terms of a single integral family with five propagators given by,

$$J^{(s)}_{\{\nu_1^{(m)}\cdots\nu_5^{(m)}\}}=\left[(4\pi)^{2-\epsilon}e^{\gamma_E\epsilon}\right]^2\int \not{d}^D l_1\not{d}^D l_2\frac{1}{D_1^{\nu_1}(m)\cdots D_5^{\nu_5}(m)}, \tag{7.122}$$

where $l_i:i=1,2$ are the loop momenta, s is the scale in the EFT formalism at which the MIs play a role, and,

$$\begin{aligned}&D_1(m)=l_1^2-m^2,\quad D_2(m)=l_2^2-m^2,\quad D_3(m)=(l_1-p)^2-m^2,\\&D_4(m)=(l_2-p)^2-m^2,\quad D_5(m)=(l_1-l_2)^2-m^2.\end{aligned} \tag{7.123}$$

To begin with, the bare vertex matching contributions at the scale $\mu\sim m_{1,2}\sim M\gg Q$, for matching from the full theory to heavy-heavy operators is represented by $V_i^{(m,M)}$. Post-reduction

one is left with the following MIs,

$$J^{(m,M)}_{1_m1_m000} = m^4\left(\frac{m^2}{\mu^2}\right)^{-2\epsilon}\left(-4\epsilon-\frac{2}{\epsilon}-\frac{1}{\epsilon^2}-2\epsilon\zeta_2-\zeta_2+\frac{2\epsilon\zeta_3}{3}-3+\mathcal{O}(\epsilon^2)\right), \tag{7.124a}$$

$$J^{(m,M)}_{1_m1_m001_m} = m^2\left(\frac{m^2}{\mu^2}\right)^{-2\epsilon}\left(-\frac{45\epsilon}{2}-\frac{9}{2\epsilon}-\frac{3}{2\epsilon^2}-\frac{27}{2}\epsilon l_3S_2+3\epsilon S_1\zeta_2+\frac{81\epsilon S_2}{2}+\frac{27S_2}{2}-9\epsilon S_3 -\frac{9\epsilon\zeta_2}{2}-\frac{3\zeta_2}{2}+\epsilon\zeta_3-\frac{21}{2}+\mathcal{O}(\epsilon^2)\right), \tag{7.124b}$$

$$J^{(m,M)}_{1_m1_m01_m0} = m^2\left(\frac{m^2}{\mu^2}\right)^{-2\epsilon}\left(-15\epsilon-\frac{3}{\epsilon}-\frac{1}{\epsilon^2}+\frac{1}{2}\epsilon l_3^2S_1-3\epsilon l_3S_1-l_3S_1-9\epsilon l_3S_2+7\epsilon S_1 +\frac{S_1}{\epsilon}+4\epsilon S_1\zeta_2+3S_1+27\epsilon S_2+9S_2-6\epsilon S_3-3\epsilon\zeta_2-\zeta_2+\frac{2\epsilon\zeta_3}{3}-7+\mathcal{O}(\epsilon^2)\right), \tag{7.124c}$$

$$J^{(m,M)}_{1_m01_m1_m1_m} = \left(\frac{m^2}{\mu^2}\right)^{-2\epsilon}\left(-\frac{65\epsilon}{2}-\frac{5}{2\epsilon}-\frac{1}{2\epsilon^2}+\frac{1}{2}\epsilon l_3^2S_1-4\epsilon l_3S_1-l_3S_1-\frac{63\epsilon l_3S_2}{4} -4\epsilon l_3\zeta_2+12\epsilon S_1+\frac{S_1}{\epsilon}-9\epsilon S_1S_2+\frac{11\epsilon S_1\zeta_2}{2}+4S_1+63\epsilon S_2+\frac{63S_2}{4}-\frac{21\epsilon S_3}{2} +\frac{7\epsilon\zeta_2}{2}+\frac{29\epsilon\zeta_3}{6}-\frac{19}{2}+\mathcal{O}(\epsilon^2)\right), \tag{7.124d}$$

$$J^{(m,M)}_{01_m1_m01_m} = m^2\left(\frac{m^2}{\mu^2}\right)^{-2\epsilon}\left(-\frac{65\epsilon}{16}-\frac{17}{4\epsilon}-\frac{3}{2\epsilon^2}-\frac{49\epsilon\zeta_2}{4}-\frac{3\zeta_2}{2}+\epsilon\zeta_3-\frac{59}{8}+\mathcal{O}(\epsilon^2)\right), \tag{7.124e}$$

$$J^{(m,M)}_{11_m01_m1)} = \left(\frac{m^2}{\mu^2}\right)^{-2\epsilon}\left(-\frac{65\epsilon}{2}-\frac{5}{2\epsilon}-\frac{1}{2\epsilon^2}+\frac{1}{2}\epsilon l_3^2S_1-4\epsilon l_3S_1-l_3S_1-\frac{63\epsilon l_3S_2}{4}+12\epsilon S_1 +\frac{S_1}{\epsilon}+\frac{23\epsilon S_1\zeta_2}{2}+4S_1+63\epsilon S_2+\frac{63S_2}{4}-\frac{21\epsilon S_3}{2}-\frac{21\epsilon\zeta_2}{2}-2\zeta_2-\frac{3\epsilon\zeta_3}{4} -\frac{19}{2}+\mathcal{O}(\epsilon^2)\right), \tag{7.124f}$$

$$J^{(m,M)}_{1_m1_m1_m1_m0} = \left(\frac{m^2}{\mu^2}\right)^{-2\epsilon}\left(-32\epsilon-\frac{4}{\epsilon}-\frac{1}{\epsilon^2}+\epsilon l_3^2S_1-8\epsilon l_3S_1-2l_3S_1-18\epsilon l_3S_2+4\epsilon l_3\zeta_2 +24\epsilon S_1+\frac{2S_1}{\epsilon}-18\epsilon S_1S_2+8\epsilon S_1\zeta_2+8S_1+72\epsilon S_2+18S_2-12\epsilon S_3-12\epsilon\zeta_2 -3\zeta_2+\frac{2\epsilon\zeta_3}{3}-12+\mathcal{O}(\epsilon^2)\right), \tag{7.124g}$$

$$J^{(m,M)}_{1_m1_m1_m1_m1_m} = \frac{1}{m^2}\left(\frac{m^2}{\mu^2}\right)^{-2\epsilon}\left(\frac{9S_1S_2}{2}-\zeta_3+\mathcal{O}(\epsilon)\right), \tag{7.124h}$$

$$J^{(m,M)}_{1001_m1} = m^2\left(\frac{m^2}{\mu^2}\right)^{-2\epsilon}\left(\frac{55\epsilon}{16}-\frac{5}{4\epsilon}-\frac{1}{2\epsilon^2}-\frac{25\epsilon\zeta_2}{4}-\frac{5\zeta_2}{2}-\frac{11\epsilon\zeta_3}{3}-\frac{11}{8}+\mathcal{O}(\epsilon^2)\right), \tag{7.124i}$$

$$J^{(m,M)}_{11_m001} = m^2\left(\frac{m^2}{\mu^2}\right)^{-2\epsilon}\left(-\frac{15\epsilon}{2}-\frac{3}{2\epsilon}-\frac{1}{2\epsilon^2}-\frac{9\epsilon\zeta_2}{2}-\frac{3\zeta_2}{2}+\frac{4\epsilon\zeta_3}{3}-\frac{7}{2}+\mathcal{O}(\epsilon^2)\right), \tag{7.124j}$$

where $l_n = \ln(n)$, $S_1 = \frac{\pi}{\sqrt{3}}$, $S_2 = \frac{4}{9\sqrt{3}}\mathrm{Ls}_2(\pi/3)$, and $S_3 = -\mathrm{Ls}_3(2\pi/3)/\sqrt{3}$, such that Ls_j can be

written in integral form as,

$$\mathrm{Ls}_j(\theta) = -\int_0^\theta d\theta' \ln^{j-1}\left|2\sin\left(\theta'/2\right)\right| : \quad 0 < \theta < 2\pi. \tag{7.125}$$

Next, we consider the bare vertex matching contributions at the scale $\mu \sim m_2 \gg m_1, M$, for matching from the full theory to heavy-light operators labelled by $V_i^{(m_2)}$. The MIs in this are,

$$J^{(m_2)}_{11001_m} = m_2^2\left(\frac{m_2^2}{\mu^2}\right)^{-2\epsilon}\left(-\frac{15\epsilon}{2} - \frac{3}{2\epsilon} - \frac{1}{2\epsilon^2} - \frac{9\epsilon\zeta_2}{2} - \frac{3\zeta_2}{2} + \frac{4\epsilon\zeta_3}{3} - \frac{7}{2} + \mathcal{O}(\epsilon^2)\right), \tag{7.126a}$$

$$J^{(m_2)}_{1_m1_m000} = m_2^4\left(\frac{m_2^2}{\mu^2}\right)^{-2\epsilon}\left(-5\epsilon^2 - 4\epsilon - \frac{2}{\epsilon} - \frac{1}{\epsilon^2} - 3\epsilon^2\zeta_2 - 2\epsilon\zeta_2 - \zeta_2 + \frac{4\epsilon^2\zeta_3}{3} + \frac{2\epsilon\zeta_3}{3} - \frac{7\epsilon^2\zeta_4}{4} - 3 + \mathcal{O}(\epsilon^3)\right), \tag{7.126b}$$

$$J^{(m_2)}_{11_m100} = m_2^2\left(\frac{m_2^2}{\mu^2}\right)^{-2\epsilon}\left(-31\epsilon^2 - 15\epsilon - \frac{3}{\epsilon} - \frac{1}{\epsilon^2} + 8\epsilon^2\zeta_3 + \frac{8\epsilon\zeta_3}{3} + 3\epsilon^2\zeta_4 - 7 + \mathcal{O}(\epsilon^3)\right), \tag{7.126c}$$

$$J^{(m_2)}_{01_m1001} = m_2^2\left(\frac{m_2^2}{\mu^2}\right)^{-2\epsilon}\left(-\frac{5\epsilon}{16} - \frac{11}{4\epsilon} - \frac{1}{\epsilon^2} + \frac{9\epsilon l_3 S_1}{2} - \frac{39\epsilon S_1}{4} - \frac{3S_1}{2} - \frac{81\epsilon S_2}{4} - \frac{11\epsilon\zeta_2}{4} - \zeta_2 + \frac{2\epsilon\zeta_3}{3} - \frac{35}{8} + \mathcal{O}(\epsilon^3)\right), \tag{7.126d}$$

$$J^{(m_2)}_{011_m02_m} = \left(\frac{m_2^2}{\mu^2}\right)^{-2\epsilon}\left(\frac{11\epsilon}{2} - \frac{1}{2\epsilon} - \frac{1}{2\epsilon^2} + 3\epsilon l_3 S_1 - 5\epsilon S_1 - S_1 - \frac{27\epsilon S_2}{2} + \frac{\epsilon\zeta_2}{6} - \frac{\zeta_2}{6} + \frac{1}{2} + \mathcal{O}(\epsilon^2)\right), \tag{7.126e}$$

$$J^{(m_2)}_{01_m1_m01_m} = m_2^2\left(\frac{m_2^2}{\mu^2}\right)^{-2\epsilon}\left(\frac{1117\epsilon^2}{32} - \frac{65\epsilon}{16} - \frac{17}{4\epsilon} - \frac{3}{2\epsilon^2} + 48\epsilon^2 l_2\zeta_2 - \frac{475\epsilon^2\zeta_2}{8} - \frac{49\epsilon\zeta_2}{4} - \frac{3\zeta_2}{2} - \frac{151\epsilon^2\zeta_3}{6} + \epsilon\zeta_3 - \frac{21\epsilon^2\zeta_4}{8} - \frac{59}{8} + \mathcal{O}(\epsilon^3)\right), \tag{7.126f}$$

$$J^{(m_2)}_{01101} = m_2^2\left(\frac{m_2^2}{\mu^2}\right)^{-2\epsilon}\left(\frac{865\epsilon^2}{32} + \frac{115\epsilon}{16} + \frac{1}{4\epsilon} - \frac{13\epsilon^2\zeta_2}{8} - \frac{\epsilon\zeta_2}{4} - \frac{8\epsilon^2\zeta_3}{3} + \frac{13}{8} + \mathcal{O}(\epsilon^3)\right), \tag{7.126g}$$

$$J^{(m_2)}_{11_m111_m} = \frac{1}{m_2^2}\left(\frac{m_2^2}{\mu^2}\right)^{-2\epsilon}\left(2\epsilon i\pi\zeta_2 + i\pi\zeta_2 + \frac{5\epsilon i\pi\zeta_3}{4} + 27\epsilon S_1S_2 + \frac{27S_1S_2}{2} + 27\epsilon S_1S_3 + \frac{729\epsilon S_2^2}{8} - 6\epsilon\zeta_3 - 3\zeta_3 - \frac{2567\epsilon\zeta_4}{36} + \mathcal{O}(\epsilon^2)\right), \tag{7.126h}$$

$$J^{(m_2)}_{1_m001_m1} = m_2^2\left(\frac{m_2^2}{\mu^2}\right)^{-2\epsilon}\left(-\frac{5\epsilon}{16} - \frac{11}{4\epsilon} - \frac{1}{\epsilon^2} + \frac{9\epsilon l_3 S_1}{2} - \frac{39\epsilon S_1}{4} - \frac{3S_1}{2} - \frac{81\epsilon S_2}{4} - \frac{11\epsilon\zeta_2}{4} - \zeta_2 + \frac{2\epsilon\zeta_3}{3} - \frac{35}{8} + \mathcal{O}(\epsilon^2)\right), \tag{7.126i}$$

$$J^{(m_2)}_{11110} = \left(\frac{m_2^2}{\mu^2}\right)^{-2\epsilon}\left(-80\epsilon^2 - 32\epsilon - \frac{4}{\epsilon} - \frac{1}{\epsilon^2} + 12\epsilon^2\zeta_2 + 4\epsilon\zeta_2 + \zeta_2 + \frac{56\epsilon^2\zeta_3}{3} + \frac{14\epsilon\zeta_3}{3} + \frac{21\epsilon^2\zeta_4}{4} - 12 + \mathcal{O}(\epsilon^3)\right), \tag{7.126j}$$

Lastly, we consider the vertex contributions, $V_i^{(m)}$, at the scale $\mu \sim m_{1,2} \gg M$, for matching from the full theory to HPET. In this case, we have the following MIs,

$$J^{(m)}_{1001^{(m)}1} = m^2 \left(\frac{m^2}{\mu^2}\right)^{-2\epsilon} \left(\frac{949\epsilon^2}{32} + \frac{55\epsilon}{16} - \frac{5}{4\epsilon} - \frac{1}{2\epsilon^2} - \frac{55\epsilon^2\zeta_2}{8} - \frac{25\epsilon\zeta_2}{4} - \frac{5\zeta_2}{2} - \frac{55\epsilon^2\zeta_3}{6} - \frac{11\epsilon\zeta_3}{3} - \frac{303\epsilon^2\zeta_4}{8} - \frac{11}{8} + \mathcal{O}(\epsilon^3)\right), \tag{7.127a}$$

$$J^{(m)}_{001^{(m)}1^{(m)}0} = m^4 \left(\frac{m^2}{\mu^2}\right)^{-2\epsilon} \left(-5\epsilon^2 - 4\epsilon - \frac{2}{\epsilon} - \frac{1}{\epsilon^2} - 3\epsilon^2\zeta_2 - 2\epsilon\zeta_2 - \zeta_2 + \frac{4\epsilon^2\zeta_3}{3} + \frac{2\epsilon\zeta_3}{3} - \frac{7\epsilon^2\zeta_4}{4} - 3 + \mathcal{O}(\epsilon^3)\right), \tag{7.127b}$$

$$J^{(m)}_{01^{(m)}1^{(m)}01^{(m)}} = m^2 \left(\frac{m^2}{\mu^2}\right)^{-2\epsilon} \left(\frac{1117\epsilon^2}{32} - \frac{65\epsilon}{16} - \frac{17}{4\epsilon} - \frac{3}{2\epsilon^2} + 48\epsilon^2 l_2\zeta_2 - \frac{475\epsilon^2\zeta_2}{8} - \frac{49\epsilon\zeta_2}{4} - \frac{3\zeta_2}{2} - \frac{151\epsilon^2\zeta_3}{6} + \epsilon\zeta_3 - \frac{21\epsilon^2\zeta_4}{8} - \frac{59}{8} + \mathcal{O}(\epsilon^3)\right). \tag{7.127c}$$

As for the full theory and SCET bare two-loop wave-function contributions, present in Appendix B.7, it is well-known that they map to MIs illustrated by Fig. 7.6, and thus we refrain from going into detail.

With regards to the effective theory MIs, the HPET vertex and wave-function contributions have MIs with topologies represented by Figs. 7.5 (d, e) and 7.7. We begin with considering the heavy-light currents in Fig. 7.5 (d), the MIs of which can be expressed in terms of a single integral family with seven propagators given by,

$$R^{(s)}_{\nu_1\ldots\nu_7} = \left[(4\pi)^{2-\epsilon}e^{\gamma_E\epsilon}\right]^2 \int \not{d}^D l_1 \not{d}^D l_2 \frac{1}{D_1^{\nu_1}\ldots D_7^{\nu_7}}, \tag{7.128}$$

where v_2 is the heavy particle velocity, p_1 and m_1 are the full theory field momentum and mass, $p_1 \cdot v_2 \equiv w'$, and thus,

$$\begin{aligned} &D_1(m) = (l_1+p_1)^2 - m^2, \quad D_2(m) = (l_2+p_1)^2 - m^2, \quad D_3 = (l_1-l_2)^2, \quad D_4 = l_2^2, \\ &D_5 = l_1\cdot v_2, \quad D_6 = l_2\cdot v_2, \quad D_7 = (l_1-l_2)\cdot v_2 + w'. \end{aligned} \tag{7.129}$$

Similarly, for the heavy-heavy vertex contributions, all sub-topologies can be mapped to the largest unique two that are shown in Fig. 7.5 (e). We can again express all MIs in terms of nine propagators given by,

$$K^{(s)}_{\nu_1\ldots\nu_9} = \left[(4\pi)^{2-\epsilon}e^{\gamma_E\epsilon}\right]^2 \int \not{d}^D l_1 \not{d}^D l_2 \frac{1}{D_1^{\nu_1}\ldots D_9^{\nu_9}}, \tag{7.130}$$

where $v_{1,2}$ are the heavy particle velocities, $v_1 \cdot v_2 \equiv w$, M is the mass of exchanged bosons, and

$$\begin{aligned} &D_1 = l_2\cdot v_1, \quad D_2 = l_1\cdot v_1, \quad D_3 = (l_1-l_2)^2 - M^2, \quad D_4 = l_1^2 - M^2, \\ &D_5(M) = l_1\cdot v_2, \quad D_6(M) = l_2\cdot v_2, \quad D_7(M) = l_2^2 - M^2, \quad D_8 = l_2^2, \quad D_9 = l_1^2 \end{aligned} \tag{7.131}$$

Finally, we examine the wave-function contributions of which all topologies are mapped to those shown in Fig. 7.7. In this case we can express all MIs in terms of six propagators given by,

$$L^{(s)}_{\nu_1\ldots\nu_8} = \left[(4\pi)^{2-\epsilon}e^{\gamma_E\epsilon}\right]^2 \int \not{d}^D l_1 \not{d}^D l_2 \frac{1}{D_1^{\nu_1}\ldots D_8^{\nu_8}}, \tag{7.132}$$

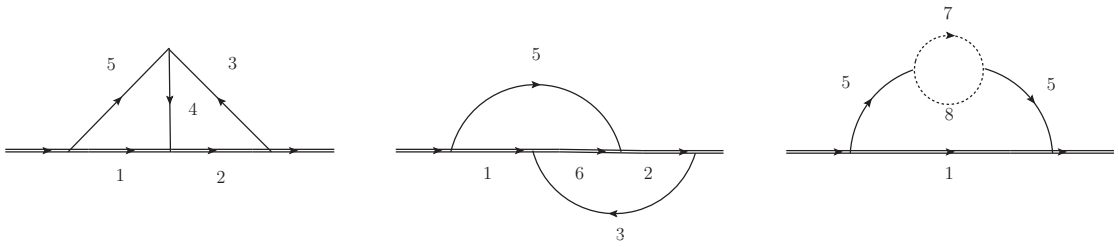

Figure 7.7: Heavy field self-energy topologies. The MIs associated to other topologies are subsets of the MIs required for topologies illustrated.

where p and v are the heavy particle residual momentum and velocity, M is the mass of exchanged bosons, and

$$D_1 = (p - l_1)\cdot v, \quad D_2 = (p + l_2)\cdot v, \quad D_3(M) = l_2^2 - M^2, \quad D_4(M) = (l_1 + l_2)^2 - M^2,$$
$$D_5(M) = l_1^2 - M^2, \quad D_6 = (p + l_2 - l_1)\cdot v, \quad D_7 = l_2^2, \quad D_8 = (l_1 - l_2)^2. \tag{7.133}$$

The evaluation of integrals of this type, i.e. massive two-loop integrals with heavy line insertions, is non-trivial and requires modern methods. In Chapter 8 we discuss the methods we employed to evaluate the MIs appearing in our calculations and generalisations thereof.

7.9 Summary

Both the massive and massless form factors are indispensable building blocks to a broad set of observables in both high and low energy regimes. Precisely studying these factors is crucial for shedding light on mysteries that remain in the Standard Model and beyond, such as the physical structure of the top quark, aspects of mass generation and the nature of dark matter. Our various composite operators, choice of model for applicability, as well as consideration of two critical energetic regimes is emblematic of the breadth of the problem at hand. Our two-loop results are not complete, as we have not calculated the bare two-loop vertex corrections for massive SCET graphs. Continuing to map this space at two-loops and beyond is essential for our predicting power to be able to match the high precision potential of a future *electron-positron collider* and the LHC in its upcoming high luminosity operating phase.

Currently, the effective theory formalism is central when it comes to tackling such complex problems by breaking them down scale by scale. By application to the SM, we have begun extending the work on EW corrections to high energy processes beyond NLO, as stated in the latest review [50]. Moreover, we are mapping other parts of the energetic landscape, aside from the Sudakov regime, which itself opens the door for further investigation. Beyond the SM, the generality of the model and operators studied means that our results can be applied to BSM models by replacement of the proper coupling and group theory factors, which would be interesting to examine further. For instance, one can apply our results to various models of dark matter [358, 359], where weak corrections are significant for indirect detection. Our full results are contained in the ancillary file submitted along with Ref. [325] on the arXiv.

Chapter 8

Massive Two-Loop Heavy Particle Diagrams

In this Chapter, we evaluate vertex and self-energy diagrams that appear in EFTs containing heavy fields. The integrals involve at least one heavy line, and the standard lines include an arbitrary mass scale. The evaluation is done analytically with modern techniques. We employ the methods of *differential equations* and *dimensional recurrence relations* to evaluate said integrals up to two-loop orders. This Chapter is based on Ref. [381], reflecting the author's contribution.

8.1 Motivation

Heavy Particle Effective Theories have a wide range of applicability, and their use cases have expanded dramatically in recent years. They are apparent when a field of arbitrary spin in a given theory is taken to have a large mass compared to other propagating massive degrees of freedom. HPETs were originally conceived in the context of QED and QCD, such as in HQET, NR QCD and QED and variations therein [64, 251, 282]. More recently, they have also been applied in the EW regime [75, 76, 161, 325, 348, 352, 353], as well as in BSM physics such as in the context of *heavy dark matter* [269, 358], *Z' bosons* [382, 383] and *black hole* interactions [242, 384, 385].

When dealing with such theories beyond leading perturbative order, one is faced with loop diagrams containing eikonal lines. In this work, we determine these at two-loop order by employing a set of modern techniques, in particular, *differential equations* and *dimensional recurrence relations* (DRR), which have been successful in similar contexts [265, 386]. We further include a non-zero mass-scale in the standard lines for theoretical models with massive propagating degrees of freedom. The mass scale bounds the IR regime for the two- and three-point diagrams studied here. Even in theories with exclusively massless propagating degrees of freedom such as QED/QCD and gravity, the IR structure needs to be correctly understood [341, 385].

The diagrams considered here are especially useful in the evaluation of *form factors* of a given model. The form factor is most well-known for its uses in perturbative analyses of scattering processes occurring at the LHC and future colliders [326, 327]. Form factors are of primary consideration instead of specific processes as they form the fundamental building blocks for a vast array of processes. For instance, they have been employed to study di-jet, $\bar{t}t$, squark pair, and DM production in various studies [353, 357–359]. It is also the simplest amplitude that can be used to study the IR behaviour of a theory. For further reference in the context of the SM, the QCD form factors of quarks have been evaluated to three-loop order [328, 330, 339–341], and the EW corrections using both EFT and IR evolution equations are currently being studied to two-loop order [75, 325, 344–350].

On the other hand, there has also been significant progress in the realm of Feynman diagram evaluation. When previously, certain classes of multi-loop diagrams were intractable, they have now become determinable with the help of revolutionary techniques. Most notably, diagrams with masses are now attainable with the differential equations method [78, 81–83]. The basis of which is set upon differentiating the master integrals of interest, forming a system of differential equations and reducing said system to so-called ϵ-form [78,387–389]. Given that such a reduction is achievable [388], the MIs are expressible in terms of *multiple polylogarithms* (MPLs) [390, 391]. The outlier systems which can not be reduced to ϵ-form are not representable as MPLs. Fortunately, even in this domain there is good progress in understanding functions beyond multiple polylogarithms such as *elliptical polylogarithms* (EPLs) [392–398], or entirely novel functions [399–402]. In our case, the diagrams we encounter are reducible to ϵ-form and thus, can be written in terms of MPLs. However, when we take external lines *off-shell*, the integrals are only reducible to $(A + B\epsilon)$-form, as we will see. This is the closest extension of ϵ-form, and one must resort to EPLs to solve such MIs. In this work, we provide results for the massive heavy-heavy, heavy-light and propagator diagrams at two-loop order. The results are explicitly give up to $\mathcal{O}(\epsilon^2)$ working in $d = 4 - 2\epsilon$ dimensions, which is the appropriate order for SM-like theories [76, 325, 352, 353]. However, this order is arbitrary as the results are attainable to any order in ϵ, given the exact *boundary integrals* provided here.

Outlining this Chapter, we begin by discussing the formalism we employ and follow by illustrating the problem. In the main sections, we tackle the on-shell diagrams under consideration by reducing the differential equations to ϵ-form. The last section illustrates the off-shell self-energy case and its reduction to $(A + B\epsilon)$-form. A description of the methods we employ in our work is given in Appendices C.1 and C.2.

8.2 Formalism and Technicalities

The massive HPET vertex and self-energy have MIs with topologies represented by Figs. 8.1 (a, b) and 8.2, respectively. We begin with considering the heavy-light currents in Figs. 8.1 (a), the master integrals of which can be expressed in terms of a single integral family with seven propagators given by,

$$R^{(s)}_{\nu_1\dots\nu_{10}} = \left[(4\pi)^{2-\epsilon} e^{\gamma_E \epsilon}\right]^2 \int \not{d}^d l_1 \not{d}^d l_2 \frac{1}{D_1^{\nu_1} \dots D_{10}^{\nu_{10}}}, \tag{8.1}$$

where v is the heavy field velocity, p is the full theory field momentum and $p^2 = m^2$, and thus,

$$\begin{aligned} &D_1(m) = (l_1 - p)^2 - m^2, \quad D_2(m) = (l_2 - p)^2 - m^2, \quad D_3 = (l_1 - l_2)^2, \quad D_4 = l_2^2, \\ &D_5 = l_1 \cdot v, \quad D_6 = l_2 \cdot v, \quad D_7 = (l_1 - l_2) \cdot v, \quad D_8(m) = (l_1 - l_2)^2 - m^2, \\ &D_9(m) = l_2^2 - m^2, \quad D_{10}(m) = (l_2 + p)^2. \end{aligned} \tag{8.2}$$

Upon momentum re-scaling with respect to m it is clear that these integrals are dependent on $w \equiv p \cdot v/m$. Thus, one can define the differential system of equations on derivatives of the MIs with respect to w. However, upon investigation it turns out that a further change of variables is necessary to reduce the system to the requisite ϵ-form. The appropriate kinematic variable was found to be,

$$\beta = \sqrt{\frac{1-w}{1+w}}, \quad w = \frac{1-\beta^2}{1+\beta^2}. \tag{8.3}$$

With this change of variables, all MIs are expressible in terms of MPLs. The *boundary conditions* are freely determined by giving a specific allowable value to w. Similarly, for the heavy-heavy

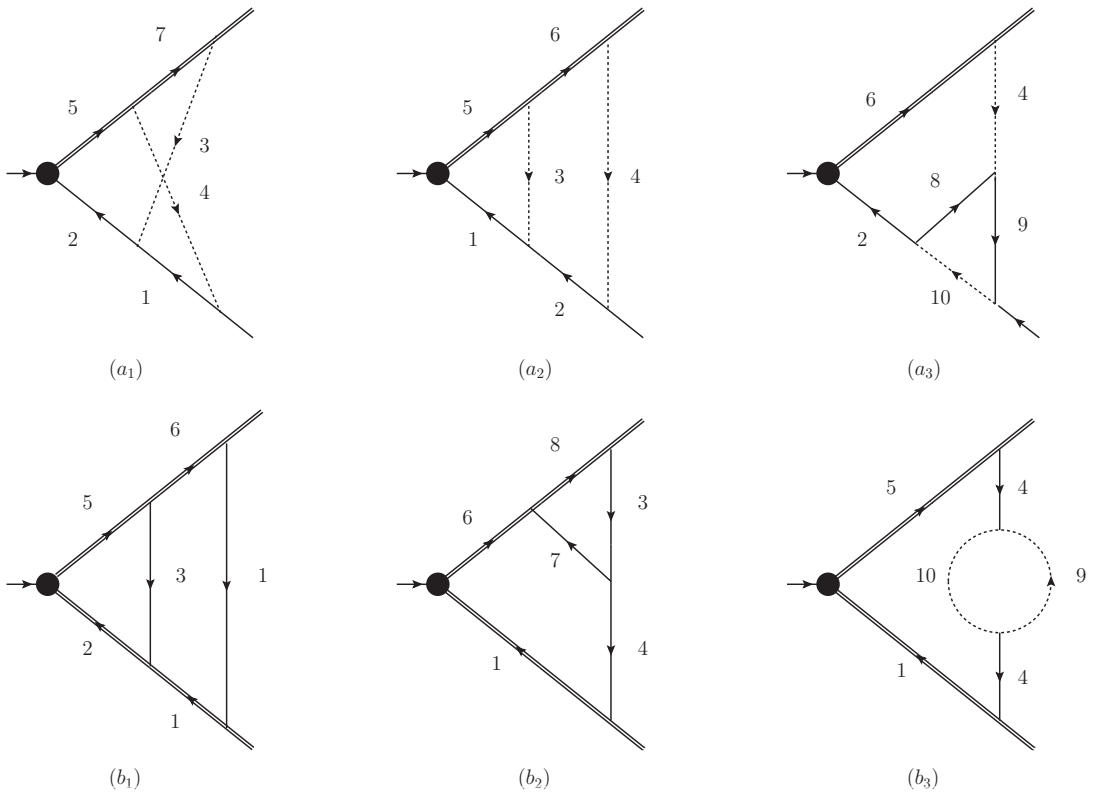

Figure 8.1: Prototype topologies of two-loop vertex diagrams. Solid lines represent massive particles, double lines represent heavy particles, dashed lines correspond to massless propagators. Arrows represent direction of momenta. (a_i) and (b_i) correspond to heavy-light and heavy-heavy topologies. We also include the case of light self-energy insertions as is apparent in (b_3).

vertex contributions, all sub-topologies can be mapped to the largest unique two that are shown in Fig. 8.1 (b). We can express all MIs in terms of ten propagators given by,

$$K^{(s)}_{\nu_1\dots\nu_{10}} = \left[(4\pi)^{2-\epsilon}e^{\gamma_E\epsilon}\right]^2 \int \not{d}^d l_1 \not{d}^d l_2 \frac{1}{D_1^{\nu_1}\dots D_{10}^{\nu_{10}}}, \tag{8.4}$$

where $v_{1,2}$ are the heavy particle velocities, M is the mass of exchanged bosons, and

$$\begin{aligned} &D_1 = l_2\cdot v_1, \quad D_2 = l_1\cdot v_1, \quad D_3 = (l_1-l_2)^2 - M^2, \quad D_4 = l_2^2 - M^2, \quad D_5(M) = l_1\cdot v_2, \\ &D_6(M) = l_2\cdot v_2, \quad D_7(M) = l_1^2 - M^2, \quad D_8 = (l_2-l_1)\cdot v_2, \quad D_9 = (l_1-l_2)^2, \quad D_{10} = l_1^2. \end{aligned} \tag{8.5}$$

Again, re-scaling the momenta with respect to M in this case gives integrals dependent on $w \equiv v_1\cdot v_2$. The appropriate kinematic variable to take derivatives with respect to was found to be β as previously defined.

Lastly, the self-energy diagrams which contribute to heavy field renormalisation and residual mass term are examined [153]. The prototype topologies are shown in Fig. 8.2. In this case, we can express all MIs in terms of the eight propagators,

$$L^{(s)}_{\nu_1\dots\nu_8} = \left[(4\pi)^{2-\epsilon}e^{\gamma_E\epsilon}\right]^2 \int \not{d}^d l_1 \not{d}^d l_2 \frac{1}{D_1^{\nu_1}\dots D_8^{\nu_8}}, \tag{8.6}$$

where p and v are the heavy particle residual momentum and velocity, M is the mass of exchanged fields,

$$\begin{aligned} &D_1 = (p-l_1)\cdot v, \quad D_2 = (p+l_2)\cdot v, \quad D_3(M) = l_2^2 - M^2, \quad D_4(M) = (l_1+l_2)^2 - M^2, \\ &D_5(M) = l_1^2 - M^2, \quad D_6 = (p+l_2-l_1)\cdot v, \quad D_7 = l_2^2, \quad D_8 = (l_1-l_2)^2. \end{aligned} \tag{8.7}$$

We note the relations between the heavy field self-energy, $\Sigma(p)$, the bare field counter-term, δZ_h, and the residual heavy field mass, δm_h, are given by,

$$\delta Z_h = i\partial_{v\cdot p}\tilde{\Sigma}|_{v\cdot p=0} \tag{8.8}$$

$$\delta m_h = -i\tilde{\Sigma}|_{v\cdot p=0}. \tag{8.9}$$

Whence, to determine these quantities one only requires the MIs on-shell at $v\cdot p = 0$, thus eliminating the momentum, p, from the propagators. This results in MIs that are simple enough to evaluate with standard techniques. Maintaining $v\cdot p \neq 0$ is interesting as it applies to off-shell studies. In this case we define $w \equiv p\cdot v/M$ and β remains the appropriate kinematic variable as previously defined. As we will see however, it is solely reducible to $(A + B\epsilon)$-form and thus requires treatment with elliptics which is more involved.

As mentioned in the previous section, in all cases, the goal is to derive a differential system for the MIs and solve *iteratively* in a small dimension parameter, ϵ. To take the derivative with respect to the product $p\cdot q$ for two arbitrary vectors p and q, it can be done in the following two equivalent ways,

$$\frac{\partial}{\partial(p\cdot q)} = \frac{(p\cdot q)p - p^2 q}{(p\cdot q)^2 - p^2q^2}\cdot\frac{\partial}{\partial p} = \frac{(p\cdot q)q - q^2 p}{(p\cdot q)^2 - p^2q^2}\cdot\frac{\partial}{\partial q} \tag{8.10}$$

In our study, we take derivatives with respect to the parameter w, as defined in each case. Upon re-reducing the differentiated results with IBP identities, one obtains a linear combination of MIs, leading to a set of coupled differential equations. More precisely, the derivative of a given MI will inevitably lie in the same *sector* or *sub-sector*, meaning they contain the same set of non-zero ν_i, or a smaller set, compared to the original MI. Thus, one can combine all MIs and

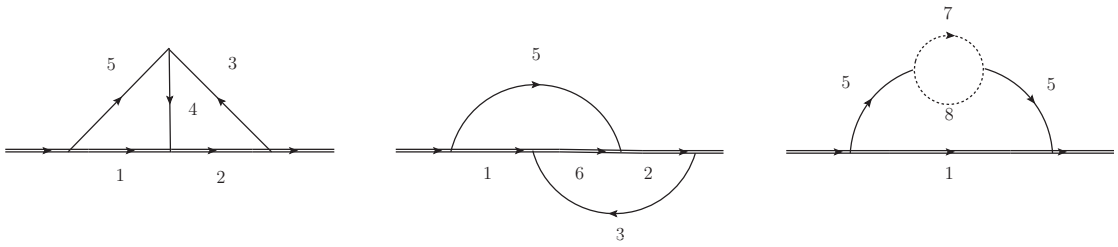

Figure 8.2: Heavy field self-energy topologies. The MIs associated to other topologies are subsets of the MIs required for topologies illustrated.

their derivatives into a linear system of differential equations. This system, in turn, will contain coupled sub-systems that may be reduced to ϵ-form. From there, we solve the system iteratively at each order in a *Laurent expansion* about small ϵ.

To achieve this technically, we obtain the Feynman diagrams with `QGRAF` [303], process the output with `FORM` [304]. We then proceed in the standard way by reducing integrals to a smaller set of so-called master integrals (MIs) using integration-by-parts identities (IBPs) [377], with the help of `LiteRed` [378] and home-grown tools. To reduce the system of differential equations to ϵ-form we employ `LIBRA` [403] and the boundary integrals that require *Mellin-Barnes* treatment are determined with the help of packages `MB` [404] and `MBsums` [405]. We also employ `HypExp2` [406] for *hypergeometric functions* and the *PSLQ algorithm* [407] for analytic expansions in ϵ.

8.3 Heavy-Heavy Vertex

To recap, the heavy-heavy N-loop master integrals with massive propagators at $d = 4 - 2\epsilon$ have the following form,

$$I = \left[(4\pi)^{2-\epsilon} e^{\gamma_E \epsilon}\right]^N \int \not{d}^d l_1 \ldots \not{d}^d l_N \frac{1}{D_1^{\nu_1} \ldots D_{n-m}^{\nu_{n-m}}} \cdot \frac{1}{\tilde{D}_{n-m+1}^{\nu_{n-m+1}} \ldots \tilde{D}_n^{\nu_n}}, \tag{8.11}$$

where n is the cardinality of the minimal set of denominators, D_i and $\tilde{D}_i$, which we separate into,

$$D_i = l_i \cdot v_i, \quad \tilde{D}_i = l_i^2 - M^2, \tag{8.12}$$

for some particular combination of loop momenta, l_i, and $v_i = v_{1,2}$ such that one preferentially works in a frame with $v_i^2 = 1$. To be able to deploy the differential equation approach to solve such master integrals one must first take a derivative of the integral with respect to some parameter. The most natural parameter in this case is $w = v_1 \cdot v_2$.

8.3.1 One-loop Case

At one-loop, all on-shell amplitudes reduce to expressions with a single MI,

$$I^{(1)} = \left[(4\pi)^{2-\epsilon} e^{\gamma_E \epsilon}\right] M^{-2\epsilon} \int \not{d}^d l \frac{1}{(l \cdot v_1)(l \cdot v_2)} \cdot \frac{1}{l^2 - 1}, \tag{8.13}$$

then we may solve this as an ODE by parameterising and taking the derivative with respect to $w = v_1 \cdot v_2$,

$$\frac{d}{dw} I^{(1)}(w) = -\frac{w}{w^2 - 1} I^{(1)}(w) + \frac{1}{w^2 - 1} \tilde{I}. \tag{8.14}$$

where the simpler integral,

$$\tilde{I} = \left[(4\pi)^{2-\epsilon} e^{\gamma_E \epsilon}\right] M^{-2\epsilon} \int \not{d}^d l \frac{1}{l^2 - 1} \cdot \frac{1}{(l \cdot v_{1,2})^2}. \tag{8.15}$$

We then reduce and evaluate,

$$\tilde{I} = \left[(4\pi)^{2-\epsilon} e^{\gamma_E \epsilon}\right] M^{-2\epsilon} (2-d) \int \not{d}^d l \frac{1}{l^2 - 1} \tag{8.16}$$

$$= 2 e^{\gamma_E \epsilon} \Gamma(\epsilon) M^{-2\epsilon} \tag{8.17}$$

One can then solve Eq. (8.14) by variation of parameters and the boundary condition, $I^{(1)}(0) = 0$, to obtain,

$$I^{(1)} = w \frac{\log(w + \sqrt{w^2 - 1})}{\sqrt{w^2 - 1}} \tilde{I} = w r(w) \tilde{I}, \tag{8.18}$$

which mimics the well-known result from *Feynman parametrisation* and its modification for HQET-like propagators [153].

8.3.2 Two-loop Case

In the two-loop case we have a column vector, $\mathbf{A}(w)$, of $n = 26$ master integrals tabulated in Table 8.1, based on our notation in Eq. (8.4). Upon differentiation of $\mathbf{A}(w)$ with respect to w and reduction by IBP identities, we have a differential system,

$$\partial_w \mathbf{A}(w) = \mathbb{M}(w, \epsilon) \mathbf{A}(w). \tag{8.19}$$

with a 26×26 matrix, $\mathbb{M}(w, \epsilon)$ which is neither Fuschian nor in ϵ-form. We may now proceed with the algorithm outlined in Section C.1. Changing variables to β, we determine a transformation matrix, $\mathbb{T}$, to attempt to reduce the differential system to one in ϵ-form. Evaluating $\mathbb{T}$ is done step-wise transforming the blocks of $\mathbb{T}$, or coupled sub-system they represent, to ϵ-form. The largest such sub-system in this case is a 3×3 block which we illustrate,

$$M_3 = \begin{pmatrix} -\frac{2w^2-\epsilon}{2(w-1)w(w+1)} & \frac{3}{4(w-1)w(w+1)} & \frac{(2w-1)(2w+1)}{4(w-1)w(w+1)\epsilon} \\ \frac{\epsilon^2}{(w-1)w(w+1)} & -\frac{2w^2-3\epsilon}{2(w-1)w(w+1)} & -\frac{1}{2(w-1)w(w+1)} \\ \frac{2\epsilon^2\left(2w^2\epsilon-2w^2-2\epsilon-1\right)}{(w-1)w(w+1)(2w-1)(2w+1)} & \frac{3\epsilon\left(2w^2\epsilon+2w^2-2\epsilon-1\right)}{(w-1)w(w+1)(2w-1)(2w+1)} & -\frac{4w^4-4w^2\epsilon-3w^2-2\epsilon-1}{(w-1)w(w+1)(2w-1)(2w+1)} \end{pmatrix}. \tag{8.20}$$

Changing variables to β and following Lee's algorithm we find a transformation matrix,

$$T_3 = \begin{pmatrix} -\frac{\beta}{w-1} & 0 & 0 \\ 0 & \frac{\beta\epsilon}{2(w-1)} & 0 \\ -\frac{2\beta\epsilon^2}{w-1} & -\frac{3\beta\epsilon^2}{2(w-1)(2w-1)(2w+1)} & \frac{w\epsilon^2}{(2w-1)(2w+1)} \end{pmatrix}, \tag{8.21}$$

which reduces M_3 to ϵ-form,

$$S_3 = \epsilon \begin{pmatrix} \frac{2w}{(w-1)(w+1)} & 0 & \frac{\beta}{4(w-1)} \\ 0 & \frac{6w}{(w-1)(w+1)(4w^2-1)} & \frac{\beta}{(w-1)(4w^2-1)} \\ \frac{16\beta}{w-1} & \frac{12\beta}{4w^3-4w^2-w+1} & -\frac{8w}{4w^2-1} \end{pmatrix}. \tag{8.22}$$

MI	ν_1	ν_2	ν_3	ν_4	ν_5	ν_6	ν_7	ν_8	ν_9	ν_{10}
A_1	0	0	1	1	0	0	0	0	0	0
A_2	0	0	1	1	0	1	0	0	0	0
A_3	0	0	1	1	1	0	0	0	0	0
A_4	0	0	1	1	1	1	0	0	0	0
A_5	0	1	1	1	0	1	0	0	0	0
A_6	0	2	1	1	0	1	0	0	0	0
A_7	0	1	2	1	0	1	0	0	0	0
A_8	0	1	1	1	1	0	0	0	0	0
A_9	0	1	1	1	0	1	0	0	0	0
A_{10}	0	1	1	1	0	1	0	0	0	0
A_{11}	0	1	1	1	1	1	0	0	0	0
A_{12}	1	1	1	1	1	1	0	0	0	0
A_{13}	0	0	1	1	0	0	1	0	0	0
A_{14}	0	0	1	1	0	0	1	1	0	0
A_{15}	0	0	1	1	0	1	0	1	0	0
A_{16}	0	0	1	1	0	1	1	1	0	0
A_{17}	1	0	1	1	0	0	1	1	0	0
A_{18}	2	0	1	1	0	0	1	1	0	0
A_{19}	1	0	1	1	0	0	2	1	0	0
A_{20}	3	0	1	1	0	0	1	1	0	0
A_{21}	1	0	1	1	0	1	1	0	0	0
A_{22}	1	0	1	1	0	1	0	1	0	0
A_{23}	1	0	1	1	0	1	1	1	0	0
A_{24}	0	0	0	1	0	0	0	0	1	1
A_{25}	0	0	0	1	0	1	0	0	1	1
A_{26}	1	0	0	1	0	1	0	0	1	1

Table 8.1: Column vector of heavy-heavy MIs with propagator exponent indices ν_i.

After repeating these steps for each block, we can consolidate each transformation matrix into a final transformation matrix. This matrix allows us to perform the complete reduction to ϵ-form as

$$\partial_w \tilde{\mathbf{A}}(w) = \epsilon \mathbb{S}(w) \tilde{\mathbf{A}}(w). \tag{8.23}$$

with Fuschian matrix $\mathbb{S}$, this system of equations is given explicitly in Appendix C.3. By analysis, $A_{1...4}$, $A_{13...16}$ and $A_{24,25}$ are w-independent and thus correspond to a portion of simpler boundary MIs. The boundary MIs require evaluation by different methods. In this work, we employ DRR to solve the boundary integrals we encounter, which provides exact results for these integrals. The DRR method is formally introduced in Appendix C.2. We present results for boundary integrals explicitly in Appendix C.4. One is not limited to DRR; however, for illustration of other methods, one can use, we solve a non-trivial example here. Consider,

$$A_{14} = C \int \not{d}^d l_1 \int \not{d}^d l_2 \frac{1}{(l_1^2-1)(l_2^2-1)((l_1-l_2)^2-1)} \frac{1}{l_2 \cdot v}, \tag{8.24}$$

where $C = -\left[(4\pi)^{2-\epsilon} e^{\gamma_E \epsilon}\right]^2 M^{2D-7}$, and we perform a shift and re-scaling in loop momenta for convenience, giving an overall negative sign. The first step involves eliminating the eikonal propagator by means of a Feynman trick developed in HQET [153],

$$\frac{1}{A^r B^s} = 2^s \frac{\Gamma(r)\Gamma(s)}{\Gamma(r+s)} \int_0^\infty d\lambda \frac{\lambda^{s-1}}{(A+2B\lambda)^{r+s}}. \tag{8.25}$$

Apply this to two of the four propgators in Eq. (8.24) and completing the square $l_{1,2} \to l_{1,2} - \lambda v/2$ gives,

$$A_{14} = C \int_0^\infty d\lambda \int \not{d}^d l_1 \int \not{d}^d l_2 \frac{2}{((l_1-v\lambda/2)^2-1)((l_2-v\lambda/2)^2-1)((l_1-l_2)^2-1-\lambda^2)^2}. \tag{8.26}$$

From here, one can proceed with standard Feynman parametrisation and application of the Cheng-Wu theorem [408], simplifying the result further. Performing the integral over λ is then straightforward, and one is left with an integral over two Feynman parameters in $d = 4-2\epsilon$ dimensions,

$$A_{14} = C \int_0^1 dx_1 \int_0^\infty dx_2 \sqrt{\pi} (x_2+1)^{1/2-2\epsilon} \Gamma(2\epsilon - 1/2)(x_1(1-x_1)+x_2)^{\epsilon-3/2}. \tag{8.27}$$

From here, it is clear that one should proceed with the *Mellin-Barnes* (MB) representation as the result will be reduced to simple Beta function integrals and a single MB integral. The MB representation is given by the well-known transformation [409],

$$\frac{1}{(A+B)^\lambda} = \frac{1}{\Gamma(\lambda)} \frac{1}{2\pi i} \int_{-i\infty}^{i\infty} dz \frac{B^z}{A^{\lambda+z}} \Gamma(\lambda+z)\Gamma(-z). \tag{8.28}$$

After transforming and performing the remaining Beta-integrals one is left with performing a sum over residues, in z, of,

$$A_{14} = C \frac{1}{2\pi i} \sqrt{\pi} \int_{-i\infty}^{i\infty} dz \frac{\Gamma(-z)\Gamma(z+1)^2 \Gamma\left(\epsilon - z - \frac{1}{2}\right) \Gamma\left(-\epsilon + z + \frac{3}{2}\right) \Gamma(\epsilon+z)}{\Gamma\left(\frac{3}{2}-\epsilon\right) \Gamma(2z+2)}. \tag{8.29}$$

which can be expanded to give,

$$A_{14} = M^{1-4\epsilon} \frac{2}{3} \pi \left(-\frac{3}{\epsilon} - 2\sqrt{3}\pi - 12 + 6l_2 + \mathcal{O}(\epsilon) \right), \tag{8.30}$$

MI	ν_1	ν_2	ν_3	ν_4	ν_5	ν_6	ν_7	ν_8	ν_9	ν_{10}
a_1	0	0	1	1	0	0	0	0	0	0
a_2	0	0	1	1	0	0	0	0	0	0
a_3	1	0	1	1	0	0	0	0	0	0
a_4	1	1	1	1	0	0	0	0	0	0
a_5	0	0	1	1	0	0	1	0	0	0
a_6	0	0	1	1	0	0	1	1	0	0
a_7	0	0	0	1	0	0	0	0	1	1
a_8	1	0	0	1	0	0	0	0	1	1

Table 8.2: Heavy-heavy boundary MIs at $w = 1$ with propagator exponent indices ν_i.

to finite order, where $l_n = \ln(n)$. Although Feynman parametrisation, MB and other techniques work well for a subset of boundary integrals it is not always possible to obtain exact results. On the other hand, with DRR, exact results are always attainable which can then be expanded to any order in ϵ, which is why we choose to employ DRR instead.

Given the boundary integrals, we can immediately determine MIs order-by-order in ϵ in terms of MPLs, up to an integration constant. To determine the MIs fully, we need to satisfy boundary conditions, as this is a first-order differential system; one only needs to enforce regularity at one of the poles. We choose $w = 1$ or $v_1 = v_2$ which leaves us with the column vector, $\mathbf{a}$, of boundary integrals present in Table 8.2. These are to be determined independently of the differential equation method. Conveniently, this is a subset of the integrals that differentiate to nil given previously, and thus no further calculation is necessary. Thus we have all the ingredients necessary to determine our result in terms of MPLs, and we perform the integrals iteratively at each order in ϵ, enforcing boundary conditions up to $\mathcal{O}(\epsilon^2)$. The full results in terms of MPLs are presented in an arXiv ancillary file of Ref. [381].

8.4 Heavy-Light Vertex

The heavy-light N-loop master integrals with massive propagators at $d = 4 - 2\epsilon$ have the following form,

$$I = \left[(4\pi)^{2-\epsilon} e^{\gamma_E \epsilon}\right]^N \int \not{d}^d l_1 \ldots \not{d}^d l_N \frac{1}{D_1^{\nu_1} \ldots D_{n-m}^{\nu_{n-m}}} \cdot \frac{1}{\tilde{D}_{n-m+1}^{\nu_{n-m+1}} \ldots \tilde{D}_n^{\nu_n}}, \tag{8.31}$$

where n is the cardinality of the minimal set of denominators, D_i can have the following forms,

$$D_i(w) = l_i \cdot v_i, \quad \tilde{D}_i(m) = l_i^2 - m^2, \quad \tilde{D}_i = l_i^2, \tag{8.32}$$

for some particular combination of loop momenta, l_i, and momentum, p, such that $w = p \cdot v/m$ where $v^2 = 1$ and $p^2 = m^2$. To use differential equation to solve the MI's we begin by taking a derivative of the integral with respect to w.

8.4.1 One-loop Case

We will go through the derivation explicitly at one-loop as a reference for the main two-loop result. At one-loop order, all on-shell amplitudes reduce to expressions with two MIs,

$$I^{(1)} = \left[(4\pi)^{2-\epsilon}e^{\gamma_E\epsilon}\right] m^{1-2\epsilon} \int \not{d}^d l \frac{1}{(l\cdot v - w)} \cdot \frac{1}{l^2-1}, \tag{8.33}$$

$$I^{(2)} = \left[(4\pi)^{2-\epsilon}e^{\gamma_E\epsilon}\right] m^{2-2\epsilon} \int \not{d}^d l \frac{1}{l^2-2} = -e^{\gamma_E\epsilon}\Gamma(\epsilon-1)m^{2-2\epsilon}, \tag{8.34}$$

then we may solve this by parameterising, taking the derivative and reducing, to obtain,

$$\frac{d}{dw}I^{(1)}(w) = \left[(4\pi)^{2-\epsilon}e^{\gamma_E\epsilon}\right] m^{1-2\epsilon} \int \not{d}^d l \left[\frac{d}{dw}\frac{1}{(l\cdot v_2 - w)}\right] \cdot \frac{1}{l^2-1} \tag{8.35}$$

$$= -m^{1-2\epsilon}\left(\frac{(D-3)}{1-w^2}wI^{(1)} + \frac{(D-2)}{1-w^2}I^{(2)}\right), \tag{8.36}$$

One can then solve Eq. (8.14) by variation of parameters and the boundary condition, $I^{(1)}(0) = 0$, to obtain,

$$I^{(1)} = 2ie^{\gamma_E\epsilon}w\Gamma(\epsilon)m^{1-2\epsilon}, \tag{8.37}$$

which is equivalent to the known heavy-light one-loop result [153].

8.4.2 Two-loop Case

At two-loop order we have a column vector, $\mathbf{B}(w)$, of $n = 33$ master integrals tabulated in Table 8.3, based on our notation for $R^{(s)}$ in Eq. (8.1). Differentiating $\mathbf{B}(w)$ with respect to w and performing the IBP reduction, the linear system obtained is in the form,

$$\partial_w \mathbf{B}(w) = \mathbb{M}(w,\epsilon)\mathbf{B}(w). \tag{8.38}$$

with a 33×33 matrix, $\mathbb{M}(w,\epsilon)$. We can again proceed with reduction in this case to ϵ-form by changing variables to β and determining the transformation matrix $\mathbb{T}$. In this case, the coupled sub-systems to transform step-wise are no greater than two, for instance,

$$M_2 = \begin{pmatrix} -\frac{2w^2\epsilon+w^2-4\epsilon}{(w-1)w(w+1)} & -\frac{4}{w} \\ -\frac{\epsilon(4\epsilon+1)}{(w-1)w(w+1)} & -\frac{w^2+4\epsilon+1}{(w-1)w(w+1)} \end{pmatrix}. \tag{8.39}$$

Changing variables to β and following Lee's algorithm we find a transformation matrix,

$$T_2 = \begin{pmatrix} \frac{1}{\beta} & 0 \\ \frac{(\beta-1)\epsilon}{2\beta} & 1 \end{pmatrix}, \tag{8.40}$$

which reduces M_2 to ϵ-form,

$$S_2 = \epsilon \begin{pmatrix} \frac{2w}{(w-1)(w+1)} & -\frac{2\beta}{w-1} \\ -\frac{4\beta}{w-1} & -\frac{4w}{w^2-1} \end{pmatrix}. \tag{8.41}$$

Repeating these steps for each block, we can consolidate each transformation matrix into a final transformation matrix. This allows us to perform the complete reduction to ϵ-form as

$$\partial_w \tilde{\mathbf{A}}(w) = \epsilon\mathbb{S}(w)\tilde{\mathbf{A}}(w). \tag{8.42}$$

MI	ν_1	ν_2	ν_3	ν_4	ν_5	ν_6	ν_7	ν_8	ν_9	ν_{10}
B_1	1	1	0	0	0	0	0	0	0	0
B_2	1	0	1	1	0	0	0	0	0	0
B_3	1	0	0	1	0	0	1	0	0	0
B_4	2	0	0	1	0	0	1	0	0	0
B_5	1	1	0	0	0	0	1	0	0	0
B_6	1	1	0	0	1	0	0	0	0	0
B_7	1	0	1	1	0	0	1	0	0	0
B_8	1	0	1	1	1	0	0	0	0	0
B_9	1	1	0	1	0	0	1	0	0	0
B_{10}	1	2	0	1	0	0	1	0	0	0
B_{11}	1	1	0	0	1	0	1	0	0	0
B_{12}	1	0	1	1	1	0	1	0	0	0
B_{13}	1	1	1	1	1	0	0	0	0	0
B_{14}	2	1	1	1	1	0	0	0	0	0
B_{15}	1	1	0	0	1	1	0	0	0	0
B_{16}	1	0	0	0	0	0	0	1	1	0
B_{17}	0	0	0	0	1	0	0	1	0	1
B_{18}	0	0	0	0	2	0	0	1	0	1
B_{19}	1	0	0	0	1	0	0	1	0	0
B_{20}	0	0	0	0	1	0	0	1	1	1
B_{21}	0	0	0	0	2	0	0	1	1	1
B_{22}	1	0	0	1	0	1	0	1	0	0
B_{23}	1	0	0	0	1	0	0	1	1	0
B_{24}	1	0	0	0	2	0	0	1	1	0
B_{25}	1	0	1	1	1	0	0	0	0	0
B_{26}	1	1	0	0	0	1	1	0	0	0
B_{27}	1	1	1	1	1	0	0	0	0	0
B_{28}	1	1	1	1	2	0	0	0	0	0
B_{29}	1	0	1	1	1	0	1	0	0	0
B_{30}	1	1	0	0	0	1	1	0	0	0
B_{31}	1	0	1	1	0	1	1	0	0	0
B_{32}	1	1	0	0	0	1	1	0	0	0
B_{33}	1	0	1	1	1	1	0	0	0	0

Table 8.3: Column vector of heavy-light MIs with propagator exponent indices ν_i.

MI	ν_1	ν_2	ν_3	ν_4	ν_5	ν_6	ν_7	ν_8	ν_9	ν_{10}
b_1	1	0	1	1	0	0	0	0	0	0
b_2	1	0	0	1	0	0	1	0	0	0
b_3	1	1	0	0	0	0	0	0	0	0
b_4	1	1	0	0	0	0	1	0	0	0
b_5	1	0	0	0	0	0	0	1	1	0

Table 8.4: Heavy-light boundary MIs at $w = 1$ with propagator exponent indices ν_i.

with the reduced system given explicitly in Appendix C.3. By analysis, in this case, $B_{1,2}$, B_5 and B_{16} are w-independent correspond to a portion of boundary MIs which we determine with DRR as in the previous case. We present exact results for boundary integrals explicitly in Appendix C.4. Moreover, as in the previous case, to determine the MIs fully, we need to satisfy boundary conditions. We select the $w = 1$ pole or $p \cdot v = m$ which leaves us with the column vector, $\mathbf{b}$, of boundary integrals present in Table 8.4. These are also evaluated with DRR and present in Appendix C.4. Thus we have all the ingredients necessary to determine our result in terms of MPLs, and we perform the integrals iteratively at each order in ϵ enforcing boundary conditions up to $\mathcal{O}(\epsilon^2)$. The full results in terms of MPLs are presented in an arXiv ancillary file of Ref. [381].

8.5 Heavy Propagator

The heavy-heavy N-loop two-point master integrals with massive propagators at $d = 4-2\epsilon$ have the following form,

$$I = \left[(4\pi)^{2-\epsilon} e^{\gamma_E \epsilon}\right]^N \int \not{d}^d l_1 \ldots \not{d}^d l_N \frac{1}{D_1^{\nu_1} \ldots D_{n-m}^{\nu_{n-m}}} \cdot \frac{1}{\tilde{D}_{n-m+1}^{\nu_{n-m+1}} \ldots \tilde{D}_n^{\nu_n}}, \tag{8.43}$$

where n is the cardinality of the minimal set of denominators, D_i can have the following forms,

$$D_i(\omega) = l_i \cdot v_i, \quad \tilde{D}_i(m_1) = l_i^2 - 1, \quad \tilde{D}_i = l_i^2, \tag{8.44}$$

for some particular combination of loop momenta, l_i, and $\omega = p \cdot v/M$ which we take the derivatives with respect to, such that $v^2 = 1$.

8.5.1 One-loop Case

We will go through the derivation explicitly at one-loop as a reference for the main two-loop result. At one-loop all on-shell amplitudes reduce to expressions with two MIs,

$$I^{(1)} = \left[(4\pi)^{2-\epsilon} e^{\gamma_E \epsilon}\right] M^{1-2\epsilon} \int \not{d}^D l \frac{1}{(l \cdot v - \omega)} \cdot \frac{1}{l^2 - 1} \tag{8.45}$$

$$I^{(2)} = \left[(4\pi)^{2-\epsilon} e^{\gamma_E \epsilon}\right] \int \not{d}^D l \frac{1}{l^2 - 1} = -e^{\gamma_E \epsilon} \Gamma(\epsilon - 1) M^{2-2\epsilon}, \tag{8.46}$$

taking the derivative and performing IBP reduction, we obtain,

$$\frac{d}{d\omega} I^{(1)}(\omega) = \left[(4\pi)^{2-\epsilon} e^{\gamma_E \epsilon}\right] \int \not{d}^D l \left[\frac{d}{d\omega} \frac{1}{(l \cdot v - \omega)}\right] \cdot \frac{1}{l^2 - 1^2} \tag{8.47}$$

$$= -\frac{(D-3)\omega}{\omega^2 - 1} I^{(1)} - \frac{(D-2)}{1 - \omega^2} I^{(2)}, \tag{8.48}$$

MI	ν_1	ν_2	ν_3	ν_4	ν_5	ν_6	ν_7	ν_8
C_1	0	0	0	1	1	0	0	0
C_2	0	0	1	1	1	0	0	0
C_3	0	0	1	0	1	1	0	0
C_4	0	1	0	1	1	0	0	0
C_5	0	2	0	1	1	0	0	0
C_6	0	1	1	1	1	0	0	0
C_7	1	1	1	1	0	0	0	0
C_8	1	1	1	0	1	0	0	0
C_9	1	1	1	1	1	0	0	0
C_{10}	0	0	0	0	1	0	1	1
C_{11}	1	0	0	0	0	0	1	1
C_{12}	1	0	0	0	1	0	1	1

Table 8.5: Column vector of heavy self-energy MIs with propagator exponent indices ν_i.

One can then solve Eq. (8.14) by variation of parameters and boundary condition, $I^{(1)}(0) = 0$, to obtain,

$$I^{(1)} = 2ie^{\gamma_E \epsilon}\omega\Gamma(\epsilon)M^{1-2\epsilon}, \tag{8.49}$$

which again equals the result obtained from the usual Feynman parametrisation [153].

8.5.2 Two-loop Case

We will start by considering the off-shell case for generality with parameter, w, non-zero. The column vector of MIs $\mathbf{C}(w)$, consists of $n = 12$ integrals. We tabulate these in Table 8.5, based on our notation for $L^{(s)}$ in Eq. (8.6). Differentiating $\mathbf{C}(w)$ with respect to w and performing IBP reduction, we have a differential system,

$$\partial_w \mathbf{C}(w) = \mathbb{M}(w, \epsilon)\mathbf{C}(w). \tag{8.50}$$

with a 12×12 matrix, $\mathbb{M}(w, \epsilon)$. Proceeding with Lee's algorithm to attempt reduction to ϵ-form. We then determine a transformation matrix $\mathbb{T}$. To evaluate $\mathbb{T}$, one starts by transforming the blocks and coupled sub-system they represent to ϵ-form. By analysis we find a non-trivial block that can only be reduced to $(A + B\epsilon)$-form,

$$M_2 = \begin{pmatrix} 0 & -1 \\ \frac{(2\epsilon-1)(4\epsilon-3)}{(w-2)(w+2)} & -\frac{\left(3w^2-4\right)(2\epsilon-1)}{(w-2)w(w+2)} \end{pmatrix}. \tag{8.51}$$

and transforming M_2 minimally gives,

$$S_2 = \epsilon \begin{pmatrix} \frac{7w^2-29w+24}{w(w^2-4)} - \frac{16((w-2)w+3)\epsilon}{w(w^2-4)} & \frac{\left(-28w^2+64w-112\right)\epsilon}{w(w^2-4)} + \frac{14w^2-65w+56}{w(w^2-4)} \\ \frac{\left(6w^2-16w+24\right)\epsilon}{w(w^2-4)} + \frac{-3w^2+13w-12}{w(w^2-4)} & \frac{\left(10w^2-32w+56\right)\epsilon}{w(w^2-4)} + \frac{-6w^2+29w-28}{w(w^2-4)} \end{pmatrix}. \tag{8.52}$$

Thus, this block requires individual treatment with EPLs to solve. The remaining blocks, however, do, reduce to ϵ-form, as can be seen in the reduced system given in Appendix C.3.

MI	ν_1	ν_2	ν_3	ν_4	ν_5	ν_6	ν_7	ν_8
c_1	0	0	1	1	0	0	0	0
c_2	0	0	1	1	1	0	0	0
c_3	0	1	1	1	0	0	0	0
c_4	0	1	0	1	1	0	0	0
c_5	0	1	1	1	1	0	0	0
c_6	1	1	1	1	0	0	0	0
c_7	1	1	1	0	1	0	0	0
c_8	1	1	1	1	1	0	0	0
c_9	0	0	0	0	1	0	1	1
c_{10}	1	0	0	0	1	0	1	1

Table 8.6: Self-energy boundary MIs at $w = 0$ with propagator exponent indices given by ν_i with $p \cdot v = 0$.

By analysis, we find that $C_{1,2}$ and C_{10} are w-independent boundary MIs, which we solve with standard methods and are present in Appendix C.4. Unlike the previous cases, our boundary condition is to enforce regularity at $w = 0$ or $p \cdot v = M$, which leaves us with the column vector, $\mathbf{c}$, of boundary integrals present in Table 8.6. Although there are more integrals to determine at $w = 0$, this point is what is needed for field renormalisation contributions in practice, as described in Section 8.2. These are to be determined independently of the differential equation method and instead with DRR. We present the exact results for these integrals in Appendix C.4. Thus we have all the ingredients necessary to determine our result in terms of MPLs and EPLs, and we perform the integrals iteratively at each order in ϵ, enforcing boundary conditions up to $\mathcal{O}(\epsilon^2)$. The full results in terms of MPLs and EPLs are presented in an arXiv ancillary file of Ref. [381].

8.6 Summary

We have employed the differential equations method and dimensional recurrence relations to treat diagrams with heavy field insertions up to three-points and two-loop order. Our analysis focused on vertex or form factor diagrams as these are fundamental for a broad class of processes and can be combined for use in studies beyond three-point order. Our results are applicable for a broader range of theories and provide an IR structure for models studied by including a mass scale. The treatment of the heavy-heavy and heavy-light vertex diagrams was shown to be straightforward, and we provide the results in terms of MPLs. The on-shell self-energy contributions give the heavy field and residual mass renormalisation. We evaluated these diagrams as they were boundary MIs for the general off-shell propagator. Determining said off-shell self-energies with differential equations leads to a sub-system of equations that required treatment with EPLs, and we describe this as well, providing results for the off- and on-shell cases. Based on this study, we have provided further proof positive of the power and simplicity of the differential equation method and advocate for its use when more exotic propagators are present. Our full results are contained in the ancillary file submitted along with Ref. [264] on the arXiv.

Chapter 9

Conclusion and Outlook

In this thesis, we incorporated electroweak corrections to fundamental parameters and EFTs arising from QCD. We focused our analysis on heavy quarks, such as top quarks in the SM, shedding light on the role of the EW sector. Our findings demonstrate that the leading EW corrections are comparable in size to current high precision QCD estimates and we therefore must take these into account. We further endeavoured to maintain generality at each stage by considering BSM theories and studying both heavy and light fields in model-independent ways.

Our analysis of heavy fields and the EW sector began in Chapter 5, in which we considered the heavy quark static potential. As the full SM is chiral and exhibits SSB, we proposed a consistent way of studying static potentials in theories with SSB. In contrast to the traditional Wilson loop approach, the method we pursued is better suited for SM-like theories and implicitly provides higher-order scalar and spin-dependent contributions. The main result we presented in this approach is the leading one-loop EW corrections to the heavy quark potential. We found the contributions from the EW regime to be significant and comparable to pure QCD contributions at NNLO. Moreover, we discussed how the theoretical framework introduced helps to study the NR regime of theories beyond the SM.

We examined analogous corrections to short-distance mass definitions with the EW corrections to the heavy quark potential at hand. The building blocks of these mass definitions are energy parameters, including the heavy quark static potential, binding energy, and residual kinetic energy. For this reason, we began Chapter 6 by elaborating on the static potential calculation and applied it to the case of top and bottom quarks. We then presented our calculation for the leading one-loop EW corrections to the heavy quark residual KE and BE. From there, we determined the leading EW corrections to often-employed threshold mass definitions for the top and bottom quarks in the SM. The numerical estimates we provided for the EW corrections indicate that they are comparable to pure QCD contributions at NNLO. Moreover, these mass definitions are useful when working with heavy quark EFTs, which we considered next.

Remaining in the vein of heavy quarks but shifting gears to an EFT perspective, we focused on HQET and NRQCD. In Chapter 7 we confirmed previous matching results in pure QCD and then studied the EW corrections to the HQET/NRQCD Lagrangian. We found the EW corrections to the matching coefficients and determined that the Lagrangian required extension. The extension was due to the SM being parity-violating, unlike pure QCD. Thus, new Lorentz structures emerged that appear as independent operators in the EFT Lagrangian with associated matching. We performed the matching at one-loop order for both form factors and four-quark operators. As in the threshold mass study, we produced numerical estimates for the one-loop matching coefficients, demonstrating the need to incorporate EW contributions in future studies.

In Chapter 8 we generalised the previous EFT analysis to the case of both massive and massless form factors. Our interest in form factors lies in their nature of primary building blocks

to a broad set of observables in both high and low energy regimes. This chapter aimed to attain a complete two-loop EFT description for each operator, mass hierarchy and energetic regime in the model we employed. We achieved a significant portion of this endeavour in both the Sudakov and threshold energetic regime for both matching and running. We further showed how the results in our model could be mapped to the SM up to and including two-loop orders. This was achieved by replacing coupling and group theory factors. We also discussed how replacements of a similar type can be used to study models beyond the SM.

Our two-loop EFT analysis opened many avenues of inquiry, one of which was the appearance of heavy field diagrams with mass scales. Analytically evaluating such integrals required treatment with modern multi-loop techniques. In Chapter 8 we evaluated all diagrams with heavy field insertions up to three points and two-loop order. We achieved this analysis with differential equations and dimensional recurrence relations, which we have shown to be the appropriate framework for dealing with non-standard multi-loop integrals. Our results are applicable to a broader range of theories and provide IR structure for models studied with the inclusion of a mass scale. The treatment of the on-shell diagrams was shown to be straightforward, and we provided the results in terms of MPLs. We further considered the off-shell case for completeness which required more delicate treatment with elliptic functions.

To conclude this thesis, the research we presented has opened new avenues of exploration into the effects of incorporating the EW sector in high precision studies. We have demonstrated that the leading EW contributions are comparable to the next-to-leading QCD corrections on a range of fronts, from fundamental SM parameters and energies to EFTs. As high precision QCD is currently providing predictions far beyond leading order, our findings indicate that the sub-leading EW sector needs accounting for at this stage. In particular, when considering specific processes of interest, approaching different energetic regimes, and delving into higher-loop orders. We hope that the framework we develop and the results we express in this thesis will help incorporate the EW sector in future studies, ultimately increasing the odds of detecting new physics at the LHC and beyond.

Appendix A

$SU(N)$-Higgs Theory Feynman Rules

We illustrate here the Feynman rules we employ for our calculations in the various theories. They may be determined from the Lagrangian described in section 7.2.1. The gauge boson fields of mass $M = M_W$ are W^a_μ (with Lorentz vector index μ). The corresponding Fadeev-Popov ghost fields are labelled c^a (and antighost $\bar{c}^a$) and Goldstone bosons are labelled ϕ^a. In the Feynman-t'Hooft gauge used by us, one sets $M_\phi = M_W$. The fields, ψ and χ denote fermions and complex scalars, respectively. The $SU(N)$ coupling is given by g and the field labelling, $\{1, 2\}$ differentiates between the particles on the grounds of mass, if two of the same kind exist in a vertex. Vertices which apply beyond two-loops are omitted here but should be included if one wants to venture beyond.

A.1 Fermion and Scalar Couplings

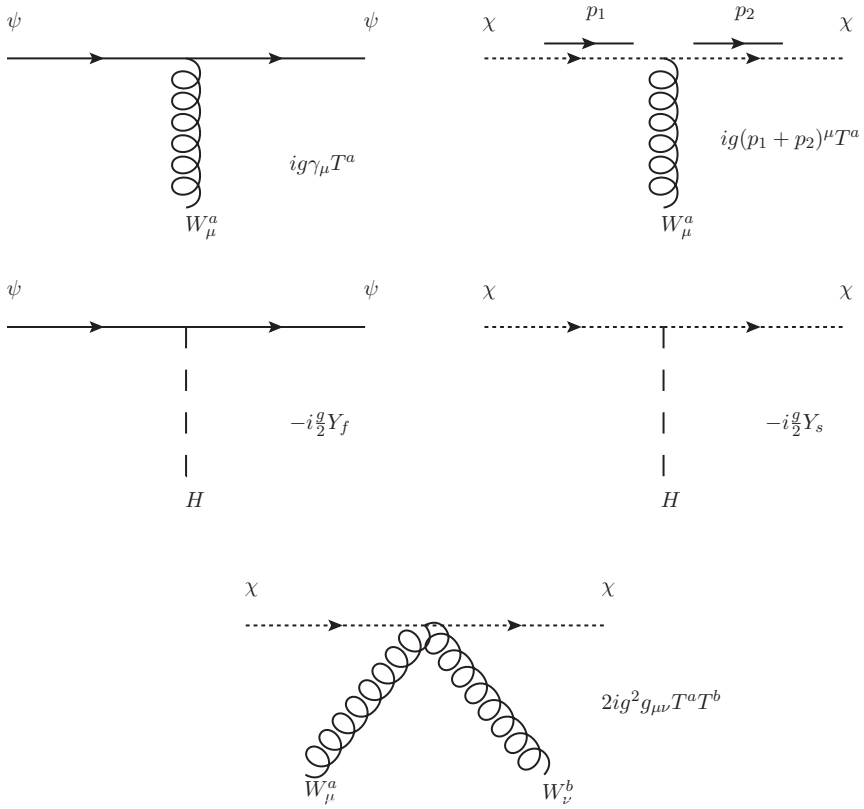

A.2 Gauge Field Self and Ghost Couplings

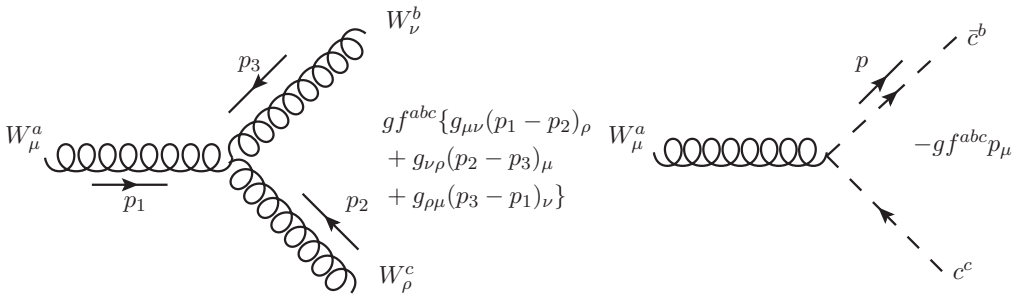

A.3 Gauge Field Higgs and Goldstone Couplings

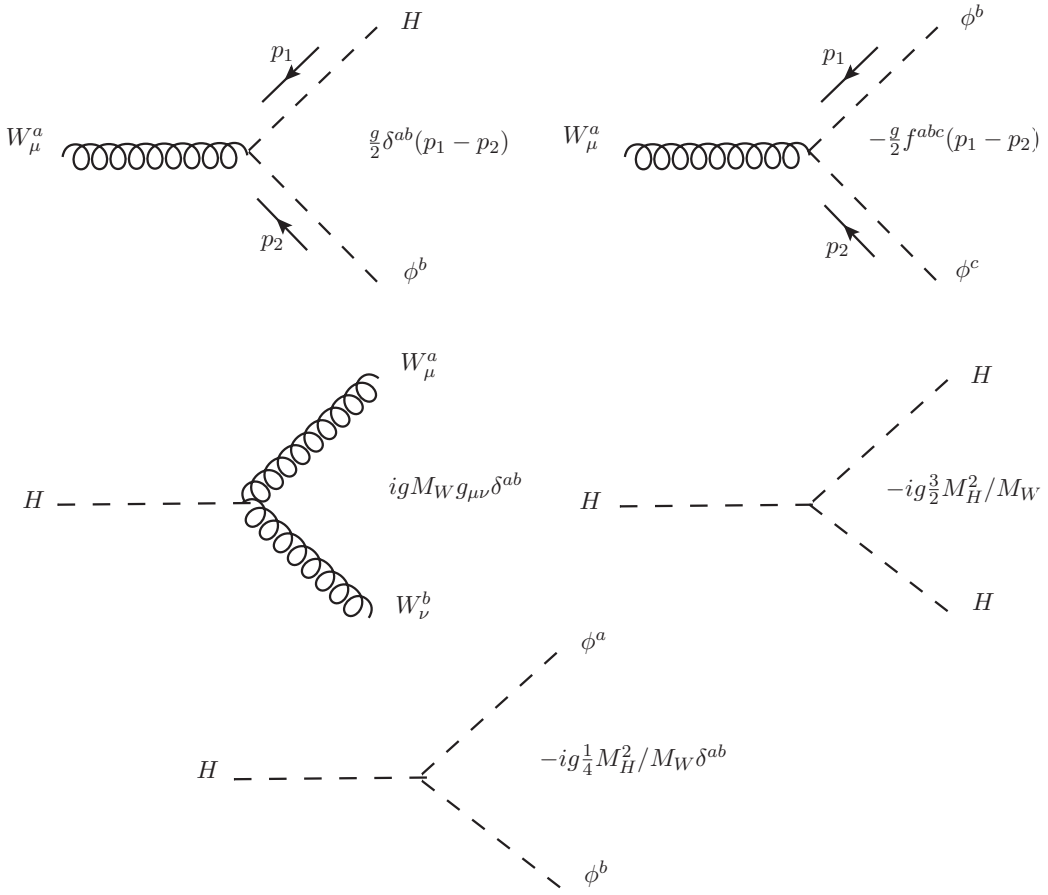

A.4 Effective theory couplings

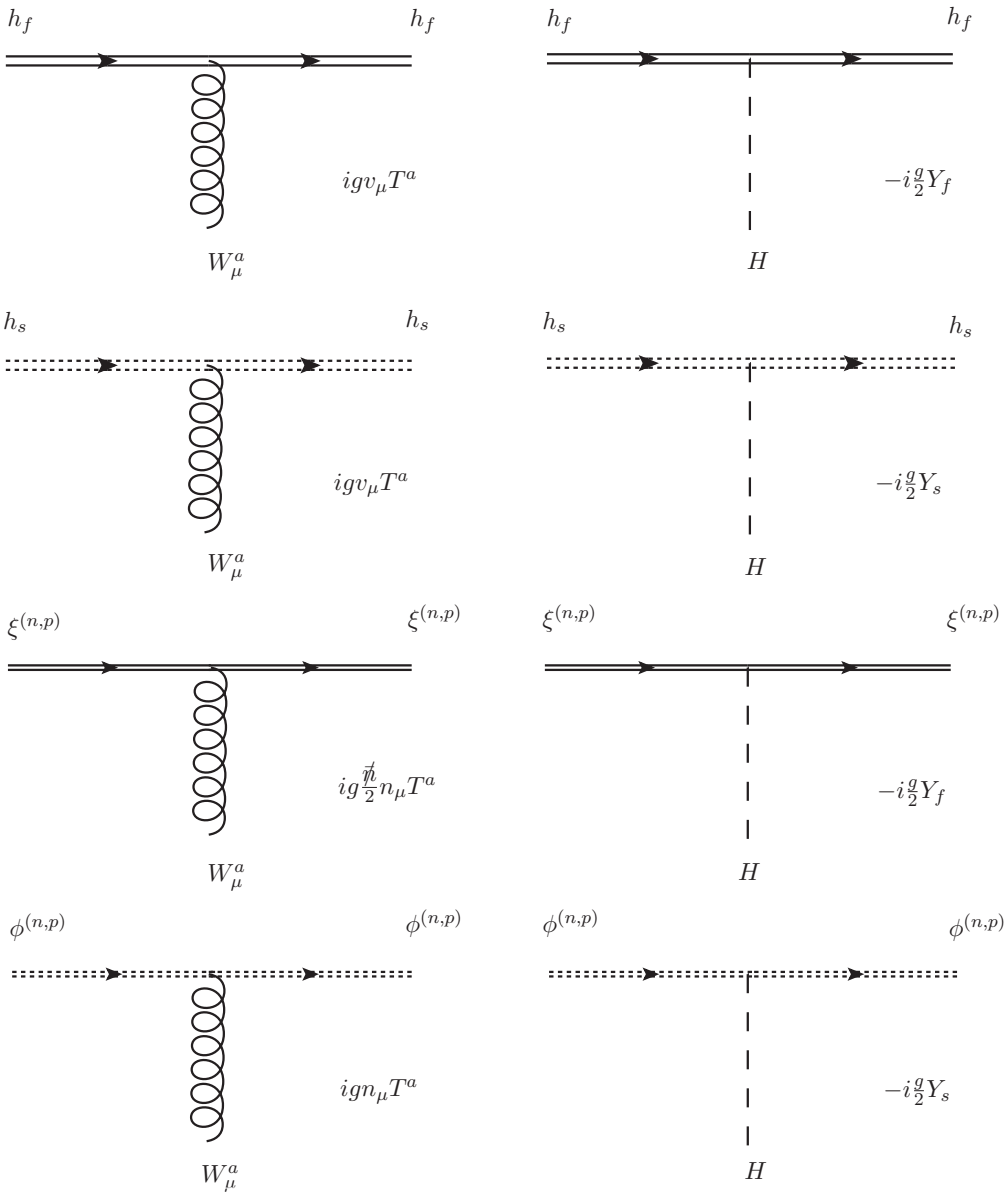

In the effective theory vertices, solid (dashed) lines correspond to fermions (scalars) and widely (thinly) spaced lines correspond to heavy (co-linear) particles. As for the co-linear vertices we do not distinguish between soft/Wilson line couplings as they are identical up to the order we are considering.

Appendix B

Form Factors Contributions

In this Chapter we present the form factor contributions compact enough to present in this thesis, for each scale hierarchy and operator considered in Chapter 8. The numbering of the contributions corresponds to their ordering in their respective tables in Chapter 8. We note further that the explicit contributions from two-loop vertex corrections, $V_i^{(2)}$, are too large to present here. We thus include the full expressions with description in the arXiv ancillary file of Ref. [325].

B.1 Matching at $\mu \sim Q$:

The coupling corrections to matching from the full theory at $\mu \sim Q$, contributing at two-loop order are given by,

$$\begin{aligned}
\Delta C_1 = &\frac{C_F}{36}\left(-2L_Q^3 + \left(\pi^2 - 12\right)L_Q - 28\zeta_3 + 24\right)\left(C_A\left(3C_A + 22\right) - 8n_f T_f - 4\right) \\
&+ \frac{Y_f^2}{288}\left\{6L_Q\left(L_Q\left(-2C_A C_F \ln L_Q + C_A\left(6C_F + 22\right) - 8n_f T_f - 1\right)\right.\right. \\
&+C_A\left(\left(\pi^2 - 36\right)C_F - 88\right) + 32n_f T_f + 4\Big) - 168\zeta_3 C_A C_F + 48C_A\left(9C_F + 22\right) \\
&\left.-2\pi^2 C_A\left(3C_F + 11\right) + \left(\pi^2 - 48\right)\left(8n_f T_f + 1\right)\right\}, \qquad \text{(B.1)} \\
\Delta C_2 = &\frac{C_F}{72}\left(2L_Q\left(\left(9 - 2L_Q\right)L_Q + \pi^2 - 48\right) - 56\zeta_3 - 3\pi^2 + 192\right)\left(C_A\left(3C_A + 22\right)\right. \\
&\left.-8n_f T_f - 4\right) + \frac{Y_f^2}{576}\left\{6L_Q^2\left(2C_A\left(6C_F - 11\right) + 8n_f T_f + 1\right)\right. \\
&+12L_Q\left(C_A\left(\left(\pi^2 - 42\right)C_F + 22\right) - 8n_f T_f - 1\right) - 24C_A C_F L_Q^3 \\
&\left.-12\left(28\zeta_3 - 90 + \pi^2\right)C_A C_F + 22\left(\pi^2 - 12\right)C_A - \left(\pi^2 - 12\right)\left(8n_f T_f + 1\right)\right\}, \qquad \text{(B.2)} \\
\Delta C_3 = &\frac{C_F}{36}\left(L_Q\left(-2\left(L_Q - 6\right)L_Q + \pi^2 - 48\right) - 28\zeta_3 - 2\pi^2 + 84\right)\left(C_A\left(3C_A + 22\right)\right. \\
&\left.-8n_f T_f - 4\right) + \frac{Y_f^2}{48}\left\{L_Q\left(-2C_A C_F\left(L_Q - 6\right)L_Q + C_A\left(\left(\pi^2 - 36\right)C_F + 44\right)\right.\right. \\
&\left.\left.-2\left(8n_f T_f + 1\right)\right) - 28\zeta_3 C_A C_F - 2C_A\left(\left(\pi^2 - 24\right)C_F + 66\right) + 48n_f T_f + 6\right\}, \qquad \text{(B.3)} \\
\Delta C_4 = &\frac{C_F}{72}\left(2L_Q\left(\left(3 - 2L_Q\right)L_Q + \pi^2 - 12\right) - 56\zeta_3 - \pi^2 + 48\right)\left(-6C_A^2 + 22C_A\right. \\
&\left.-8n_f T_f + 5\right), \qquad \text{(B.4)} \\
\Delta C_5 = &\frac{C_F}{36}\left(L_Q\left(-2\left(L_Q - 6\right)L_Q + \pi^2 - 48\right) - 28\zeta_3 - 2\pi^2 + 96\right)\left(-6C_A^2 + 22C_A\right.
\end{aligned}$$

$$-8n_f T_f + 5)\,, \tag{B.5}$$

$$\Delta C_6 = \frac{C_F}{576}\left(-2L_Q\left((9-2L_Q)\,L_Q + \pi^2 - 36\right) + 56\zeta_3 + 3\pi^2 - 144\right)\left(C_A\left(-12C_A + 3Y_f^2 - 176\right) + 64n_f T_f + 20\right). \tag{B.6}$$

B.2 SCET Matching at $\mu \sim M$:

The SCET form factor contributions at two-loop order from mass and coupling renormalisation are given by,

$$\begin{aligned}
\Delta D_1 = & -\frac{C_F}{72M_W^6}\Big\{M_W^6\left(\left(99\sqrt{3}\pi - 690\right)C_A + 32(5+3i\pi)n_f T_f + 124\right) \\
& +3M_W^4\left(L_{M_W}\left(M_W^2\left(141C_A - 32n_f T_f - 20\right) + 10M_H^2\right) - 8M_H^2 L_{M_H}\right) \\
& -54M_W^4 M_H^2 + 6M_W^2 M_H^4 - 6M_H s\left(12M_W^4 - 4M_W^2 M_H^2 + M_H^4\right)\ln(w) \\
& +6\left(8M_W^4 M_H^2 - 6M_W^2 M_H^4 + M_H^6\right)\ln\left(M_W/M_H\right)\Big\}\left(2L_{M_W} - 2L_Q + 3\right),
\end{aligned} \tag{B.7}$$

$$\begin{aligned}
\Delta D_2 = & -\frac{C_F}{36M_W^6}\left\{3M_W^4\left(L_{M_W}\left(M_W^2\left(141C_A - 32n_f T_f - 20\right) + 10M_H^2\right) - 8M_H^2 L_{M_H}\right)\right. \\
& +M_W^6\left(\left(99\sqrt{3}\pi - 690\right)C_A + 32(5+3i\pi)n_f T_f + 124\right) + 6M_H^4 M_W^2 \\
& -54M_H^2 M_W^4 - 6M_H s\left(M_H^4 - 4M_H^2 M_W^2 + 12M_W^4\right)\ln(w) \\
& \left.+6\left(M_H^6 - 6M_H^4 M_W^2 + 8M_H^2 M_W^4\right)\ln\left(M_W/M_H\right)\right\}\left(L_{M_W} - L_Q + 2\right),
\end{aligned} \tag{B.8}$$

$$\begin{aligned}
\Delta D_3 = & -\frac{C_F}{14M_W^6}\left\{3M_W^4\left(L_{M_W}\left(M_W^2\left(141C_A - 32n_f T_f - 20\right) + 10M_H^2\right) - 8M_H^2 L_{M_H}\right)\right. \\
& +M_W^6\left(\left(99\sqrt{3}\pi - 690\right)C_A + 32(5+3i\pi)n_f T_f + 124\right) + 6M_H^4 M_W^2 \\
& -54M_H^2 M_W^4 - 6M_H s\left(M_H^4 - 4M_H^2 M_W^2 + 12M_W^4\right)\ln(w) \\
& \left.+6\left(M_H^6 - 6M_H^4 M_W^2 + 8M_H^2 M_W^4\right)\ln\left(M_W/M_H\right)\right\}\left(4L_{M_W} - 4L_Q + 7\right).
\end{aligned} \tag{B.9}$$

B.3 HPET Matching at $\mu \sim M$:

The two-loop HPET matching contribution at $\mu \sim M$, are given by,

$$\begin{aligned}
U_1^{(2)} = & \left(V_1^{(M)} + F_h^{(M)} + \Delta U_1\right) + \frac{2}{3}wC_F^2\left(12(L_{M_W}-1)L_{M_W} + \pi^2\right)h(w) \\
& + \frac{1}{24}Y_f^4\left(12(L_{M_H}-1)L_{M_H} + \pi^2\right)h(w) \\
& - \frac{1}{6}C_F Y_f^2 h(w)\left(6L_{M_W}((w+1)L_{M_H} - 2) + 3(w+1)L_{M_W}^2\right. \\
& \left.+3L_{M_H}((w+1)L_{M_H} - 4w) + \pi^2(w+1)\right),
\end{aligned} \tag{B.10}$$

$$\begin{aligned}
U_2^{(2)} = & \left(V_2^{(M)} + F_h^{(M)} + \Delta U_2\right) + \frac{2}{3}wC_F^2\left(12(L_{M_W}-1)L_{M_W} + \pi^2\right)h(w) \\
& + \frac{1}{24}Y_s^4\left(12(L_{M_H}-1)L_{M_H} + \pi^2\right)h(w) \\
& - \frac{1}{6}C_F Y_s^2 h(w)\left(6L_{M_W}((w+1)L_{M_H} - 2) + 3(w+1)L_{M_W}^2\right. \\
& \left.+3L_{M_H}((w+1)L_{M_H} - 4w) + \pi^2(w+1)\right),
\end{aligned} \tag{B.11}$$

$$U_3^{(2)} = \left(V_3^{(M)} + F_h^{(M)} + \Delta U_3\right) + \frac{2}{3}wC_F^2\left(12(L_{M_W}-1)L_{M_W} + \pi^2\right)h(w)$$

$$
\begin{aligned}
&+\frac{1}{48}(Y_f^3 Y_s + Y_s^3 Y_f)\left(12(L_{M_H}-1)L_{M_H}+\pi^2\right)\\
&-\frac{1}{6}C_F Y_f Y_s h(w)\left(3\left(2L_{M_W}(L_{M_H}-2)+L_{M_W}^2+L_{M_H}^2\right)+\pi^2\right)\\
&-\frac{1}{12}wC_F(Y_f^2+Y_s^2)h(w)\left(3(L_{M_W}+L_{M_H})^2-12L_{M_H}+\pi^2\right)h(w). \qquad \text{(B.12)}
\end{aligned}
$$

The terms, $V_i^{(M)}$ and F_I are the bare two-loop vertex and wave-function corrections and ΔU_i are the associated mass and coupling renormalisation contributions.

B.4 Matching at $\mu \sim m_{1,2}$:

Matching corrections at one- and two-loop order to the threshold form factor at $\mu \sim m_{1,2}$ are represented by,

$$
\begin{aligned}
B_1^{(1)} =& \frac{C_F}{2m_-m_+}\left\{L_{m_2}^2\left(m_1^2+m_2^2\right)-L_{m_2}\left(m_1^2-4m_1m_2-m_2^2\right)\right\}-\frac{Y_f^2L_{m_2}}{16m_-m_+}\left\{9m_1^2-8m_1m_2\right.\\
&\left.-5m_2^2\right\}-\frac{Y_f^2}{16m_-m_+}\left\{5m_1^2L_{m_1}-9m_2^2L_{m_1}-4m_1m_2L_{m_1}^2+8m_1m_2L_{m_1}-6m_1^2+6m_2^2\right\}\\
&-\frac{Y_f^2m_1m_2L_{m_2}^2}{4m_-m_+}-\frac{C_FL_{m_1}}{2m_-m_+}\left\{m_1^2L_{m_1}+m_2^2L_{m_1}+m_1^2+4m_1m_2-m_2^2\right\}, \qquad \text{(B.13)}\\
B_2^{(1)} =& -\frac{C_FL_{m_2}}{2m_-m_+}\left\{m_1^2-4m_1m_2+5m_2^2\right\}+\frac{m_-C_FL_{m_2}^2}{2m_+}-\frac{Y_f^2L_{m_2}}{16m_-m_+^2}\left\{9m_1^3+9m_1^2m_2\right.\\
&\left.-3m_1m_2^2-11m_2^3\right\}-\frac{C_F}{2m_-m_+}\left\{m_1^2L_{m_1}^2-5m_1^2L_{m_1}+m_2^2L_{m_1}^2-m_2^2L_{m_1}-2m_1m_2L_{m_1}^2\right.\\
&\left.+4m_1m_2L_{m_1}+6m_1^2-6m_2^2\right\}-\frac{Y_f^2}{16m_-m_+^2}\left\{11m_1^3L_{m_1}+11m_1^2m_2L_{m_1}-9m_2^3L_{m_1}\right.\\
&\left.-17m_1m_2^2L_{m_1}-18m_1^3-26m_1^2m_2+18m_1m_2^2+26m_2^3\right\}, \qquad \text{(B.14)}\\
B_3^{(1)} =& \frac{C_F}{2m_-m_+}\left\{L_{m_2}^2\left(m_1^2+m_2^2\right)-L_{m_2}\left(m_1^2-4m_1m_2+7m_2^2\right)\right\}-\frac{Y_f^2L_{m_2}}{16m_-m_+}\left\{9m_1^2-8m_1m_2\right.\\
&\left.-9m_2^2\right\}-\frac{C_F}{2m_-m_+}\left\{m_1^2L_{m_1}^2-7m_1^2L_{m_1}+m_2^2L_{m_1}^2-m_2^2L_{m_1}+4m_1m_2L_{m_1}+4m_1^2\right.\\
&\left.-4m_2^2\right\}-\frac{Y_f^2m_1m_2L_{m_2}^2}{4m_-m_+}-\frac{Y_f^2}{16m_-m_+}\left\{9m_1^2L_{m_1}-9m_2^2L_{m_1}-4m_1m_2L_{m_1}^2+8m_1m_2L_{m_1}\right.\\
&\left.-14m_1^2+14m_2^2\right\}, \qquad \text{(B.15)}\\
B_4^{(1)} =& \frac{C_F}{2m_-m_+}\left\{L_{m_2}^2\left(m_1^2+m_2^2\right)-2m_2^2L_{m_2}\right\}-\frac{Y_s^2L_{m_2}}{8m_2^2}-\frac{C_F}{2m_-m_+}\left\{m_1^2L_{m_1}^2-2m_1^2L_{m_1}\right.\\
&\left.+m_2^2L_{m_1}^2-6m_1^2+6m_2^2\right\}+\frac{Y_s^2}{16m_1^2m_2^2m_-m_+}\left\{m_1^2m_2^2L_{m_1}^2-2m_1^2m_2^2L_{m_1}+2m_2^4L_{m_1}\right.\\
&\left.+2m_1^4-2m_2^4\right\}-\frac{Y_s^2L_{m_2}^2}{16m_-m_+}, \qquad \text{(B.16)}\\
B_5^{(1)} =& -\frac{C_F2m_2^2L_{m_2}\left(m_1^2+8m_2^2\right)}{m_-m_+\left(m_1^2+m_2^2\right)}+\frac{C_FL_{m_2}^2\left(m_1^2+m_2^2\right)}{2m_-m_+}-\frac{Y_s^2L_{m_2}\left(m_1^2-2m_2^2\right)}{2m_2^2m_-m_+}-\frac{Y_s^2L_{m_2}^2}{16m_-m_+}\\
&-\frac{C_F}{2m_-m_+\left(m_1^2+m_2^2\right)}\left\{m_1^4L_{m_1}^2-32m_1^4L_{m_1}+2m_1^2m_2^2L_{m_1}^2-4m_1^2m_2^2L_{m_1}+m_2^4L_{m_1}^2\right.
\end{aligned}
$$

$$
\begin{aligned}
&+18m_1^4-18m_2^4\big\}+\frac{Y_s^2}{16m_1^2m_2^2m_-m_+\left(m_1^2+m_2^2\right)}\big\{M_1^4m_2^2L_{m_1}^2-16m_1^4m_2^2L_{m_1}\\
&+m_1^2m_2^4L_{m_1}^2-8m_1^2m_2^4L_{m_1}+8m_2^6L_{m_1}+8m_1^6\big\}+\frac{Y_s^2}{16m_1^2m_2^2m_-m_+\left(m_1^2+m_2^2\right)}\big\{-8m_1^4m_2^2\\
&+8m_1^2m_2^4-8m_2^6\big\}, \qquad \text{(B.17)}\\
B_6^{(1)}=&\frac{C_FL_{m_2}^2\left(m_1^2+m_2^2\right)}{2m_-m_+}-\frac{2m_2^3C_FL_{m_2}}{m_-m_+^2}+\frac{Y_sL_{m_2}}{8m_2^2m_-m_+^2}\big\{2Y_fm_1m_2^3-Y_sm_1^3-Y_sm_1^2m_2\\
&+Y_sm_1m_2^2+Y_sm_2^3\big\}+\frac{Y_f^2}{16m_2^2m_-m_+^2}\big\{-9m_1^3m_2^2L_{m_1}-9m_1^2m_2^3L_{m_1}+9m_2^5L_{m_1}\\
&+9m_1m_2^4L_{m_1}+9m_1^3m_2^2+9m_1^2m_2^3\big\}+\frac{Y_f^2}{16m_2^2m_-m_+^2}\big\{-9m_1m_2^4-9m_2^5\big\}\\
&+\frac{Y_fY_s}{16m_2^2m_-m_+^2}\big\{2m_1^2m_2^2L_{m_1}^2+2m_1m_2^3L_{m_1}^2-4m_1m_2^3L_{m_1}-4m_1^2m_2^2\big\}+\frac{Y_fY_sm_2^2}{4m_-m_+^2}\\
&+\frac{Y_s^2}{16m_2^2m_-m_+^2}\big\{2m_1^3+2m_1^2m_2-2m_1m_2^2-2m_2^3\big\}-\frac{Y_fY_sm_1L_{m_2}^2}{8m_-m_+}\\
&-\frac{C_F}{2m_-m_+^2}\big\{m_1^3L_{m_1}^2-3m_1^3L_{m_1}\big\}-\frac{C_F}{2m_-m_+^2}\big\{m_1^2m_2L_{m_1}^2-3m_1^2m_2L_{m_1}\\
&+m_2^3L_{m_1}^2-m_2^3L_{m_1}+m_1m_2^2L_{m_1}^2+3m_1m_2^2L_{m_1}-4m_1^3+4m_1m_2^2\big\}. \qquad \text{(B.18)}
\end{aligned}
$$

$$
\begin{aligned}
B_1^{(2)}=&\left(V_1^{(m_{1,2})}+\frac{1}{2}F_\psi^{(m_2)}+\frac{1}{2}F_\psi^{(m_1)}+\Delta B_1\right)\\
&+\frac{C_F^2}{2m_1^2}\left(60m_1^2L_{m_1}^2-80m_1^2L_{m_1}-12L_{m_1}^2+28L_{m_1}+5\pi^2m_1^2+104m_1^2-\pi^2-36\right)\\
&+\frac{Y_f^4}{64m_1^2}\left(72m_1^2L_{m_1}^2-144m_1^2L_{m_1}-36L_{m_1}^2+72L_{m_1}+6\pi^2m_1^2+176m_1^2-3\pi^2-88\right)\\
&-\frac{C_FY_f^2}{32m_1^3}\left(252L_{m_1}^2-768L_{m_1}+\pi^2m_1^2-366m_1^2+21\pi^2+912\right)m_-\\
&-\frac{C_FY_f^2}{32m_1^3}\left(12m_1^2L_{m_1}^2+764m_1^2L_{m_1}\right)m_-\\
&-\frac{Y_f^4m_-}{128m_1^3}\left(36m_1^2L_{m_1}^2-324m_1^2L_{m_1}-108L_{m_1}^2\right)\\
&-\frac{Y_f^4m_-}{128m_1^3}\left(360L_{m_1}+3\pi^2m_1^2+322m_1^2-9\pi^2-408\right)\\
&+\frac{C_F^2}{4m_1^3}\left(12m_1^2L_{m_1}^2+176m_1^2L_{m_1}+60L_{m_1}^2\right)m_-\\
&-\frac{C_FY_f^2}{16m_1^2}\left(19\pi^2m_1^2+386m_1^2-5\pi^2-160\right)\\
&+\frac{C_F^2}{4m_1^3}\left(\pi^2m_1^2-188L_{m_1}-64m_1^2+5\pi^2+236\right)m_-\\
&-\frac{C_FY_f^2}{16m_1^2}\left(228m_1^2L_{m_1}^2-292m_1^2L_{m_1}-60L_{m_1}^2+128L_{m_1}\right), \qquad \text{(B.19)}
\end{aligned}
$$

$$
\begin{aligned}
B_2^{(2)} = (V_2^{(m_{1,2})} &+ \frac{1}{2}F_\psi^{(m_2)} + \frac{1}{2}F_\psi^{(m_1)} + \Delta B_2) \\
&- \frac{C_F^2}{4m_1 m_-}\left(12m_1^2L_{m_1}^2 - 28m_1^2L_{m_1} + 12L_{m_1}^2 - 16L_{m_1} + \pi^2m_1^2 + 30m_1^2 + \pi^2 + 16\right) \\
&- \frac{C_F^2}{8m_1^2}\left(36m_1^2L_{m_1}^2 + 36m_1^2L_{m_1} + 36L_{m_1}^2 + 3\pi^2m_1^2 - 74m_1^2 + 3\pi^2 + 40\right) \\
&+ \frac{C_F Y_f^2}{16m_1 m_-}\left(12m_1^2L_{m_1}^2 - 16m_1^2L_{m_1} + 12L_{m_1}^2 - 4L_{m_1} + \pi^2m_1^2 + 10m_1^2 + \pi^2 + 2\right) \\
&+ \frac{C_F Y_f^2}{32m_1^2}\left(36m_1^2L_{m_1}^2 + 72m_1^2L_{m_1} + 36L_{m_1}^2 + 36L_{m_1} + 3\pi^2m_1^2 - 74m_1^2 + 3\pi^2 + 22\right) \\
&+ \frac{3}{512m_1^2}\left(36m_1^2L_{m_1}^2 + 12m_1^2L_{m_1} + 36L_{m_1}^2 - 24L_{m_1} + 3\pi^2m_1^2 - 80m_1^2 + 3\pi^2 + 46\right) \\
&- \frac{C_F Y_f^2}{192m_1^3}\left(324m_1^2L_{m_1}^2 - 1512m_1^2L_{m_1} + 900L_{m_1}^2 - 1284L_{m_1}\right)m_- \\
&- \frac{C_F Y_f^2}{192m_1^3}\left(27\pi^2m_1^2 + 1278m_1^2 + 75\pi^2 + 1202\right)m_- \\
&+ \frac{Y_f^4}{256m_1 m_-}\left(3\pi^2m_1^2 + 124m_1^2 + 3\pi^2 + 70\right) \\
&+ \frac{Y_f^4}{256m_1 m_-}\left(36m_1^2L_{m_1}^2 - 108m_1^2L_{m_1} + 36L_{m_1}^2 - 72L_{m_1}\right) \\
&+ \frac{m_-}{1024m_1^3}\left(324m_1^2L_{m_1}^2 + 324m_1^2L_{m_1} - 252L_{m_1}^2\right) \\
&+ \frac{m_-}{1024m_1^3}\left(840L_{m_1} + 27\pi^2m_1^2 - 36m_1^2 - 21\pi^2 - 778\right), \qquad \text{(B.20)}
\end{aligned}
$$

$$
\begin{aligned}
B_3^{(2)} = (V_3^{(m_{1,2})} &+ \frac{1}{2}F_\psi^{(m_2)} + \frac{1}{2}F_\psi^{(m_1)} + \Delta B_3) \\
&+ \frac{C_F^2}{2m_1^2}\left(12m_1^2L_{m_1}^2 - 58m_1^2L_{m_1} - 12L_{m_1}^2 + 34L_{m_1} + \pi^2m_1^2 + 80m_1^2 - \pi^2 - 55\right) \\
&+ \frac{C_F^2 m_-}{4m_1^3}\left(12m_1^2L_{m_1}^2 - 22m_1^2L_{m_1} + 60L_{m_1}^2 - 194L_{m_1} + \pi^2m_1^2 - 10m_1^2 + 5\pi^2 + 263\right) \\
&- \frac{C_F Y_f^2}{32m_1^2}\left(84m_1^2L_{m_1}^2 - 388m_1^2L_{m_1} - 108L_{m_1}^2 + 216L_{m_1} + 7\pi^2m_1^2 + 548m_1^2 - 9\pi^2 - 342\right) \\
&- \frac{Y_f^4}{128m_1 m_-}\left(36m_1^2L_{m_1}^2 - 108m_1^2L_{m_1} + 36L_{m_1}^2 - 72L_{m_1} + 3\pi^2m_1^2 + 124m_1^2 + 3\pi^2 + 70\right) \\
&+ \frac{Y_f^4}{256m_1^2}\left(36m_1^2L_{m_1}^2 - 180m_1^2L_{m_1} - 108L_{m_1}^2 + 72L_{m_1} + 3\pi^2m_1^2 + 376m_1^2 - 9\pi^2 - 138\right) \\
&+ \frac{C_F Y_f^2}{16m_1 m_-}\left(12m_1^2L_{m_1}^2 - 4m_1^2L_{m_1} + 12L_{m_1}^2 + 8L_{m_1} + \pi^2m_1^2 - 4m_1^2 + \pi^2 - 6\right) \\
&- \frac{C_F^2}{m_1 m_-}\left(6m_1^2L_{m_1} + 6L_{m_1} - 10m_1^2 - 7\right) \\
&- \frac{C_F Y_f^2 m_-}{192m_1^3}\left(36m_1^2L_{m_1}^2 + 132m_1^2L_{m_1} + 1476L_{m_1}^2 - 4392L_{m_1}\right)
\end{aligned}
$$

$$
\begin{aligned}
&- \frac{C_F Y_f^2 m_-}{192 m_1^3}\left(3\pi^2 m_1^2 - 936 m_1^2 + 123\pi^2 + 5378\right) \\
&+ \frac{m_-}{512 m_1^3}\left(1128 L_{m_1} + 15\pi^2 m_1^2 + 548 m_1^2 - 33\pi^2 - 1130\right) \\
&+ \frac{m_-}{512 m_1^3}\left(180 m_1^2 L_{m_1}^2 - 396 m_1^2 L_{m_1} - 396 L_{m_1}^2\right), \qquad \text{(B.21)}
\end{aligned}
$$

$$
\begin{aligned}
B_4^{(2)} = &(V_4^{(m_{1,2})} + \frac{1}{2}F_\chi^{(m_2)} + \frac{1}{2}F_\chi^{(m_1)} + \Delta B_4) \\
&+ \frac{C_F^2}{3 m_1^2}\left(24 m_1^2 L_{m_1}^2 - 24 m_1^2 L_{m_1} - 12 L_{m_1}^2 + 12 L_{m_1} + 2\pi^2 m_1^2 + 24 m_1^2 - \pi^2 - 12\right) \\
&+ \frac{2 C_F^2 m_-}{3 m_1^3}\left(18 m_1^2 L_{m_1} + 12 L_{m_1}^2 - 24 L_{m_1} - 6 m_1^2 + \pi^2 + 18\right) \\
&+ \frac{C_F Y_s^2 m_-}{8 m_1^5}\left(12 m_1^2 L_{m_1}^2 - 36 m_1^2 L_{m_1} - 12 L_{m_1}^2 + 32 L_{m_1} + \pi^2 m_1^2 + 30 m_1^2 - \pi^2 - 38\right) \\
&- \frac{C_F Y_s^2}{24 m_1^4}\left(36 m_1^2 L_{m_1}^2 - 48 m_1^2 L_{m_1} - 12 L_{m_1}^2 + 24 L_{m_1} + 3\pi^2 m_1^2 + 60 m_1^2 - \pi^2 - 30\right) \\
&+ \frac{Y_s^4}{192 m_1^4}\left(12 L_{m_1}^2 - 12 L_{m_1} + \pi^2 + 12\right) - \frac{Y_s^4 m_-}{96 m_1^5}\left(12 L_{m_1}^2 - 24 L_{m_1} + \pi^2 + 18\right), \qquad \text{(B.22)}
\end{aligned}
$$

$$
\begin{aligned}
B_5^{(2)} = &(V_5^{(m_{1,2})} + \frac{1}{2}F_\chi^{(m_2)} + \frac{1}{2}F_\chi^{(m_1)} + \Delta B_5) \\
&+ \frac{C_F^2 m_-}{12 m_1^3}\left(36 m_1^2 L_{m_1}^2 - 120 m_1^2 L_{m_1} + 60 L_{m_1}^2 - 72 L_{m_1} + 3\pi^2 m_1^2 + 108 m_1^2 + 5\pi^2 + 48\right) \\
&- \frac{C_F Y_s^2 m_-}{48 m_1^5}\left(12 m_1^2 L_{m_1}^2 - 54 m_1^2 L_{m_1} + 72 L_{m_1}^2 - 132 L_{m_1} + \pi^2 m_1^2 + 78 m_1^2 + 6\pi^2 + 126\right) \\
&- \frac{C_F Y_s^2}{96 m_1^4}\left(12 m_1^2 L_{m_1}^2 - 24 m_1^2 L_{m_1} - 36 L_{m_1}^2 + 36 L_{m_1} + \pi^2 m_1^2 + 24 m_1^2 - 3\pi^2 - 36\right) \\
&+ \frac{1}{384 m_1^6}\left(12 m_1^2 L_{m_1}^2 - 36 m_1^2 L_{m_1} - 12 L_{m_1}^2 + 24 L_{m_1} + \pi^2 m_1^2 + 48 m_1^2 - \pi^2 - 30\right) \\
&+ \frac{m_-}{192 m_1^7}\left(12 m_1^2 L_{m_1}^2 - 42 m_1^2 L_{m_1} - 24 L_{m_1}^2 + 60 L_{m_1} + \pi^2 m_1^2 + 57 m_1^2 - 2\pi^2 - 72\right) \\
&- \frac{C_F^2}{12 m_1^2}\left(12 m_1^2 L_{m_1}^2 - 12 m_1^2 L_{m_1} + 12 L_{m_1}^2 + \pi^2 m_1^2 + 6 m_1^2 + \pi^2\right), \qquad \text{(B.23)}
\end{aligned}
$$

$$
\begin{aligned}
B_6^{(2)} = &(V_6^{(m_{1,2})} + \frac{1}{2}F_\chi^{(m_2)} + \frac{1}{2}F_\psi^{(m_1)} + \Delta B_6) \\
&- \frac{C_F Y_s^2}{96 m_1^4}\left(60 m_1^2 L_{m_1}^2 - 132 m_1^2 L_{m_1} - 12 L_{m_1}^2 + 24 L_{m_1} + 5\pi^2 m_1^2 + 168 m_1^2 - \pi^2 - 30\right) \\
&- \frac{C_F Y_f^2}{64 m_1^2}\left(180 m_1^2 L_{m_1}^2 - 396 m_1^2 L_{m_1} - 36 L_{m_1}^2 + 72 L_{m_1} + 15\pi^2 m_1^2 + 494 m_1^2 - 3\pi^2 - 88\right) \\
&- \frac{C_F Y_f^2 m_-}{64 m_1^3}\left(36 m_1^2 L_{m_1}^2 + 36 m_1^2 L_{m_1} + 108 L_{m_1}^2 - 252 L_{m_1} + 3\pi^2 m_1^2 - 2 m_1^2 + 9\pi^2 + 300\right) \\
&+ \frac{Y_f^3 Y_s}{512 m_1^3}\left(108 m_1^2 L_{m_1}^2 - 180 m_1^2 L_{m_1} - 36 L_{m_1}^2 + 72 L_{m_1} + 9\pi^2 m_1^2 + 210 m_1^2 - 3\pi^2 - 88\right) \\
&+ \frac{C_F^2}{24 m_1^2}\left(108 L_{m_1} + 25\pi^2 m_1^2 + 744 m_1^2 - 5\pi^2 - 132\right)
\end{aligned}
$$

$$
\begin{aligned}
&+\frac{C_F^2 m_-}{24m_1^3}\left(5\pi^2 m_1^2-432L_{m_1}-144m_1^2+15\pi^2+474\right)\\
&-\frac{Y_f^3 Y_s m_-}{256m_1^4}\left(90L_{m_1}+6\pi^2 m_1^2+140m_1^2-3\pi^2-106\right)\\
&+\frac{Y_s^3 Y_f}{768m_1^5}\left(24L_{m_1}+3\pi^2 m_1^2+72m_1^2-\pi^2-30\right)\\
&-\frac{Y_s^3 Y_f m_-}{384m_1^6}\left(66L_{m_1}+5\pi^2 m_1^2+150m_1^2-2\pi^2-78\right)\\
&+\frac{C_F Y_f Y_s m_-}{96m_1^4}\left(162L_{m_1}+10\pi^2 m_1^2+228m_1^2-5\pi^2-171\right)\\
&-\frac{C_F Y_f Y_s}{192m_1^3}\left(108L_{m_1}+15\pi^2 m_1^2+312m_1^2-5\pi^2-132\right)\\
&+\frac{C_F Y_s^2 m_-}{96m_1^5}\left(156L_{m_1}+9\pi^2 m_1^2+468m_1^2-5\pi^2-186\right)\\
&+\frac{C_F^2}{24m_1^2}\left(300m_1^2L_{m_1}^2-600m_1^2L_{m_1}-60L_{m_1}^2\right)\\
&+\frac{C_F^2 m_-}{24m_1^3}\left(60m_1^2L_{m_1}^2+312m_1^2L_{m_1}+180L_{m_1}^2\right)\\
&-\frac{Y_f^3 Y_s m_-}{256m_1^4}\left(72m_1^2L_{m_1}^2-144m_1^2L_{m_1}-36L_{m_1}^2\right)\\
&+\frac{Y_s^3 Y_f}{768m_1^5}\left(36m_1^2L_{m_1}^2-60m_1^2L_{m_1}-12L_{m_1}^2\right)\\
&-\frac{Y_s^3 Y_f m_-}{384m_1^6}\left(60m_1^2L_{m_1}^2-144m_1^2L_{m_1}-24L_{m_1}^2\right)\\
&+\frac{C_F Y_f Y_s m_-}{96m_1^4}\left(120m_1^2L_{m_1}^2-288m_1^2L_{m_1}-60L_{m_1}^2\right)\\
&-\frac{C_F Y_f Y_s}{192m_1^3}\left(180m_1^2L_{m_1}^2-264m_1^2L_{m_1}-60L_{m_1}^2\right)\\
&+\frac{C_F Y_s^2 m_-}{96m_1^5}\left(108m_1^2L_{m_1}^2-396m_1^2L_{m_1}-60L_{m_1}^2\right). \qquad \text{(B.24)}
\end{aligned}
$$

The notation $m_\pm = m_2 \pm m_1$. $V_i^{(m_{1,2})}$ and F_I are bare two-loop vertex and wave-function corrections. ΔB_i are the two-loop order contribution from mass and coupling renormalisation.

B.5 Matching at $\mu \sim m_2$:

Matching corrections to the threshold form factor at $\mu \sim m_2$ are given by,

$$
\begin{aligned}
\tilde{B}_1^{(2)} = &\left(V_1^{(m_2)}+\frac{1}{2}F_\psi^{(m_2,0)}+\frac{1}{2}F_\psi^{(0,0)}\right)\\
&+\frac{1}{6}C_F^2\left(3L_{m_2}\left(4\left(L_{m_2}-2\right)L_{m_2}+\pi^2+16\right)+6\zeta_3-2\pi^2-48\right)\\
&-\frac{1}{32}C_F Y_f^2\left(2L_{m_2}\left(6L_{m_2}\left(2L_{m_2}+1\right)+3\pi^2-46\right)+12\zeta_3+\pi^2+158\right)\\
&+\frac{1}{64}Y_f^4\left(36\left(L_{m_2}-3\right)L_{m_2}+3\pi^2+142\right), \qquad \text{(B.25)}
\end{aligned}
$$

$$\tilde{B}_2^{(2)} = (V_2^{(m_2)} + \frac{1}{2}F_\psi^{(m_2,0)} + \frac{1}{2}F_\psi^{(0,0)})$$
$$+ \frac{1}{12}C_F^2\left(6L_{m_2}\left(4L_{m_2}^2 - 2L_{m_2} + \pi^2 + 26\right) + 12\zeta_3 - \pi^2 - 246\right)$$
$$+ \frac{1}{32}C_F Y_f^2\left(-6L_{m_2}\left(4L_{m_2}^2 - 2L_{m_2} + \pi^2 + 30\right) + \pi^2 + 262 - 12\zeta_3\right)$$
$$- \frac{1}{256}Y_f^4\left(36\left(L_{m_2} - 3\right)L_{m_2} + 3\pi^2 + 124\right), \tag{B.26}$$

$$\tilde{B}_3^{(2)} = (V_3^{(m_2)} + \frac{1}{2}F_\psi^{(m_2,0)} + \frac{1}{2}F_\psi^{(0,0)})$$
$$+ \frac{1}{6}C_F^2\left(3L_{m_2}\left(4\left(L_{m_2} - 2\right)L_{m_2} + \pi^2 + 28\right) + 6\zeta_3 - 2\pi^2 - 108\right)$$
$$- \frac{1}{32}C_F Y_f^2\left(2L_{m_2}\left(6L_{m_2}\left(2L_{m_2} + 3\right) + 3\pi^2 - 50\right)\right.$$
$$\left.+3\left(4\zeta_3 + 50 + \pi^2\right)\right) + \frac{3}{128}Y_f^4\left(36\left(L_{m_2} - 3\right)L_{m_2} + 3\pi^2 + 136\right), \tag{B.27}$$

$$\tilde{B}_4^{(2)} = (V_4^{(m_2)} + \frac{1}{2}F_\chi^{(m_2,0)} + \frac{1}{2}F_\chi^{(0,0)})$$
$$+ \frac{1}{6}C_F^2\left(2L_{m_2}\left(4L_{m_2}^2 + 6L_{m_2} + \pi^2 - 12\right) + 4\zeta_3 + \pi^2 + 24\right) +$$
$$\frac{1}{12m_2^2}C_F Y_s^2\left(-L_{m_2}\left(4L_{m_2}^2 + \pi^2 - 3\right) - 6 + \psi^{(2)}(1)\right)$$
$$+ \frac{1}{384m_2^4}Y_s^4\left(2L_{m_2}\left(4L_{m_2}^2 - 6L_{m_2} + \pi^2 + 12\right) + 4\zeta_3 - \pi^2 - 24\right), \tag{B.28}$$

$$\tilde{B}_5^{(2)} = (V_5^{(m_2)} + \frac{1}{2}F_\chi^{(m_2,0)} + \frac{1}{2}F_\chi^{(0,0)})$$
$$+ \frac{1}{12}C_F^2\left(4L_{m_2}\left(L_{m_2}\left(4L_{m_2} - 9\right) + \pi^2 + 15\right) + 8\zeta_3 - 3\pi^2 - 54\right) +$$
$$\frac{1}{96m_2^2}C_F Y_s^2\left(-4L_{m_2}\left(8L_{m_2}^2 - 9L_{m_2} + 2\pi^2 + 24\right) + 3\pi^2 + 8(15 + \psi^{(2)}(1))\right)$$
$$+ \frac{1}{192m_2^4}Y_s^4\left(4L_{m_2}^3 + \left(\pi^2 - 6\right)L_{m_2} + 2(\zeta_3 + 6)\right), \tag{B.29}$$

$$\tilde{B}_6^{(2)} = (V_6^{(m_2)} + \frac{1}{2}F_\chi^{(m_2,0)} + \frac{1}{2}F_\psi^{(0,0)})$$
$$+ \frac{1}{3}C_F^2\left(L_{m_2}\left(4L_{m_2}\left(L_{m_2} + 3\right) + \pi^2 - 24\right) + 2\zeta_3 + \pi^2 + 24\right) -$$
$$\frac{1}{24m_2}C_F Y_f Y_s\left(2L_{m_2}\left(4L_{m_2}^2 + 6L_{m_2} + \pi^2 - 12\right) + 4\zeta_3 + \pi^2 + 24\right)$$
$$- \frac{1}{48m_2^2}C_F Y_s^2\left(2L_{m_2}\left(4L_{m_2}^2 + 6L_{m_2} + \pi^2 - 24\right) + 4\zeta_3 + \pi^2 + 72\right) +$$
$$\frac{1}{96m_2^3}Y_s^3 Y_f\left(4L_{m_2}^3 + \left(\pi^2 - 6\right)L_{m_2} + 2(\zeta_3 + 6)\right), \tag{B.30}$$

$$\tilde{B}_7^{(2)} = (V_7^{(m_2)} + \frac{1}{2}F_\psi^{(m_2,0)} + \frac{1}{2}F_\chi^{(0,0)})$$
$$+ \frac{1}{12}C_F^2\left(6L_{m_2}\left(2L_{m_2}\left(2L_{m_2} - 7\right) + \pi^2 + 36\right) + 12\zeta_3 - 7\pi^2 - 264\right)$$
$$- \frac{1}{16m_2}C_F Y_f Y_s\left(4L_{m_2}\left(3L_{m_2} - 10\right) + \pi^2 + 56\right)$$
$$+ \frac{1}{16}C_F Y_f^2\left(-L_{m_2}\left(12\left(L_{m_2} - 3\right)L_{m_2} + 3\pi^2 + 88\right) - 6\zeta_3 + 3\pi^2 + 104\right)$$

$$+\frac{1}{128m_2}Y_f^3Y_s\left(36\left(L_{m_2}-3\right)L_{m_2}+3\pi^2+142\right). \tag{B.31}$$

$V_i^{(m_2)}$ and F_I are two-loop vertex and wave-function corrections. The mass and coupling renormalisation contributions contributing at two-loop order are given by,

$$\begin{aligned}
\Delta\tilde{B}_1 = \frac{1}{24}C_F\{&-2L_{m_2}\left(3L_{m_2}\left(\beta_0-48C_F\right)+120C_F+\left(24+\pi^2\right)\beta_0\right.\\
&\left.+2\beta_0L_{m_2}^2\right)+24\left(24+\pi^2\right)C_F-\left(\pi^2-96\right)\beta_0-8\beta_0\zeta_3\}\\
&-\frac{1}{192}Y_f^2\{6L_{m_2}\left(L_{m_2}\left(48C_F+5\beta_0\right)-208C_F+6\beta_0\right)\\
&+24\left(46+\pi^2\right)C_F+\left(5\pi^2-132\right)\beta_0\}+\frac{1}{32}Y_f^4(13-15L_{m_2}),
\end{aligned} \tag{B.32}$$

$$\begin{aligned}
\Delta\tilde{B}_2 = \frac{1}{24}C_F\{&-2L_{m_2}\left(-3L_{m_2}\left(48C_F+5\beta_0\right)+552C_F+\left(60+\pi^2\right)\beta_0\right.\\
&\left.+2\beta_0L_{m_2}^2\right)+24\left(66+\pi^2\right)C_F+\left(264+5\pi^2\right)\beta_0-8\beta_0\zeta_3\}\\
&-\frac{1}{192}Y_f^2\{6L_{m_2}\left(48C_FL_{m_2}-496C_F-18\beta_0+11\beta_0L_{m_2}\right)\\
&+24\left(166+\pi^2\right)C_F+\left(180+11\pi^2\right)\beta_0\}+\frac{1}{32}Y_f^4(52-33L_{m_2}),
\end{aligned} \tag{B.33}$$

$$\begin{aligned}
\Delta\tilde{B}_3 = \frac{1}{24}C_F\{&-2L_{m_2}\left(-3L_{m_2}\left(48C_F+7\beta_0\right)+696C_F+\left(48+\pi^2\right)\beta_0\right.\\
&\left.+2\beta_0L_{m_2}^2\right)+24\left(68+\pi^2\right)C_F+\left(96+7\pi^2\right)\beta_0-8\beta_0\zeta_3\}\\
&-\frac{1}{64}Y_f^2\{2L_{m_2}\left(48C_FL_{m_2}-496C_F-10\beta_0+9\beta_0L_{m_2}\right)\\
&+8\left(154+\pi^2\right)C_F+\left(4+3\pi^2\right)\beta_0\}+\frac{3}{32}Y_f^4(13-9L_{m_2}),
\end{aligned} \tag{B.34}$$

$$\begin{aligned}
\Delta\tilde{B}_4 = \frac{1}{12}C_F\{&6L_{m_2}^2\left(12C_F+\beta_0\right)-L_{m_2}\left(240C_F+\left(\pi^2-12\right)\beta_0\right)\\
&+6\left(38+\pi^2\right)C_F-2\beta_0L_{m_2}^3+\beta_0\left(\pi^2-4(\zeta_3+9)\right)\}\\
&+\frac{Y_s^2}{96m_2^2}\{L_{m_2}\left(-6L_{m_2}\left(20C_F+\beta_0\right)+384C_F+\left(12+\pi^2\right)\beta_0\right.\\
&\left.+2\beta_0L_{m_2}^2\right)-10\left(42+\pi^2\right)C_F-\left(24+\pi^2\right)\beta_0+4\beta_0\zeta_3\}\\
&+\frac{Y_s^4}{192m_2^4}\left(12(L_{m_2}-3)L_{m_2}+\pi^2+42\right)+\frac{1}{32}Y_f^4(13-15L_{m_2}),
\end{aligned} \tag{B.35}$$

$$\begin{aligned}
\Delta\tilde{B}_5 = \frac{1}{24}C_F\{&-2L_{m_2}\left(-24L_{m_2}\left(3C_F+\beta_0\right)+456C_F+\left(51+\pi^2\right)\beta_0\right.\\
&\left.+2\beta_0L_{m_2}^2\right)+6\left(223+2\pi^2\right)C_F+\left(153+8\pi^2\right)\beta_0-8\beta_0\zeta_3\}\\
&+\frac{Y_s^2}{96m_2^2}\{-2\left(\left(387+5\pi^2\right)C_F+\pi^2\beta_0\right)+L_{m_2}\left(2L_{m_2}\left(\beta_0L_{m_2}\right.\right.\\
&\left.\left.-6\left(10C_F+\beta_0\right)\right)+600C_F+\left(12+\pi^2\right)\beta_0\right)+4\beta_0\zeta_3\}\\
&+\frac{Y_s^4}{192m_2^4}\left(12(L_{m_2}-4)L_{m_2}+\pi^2+54\right),
\end{aligned} \tag{B.36}$$

$$\begin{aligned}
\Delta\tilde{B}_6 = \frac{1}{12}C_F\{&6L_{m_2}^2\left(12C_F+\beta_0\right)-L_{m_2}\left(240C_F+\left(\pi^2-24\right)\beta_0\right)\\
&+6\left(32+\pi^2\right)C_F-2\beta_0L_{m_2}^3+\beta_0\left(-4\zeta_3-72+\pi^2\right)\}\\
&-\frac{Y_s^2}{96m_2^2}\{6L_{m_2}\left(L_{m_2}\left(8C_F+\beta_0\right)-2\left(18C_F+\beta_0\right)\right)+4\left(54\right.
\end{aligned}$$

$$
\begin{aligned}
&+\pi^2)\,C_F+\left(24+\pi^2\right)\beta_0\big\}+\frac{Y_fY_s}{48m_2}\left\{L_{m_2}\left(168C_F+\left(\pi^2-12\right)\beta_0\right)\right.\\
&\left.-72C_FL_{m_2}^2-6\left(24+\pi^2\right)C_F+2\beta_0L_{m_2}^3+4\beta_0(\zeta_3+9)\right\}\\
&\frac{Y_fY_s^3}{96m_2^3}\left(12(L_{m_2}-2)L_{m_2}+\pi^2+18\right)-\frac{Y_s^4}{32m_2^4}(2L_{m_2}-3),
\end{aligned}
\tag{B.37}
$$

$$
\begin{aligned}
\Delta\tilde{B}_7=&\frac{1}{24}C_F\left\{-2L_{m_2}\left(-3L_{m_2}\left(48C_F+5\beta_0\right)+552C_F+\left(48+\pi^2\right)\beta_0\right.\right.\\
&\left.+2\beta_0L_{m_2}^2\right)+24\left(60+\pi^2\right)C_F+\left(192+5\pi^2\right)\beta_0-8\beta_0\zeta_3\big\}\\
&-\frac{1}{64}Y_f^2\left\{2L_{m_2}\left(48C_FL_{m_2}-448C_F-18\beta_0+9\beta_0L_{m_2}\right)\right.\\
&\left.+8\left(152+\pi^2\right)C_F+\left(68+3\pi^2\right)\beta_0\right\}+\frac{9}{32}Y_f^4(5-3L_{m_2})\\
&+\frac{Y_fY_s}{4m_2}\left(-L_{m_2}\left(6C_F+\beta_0\right)+19C_F+3\beta_0\right)+\frac{Y_f^3Y_s}{16m_2}(3L_{m_2}-11).
\end{aligned}
\tag{B.38}
$$

B.6 Matching at $\mu\sim m_1$:

Matching corrections to the threshold form factor at $\mu\sim m_1$ are given by,

$$
\begin{aligned}
G_1^{(2)}=&(V_1^{(m_1)}+\frac{1}{2}F_\psi^{(m_1,0)}+\frac{1}{2}F_h^{(0)})\\
&-\frac{1}{8}C_F^2\left(4L_{m_1}(3L_{m_1}-10)+\pi^2+56\right)+\\
&C_F\frac{Y_f^2}{96m_1^2}\left\{-2L_{m_1}\left(2L_{m_1}(2L_{m_1}-9)+\pi^2+48\right)\right.\\
&\left.-4\zeta_3+3\pi^2+120\right\}-\frac{1}{256}Y_f^4\left(36(L_{m_1}-3)L_{m_1}+3\pi^2+142\right),
\end{aligned}
\tag{B.39}
$$

$$
\begin{aligned}
G_2^{(2)}=&(V_2^{(m_1)}+\frac{1}{2}F_\chi^{(m_1,0)}+\frac{1}{2}F_h^{(0)})\\
&-\frac{1}{6}C_F^2\left\{L_{m_1}\left(4(L_{m_1}-3)L_{m_1}+\pi^2+24\right)\right.\\
&\left.+2\zeta_3-\pi^2-24\right\}+C_F\frac{Y_s^2}{96m_1^2}\left\{-2L_{m_1}\left(2L_{m_1}(2L_{m_1}-9)+\pi^2\right.\right.\\
&\left.\left.+48\right)-4\zeta_3+3\pi^2+120\right\},
\end{aligned}
\tag{B.40}
$$

$$
\begin{aligned}
G_3^{(2)}=&(V_3^{(m_1)}+\frac{1}{2}F_\chi^{(m_1,0)}+\frac{1}{2}F_h^{(0)})\\
&+\frac{1}{3}C_F^2\left\{L_{m_1}\left(4(L_{m_1}-3)L_{m_1}+\pi^2+24\right)\right.\\
&\left.+2\zeta_3-\pi^2-24\right\}+C_F\frac{Y_s^2}{48m_1^2}\left\{-2L_{m_1}\left(2L_{m_1}(2L_{m_1}-9)+\pi^2\right.\right.\\
&\left.\left.+48\right)-4\zeta_3+3\pi^2+120\right\},
\end{aligned}
\tag{B.41}
$$

$$
\begin{aligned}
G_4^{(2)}=&(V_4^{(m_1)}+\frac{1}{2}F_\psi^{(m_1,0)}+\frac{1}{2}F_h^{(0)})\\
&-\frac{1}{12}C_F^2\left(12(L_{m_1}-2)L_{m_1}+\pi^2+24\right)+\frac{1}{48}C_FY_fY_s\left(\pi^2\right.\\
&\left.+24+12(L_{m_1}-2)L_{m_1}\right)+C_F\frac{Y_s^2}{96m_1^2}\left\{12(L_{m_1}-3)L_{m_1}+\pi^2\right.
\end{aligned}
$$

$$+48\} - \frac{Y_s^3 Y_f}{384 m_1^2}\left(12(L_{m_1}-3)L_{m_1}+\pi^2+48\right), \tag{B.42}$$

$$\begin{aligned} G_5^{(2)} = (V_5^{(m_1)} &+ \frac{1}{2}F_\chi^{(m_1,0)} + \frac{1}{2}F_h^{(0)}) \\ &+ \frac{1}{12}C_F^2\left(3L_{m_1}\left(4(L_{m_1}-5)L_{m_1}+\pi^2+56\right)\right. \\ &\left.+6\zeta_3 - 5\pi^2 - 216\right) + C_F\frac{Y_f^2}{64}\{-2L_{m_1}\left(6L_{m_1}(2L_{m_1}-9)\right. \\ &\left.+3\pi^2+142\right) + 9\pi^2 + 350 + 6\psi^{(2)}(1)\Big\}. \end{aligned} \tag{B.43}$$

$V_i^{(m_1)}$ and F_I are two-loop vertex and wave-function corrections. The mass and coupling renormalisation contributions contributing at two-loop order are given by,

$$\begin{aligned} \Delta G_1 = \frac{1}{12}C_F\{&6L_{m_1}\left(\beta_0 L_{m_1} - 2\left(12C_F+\beta_0\right)\right) \\ &+168C_F + \left(24+\pi^2\right)\beta_0\} + \frac{1}{192}Y_f^2\{6L_{m_1}\left(216C_F\right. \\ &\left.+10\beta_0 - 7\beta 0 L_{m_1}\right) - 1512C_F - \left(108+7\pi^2\right)\beta_0\} \\ &+ \frac{1}{32}Y_f^4(32-21L_{m_1}), \end{aligned} \tag{B.44}$$

$$\begin{aligned} \Delta G_2 = \frac{1}{24}C_F\{&-144C_F L_{m_1} + 2\beta_0 L_{m_1}^3 + \left(48+\pi^2\right)\beta_0 L_{m_1} \\ &+168C_F + 4\beta_0(\zeta_3-24)\} + \frac{Y_s^2}{96m_1^2}\{6L_{m_1}\left(20C_F+2\beta_0\right. \\ &\left.-\beta_0 L_{m_1}\right) - 168C_F - \left(24+\pi^2\right)\beta_0\} - \frac{Y_s^4(2L_{m_1}-3)}{32m_1^4}, \end{aligned} \tag{B.45}$$

$$\begin{aligned} \Delta G_3 = \frac{1}{12}C_F\{&L_{m_1}\left(\left(48+\pi^2\right)\beta_0 - 72C_F\right) + 84C_F + \\ &2\beta_0 L_{m_1}^3 - 6\beta_0 L_{m_1}^2 - \beta_0\left(-4\zeta_3 + 96 + \pi^2\right)\} \\ &+ \frac{Y_s^2}{96m_1^2}\{6L_{m_1}\left(20C_F+2\beta_0-\beta_0 L_{m_1}\right) - 168C_F - (24 \\ &+\pi^2)\beta_0\} - \frac{Y_s^4(2L_{m_1}-3)}{32m_1^4}, \end{aligned} \tag{B.46}$$

$$\begin{aligned} \Delta G_4 = \frac{1}{12}C_F\{&6L_{m_1}\left(\beta_0 L_{m_1} - 2\left(12C_F+\beta_0\right)\right) + \left(24+\pi^2\right)\beta_0 \\ &+168C_F\} + \frac{1}{64}Y_f^2\{6L_{m_1}\left(88C_F+6\beta_0-3\beta_0 L_{m_1}\right) - \left(68+3\pi^2\right)\beta_0 \\ &-664C_F\} + \frac{1}{96}Y_f Y_s\{6L_{m_1}\left(\beta_0 L_{m_1} - 4\left(6C_F+\beta_0\right)\right) + 240C_F \\ &+\left(48+\pi^2\right)\beta_0\} + \frac{1}{32}Y_f^3 Y_s(6L_{m_1}-13) + \frac{9}{32}Y_f^4(5-3L_{m_1}), \end{aligned} \tag{B.47}$$

$$\begin{aligned} \Delta G_5 = \frac{1}{24}C_F\{&-144C_F L_{m_1} + 168C_F + 2\beta_0 L_{m_1}^3 + \left(48+\pi^2\right)\beta_0 L_{m_1} \\ &+4\beta_0(\zeta_3-24)\} + \frac{Y_s^2}{96m_1^2}\{6L_{m_1}\left(20C_F+2\beta_0-\beta_0 L_{m_1}\right) \\ &-168C_F - \left(24+\pi^2\right)\beta_0\} - \frac{Y_s^4}{32m_1^4}(2L_{m_1}-3). \end{aligned} \tag{B.48}$$

The contributions from bare two-loop vertex contributions, $V_i^{(m_1)}$, are too large to present here. We thus include the full expressions with description in the arXiv ancillary file of Ref. [325]. The contributions from two-loop vertex corrections, $V_i^{(M)}$, are too large to present here. We thus include the full expressions with description in the arXiv ancillary file of Ref. [325]. The contributions from all corrections both one- and two-loop are too large to present here. We thus include the full expressions with description in the arXiv ancillary file of Ref. [325].

B.7 Two-Loop Field Renormalisation

The bare two-loop wave-function contributions are presented here for reference. As with all other contributions, these too are available in the arXiv ancillary file of Ref. [325].

B.7.1 Fermion and Scalar Field at $m = 0$ and $M = 0$:

$$
\begin{aligned}
F_{\psi}^{(0,0)} = &\frac{2291C_AC_F}{16\epsilon_{\rm IR}} - \frac{3C_AC_F}{\epsilon_{\rm IR}^2} - \frac{1025S_1C_AC_F}{12\epsilon_{\rm IR}} + \frac{57S_1Y_f^2C_AC_F}{32\epsilon_{\rm IR}} + \frac{3C_AC_F}{\epsilon_{\rm IR}\epsilon_{\rm UV}} + \frac{Y_f^2C_AC_F}{8\epsilon_{\rm IR}\epsilon_{\rm UV}} - \\
&\frac{59Y_f^2C_AC_F}{32\epsilon_{\rm IR}} - \frac{Y_f^2C_AC_F}{8\epsilon_{\rm IR}^2} + \frac{1025S_1C_AC_F}{24\epsilon_{\rm UV}} - \frac{57S_1Y_f^2C_AC_F}{64\epsilon_{\rm UV}} - \frac{2291C_AC_F}{32\epsilon_{\rm UV}} - \frac{3C_AC_F}{2\epsilon_{\rm UV}^2} + \\
&\frac{59Y_f^2C_AC_F}{64\epsilon_{\rm UV}} - \frac{Y_f^2C_AC_F}{16\epsilon_{\rm UV}^2} + \frac{50n_fS_1C_FT_f}{9\epsilon_{\rm IR}} - \frac{55n_fC_FT_f}{6\epsilon_{\rm IR}} - \frac{25n_fS_1C_FT_f}{9\epsilon_{\rm UV}} + \frac{55n_fC_FT_f}{12\epsilon_{\rm UV}} + \\
&\frac{19C_F^2}{2\epsilon_{\rm IR}} - \frac{199C_F}{24\epsilon_{\rm IR}} + \frac{C_F^2}{\epsilon_{\rm IR}^2} - \frac{6S_1C_F^2}{\epsilon_{\rm IR}} + \frac{85S_1C_F}{18\epsilon_{\rm IR}} + \frac{41S_1Y_f^2C_F}{4\epsilon_{\rm IR}} - \frac{C_F^2}{\epsilon_{\rm IR}\epsilon_{\rm UV}} + \frac{3Y_f^2C_F}{8\epsilon_{\rm IR}\epsilon_{\rm UV}} - \\
&\frac{293Y_f^2C_F}{16\epsilon_{\rm IR}} - \frac{3Y_f^2C_F}{8\epsilon_{\rm IR}^2} + \frac{3S_1C_F^2}{\epsilon_{\rm UV}} - \frac{85S_1C_F}{36\epsilon_{\rm UV}} - \frac{41S_1Y_f^2C_F}{8\epsilon_{\rm UV}} - \frac{19C_F^2}{4\epsilon_{\rm UV}} + \frac{199C_F}{48\epsilon_{\rm UV}} + \frac{C_F^2}{2\epsilon_{\rm UV}^2} + \\
&\frac{293Y_f^2C_F}{32\epsilon_{\rm UV}} - \frac{3Y_f^2C_F}{16\epsilon_{\rm UV}^2} - \frac{39S_1Y_f^4}{32\epsilon_{\rm IR}} + \frac{9S_1Y_f^2}{16\epsilon_{\rm IR}} - \frac{5Y_f^4}{64\epsilon_{\rm IR}\epsilon_{\rm UV}} + \frac{271Y_f^4}{128\epsilon_{\rm IR}} + \frac{5Y_f^4}{64\epsilon_{\rm IR}^2} - \frac{9Y_f^2}{16\epsilon_{\rm IR}} + \\
&\frac{39S_1Y_f^4}{64\epsilon_{\rm UV}} - \frac{9S_1Y_f^2}{32\epsilon_{\rm UV}} - \frac{271Y_f^4}{256\epsilon_{\rm UV}} + \frac{5Y_f^4}{128\epsilon_{\rm UV}^2} + \frac{9Y_f^2}{32\epsilon_{\rm UV}}
\end{aligned}
\tag{B.49}
$$

$$
\begin{aligned}
F_{\chi}^{(0,0)} = &-\frac{343C_AC_F}{16\epsilon_{\rm IR}} + \frac{105C_AC_F}{8\epsilon_{\rm IR}^2} + \frac{7S_1Y_s^2C_AC_F}{32m^2\epsilon_{\rm IR}} - \frac{5Y_s^2C_AC_F}{32m^2\epsilon_{\rm IR}} + \frac{53S_1C_AC_F}{4\epsilon_{\rm IR}} - \frac{105C_AC_F}{8\epsilon_{\rm IR}\epsilon_{\rm UV}} - \\
&\frac{7S_1Y_s^2C_AC_F}{64m^2\epsilon_{\rm UV}} + \frac{5Y_s^2C_AC_F}{64m^2\epsilon_{\rm UV}} - \frac{53S_1C_AC_F}{8\epsilon_{\rm UV}} + \frac{343C_AC_F}{32\epsilon_{\rm UV}} + \frac{105C_AC_F}{16\epsilon_{\rm UV}^2} - \frac{2n_fS_1C_FT_f}{3\epsilon_{\rm IR}} + \\
&\frac{3n_fC_FT_f}{2\epsilon_{\rm IR}} - \frac{n_fC_FT_f}{\epsilon_{\rm IR}^2} + \frac{n_fC_FT_f}{\epsilon_{\rm IR}\epsilon_{\rm UV}} + \frac{n_fS_1C_FT_f}{3\epsilon_{\rm UV}} - \frac{3n_fC_FT_f}{4\epsilon_{\rm UV}} - \frac{n_fC_FT_f}{2\epsilon_{\rm UV}^2} + \frac{9C_F^2}{2\epsilon_{\rm IR}} + \\
&\frac{21C_F}{8\epsilon_{\rm IR}} - \frac{8C_F^2}{\epsilon_{\rm IR}^2} - \frac{C_F}{4\epsilon_{\rm IR}^2} + \frac{3S_1Y_s^2C_F}{2m^2\epsilon_{\rm IR}} - \frac{3Y_s^2C_F}{m^2\epsilon_{\rm IR}} - \frac{4S_1Y_sC_F}{m\epsilon_{\rm IR}} + \frac{6Y_sC_F}{m\epsilon_{\rm IR}} + \frac{41S_1C_F}{6\epsilon_{\rm IR}} + \\
&\frac{8C_F^2}{\epsilon_{\rm IR}\epsilon_{\rm UV}} + \frac{C_F}{4\epsilon_{\rm IR}\epsilon_{\rm UV}} - \frac{3S_1Y_s^2C_F}{4m^2\epsilon_{\rm UV}} + \frac{3Y_s^2C_F}{2m^2\epsilon_{\rm UV}} + \frac{2S_1Y_sC_F}{m\epsilon_{\rm UV}} - \frac{3Y_sC_F}{m\epsilon_{\rm UV}} - \frac{41S_1C_F}{12\epsilon_{\rm UV}} - \frac{9C_F^2}{4\epsilon_{\rm UV}} - \\
&\frac{21C_F}{16\epsilon_{\rm UV}} - \frac{4C_F^2}{\epsilon_{\rm UV}^2} - \frac{C_F}{8\epsilon_{\rm UV}^2} - \frac{S_1Y_s^4}{72m^4\epsilon_{\rm IR}} + \frac{Y_s^4}{24m^4\epsilon_{\rm IR}} - \frac{S_1Y_s^2}{16m^2\epsilon_{\rm IR}} + \frac{3Y_s^2}{16m^2\epsilon_{\rm IR}} + \frac{S_1Y_s^4}{144m^4\epsilon_{\rm UV}} - \\
&\frac{Y_s^4}{48m^4\epsilon_{\rm UV}} + \frac{S_1Y_s^2}{32m^2\epsilon_{\rm UV}} - \frac{3Y_s^2}{32m^2\epsilon_{\rm UV}}
\end{aligned}
\tag{B.50}
$$

B.7.2 Fermion and Scalar Field at $m = 0$ and $M \neq 0$ ($\Delta_M \equiv M_H - M_W$):

$$
\begin{aligned}
F_{\psi}^{(0,M)} = & -\frac{4C_AC_FL(M_W)}{\epsilon_{\rm UV}} - 64C_AC_F^5L(M_W)^2 - 64C_AC_F^3L(M_W)^2 - 8C_AC_FL(M_W)^2 - \\
& 144S_2C_AC_F^5 - 144S_2C_AC_F^3 - 18S_2C_AC_F + \frac{2C_AC_F}{\epsilon_{\rm UV}^2} - 64\zeta_2C_AC_F^5 - 64\zeta_2C_AC_F^3 - \\
& 8\zeta_2C_AC_F + 96C_AC_F^5 + 96C_AC_F^3 + 14C_AC_F + 2C_A^6L(M_W)^2 + \frac{9S_2C_A^6}{2} + 2\zeta_2C_A^6 - \\
& 3C_A^6 - \frac{4\Delta_MY_f^2C_FL(M_W)}{M_W} - \frac{9\Delta_MS_2C_F}{M_W} + \frac{2\Delta_MY_f^2C_F}{M_W\epsilon_{\rm UV}} - \frac{3\Delta_MY_f^2\zeta_2C_F}{M_W} + \\
& \frac{4\Delta_MY_f^2C_F}{M_W} + \frac{2\Delta_MC_F}{M_W} + \frac{n_fC_FT_fL(M_W)}{\epsilon_{\rm UV}} - n_fC_FT_fL(M_W)^2 + n_fC_FT_fL(M_W) - \\
& \frac{n_fC_FT_f}{2\epsilon_{\rm UV}} - \frac{n_fC_FT_f}{2\epsilon_{\rm UV}^2} - \frac{3}{2}n_f\zeta_2C_FT_f - \frac{1}{2}n_fC_FT_f + \frac{Y_f^2C_FL(M_W)}{2\epsilon_{\rm UV}} - \frac{1}{2}Y_f^2C_FL(M_W)^2 + \\
& \frac{1}{2}Y_f^2C_FL(M_W) - 32C_F^4L(M_W)^2 - 24C_F^2L(M_W)^2 - 72S_2C_F^4 - 54S_2C_F^2 - \frac{Y_f^2C_F}{4\epsilon_{\rm UV}} - \\
& \frac{Y_f^2C_F}{4\epsilon_{\rm UV}^2} - \frac{3}{4}Y_f^2\zeta_2C_F - Y_f^2C_F - 32\zeta_2C_F^4 - 24\zeta_2C_F^2 + 48C_F^4 + 32C_F^2 + \frac{\Delta_MY_f^4L(M_W)}{2M_W} - \\
& \frac{\Delta_MY_f^4}{4M_W\epsilon_{\rm UV}} - \frac{5\Delta_MY_f^4}{8M_W} - \frac{Y_f^4L(M_W)}{8\epsilon_{\rm UV}} + \frac{1}{8}Y_f^4L(M_W)^2 - \frac{5}{16}Y_f^4L(M_W) - 2L(M_W)^2 - \\
& \frac{9S_2}{2} + \frac{5Y_f^4}{32\epsilon_{\rm UV}} + \frac{Y_f^4}{16\epsilon_{\rm UV}^2} + \frac{Y_f^4}{4} - 2\zeta_2 + 3
\end{aligned}
\tag{B.51}
$$

$$
\begin{aligned}
F_{\chi}^{(0,M)} = & -\frac{5L(M_W)^2Y_s^4}{16M_W^4} + \frac{5\Delta_ML(M_W)^2Y_s^4}{4M_W^5} - \frac{3\zeta_2Y_s^4}{32M_W^4} + \frac{3\Delta_M\zeta_2Y_s^4}{8M_W^5} + \frac{5L(M_W)Y_s^4}{16\epsilon_{\rm UV}M_W^4} + \\
& \frac{9L(M_W)Y_s^4}{16M_W^4} - \frac{7\Delta_ML(M_W)Y_s^4}{2M_W^5} - \frac{5\Delta_ML(M_W)Y_s^4}{4\epsilon_{\rm UV}M_W^5} - \frac{9Y_s^4}{32\epsilon_{\rm UV}M_W^4} - \frac{5Y_s^4}{32\epsilon_{\rm UV}^2M_W^4} - \\
& \frac{17Y_s^4}{32M_W^4} + \frac{13\Delta_MY_s^4}{4M_W^5} + \frac{7\Delta_MY_s^4}{4\epsilon_{\rm UV}M_W^5} + \frac{5\Delta_MY_s^4}{8\epsilon_{\rm UV}^2M_W^5} + \frac{81S_2Y_s^3}{16M_W^3} - \frac{81\Delta_MS_2Y_s^3}{8M_W^4} - \\
& \frac{3L(M_W)Y_s^3}{4M_W^3} + \frac{3\Delta_ML(M_W)Y_s^3}{2M_W^4} + \frac{3Y_s^3}{8\epsilon_{\rm UV}M_W^3} - \frac{3Y_s^3}{8M_W^3} - \frac{3\Delta_MY_s^3}{4M_W^4} - \frac{3\Delta_MY_s^3}{4\epsilon_{\rm UV}M_W^4} - \\
& \frac{3C_FL(M_W)^2Y_s^2}{M_W^2} + \frac{10C_F\Delta_ML(M_W)^2Y_s^2}{M_W^3} + \frac{1005C_AC_FS_2Y_s^2}{128M_W^2} + \frac{189S_2Y_s^2}{64M_W^2} - \\
& \frac{417C_AC_F\Delta_MS_2Y_s^2}{8M_W^3} - \frac{27\Delta_MS_2Y_s^2}{16M_W^3} - \frac{5C_F\zeta_2Y_s^2}{4M_W^2} + \frac{11C_F\Delta_M\zeta_2Y_s^2}{2M_W^3} + \\
& \frac{65C_AC_FL(M_W)Y_s^2}{32M_W^2} + \frac{4C_FL(M_W)Y_s^2}{M_W^2} + \frac{3C_FL(M_W)Y_s^2}{\epsilon_{\rm UV}M_W^2} + \frac{9L(M_W)Y_s^2}{16M_W^2} - \\
& \frac{153C_AC_F\Delta_ML(M_W)Y_s^2}{16M_W^3} - \frac{37C_F\Delta_ML(M_W)Y_s^2}{2M_W^3} - \frac{9\Delta_ML(M_W)Y_s^2}{8M_W^3} - \\
& \frac{10C_F\Delta_ML(M_W)Y_s^2}{\epsilon_{\rm UV}M_W^3} - \frac{213C_AC_FY_s^2}{64M_W^2} - \frac{3C_FY_s^2}{M_W^2} - \frac{65C_AC_FY_s^2}{64\epsilon_{\rm UV}M_W^2} - \frac{2C_FY_s^2}{\epsilon_{\rm UV}M_W^2} - \\
& \frac{9Y_s^2}{32\epsilon_{\rm UV}M_W^2} - \frac{3C_FY_s^2}{2\epsilon_{\rm UV}^2M_W^2} - \frac{45Y_s^2}{32M_W^2} + \frac{645C_AC_F\Delta_MY_s^2}{32M_W^3} + \frac{45C_F\Delta_MY_s^2}{4M_W^3} + \frac{45\Delta_MY_s^2}{16M_W^3} +
\end{aligned}
$$

$$\frac{153C_AC_F\Delta_MY_s^2}{32\epsilon_{\rm UV}M_W^3}+\frac{37C_F\Delta_MY_s^2}{4\epsilon_{\rm UV}M_W^3}+\frac{9\Delta_MY_s^2}{16\epsilon_{\rm UV}M_W^3}+\frac{5C_F\Delta_MY_s^2}{\epsilon_{\rm UV}^2M_W^3}-\frac{7C_FL(M_W)^2Y_s}{M_W}+$$
$$\frac{14C_F\Delta_ML(M_W)^2Y_s}{M_W^2}+\frac{261C_FS_2Y_s}{4M_W}-\frac{192C_F\Delta_MS_2Y_s}{M_W^2}-\frac{4C_F\zeta_2Y_s}{M_W}+\frac{9C_F\Delta_M\zeta_2Y_s}{M_W^2}+$$
$$\frac{4C_FL(M_W)Y_s}{M_W}+\frac{7C_FL(M_W)Y_s}{\epsilon_{\rm UV}M_W}-\frac{22C_F\Delta_ML(M_W)Y_s}{M_W^2}-\frac{14C_F\Delta_ML(M_W)Y_s}{\epsilon_{\rm UV}M_W^2}-$$
$$\frac{35C_FY_s}{2M_W}-\frac{2C_FY_s}{\epsilon_{\rm UV}M_W}-\frac{7C_FY_s}{2\epsilon_{\rm UV}^2M_W}+\frac{54C_F\Delta_MY_s}{M_W^2}+\frac{11C_F\Delta_MY_s}{\epsilon_{\rm UV}M_W^2}+\frac{7C_F\Delta_MY_s}{\epsilon_{\rm UV}^2M_W^2}-8C_F^2-$$
$$14C_F^2L(M_W)^2+\frac{47}{4}C_AC_FL(M_W)^2+\frac{7}{2}C_FL(M_W)^2-2C_Fn_fT_fL(M_W)^2+\frac{97C_AC_F}{4}+$$
$$\frac{19C_F}{2}-\frac{141}{2}C_AC_FS_2-6C_FS_2-\frac{21C_F\Delta_MS_2}{M_W}-C_Fn_fT_f-\frac{C_Fn_fT_f}{\epsilon_{\rm UV}}-\frac{C_Fn_fT_f}{\epsilon_{\rm UV}^2}-$$
$$14C_F^2\zeta_2+\frac{39}{8}C_AC_F\zeta_2+\frac{7C_F\zeta_2}{4}-3C_Fn_fT_f\zeta_2+24C_F^2L(M_W)-\frac{73}{2}C_AC_FL(M_W)+$$
$$5C_FL(M_W)+2C_Fn_fT_fL(M_W)+\frac{2C_Fn_fT_fL(M_W)}{\epsilon_{\rm UV}}+\frac{14C_F^2L(M_W)}{\epsilon_{\rm UV}}-$$
$$\frac{47C_AC_FL(M_W)}{4\epsilon_{\rm UV}}-\frac{7C_FL(M_W)}{2\epsilon_{\rm UV}}-\frac{2C_F\Delta_ML(M_W)}{M_W}-\frac{12C_F^2}{\epsilon_{\rm UV}}+\frac{73C_AC_F}{4\epsilon_{\rm UV}}-\frac{5C_F}{2\epsilon_{\rm UV}}+$$
$$\frac{4C_F\Delta_M}{M_W}+\frac{C_F\Delta_M}{\epsilon_{\rm UV}M_W}-\frac{7C_F^2}{\epsilon_{\rm UV}^2}+\frac{47C_AC_F}{8\epsilon_{\rm UV}^2}+\frac{7C_F}{4\epsilon_{\rm UV}^2} \tag{B.52}$$

B.7.3 Fermion and Scalar Field at $m \neq 0$ and $M = 0$:

$$F_\psi^{(m,0)}=\frac{17C_AC_FY_f^2M_H^4}{128M_W^2}+\frac{5C_AC_FY_f^2M_H^4}{256\epsilon_{\rm IR}M_W^2}+\frac{45Y_f^2M_H^4}{128\epsilon_{\rm IR}M_W^2}+\frac{C_AC_FY_f^2M_H^4}{128\epsilon_{\rm IR}^2M_W^2}+\frac{9Y_f^2M_H^4}{64\epsilon_{\rm IR}^2M_W^2}+$$
$$\frac{53C_AC_FY_f^2M_H^4}{256m^2M_W^2}+\frac{C_AC_FY_f^2M_H^4}{64\epsilon_{\rm IR}^2m^2M_W^2}+\frac{9Y_f^2M_H^4}{32\epsilon_{\rm IR}^2m^2M_W^2}+\frac{477Y_f^2M_H^4}{128m^2M_W^2}+\frac{153Y_f^2M_H^4}{64M_W^2}+$$
$$\frac{C_AC_FY_f^2L(m)^2M_H^4}{64M_W^2}+\frac{C_AC_FY_f^2L(m)^2M_H^4}{32m^2M_W^2}+\frac{9Y_f^2L(m)^2M_H^4}{16m^2M_W^2}+\frac{9Y_f^2L(m)^2M_H^4}{32M_W^2}+$$
$$\frac{5C_AC_FY_f^2\zeta_2M_H^4}{128M_W^2}+\frac{5C_AC_FY_f^2\zeta_2M_H^4}{64m^2M_W^2}+\frac{45Y_f^2\zeta_2M_H^4}{32m^2M_W^2}+\frac{45Y_f^2\zeta_2M_H^4}{64M_W^2}-$$
$$\frac{5C_AC_FY_f^2L(m)M_H^4}{128M_W^2}-\frac{C_AC_FY_f^2L(m)M_H^4}{64\epsilon_{\rm IR}M_W^2}-\frac{9Y_f^2L(m)M_H^4}{32\epsilon_{\rm IR}M_W^2}-\frac{C_AC_FY_f^2L(m)M_H^4}{32\epsilon_{\rm IR}m^2M_W^2}-$$
$$\frac{9Y_f^2L(m)M_H^4}{16\epsilon_{\rm IR}m^2M_W^2}-\frac{45Y_f^2L(m)M_H^4}{64M_W^2}+\frac{3mY_f^3M_H^2}{32\epsilon_{\rm IR}M_W}+\frac{3mY_f^3M_H^2}{64\epsilon_{\rm IR}^2M_W}+\frac{3mY_f^3M_H^2}{16M_W}-$$
$$\frac{39Y_f^3M_H^2}{32\epsilon_{\rm IR}mM_W}+\frac{33Y_f^3M_H^2}{64\epsilon_{\rm IR}^2mM_W}+\frac{99Y_f^3M_H^2}{16mM_W}+\frac{3mY_f^3L(m)^2M_H^2}{32M_W}+\frac{33Y_f^3L(m)^2M_H^2}{32mM_W}-$$
$$\frac{3mY_f^3\zeta_2M_H^2}{16\epsilon_{\rm IR}M_W}-\frac{57mY_f^3\zeta_2M_H^2}{64M_W}-\frac{21Y_f^3\zeta_2M_H^2}{16\epsilon_{\rm IR}mM_W}-\frac{99Y_f^3\zeta_2M_H^2}{64mM_W}-\frac{3mY_f^3\zeta_3M_H^2}{8M_W}-$$
$$\frac{21Y_f^3\zeta_3M_H^2}{8mM_W}-\frac{3mY_f^3L(m)M_H^2}{32\epsilon_{\rm IR}M_W}-\frac{3mY_f^3L(m)M_H^2}{16M_W}-\frac{33Y_f^3L(m)M_H^2}{32\epsilon_{\rm IR}mM_W}+$$
$$\frac{39Y_f^3L(m)M_H^2}{16mM_W}+\frac{3mY_f^3\zeta_2L(m)M_H^2}{8M_W}+\frac{21Y_f^3\zeta_2L(m)M_H^2}{8mM_W}-\frac{21m^2Y_f^4}{32\epsilon_{\rm IR}}-\frac{11m^2Y_f^4}{64\epsilon_{\rm IR}^2}-$$

$$\frac{89m^2Y_f^4}{32}-\frac{539Y_f^4}{256\epsilon_{\rm IR}}-\frac{Y_f^4}{8\epsilon_{\rm IR}\epsilon_{\rm UV}}+\frac{5Y_f^4}{32\epsilon_{\rm UV}}-\frac{93Y_f^4}{128\epsilon_{\rm IR}^2}+\frac{Y_f^4}{16\epsilon_{\rm UV}^2}-\frac{3053Y_f^4}{512}-\frac{819C_F^2}{8}+$$
$$\frac{187}{4}C_F^2m^2-\frac{923}{32}C_AC_Fm^2-\frac{29C_Fm^2}{16}+\frac{21C_F^2m^2}{2\epsilon_{\rm IR}}+\frac{379C_AC_Fm^2}{32\epsilon_{\rm IR}}-\frac{C_Fm^2}{16\epsilon_{\rm IR}}+$$
$$\frac{8C_F^2m^2}{\epsilon_{\rm IR}^2}-\frac{33C_AC_Fm^2}{16\epsilon_{\rm IR}^2}-\frac{C_Fm^2}{8\epsilon_{\rm IR}^2}+\frac{29C_FM_W^2}{2}+\frac{3C_FM_W^2}{2\epsilon_{\rm IR}}+\frac{C_FM_W^2}{\epsilon_{\rm IR}^2}-\frac{19C_FM_W^2}{2m^2}+$$
$$\frac{9C_FM_W^2}{2\epsilon_{\rm IR}m^2}-\frac{C_FM_W^2}{\epsilon_{\rm IR}^2m^2}-\frac{13}{32}C_AC_Fm^2Y_f^2+\frac{113}{64}C_Fm^2Y_f^2+\frac{C_AC_Fm^2Y_f^2}{32\epsilon_{\rm IR}}+\frac{55C_Fm^2Y_f^2}{32\epsilon_{\rm IR}}-$$
$$\frac{C_AC_Fm^2Y_f^2}{16\epsilon_{\rm IR}^2}+\frac{3C_Fm^2Y_f^2}{16\epsilon_{\rm IR}^2}+\frac{63}{8}C_AC_FM_W^2Y_f^2+\frac{C_AC_FM_W^2Y_f^2}{\epsilon_{\rm IR}}+\frac{C_AC_FM_W^2Y_f^2}{2\epsilon_{\rm IR}^2}+$$
$$\frac{53C_AC_FM_W^2Y_f^2}{4m^2}-\frac{C_AC_FM_W^2Y_f^2}{2\epsilon_{\rm IR}m^2}+\frac{C_AC_FM_W^2Y_f^2}{\epsilon_{\rm IR}^2m^2}+\frac{389}{64}C_AC_FY_f^2+\frac{1963C_FY_f^2}{32}+$$
$$\frac{5C_AC_FY_f^2}{4\epsilon_{\rm IR}}+\frac{201C_FY_f^2}{16\epsilon_{\rm IR}}-\frac{C_FY_f^2}{4\epsilon_{\rm UV}}+\frac{C_FY_f^2}{2\epsilon_{\rm IR}\epsilon_{\rm UV}}+\frac{C_AC_FY_f^2}{4\epsilon_{\rm IR}^2}+\frac{61C_FY_f^2}{8\epsilon_{\rm IR}^2}-\frac{C_FY_f^2}{4\epsilon_{\rm UV}^2}-$$
$$\frac{11}{32}m^2Y_f^4L(m)^2-\frac{101}{64}Y_f^4L(m)^2-43C_F^2L(m)^2+16C_F^2m^2L(m)^2-$$
$$\frac{33}{8}C_AC_Fm^2L(m)^2-\frac{1}{4}C_Fm^2L(m)^2+2C_FM_W^2L(m)^2-\frac{2C_FM_W^2L(m)^2}{m^2}-$$
$$\frac{1}{8}C_AC_Fm^2Y_f^2L(m)^2+\frac{3}{8}C_Fm^2Y_f^2L(m)^2+C_AC_FM_W^2Y_f^2L(m)^2+$$
$$\frac{2C_AC_FM_W^2Y_f^2L(m)^2}{m^2}+\frac{1}{2}C_AC_FY_f^2L(m)^2+\frac{63}{4}C_FY_f^2L(m)^2-\frac{63}{4}C_AC_FL(m)^2+$$
$$\frac{1}{2}C_FL(m)^2+C_Fm^2n_fT_fL(m)^2+\frac{1}{2}C_FmM_WY_fL(m)^2-\frac{13C_FM_WY_fL(m)^2}{2m}-$$
$$\frac{5209C_AC_F}{64}+\frac{139C_F}{32}+\frac{25}{4}C_Fm^2n_fT_f+\frac{C_Fm^2n_fT_f}{2\epsilon_{\rm IR}}+\frac{C_Fm^2n_fT_f}{2\epsilon_{\rm IR}^2}+\frac{9}{8}C_Fn_fT_f+$$
$$\frac{9C_Fn_fT_f}{4\epsilon_{\rm IR}}-\frac{C_Fn_fT_f}{2\epsilon_{\rm UV}}+\frac{C_Fn_fT_f}{\epsilon_{\rm IR}\epsilon_{\rm UV}}-\frac{C_Fn_fT_f}{2\epsilon_{\rm IR}^2}-\frac{C_Fn_fT_f}{2\epsilon_{\rm UV}^2}+\frac{41}{4}C_FmM_WY_f-$$
$$\frac{C_FmM_WY_f}{\epsilon_{\rm IR}}+\frac{C_FmM_WY_f}{4\epsilon_{\rm IR}^2}-\frac{241C_FM_WY_f}{4m}+\frac{12C_FM_WY_f}{\epsilon_{\rm IR}m}-\frac{13C_FM_WY_f}{4\epsilon_{\rm IR}^2m}+$$
$$\frac{3}{4}l_2m^2Y_f^4\zeta_2-\frac{11}{64}m^2Y_f^4\zeta_2+\frac{21}{4}l_2Y_f^4\zeta_2-\frac{449Y_f^4\zeta_2}{128}-\frac{79C_F^2\zeta_2}{2}+8C_F^2m^2\zeta_2+$$
$$\frac{27}{16}C_AC_Fm^2\zeta_2-\frac{5}{8}C_Fm^2\zeta_2+\frac{6C_AC_Fm^2\zeta_2}{\epsilon_{\rm IR}}+5C_FM_W^2\zeta_2-\frac{5C_FM_W^2\zeta_2}{m^2}-$$
$$\frac{5}{16}C_AC_Fm^2Y_f^2\zeta_2+\frac{35}{16}C_Fm^2Y_f^2\zeta_2+6C_Fl_2m^2Y_f^2\zeta_2+\frac{5}{2}C_AC_FM_W^2Y_f^2\zeta_2+$$
$$\frac{5C_AC_FM_W^2Y_f^2\zeta_2}{m^2}+\frac{5}{4}C_AC_FY_f^2\zeta_2+\frac{107}{8}C_FY_f^2\zeta_2-30C_Fl_2Y_f^2\zeta_2-\frac{91}{8}C_AC_F\zeta_2+$$
$$\frac{5C_F\zeta_2}{4}+\frac{5}{2}C_Fm^2n_fT_f\zeta_2-\frac{11}{4}C_FmM_WY_f\zeta_2-\frac{2C_FmM_WY_f\zeta_2}{\epsilon_{\rm IR}}+\frac{47C_FM_WY_f\zeta_2}{4m}+$$
$$\frac{14C_FM_WY_f\zeta_2}{\epsilon_{\rm IR}m}-\frac{6C_AC_F\zeta_2}{\epsilon_{\rm IR}}-\frac{3}{16}m^2Y_f^4\zeta_3-\frac{21Y_f^4\zeta_3}{16}+12C_AC_Fm^2\zeta_3-\frac{3}{2}C_Fm^2Y_f^2\zeta_3+$$
$$\frac{15}{2}C_FY_f^2\zeta_3-12C_AC_F\zeta_3-4C_FmM_WY_f\zeta_3+\frac{28C_FM_WY_f\zeta_3}{m}+\frac{11m^2Y_f^4L(m)}{32\epsilon_{\rm IR}}+$$

$$\frac{21}{16}m^2Y_f^4L(m)+\frac{101Y_f^4L(m)}{64\epsilon_{\rm IR}}+\frac{499}{128}Y_f^4L(m)+\frac{57}{2}C_F^2L(m)-21C_F^2m^2L(m)-$$
$$\frac{379}{16}C_AC_Fm^2L(m)+\frac{1}{8}C_Fm^2L(m)-\frac{16C_F^2m^2L(m)}{\epsilon_{\rm IR}}+\frac{33C_AC_Fm^2L(m)}{8\epsilon_{\rm IR}}+$$
$$\frac{C_Fm^2L(m)}{4\epsilon_{\rm IR}}-3C_FM_W^2L(m)-\frac{2C_FM_W^2L(m)}{\epsilon_{\rm IR}}-\frac{9C_FM_W^2L(m)}{m^2}+\frac{2C_FM_W^2L(m)}{\epsilon_{\rm IR}m^2}-$$
$$\frac{1}{16}C_AC_Fm^2Y_f^2L(m)-\frac{55}{16}C_Fm^2Y_f^2L(m)+\frac{C_AC_Fm^2Y_f^2L(m)}{8\epsilon_{\rm IR}}-\frac{3C_Fm^2Y_f^2L(m)}{8\epsilon_{\rm IR}}-$$
$$2C_AC_FM_W^2Y_f^2L(m)-\frac{C_AC_FM_W^2Y_f^2L(m)}{\epsilon_{\rm IR}}+\frac{C_AC_FM_W^2Y_f^2L(m)}{m^2}-$$
$$\frac{2C_AC_FM_W^2Y_f^2L(m)}{\epsilon_{\rm IR}m^2}-\frac{5}{2}C_AC_FY_f^2L(m)-\frac{197}{8}C_FY_f^2L(m)-\frac{C_AC_FY_f^2L(m)}{2\epsilon_{\rm IR}}-$$
$$\frac{63C_FY_f^2L(m)}{4\epsilon_{\rm IR}}+93C_AC_FL(m)-\frac{3}{2}C_FL(m)-C_Fm^2n_fT_fL(m)-\frac{C_Fm^2n_fT_fL(m)}{\epsilon_{\rm IR}}-$$
$$\frac{7}{2}C_Fn_fT_fL(m)+2C_FmM_WY_fL(m)-\frac{C_FmM_WY_fL(m)}{2\epsilon_{\rm IR}}-\frac{24C_FM_WY_fL(m)}{m}+$$
$$\frac{13C_FM_WY_fL(m)}{2\epsilon_{\rm IR}m}-12C_AC_Fm^2\zeta_2L(m)+12C_AC_F\zeta_2L(m)+4C_FmM_WY_f\zeta_2L(m)-$$
$$\frac{28C_FM_WY_f\zeta_2L(m)}{m}+\frac{43C_F^2L(m)}{\epsilon_{\rm IR}}+\frac{63C_AC_FL(m)}{4\epsilon_{\rm IR}}-\frac{C_FL(m)}{2\epsilon_{\rm IR}}-\frac{57C_F^2}{4\epsilon_{\rm IR}}-\frac{93C_AC_F}{2\epsilon_{\rm IR}}+$$
$$\frac{3C_F}{4\epsilon_{\rm IR}}-\frac{4C_AC_F}{\epsilon_{\rm IR}\epsilon_{\rm UV}}-\frac{43C_F^2}{2\epsilon_{\rm IR}^2}-\frac{47C_AC_F}{8\epsilon_{\rm IR}^2}+\frac{C_F}{4\epsilon_{\rm IR}^2}+\frac{2C_AC_F}{\epsilon_{\rm UV}^2} \tag{B.53}$$

$$F_\chi^{(m,0)}=\frac{11C_A^2Y_s^2M_H^4}{512m^4M_W^2}-\frac{3C_AC_FY_s^2M_H^4}{512\epsilon_{\rm IR}m^4M_W^2}-\frac{27Y_s^2M_H^4}{256\epsilon_{\rm IR}m^4M_W^2}+\frac{C_AC_FY_s^2M_H^4}{256\epsilon_{\rm IR}^2m^4M_W^2}+\frac{9Y_s^2M_H^4}{128\epsilon_{\rm IR}^2m^4M_W^2}+$$
$$\frac{385Y_s^2M_H^4}{512m^4M_W^2}+\frac{C_A^2Y_s^2L(m)^2M_H^4}{256m^4M_W^2}+\frac{35Y_s^2L(m)^2M_H^4}{256m^4M_W^2}+\frac{5C_A^2Y_s^2\zeta_2M_H^4}{512m^4M_W^2}+\frac{175Y_s^2\zeta_2M_H^4}{512m^4M_W^2}+$$
$$\frac{3C_A^2Y_s^2L(m)M_H^4}{512m^4M_W^2}-\frac{C_AC_FY_s^2L(m)M_H^4}{128\epsilon_{\rm IR}m^4M_W^2}-\frac{9Y_s^2L(m)M_H^4}{64\epsilon_{\rm IR}m^4M_W^2}+\frac{105Y_s^2L(m)M_H^4}{512m^4M_W^2}-$$
$$\frac{3Y_s^3M_H^2}{16\epsilon_{\rm IR}m^4M_W}+\frac{3Y_s^3M_H^2}{64\epsilon_{\rm IR}^2m^4M_W}+\frac{3Y_s^3M_H^2}{4m^4M_W}+\frac{3Y_s^3L(m)^2M_H^2}{32m^4M_W}-\frac{3Y_s^3\zeta_2M_H^2}{16\epsilon_{\rm IR}m^4M_W}-$$
$$\frac{9Y_s^3\zeta_2M_H^2}{64m^4M_W}-\frac{3Y_s^3\zeta_3M_H^2}{8m^4M_W}-\frac{3Y_s^3L(m)M_H^2}{32\epsilon_{\rm IR}m^4M_W}+\frac{3Y_s^3L(m)M_H^2}{8m^4M_W}+\frac{3Y_s^3\zeta_2L(m)M_H^2}{8m^4M_W}-$$
$$\frac{5Y_s^4}{128\epsilon_{\rm IR}^2m^4}-\frac{3Y_s^4}{32m^4}+\frac{9Y_s^4}{32\epsilon_{\rm IR}M_W^4}+\frac{5Y_s^4}{16\epsilon_{\rm IR}\epsilon_{\rm UV}M_W^4}-\frac{9Y_s^4}{32\epsilon_{\rm UV}M_W^4}-\frac{5Y_s^4}{32\epsilon_{\rm IR}^2M_W^4}-$$
$$\frac{5Y_s^4}{32\epsilon_{\rm UV}^2M_W^4}-\frac{3Y_s^3}{8\epsilon_{\rm IR}M_W^3}+\frac{3Y_s^3}{8\epsilon_{\rm UV}M_W^3}-\frac{2811C_A^2}{128}-\frac{11C_AM_W^2}{2m^2}+\frac{11M_W^2}{2C_Am^2}-\frac{C_AM_W^2}{2\epsilon_{\rm IR}m^2}+$$
$$\frac{M_W^2}{2C_A\epsilon_{\rm IR}m^2}-\frac{3C_AM_W^2}{8\epsilon_{\rm IR}^2m^2}+\frac{3M_W^2}{8C_A\epsilon_{\rm IR}^2m^2}+\frac{47C_A^2M_W^2Y_s^2}{32m^4}-\frac{C_AC_FM_W^2Y_s^2}{2\epsilon_{\rm IR}m^4}+$$
$$\frac{C_AC_FM_W^2Y_s^2}{4\epsilon_{\rm IR}^2m^4}-\frac{47M_W^2Y_s^2}{32m^4}+\frac{3C_A^2Y_s^2}{4m^2}+\frac{5C_AY_s^2}{m^2}-\frac{5Y_s^2}{C_Am^2}+\frac{3C_AY_s^2}{2\epsilon_{\rm IR}m^2}+\frac{3C_AC_FY_s^2}{8\epsilon_{\rm IR}m^2}-$$
$$\frac{3Y_s^2}{2C_A\epsilon_{\rm IR}m^2}+\frac{5C_AY_s^2}{8\epsilon_{\rm IR}^2m^2}+\frac{C_AC_FY_s^2}{16\epsilon_{\rm IR}^2m^2}-\frac{5Y_s^2}{8C_A\epsilon_{\rm IR}^2m^2}-\frac{3Y_s^2}{4m^2}+\frac{65C_AC_FY_s^2}{64\epsilon_{\rm IR}M_W^2}+\frac{2C_FY_s^2}{\epsilon_{\rm IR}M_W^2}+$$

$$\frac{9Y_s^2}{32\epsilon_{\rm IR}M_W^2}-\frac{65C_AC_FY_s^2}{64\epsilon_{\rm UV}M_W^2}-\frac{2C_FY_s^2}{\epsilon_{\rm UV}M_W^2}+\frac{3C_FY_s^2}{\epsilon_{\rm IR}\epsilon_{\rm UV}M_W^2}-\frac{9Y_s^2}{32\epsilon_{\rm UV}M_W^2}-\frac{3C_FY_s^2}{2\epsilon_{\rm IR}^2M_W^2}-$$
$$\frac{3C_FY_s^2}{2\epsilon_{\rm UV}^2M_W^2}-\frac{5Y_s^4L(m)^2}{64m^4}-\frac{27}{8}C_A^2L(m)^2-\frac{3C_AM_W^2L(m)^2}{4m^2}+\frac{3M_W^2L(m)^2}{4C_Am^2}+$$
$$\frac{C_A^2M_W^2Y_s^2L(m)^2}{4m^4}-\frac{M_W^2Y_s^2L(m)^2}{4m^4}+\frac{C_A^2Y_s^2L(m)^2}{16m^2}+\frac{5C_AY_s^2L(m)^2}{4m^2}-\frac{5Y_s^2L(m)^2}{4C_Am^2}-$$
$$\frac{Y_s^2L(m)^2}{16m^2}+6C_AL(m)^2-\frac{3C_AM_WY_sL(m)^2}{m^2}+\frac{3M_WY_sL(m)^2}{C_Am^2}-\frac{6L(m)^2}{C_A}+\frac{27L(m)^2}{8}+$$
$$\frac{781C_A}{64}+\frac{11}{16}C_An_fT_f-\frac{11n_fT_f}{16C_A}+\frac{C_An_fT_f}{8\epsilon_{\rm IR}}+\frac{C_Fn_fT_f}{\epsilon_{\rm IR}}-\frac{n_fT_f}{8C_A\epsilon_{\rm IR}}-\frac{C_Fn_fT_f}{\epsilon_{\rm UV}}+$$
$$\frac{2C_Fn_fT_f}{\epsilon_{\rm IR}\epsilon_{\rm UV}}-\frac{C_Fn_fT_f}{\epsilon_{\rm IR}^2}-\frac{C_Fn_fT_f}{\epsilon_{\rm UV}^2}-\frac{81C_AM_WY_s}{4m^2}+\frac{81M_WY_s}{4C_Am^2}+\frac{C_AM_WY_s}{4\epsilon_{\rm IR}m^2}-$$
$$\frac{M_WY_s}{4C_A\epsilon_{\rm IR}m^2}-\frac{3C_AM_WY_s}{2\epsilon_{\rm IR}^2m^2}+\frac{3M_WY_s}{2C_A\epsilon_{\rm IR}^2m^2}+\frac{2C_FY_s}{\epsilon_{\rm IR}M_W}-\frac{2C_FY_s}{\epsilon_{\rm UV}M_W}+\frac{7C_FY_s}{\epsilon_{\rm IR}\epsilon_{\rm UV}M_W}-$$
$$\frac{7C_FY_s}{2\epsilon_{\rm IR}^2M_W}-\frac{7C_FY_s}{2\epsilon_{\rm UV}^2M_W}+\frac{3l_2Y_s^4\zeta_2}{8m^4}-\frac{15Y_s^4\zeta_2}{128m^4}-\frac{27C_A^2\zeta_2}{16}-\frac{15C_AM_W^2\zeta_2}{8m^2}+\frac{15M_W^2\zeta_2}{8C_Am^2}+$$
$$\frac{5C_A^2M_W^2Y_s^2\zeta_2}{8m^4}-\frac{5M_W^2Y_s^2\zeta_2}{8m^4}+\frac{5C_A^2Y_s^2\zeta_2}{32m^2}+\frac{17C_AY_s^2\zeta_2}{8m^2}-\frac{9C_Al_2Y_s^2\zeta_2}{4m^2}+\frac{9l_2Y_s^2\zeta_2}{4C_Am^2}-$$
$$\frac{17Y_s^2\zeta_2}{8C_Am^2}-\frac{5Y_s^2\zeta_2}{32m^2}+3C_A\zeta_2-\frac{C_AM_WY_s\zeta_2}{2m^2}+\frac{M_WY_s\zeta_2}{2C_Am^2}+\frac{2C_AM_WY_s\zeta_2}{\epsilon_{\rm IR}m^2}-\frac{2M_WY_s\zeta_2}{C_A\epsilon_{\rm IR}m^2}-$$
$$\frac{3\zeta_2}{C_A}+\frac{3\zeta_2}{2C_A^2}+\frac{3\zeta_2}{16}-\frac{3Y_s^4\zeta_3}{32m^4}+\frac{9C_AY_s^2\zeta_3}{16m^2}-\frac{9Y_s^2\zeta_3}{16C_Am^2}+\frac{4C_AM_WY_s\zeta_3}{m^2}-\frac{4M_WY_s\zeta_3}{C_Am^2}+$$
$$\frac{5Y_s^4L(m)}{64\epsilon_{\rm IR}m^4}+\frac{335}{32}C_A^2L(m)+\frac{C_AM_W^2L(m)}{m^2}-\frac{M_W^2L(m)}{C_Am^2}+\frac{3C_AM_W^2L(m)}{4\epsilon_{\rm IR}m^2}-$$
$$\frac{3M_W^2L(m)}{4C_A\epsilon_{\rm IR}m^2}+\frac{C_A^2M_W^2Y_s^2L(m)}{2m^4}-\frac{C_AC_FM_W^2Y_s^2L(m)}{2\epsilon_{\rm IR}m^4}-\frac{M_W^2Y_s^2L(m)}{2m^4}-\frac{3C_A^2Y_s^2L(m)}{8m^2}-$$
$$\frac{3C_AY_s^2L(m)}{m^2}+\frac{3Y_s^2L(m)}{C_Am^2}-\frac{5C_AY_s^2L(m)}{4\epsilon_{\rm IR}m^2}-\frac{C_AC_FY_s^2L(m)}{8\epsilon_{\rm IR}m^2}+\frac{5Y_s^2L(m)}{4C_A\epsilon_{\rm IR}m^2}+$$
$$\frac{3Y_s^2L(m)}{8m^2}-\frac{17}{16}C_AL(m)-\frac{1}{4}C_An_fT_fL(m)+\frac{n_fT_fL(m)}{4C_A}-\frac{C_AM_WY_sL(m)}{2m^2}+$$
$$\frac{M_WY_sL(m)}{2C_Am^2}+\frac{3C_AM_WY_sL(m)}{\epsilon_{\rm IR}m^2}-\frac{3M_WY_sL(m)}{C_A\epsilon_{\rm IR}m^2}-\frac{4C_AM_WY_s\zeta_2L(m)}{m^2}+$$
$$\frac{4M_WY_s\zeta_2L(m)}{C_Am^2}+\frac{17L(m)}{16C_A}-\frac{6C_AL(m)}{\epsilon_{\rm IR}}+\frac{27C_AC_FL(m)}{4\epsilon_{\rm IR}}+\frac{6L(m)}{C_A\epsilon_{\rm IR}}-\frac{47L(m)}{8C_A^2}-$$
$$\frac{147L(m)}{32}-\frac{781}{64C_A}+\frac{12C_F^2}{\epsilon_{\rm IR}}+\frac{17C_A}{32\epsilon_{\rm IR}}-\frac{919C_AC_F}{32\epsilon_{\rm IR}}+\frac{5C_F}{2\epsilon_{\rm IR}}-\frac{17}{32C_A\epsilon_{\rm IR}}+\frac{47}{16C_A^2\epsilon_{\rm IR}}-$$
$$\frac{47}{16\epsilon_{\rm IR}}-\frac{12C_F^2}{\epsilon_{\rm UV}}+\frac{73C_AC_F}{4\epsilon_{\rm UV}}-\frac{5C_F}{2\epsilon_{\rm UV}}+\frac{14C_F^2}{\epsilon_{\rm IR}\epsilon_{\rm UV}}-\frac{47C_AC_F}{4\epsilon_{\rm IR}\epsilon_{\rm UV}}-\frac{7C_F}{2\epsilon_{\rm IR}\epsilon_{\rm UV}}+\frac{217}{32C_A^2}-\frac{7C_F^2}{\epsilon_{\rm IR}^2}+$$
$$\frac{3C_A}{\epsilon_{\rm IR}^2}+\frac{5C_AC_F}{2\epsilon_{\rm IR}^2}+\frac{7C_F}{4\epsilon_{\rm IR}^2}-\frac{3}{C_A\epsilon_{\rm IR}^2}-\frac{7C_F^2}{\epsilon_{\rm UV}^2}+\frac{47C_AC_F}{8\epsilon_{\rm UV}^2}+\frac{7C_F}{4\epsilon_{\rm UV}^2}+\frac{1943}{128} \tag{B.54}$$

B.7.4 Fermion and Scalar Field at $m \neq 0$ and $M \neq 0$ ($\Delta_M \equiv M_H - M_W$, $\Delta_{m,M} \equiv M_W - m$):

$$
\begin{aligned}
F_{\psi}^{(m,M)} = {} & \frac{5}{64}L(m)^2Y_f^4 - \frac{39}{64}l_3S_1Y_f^4 + \frac{39S_1Y_f^4}{64\epsilon_{\rm UV}} + \frac{25\Delta_M S_1Y_f^4}{12m} + \frac{25\Delta_{m,M}S_1Y_f^4}{12m} - \frac{3\Delta_M l_3S_1Y_f^4}{16m} - \\
& \frac{3\Delta_{m,M}l_3S_1Y_f^4}{16m} + \frac{3\Delta_M S_1Y_f^4}{16\epsilon_{\rm UV}m} + \frac{3\Delta_{m,M}S_1Y_f^4}{16\epsilon_{\rm UV}m} + \frac{9S_1Y_f^4}{4} - \frac{117\Delta_M S_1S_2Y_f^4}{16m} - \\
& \frac{117\Delta_{m,M}S_1S_2Y_f^4}{16m} + \frac{81}{64}S_1S_2Y_f^4 - \frac{351\Delta_M S_2Y_f^4}{16m} - \frac{351\Delta_{m,M}S_2Y_f^4}{16m} + \frac{2295S_2Y_f^4}{256} + \\
& \frac{9\Delta_M\zeta_2Y_f^4}{8m} + \frac{9\Delta_{m,M}\zeta_2Y_f^4}{8m} - \frac{25\zeta_2Y_f^4}{32} + \frac{13\Delta_M\zeta_3Y_f^4}{8m} + \frac{13\Delta_{m,M}\zeta_3Y_f^4}{8m} - \frac{9\zeta_3Y_f^4}{32} - \\
& \frac{3\Delta_M S_1L(m)Y_f^4}{8m} - \frac{3\Delta_{m,M}S_1L(m)Y_f^4}{8m} - \frac{39}{32}S_1L(m)Y_f^4 - \frac{5L(m)Y_f^4}{64\epsilon_{\rm UV}} + \frac{7\Delta_M L(m)Y_f^4}{8m} + \\
& \frac{7\Delta_{m,M}L(m)Y_f^4}{8m} + \frac{271}{128}L(m)Y_f^4 - \frac{271Y_f^4}{256\epsilon_{\rm UV}} + \frac{37\Delta_M Y_f^4}{16m} + \frac{37\Delta_{m,M}Y_f^4}{16m} - \frac{7\Delta_M Y_f^4}{16\epsilon_{\rm UV}m} - \\
& \frac{7\Delta_{m,M}Y_f^4}{16\epsilon_{\rm UV}m} + \frac{5Y_f^4}{128\epsilon_{\rm UV}^2} - \frac{2229Y_f^4}{512} - \frac{13\Delta_M S_1Y_f^3}{4m} - \frac{23\Delta_{m,M}S_1Y_f^3}{8m} - \frac{3S_1Y_f^3}{8} - \\
& \frac{27\Delta_{m,M}S_1S_2Y_f^3}{8m} + \frac{27}{8}S_1S_2Y_f^3 + \frac{405\Delta_M S_2Y_f^3}{32m} + \frac{405\Delta_{m,M}S_2Y_f^3}{32m} + \frac{33\Delta_M\zeta_2Y_f^3}{16m} + \\
& \frac{33\Delta_{m,M}\zeta_2Y_f^3}{16m} + \frac{3\Delta_{m,M}\zeta_3Y_f^3}{4m} - \frac{3\zeta_3Y_f^3}{4} - \frac{3\Delta_M Y_f^3}{4m} - \frac{3\Delta_{m,M}Y_f^3}{8m} - \frac{3Y_f^3}{8} - \\
& \frac{1}{8}C_AC_FL(m)^2Y_f^2 - \frac{3}{8}C_FL(m)^2Y_f^2 + \frac{861}{128}C_AC_FY_f^2 + \frac{2327C_FY_f^2}{64} - \frac{521}{128}C_AC_FS_1Y_f^2 - \\
& \frac{19}{2}C_FS_1Y_f^2 + \frac{57}{64}C_AC_Fl_3S_1Y_f^2 + \frac{41}{8}C_Fl_3S_1Y_f^2 + \frac{9}{32}l_3S_1Y_f^2 - \frac{57C_AC_FS_1Y_f^2}{64\epsilon_{\rm UV}} - \\
& \frac{41C_FS_1Y_f^2}{8\epsilon_{\rm UV}} - \frac{9S_1Y_f^2}{32\epsilon_{\rm UV}} + \frac{1891C_AC_F\Delta_M S_1Y_f^2}{192m} + \frac{5C_F\Delta_M S_1Y_f^2}{6m} - \frac{193\Delta_M S_1Y_f^2}{32m} + \\
& \frac{C_AC_F\Delta_{m,M}S_1Y_f^2}{8m} - \frac{245C_F\Delta_{m,M}S_1Y_f^2}{36m} - \frac{11\Delta_{m,M}S_1Y_f^2}{4m} + \frac{25C_AC_F\Delta_M l_3S_1Y_f^2}{32m} + \\
& \frac{5C_F\Delta_M l_3S_1Y_f^2}{2m} + \frac{33\Delta_M l_3S_1Y_f^2}{16m} + \frac{9C_AC_F\Delta_{m,M}l_3S_1Y_f^2}{4m} + \frac{15C_F\Delta_{m,M}l_3S_1Y_f^2}{2m} + \\
& \frac{3\Delta_{m,M}l_3S_1Y_f^2}{2m} - \frac{25C_AC_F\Delta_M S_1Y_f^2}{32\epsilon_{\rm UV}m} - \frac{5C_F\Delta_M S_1Y_f^2}{2\epsilon_{\rm UV}m} - \frac{33\Delta_M S_1Y_f^2}{16\epsilon_{\rm UV}m} - \\
& \frac{9C_AC_F\Delta_{m,M}S_1Y_f^2}{4\epsilon_{\rm UV}m} - \frac{15C_F\Delta_{m,M}S_1Y_f^2}{2\epsilon_{\rm UV}m} - \frac{3\Delta_{m,M}S_1Y_f^2}{2\epsilon_{\rm UV}m} - \frac{105S_1Y_f^2}{64} + \\
& \frac{171}{64}C_AC_FS_2Y_f^2 - \frac{3501}{32}C_FS_2Y_f^2 - \frac{63}{4}C_FS_1S_2Y_f^2 + \frac{81C_F\Delta_M S_1S_2Y_f^2}{4m} - \\
& \frac{9C_F\Delta_{m,M}S_1S_2Y_f^2}{4m} - \frac{10317C_AC_F\Delta_M S_2Y_f^2}{128m} - \frac{99C_F\Delta_M S_2Y_f^2}{2m} - \frac{513\Delta_M S_2Y_f^2}{32m} - \\
& \frac{3051C_AC_F\Delta_{m,M}S_2Y_f^2}{64m} - \frac{639C_F\Delta_{m,M}S_2Y_f^2}{4m} - \frac{675\Delta_{m,M}S_2Y_f^2}{32m} + \frac{81S_2Y_f^2}{32} - \\
& \frac{57}{64}C_AC_F\zeta_2Y_f^2 + \frac{5}{2}C_F\zeta_2Y_f^2 + \frac{101C_AC_F\Delta_M\zeta_2Y_f^2}{64m} + \frac{C_F\Delta_M\zeta_2Y_f^2}{m} - \frac{9\Delta_M\zeta_2Y_f^2}{8m} -
\end{aligned}
$$

$$\frac{33C_AC_F\Delta_{m,M}\zeta_2Y_f^2}{32m}+\frac{35C_F\Delta_{m,M}\zeta_2Y_f^2}{3m}-\frac{9\Delta_{m,M}\zeta_2Y_f^2}{16m}-\frac{9\zeta_2Y_f^2}{32}+\frac{7}{2}C_F\zeta_3Y_f^2-$$
$$\frac{9C_F\Delta_M\zeta_3Y_f^2}{2m}+\frac{C_F\Delta_{m,M}\zeta_3Y_f^2}{2m}-\frac{59}{32}C_AC_FL(m)Y_f^2-\frac{293}{16}C_FL(m)Y_f^2+$$
$$\frac{57}{32}C_AC_FS_1L(m)Y_f^2+\frac{41}{4}C_FS_1L(m)Y_f^2+\frac{25C_AC_F\Delta_MS_1L(m)Y_f^2}{16m}+$$
$$\frac{5C_F\Delta_MS_1L(m)Y_f^2}{m}+\frac{33\Delta_MS_1L(m)Y_f^2}{8m}+\frac{9C_AC_F\Delta_{m,M}S_1L(m)Y_f^2}{2m}+$$
$$\frac{15C_F\Delta_{m,M}S_1L(m)Y_f^2}{m}+\frac{3\Delta_{m,M}S_1L(m)Y_f^2}{m}+\frac{9}{16}S_1L(m)Y_f^2+\frac{C_AC_FL(m)Y_f^2}{8\epsilon_{\rm UV}}+$$
$$\frac{3C_FL(m)Y_f^2}{8\epsilon_{\rm UV}}-\frac{51C_AC_F\Delta_ML(m)Y_f^2}{8m}-\frac{9C_F\Delta_ML(m)Y_f^2}{m}-\frac{27\Delta_ML(m)Y_f^2}{4m}-$$
$$\frac{149C_AC_F\Delta_{m,M}L(m)Y_f^2}{16m}-\frac{27C_F\Delta_{m,M}L(m)Y_f^2}{m}-\frac{45\Delta_{m,M}L(m)Y_f^2}{8m}-\frac{9}{16}L(m)Y_f^2+$$
$$\frac{59C_AC_FY_f^2}{64\epsilon_{\rm UV}}+\frac{293C_FY_f^2}{32\epsilon_{\rm UV}}+\frac{9Y_f^2}{32\epsilon_{\rm UV}}-\frac{29C_AC_F\Delta_MY_f^2}{64m}-\frac{2C_F\Delta_MY_f^2}{m}+\frac{435\Delta_MY_f^2}{32m}+$$
$$\frac{191C_AC_F\Delta_{m,M}Y_f^2}{16m}+\frac{197C_F\Delta_{m,M}Y_f^2}{12m}+\frac{75\Delta_{m,M}Y_f^2}{8m}+\frac{51C_AC_F\Delta_MY_f^2}{16\epsilon_{\rm UV}m}+$$
$$\frac{9C_F\Delta_MY_f^2}{2\epsilon_{\rm UV}m}+\frac{27\Delta_MY_f^2}{8\epsilon_{\rm UV}m}+\frac{149C_AC_F\Delta_{m,M}Y_f^2}{32\epsilon_{\rm UV}m}+\frac{27C_F\Delta_{m,M}Y_f^2}{2\epsilon_{\rm UV}m}+\frac{45\Delta_{m,M}Y_f^2}{16\epsilon_{\rm UV}m}-$$
$$\frac{C_AC_FY_f^2}{16\epsilon_{\rm UV}^2}-\frac{3C_FY_f^2}{16\epsilon_{\rm UV}^2}+\frac{135Y_f^2}{64}-\frac{22C_F\Delta_MS_1Y_f}{3m}+\frac{8C_F\Delta_{m,M}S_1Y_f}{m}-54C_FS_1S_2Y_f+$$
$$\frac{72C_F\Delta_MS_1S_2Y_f}{m}-\frac{54C_F\Delta_{m,M}S_1S_2Y_f}{m}+\frac{297C_F\Delta_MS_2Y_f}{2m}+\frac{108C_F\Delta_{m,M}S_2Y_f}{m}+$$
$$8C_F\zeta_2Y_f-\frac{77C_F\Delta_M\zeta_2Y_f}{3m}-\frac{64C_F\Delta_{m,M}\zeta_2Y_f}{3m}+12C_F\zeta_3Y_f-\frac{16C_F\Delta_M\zeta_3Y_f}{m}+$$
$$\frac{12C_F\Delta_{m,M}\zeta_3Y_f}{m}-\frac{21C_F^2}{8}+C_F^2L(m)^2-3C_AC_FL(m)^2-\frac{45233C_AC_F}{192}+\frac{1231C_F}{96}-$$
$$\frac{86C_F^2S_1}{3}+\frac{3461}{36}C_AC_FS_1-\frac{29C_FS_1}{18}-3C_F^2l_3S_1-\frac{1025}{24}C_AC_Fl_3S_1+\frac{85}{36}C_Fl_3S_1+$$
$$\frac{3C_F^2S_1}{\epsilon_{\rm UV}}+\frac{1025C_AC_FS_1}{24\epsilon_{\rm UV}}-\frac{85C_FS_1}{36\epsilon_{\rm UV}}+\frac{79C_F\Delta_MS_1}{18m}-\frac{536C_F^2\Delta_{m,M}S_1}{9m}+$$
$$\frac{2779C_AC_F\Delta_{m,M}S_1}{36m}+\frac{233C_F\Delta_{m,M}S_1}{54m}-\frac{5C_F\Delta_Ml_3S_1}{3m}-\frac{100C_F^2\Delta_{m,M}l_3S_1}{3m}-$$
$$\frac{93C_AC_F\Delta_{m,M}l_3S_1}{2m}+\frac{19C_F\Delta_{m,M}l_3S_1}{9m}+\frac{5C_F\Delta_MS_1}{3\epsilon_{\rm UV}m}+\frac{100C_F^2\Delta_{m,M}S_1}{3\epsilon_{\rm UV}m}+$$
$$\frac{93C_AC_F\Delta_{m,M}S_1}{2\epsilon_{\rm UV}m}-\frac{19C_F\Delta_{m,M}S_1}{9\epsilon_{\rm UV}m}+\frac{999C_F^2S_2}{4}+\frac{19167}{32}C_AC_FS_2-\frac{817C_FS_2}{16}+$$
$$72C_AC_FS_1S_2+\frac{225C_AC_F\Delta_{m,M}S_1S_2}{m}+\frac{27C_F\Delta_MS_2}{2m}+\frac{1164C_F^2\Delta_{m,M}S_2}{m}+$$
$$\frac{4113C_AC_F\Delta_{m,M}S_2}{8m}-\frac{427C_F\Delta_{m,M}S_2}{4m}+\frac{377}{24}C_Fn_fT_f+\frac{55C_Fn_fT_f}{12\epsilon_{\rm UV}}+$$
$$\frac{134C_F\Delta_{m,M}n_fT_f}{9m}+\frac{6C_F\Delta_{m,M}n_fT_f}{\epsilon_{\rm UV}m}-5C_Fn_fS_1T_f+\frac{25}{9}C_Fl_3n_fS_1T_f-$$

$$\frac{25C_F n_f S_1 T_f}{9\epsilon_{\rm UV}} + \frac{46C_F\Delta_{m,M} n_f S_1 T_f}{27m} + \frac{28C_F\Delta_{m,M} l_3 n_f S_1 T_f}{9m} - \frac{28C_F\Delta_{m,M} n_f S_1 T_f}{9\epsilon_{\rm UV} m} -$$
$$\frac{175}{4}C_F n_f S_2 T_f - \frac{49C_F\Delta_{m,M} n_f S_2 T_f}{m} - 8C_F^2\zeta_2 - \frac{287}{16}C_A C_F\zeta_2 - \frac{5C_F\zeta_2}{24} -$$
$$\frac{1}{2}C_F n_f T_f\zeta_2 - \frac{6C_F\Delta_{m,M} n_f T_f\zeta_2}{m} + \frac{7C_F\Delta_M\zeta_2}{9m} - \frac{56C_F^2\Delta_{m,M}\zeta_2}{m} -$$
$$\frac{223C_A C_F\Delta_{m,M}\zeta_2}{12m} + \frac{55C_F\Delta_{m,M}\zeta_2}{18m} - 16C_A C_F\zeta_3 - \frac{50C_A C_F\Delta_{m,M}\zeta_3}{m} + \frac{19}{2}C_F^2 L(m) +$$
$$\frac{2291}{16}C_A C_F L(m) - \frac{199}{24}C_F L(m) - 6C_F^2 S_1 L(m) - \frac{1025}{12}C_A C_F S_1 L(m) +$$
$$\frac{85}{18}C_F S_1 L(m) - \frac{10C_F\Delta_M S_1 L(m)}{3m} - \frac{200C_F^2\Delta_{m,M} S_1 L(m)}{3m} -$$
$$\frac{93C_A C_F\Delta_{m,M} S_1 L(m)}{m} + \frac{38C_F\Delta_{m,M} S_1 L(m)}{9m} - \frac{55}{6}C_F n_f T_f L(m) -$$
$$\frac{12C_F\Delta_{m,M} n_f T_f L(m)}{m} + \frac{50}{9}C_F n_f S_1 T_f L(m) + \frac{56C_F\Delta_{m,M} n_f S_1 T_f L(m)}{9m} -$$
$$\frac{C_F^2 L(m)}{\epsilon_{\rm UV}} + \frac{3C_A C_F L(m)}{\epsilon_{\rm UV}} + \frac{6C_F\Delta_M L(m)}{m} + \frac{120C_F^2\Delta_{m,M} L(m)}{m} +$$
$$\frac{329C_A C_F\Delta_{m,M} L(m)}{2m} - \frac{7C_F\Delta_{m,M} L(m)}{m} - \frac{19C_F^2}{4\epsilon_{\rm UV}} - \frac{2291C_A C_F}{32\epsilon_{\rm UV}} + \frac{199C_F}{48\epsilon_{\rm UV}} -$$
$$\frac{61C_F\Delta_M}{6m} - \frac{76C_F^2\Delta_{m,M}}{3m} - \frac{626C_A C_F\Delta_{m,M}}{3m} + \frac{104C_F\Delta_{m,M}}{9m} - \frac{3C_F\Delta_M}{\epsilon_{\rm UV} m} -$$
$$\frac{60C_F^2\Delta_{m,M}}{\epsilon_{\rm UV} m} - \frac{329C_A C_F\Delta_{m,M}}{4\epsilon_{\rm UV} m} + \frac{7C_F\Delta_{m,M}}{2\epsilon_{\rm UV} m} + \frac{C_F^2}{2\epsilon_{\rm UV}^2} - \frac{3C_A C_F}{2\epsilon_{\rm UV}^2} \qquad \text{(B.55)}$$

$$F_\chi^{(m,M)} = -\frac{l_3 S_1 Y_s^4}{144m^4} + \frac{S_1 Y_s^4}{144\epsilon_{\rm UV} m^4} - \frac{5S_1 Y_s^4}{144m^4} + \frac{31\Delta_M S_1 Y_s^4}{216m^5} + \frac{31\Delta_{m,M} S_1 Y_s^4}{216m^5} - \frac{\Delta_M l_3 S_1 Y_s^4}{18m^5} -$$
$$\frac{\Delta_{m,M} l_3 S_1 Y_s^4}{18m^5} + \frac{\Delta_M S_1 Y_s^4}{18\epsilon_{\rm UV} m^5} + \frac{\Delta_{m,M} S_1 Y_s^4}{18\epsilon_{\rm UV} m^5} + \frac{9S_1 S_2 Y_s^4}{32m^4} + \frac{31S_2 Y_s^4}{64m^4} + \frac{61\Delta_M S_2 Y_s^4}{32m^5} +$$
$$\frac{61\Delta_{m,M} S_2 Y_s^4}{32m^5} - \frac{5\zeta_2 Y_s^4}{96m^4} - \frac{13\Delta_M\zeta_2 Y_s^4}{48m^5} - \frac{13\Delta_{m,M}\zeta_2 Y_s^4}{48m^5} - \frac{\zeta_3 Y_s^4}{16m^4} - \frac{S_1 L(m) Y_s^4}{72m^4} -$$
$$\frac{\Delta_M S_1 L(m) Y_s^4}{9m^5} - \frac{\Delta_{m,M} S_1 L(m) Y_s^4}{9m^5} + \frac{L(m) Y_s^4}{24m^4} + \frac{\Delta_M L(m) Y_s^4}{6m^5} + \frac{\Delta_{m,M} L(m) Y_s^4}{6m^5} -$$
$$\frac{Y_s^4}{48\epsilon_{\rm UV} m^4} - \frac{Y_s^4}{24m^4} - \frac{5\Delta_M Y_s^4}{36m^5} - \frac{5\Delta_{m,M} Y_s^4}{36m^5} - \frac{\Delta_M Y_s^4}{12\epsilon_{\rm UV} m^5} - \frac{\Delta_{m,M} Y_s^4}{12\epsilon_{\rm UV} m^5} - \frac{\Delta_M S_1 Y_s^3}{8m^4} -$$
$$\frac{\Delta_{m,M} S_1 Y_s^3}{8m^4} + \frac{27S_1 S_2 Y_s^3}{32m^3} + \frac{27\Delta_M S_1 S_2 Y_s^3}{16m^4} + \frac{27\Delta_{m,M} S_1 S_2 Y_s^3}{32m^4} - \frac{27\Delta_M S_2 Y_s^3}{16m^4} -$$
$$\frac{27\Delta_{m,M} S_2 Y_s^3}{16m^4} - \frac{\zeta_2 Y_s^3}{8m^3} + \frac{5\Delta_M\zeta_2 Y_s^3}{24m^4} + \frac{\Delta_{m,M}\zeta_2 Y_s^3}{3m^4} - \frac{3\zeta_3 Y_s^3}{16m^3} - \frac{3\Delta_M\zeta_3 Y_s^3}{8m^4} -$$
$$\frac{3\Delta_{m,M}\zeta_3 Y_s^3}{16m^4} - \frac{191C_A C_F S_1 Y_s^2}{192m^2} - \frac{101C_F S_1 Y_s^2}{36m^2} + \frac{7C_A C_F l_3 S_1 Y_s^2}{64m^2} + \frac{3C_F l_3 S_1 Y_s^2}{4m^2} -$$
$$\frac{l_3 S_1 Y_s^2}{32m^2} - \frac{7C_A C_F S_1 Y_s^2}{64\epsilon_{\rm UV} m^2} - \frac{3C_F S_1 Y_s^2}{4\epsilon_{\rm UV} m^2} + \frac{S_1 Y_s^2}{32\epsilon_{\rm UV} m^2} - \frac{5S_1 Y_s^2}{32m^2} + \frac{59C_A C_F\Delta_M S_1 Y_s^2}{48m^3} -$$
$$\frac{35C_F\Delta_M S_1 Y_s^2}{18m^3} - \frac{19\Delta_M S_1 Y_s^2}{24m^3} - \frac{109C_A C_F\Delta_{m,M} S_1 Y_s^2}{288m^3} - \frac{29C_F\Delta_{m,M} S_1 Y_s^2}{6m^3} -$$
$$\frac{23\Delta_{m,M} S_1 Y_s^2}{48m^3} + \frac{9C_A C_F\Delta_M l_3 S_1 Y_s^2}{16m^3} + \frac{C_F\Delta_M l_3 S_1 Y_s^2}{6m^3} + \frac{\Delta_M l_3 S_1 Y_s^2}{8m^3} +$$

$$\frac{115C_AC_F\Delta_{m,M}l_3S_1Y_s^2}{288m^3}+\frac{C_F\Delta_{m,M}l_3S_1Y_s^2}{2m^3}+\frac{3\Delta_{m,M}l_3S_1Y_s^2}{16m^3}-\frac{9C_AC_F\Delta_MS_1Y_s^2}{16\epsilon_{\rm UV}m^3}-$$
$$\frac{C_F\Delta_MS_1Y_s^2}{6\epsilon_{\rm UV}m^3}-\frac{\Delta_MS_1Y_s^2}{8\epsilon_{\rm UV}m^3}-\frac{115C_AC_F\Delta_{m,M}S_1Y_s^2}{288\epsilon_{\rm UV}m^3}-\frac{C_F\Delta_{m,M}S_1Y_s^2}{2\epsilon_{\rm UV}m^3}-\frac{3\Delta_{m,M}S_1Y_s^2}{16\epsilon_{\rm UV}m^3}+$$
$$\frac{9C_F\Delta_MS_1S_2Y_s^2}{2m^3}+\frac{27C_F\Delta_{m,M}S_1S_2Y_s^2}{4m^3}+\frac{855C_AC_FS_2Y_s^2}{256m^2}-\frac{63C_FS_2Y_s^2}{4m^2}+\frac{279S_2Y_s^2}{128m^2}-$$
$$\frac{1467C_AC_F\Delta_MS_2Y_s^2}{64m^3}+\frac{27C_F\Delta_MS_2Y_s^2}{8m^3}+\frac{63\Delta_MS_2Y_s^2}{16m^3}-\frac{523C_AC_F\Delta_{m,M}S_2Y_s^2}{128m^3}+$$
$$\frac{147C_F\Delta_{m,M}S_2Y_s^2}{8m^3}-\frac{27\Delta_{m,M}S_2Y_s^2}{64m^3}-\frac{73C_AC_F\zeta_2Y_s^2}{384m^2}+\frac{3C_F\zeta_2Y_s^2}{4m^2}-\frac{3\zeta_2Y_s^2}{64m^2}+$$
$$\frac{5C_AC_F\Delta_M\zeta_2Y_s^2}{32m^3}-\frac{5C_F\Delta_M\zeta_2Y_s^2}{6m^3}-\frac{13\Delta_M\zeta_2Y_s^2}{48m^3}-\frac{457C_AC_F\Delta_{m,M}\zeta_2Y_s^2}{1728m^3}-$$
$$\frac{19C_F\Delta_{m,M}\zeta_2Y_s^2}{12m^3}-\frac{17\Delta_{m,M}\zeta_2Y_s^2}{96m^3}-\frac{C_F\Delta_M\zeta_3Y_s^2}{m^3}-\frac{3C_F\Delta_{m,M}\zeta_3Y_s^2}{2m^3}+$$
$$\frac{7C_AC_FS_1L(m)Y_s^2}{32m^2}+\frac{3C_FS_1L(m)Y_s^2}{2m^2}-\frac{S_1L(m)Y_s^2}{16m^2}+\frac{9C_AC_F\Delta_MS_1L(m)Y_s^2}{8m^3}+$$
$$\frac{C_F\Delta_MS_1L(m)Y_s^2}{3m^3}+\frac{\Delta_MS_1L(m)Y_s^2}{4m^3}+\frac{115C_AC_F\Delta_{m,M}S_1L(m)Y_s^2}{144m^3}+$$
$$\frac{C_F\Delta_{m,M}S_1L(m)Y_s^2}{m^3}+\frac{3\Delta_{m,M}S_1L(m)Y_s^2}{8m^3}-\frac{5C_AC_FL(m)Y_s^2}{32m^2}-\frac{3C_FL(m)Y_s^2}{m^2}+$$
$$\frac{3L(m)Y_s^2}{16m^2}-\frac{43C_AC_F\Delta_ML(m)Y_s^2}{16m^3}-\frac{C_F\Delta_ML(m)Y_s^2}{m^3}-\frac{3\Delta_ML(m)Y_s^2}{8m^3}-$$
$$\frac{41C_AC_F\Delta_{m,M}L(m)Y_s^2}{24m^3}-\frac{C_F\Delta_{m,M}L(m)Y_s^2}{m^3}-\frac{3\Delta_{m,M}L(m)Y_s^2}{4m^3}+\frac{33C_AC_FY_s^2}{32m^2}+$$
$$\frac{20C_FY_s^2}{3m^2}+\frac{5C_AC_FY_s^2}{64\epsilon_{\rm UV}m^2}+\frac{3C_FY_s^2}{2\epsilon_{\rm UV}m^2}-\frac{3Y_s^2}{32\epsilon_{\rm UV}m^2}-\frac{3Y_s^2}{16m^2}+\frac{83C_AC_F\Delta_MY_s^2}{32m^3}+$$
$$\frac{8C_F\Delta_MY_s^2}{3m^3}+\frac{11\Delta_MY_s^2}{16m^3}+\frac{57C_AC_F\Delta_{m,M}Y_s^2}{32m^3}+\frac{10C_F\Delta_{m,M}Y_s^2}{3m^3}+\frac{17\Delta_{m,M}Y_s^2}{16m^3}+$$
$$\frac{43C_AC_F\Delta_MY_s^2}{32\epsilon_{\rm UV}m^3}+\frac{C_F\Delta_MY_s^2}{2\epsilon_{\rm UV}m^3}+\frac{3\Delta_MY_s^2}{16\epsilon_{\rm UV}m^3}+\frac{41C_AC_F\Delta_{m,M}Y_s^2}{48\epsilon_{\rm UV}m^3}+\frac{C_F\Delta_{m,M}Y_s^2}{2\epsilon_{\rm UV}m^3}+$$
$$\frac{3\Delta_{m,M}Y_s^2}{8\epsilon_{\rm UV}m^3}+\frac{43C_FS_1Y_s}{6m}-\frac{2C_Fl_3S_1Y_s}{m}+\frac{2C_FS_1Y_s}{\epsilon_{\rm UV}m}-\frac{17C_F\Delta_MS_1Y_s}{18m^2}+$$
$$\frac{107C_F\Delta_{m,M}S_1Y_s}{9m^2}-\frac{2C_F\Delta_Ml_3S_1Y_s}{3m^2}-\frac{8C_F\Delta_{m,M}l_3S_1Y_s}{3m^2}+\frac{2C_F\Delta_MS_1Y_s}{3\epsilon_{\rm UV}m^2}+$$
$$\frac{8C_F\Delta_{m,M}S_1Y_s}{3\epsilon_{\rm UV}m^2}-\frac{63C_FS_1S_2Y_s}{8m}+\frac{27C_F\Delta_MS_1S_2Y_s}{4m^2}+\frac{99C_F\Delta_{m,M}S_1S_2Y_s}{8m^2}+$$
$$\frac{18C_FS_2Y_s}{m}+\frac{24C_F\Delta_MS_2Y_s}{m^2}+\frac{39C_F\Delta_{m,M}S_2Y_s}{2m^2}+\frac{C_F\zeta_2Y_s}{m}-\frac{7C_F\Delta_M\zeta_2Y_s}{3m^2}-$$
$$\frac{25C_F\Delta_{m,M}\zeta_2Y_s}{3m^2}+\frac{7C_F\zeta_3Y_s}{4m}-\frac{3C_F\Delta_M\zeta_3Y_s}{2m^2}-\frac{11C_F\Delta_{m,M}\zeta_3Y_s}{4m^2}-\frac{4C_FS_1L(m)Y_s}{m}-$$
$$\frac{4C_F\Delta_MS_1L(m)Y_s}{3m^2}-\frac{16C_F\Delta_{m,M}S_1L(m)Y_s}{3m^2}+\frac{6C_FL(m)Y_s}{m}+\frac{4C_F\Delta_ML(m)Y_s}{m^2}+$$
$$\frac{10C_F\Delta_{m,M}L(m)Y_s}{m^2}-\frac{23C_FY_s}{2m}-\frac{3C_FY_s}{\epsilon_{\rm UV}m}-\frac{8C_F\Delta_MY_s}{3m^2}-\frac{85C_F\Delta_{m,M}Y_s}{6m^2}-$$
$$\frac{2C_F\Delta_MY_s}{\epsilon_{\rm UV}m^2}-\frac{5C_F\Delta_{m,M}Y_s}{\epsilon_{\rm UV}m^2}-\frac{131C_F^2}{8}-8C_F^2L(m)^2+\frac{105}{8}C_AC_FL(m)^2-$$

$$\frac{1}{4}C_F L(m)^2 - C_F n_f T_f L(m)^2 + \frac{2045 C_A C_F}{64} + \frac{659 C_F}{96} - \frac{493}{24} C_A C_F S_1 - \frac{89 C_F S_1}{12} +$$
$$\frac{53}{8} C_A C_F l_3 S_1 + \frac{41}{12} C_F l_3 S_1 - \frac{53 C_A C_F S_1}{8\epsilon_{\rm UV}} - \frac{41 C_F S_1}{12\epsilon_{\rm UV}} - \frac{5 C_F \Delta_M S_1}{3m} +$$
$$\frac{134 C_F^2 \Delta_{m,M} S_1}{3m} - \frac{1243 C_A C_F \Delta_{m,M} S_1}{18m} + \frac{16 C_F \Delta_{m,M} S_1}{3m} + \frac{C_F \Delta_M l_3 S_1}{2m} -$$
$$\frac{2 C_F^2 \Delta_{m,M} l_3 S_1}{m} + \frac{185 C_A C_F \Delta_{m,M} l_3 S_1}{6m} + \frac{29 C_F \Delta_{m,M} l_3 S_1}{9m} - \frac{C_F \Delta_M S_1}{2\epsilon_{\rm UV} m} +$$
$$\frac{2 C_F^2 \Delta_{m,M} S_1}{\epsilon_{\rm UV} m} - \frac{185 C_A C_F \Delta_{m,M} S_1}{6\epsilon_{\rm UV} m} - \frac{29 C_F \Delta_{m,M} S_1}{9\epsilon_{\rm UV} m} + \frac{81 C_F^2 S_2}{2} - \frac{1089}{32} C_A C_F S_2 -$$
$$\frac{609 C_F S_2}{16} + \frac{63}{8} C_A C_F S_1 S_2 - \frac{9 C_A C_F \Delta_{m,M} S_1 S_2}{2m} + \frac{3 C_F \Delta_M S_2}{8m} - \frac{99 C_F^2 \Delta_{m,M} S_2}{2m} -$$
$$\frac{2787 C_A C_F \Delta_{m,M} S_2}{8m} - \frac{53 C_F \Delta_{m,M} S_2}{4m} - \frac{55}{24} C_F n_f T_f - \frac{3 C_F n_f T_f}{4\epsilon_{\rm UV}} - \frac{8 C_F \Delta_{m,M} n_f T_f}{m} -$$
$$\frac{4 C_F \Delta_{m,M} n_f T_f}{3\epsilon_{\rm UV} m} - \frac{C_F n_f T_f}{2\epsilon_{\rm UV}^2} + \frac{4}{3} C_F n_f S_1 T_f - \frac{1}{3} C_F l_3 n_f S_1 T_f + \frac{C_F n_f S_1 T_f}{3\epsilon_{\rm UV}} +$$
$$\frac{8 C_F \Delta_{m,M} n_f S_1 T_f}{3m} - \frac{16 C_F \Delta_{m,M} l_3 n_f S_1 T_f}{9m} + \frac{16 C_F \Delta_{m,M} n_f S_1 T_f}{9\epsilon_{\rm UV} m} + \frac{21}{4} C_F n_f S_2 T_f +$$
$$\frac{28 C_F \Delta_{m,M} n_f S_2 T_f}{m} - C_F^2 \zeta_2 + \frac{C_F \zeta_2}{4} - 2 C_F n_f T_f \zeta_2 + \frac{C_F \Delta_M \zeta_2}{12m} - \frac{5 C_F^2 \Delta_{m,M} \zeta_2}{m} +$$
$$\frac{29 C_A C_F \Delta_{m,M} \zeta_2}{4m} - \frac{43 C_F \Delta_{m,M} \zeta_2}{6m} - \frac{7}{4} C_A C_F \zeta_3 + \frac{C_A C_F \Delta_{m,M} \zeta_3}{m} + \frac{9}{2} C_F^2 L(m) -$$
$$\frac{343}{16} C_A C_F L(m) + \frac{21}{8} C_F L(m) + \frac{53}{4} C_A C_F S_1 L(m) + \frac{41}{6} C_F S_1 L(m) +$$
$$\frac{C_F \Delta_M S_1 L(m)}{m} - \frac{4 C_F^2 \Delta_{m,M} S_1 L(m)}{m} + \frac{185 C_A C_F \Delta_{m,M} S_1 L(m)}{3m} +$$
$$\frac{58 C_F \Delta_{m,M} S_1 L(m)}{9m} + \frac{3}{2} C_F n_f T_f L(m) + \frac{C_F n_f T_f L(m)}{\epsilon_{\rm UV}} + \frac{8 C_F \Delta_{m,M} n_f T_f L(m)}{3m} -$$
$$\frac{2}{3} C_F n_f S_1 T_f L(m) - \frac{32 C_F \Delta_{m,M} n_f S_1 T_f L(m)}{9m} + \frac{8 C_F^2 L(m)}{\epsilon_{\rm UV}} - \frac{105 C_A C_F L(m)}{8\epsilon_{\rm UV}} +$$
$$\frac{C_F L(m)}{4\epsilon_{\rm UV}} - \frac{36 C_F^2 \Delta_{m,M} L(m)}{m} - \frac{64 C_A C_F \Delta_{m,M} L(m)}{m} - \frac{124 C_F \Delta_{m,M} L(m)}{3m} - \frac{9 C_F^2}{4\epsilon_{\rm UV}} +$$
$$\frac{343 C_A C_F}{32\epsilon_{\rm UV}} - \frac{21 C_F}{16\epsilon_{\rm UV}} + \frac{C_F \Delta_M}{2m} - \frac{50 C_F^2 \Delta_{m,M}}{m} + \frac{913 C_A C_F \Delta_{m,M}}{6m} + \frac{33 C_F \Delta_{m,M}}{m} +$$
$$\frac{18 C_F^2 \Delta_{m,M}}{\epsilon_{\rm UV} m} + \frac{32 C_A C_F \Delta_{m,M}}{\epsilon_{\rm UV} m} + \frac{62 C_F \Delta_{m,M}}{3\epsilon_{\rm UV} m} - \frac{4 C_F^2}{\epsilon_{\rm UV}^2} + \frac{105 C_A C_F}{16\epsilon_{\rm UV}^2} - \frac{C_F}{8\epsilon_{\rm UV}^2} \qquad \text{(B.56)}$$

B.8 Parametric Integrals:

$$P(z) = -\int_0^1 dx \left\{ 2(1-x) \ln\left(\frac{1-x+z^2x^2}{1-x} \right) + \frac{4z^2 x(1-x^2)}{1-x+z^2x^2} \right\}$$
$$= \frac{3}{z^2} + \left\{ \frac{3}{2z^4} - 3 \right\} \ln z^2 + \frac{(3-6z^2-12z^4)}{z^4\sqrt{1-4z^2}} \tanh^{-1}\left(\sqrt{1-4z^2}\right) \qquad \text{(B.57)}$$

$$P^{'}(z) = -\int_0^1 dx \left\{(1-x)\ln\left(\frac{1-x+z^2x^2}{1-x}\right) - \frac{2z^2x(1-x)(2-x)}{1-x+z^2x^2}\right\}$$
$$= \frac{3}{2z^2} - \left\{\frac{3}{z^2} - \frac{3}{4z^4} - \frac{3}{2}\right\}\ln z^2 + \frac{(3-6z^2)\sqrt{1-4z^2}}{2z^4}\tanh^{-1}\left(\sqrt{1-4z^2}\right) \tag{B.58}$$

$$S(z) = \int_0^1 dx \left\{(3x^2-6x+4)\ln\left(\frac{1-x+z^2x^2}{1-x}\right) - \frac{z^2x(1-x^2)}{(1-x)(2-x)^2}\right\}$$
$$= -\frac{1}{z^2} + \left\{\frac{3}{2z^2} - \frac{1}{2z^4}\right\}\ln z^2 + \frac{(z^2-1)\sqrt{1-4z^2}}{z^4}\tanh^{-1}\left(\sqrt{1-4z^2}\right) \tag{B.59}$$

$$S^{'}(z) = -\int_0^1 dx \left\{\frac{z^2x^3}{1-x+z^2x^2}\right\}$$
$$= -\frac{1}{z^2} + \left\{\frac{1}{2z^2} - \frac{1}{2z^4}\right\}\ln z^2 + \frac{3z^2-1}{z^4\sqrt{1-4z^2}}\tanh^{-1}\left(\sqrt{1-4z^2}\right) \tag{B.60}$$

The integrals may be analytically continued in the regime, $4z^2 \geq 1$, using $\sqrt{1-4z^2} \mapsto i\sqrt{4z^2-1}$ and therefore $\tanh^{-1}(\sqrt{1-4z^2}) \mapsto i\tanh^{-1}(\sqrt{4z^2-1})$, and plugging this back into the integrals one can verify that the integral remains real.

B.9 Remaining Matching Contributions:

All remaining matching coefficient contributions are too large to present here, which includes: The bare two-loop vertex contributions in all cases, the heavy bare two-loop field renormalisation contributions, both the one- and two-loop contributions of $\tilde{D}(\mu)$, the coupling and mass renormalisation contributions labelled by $\Delta B(\mu)$ and $\Delta U(\mu)$. We thus present their full expressions with description in the arXiv ancillary file of Ref. [325].

Appendix C

Heavy Master Integrals

C.1 Differential Equations Algorithm

We briefly introduce the algorithm for reducing a coupled differential system to ϵ-form in the context of multi-loop integrals, for further detail see [389]. Given a family of n master integrals in a column, $\mathbf{J}(x)$, arising from the same types of diagrams and dependent on a single parameter x, a differential system may be defined,

$$\partial_x \mathbf{J}(x) = \mathbb{M}(\epsilon, x)\mathbf{J}(x). \tag{C.1}$$

The matrix $\mathbb{M}(\epsilon, x)$ is obtained after IBP reduction of the differentiated MIs, where $d = 4 - 2\epsilon$. Given this linear system one can then proceed with *Lee's algorithm* [389], which reduces the system to one which can be solved iteratively order-by-order in ϵ. Firstly, a reduction to so-called *Fuschian form* is necessary for $\mathbb{M}(\epsilon, x)$ in which only *simple poles* in x arise. If the system exhibits regular singularities this can always be achieved [410]. Specifically, one can always define a transformation matrix, $\mathbb{T}(\epsilon, x)$, such that

$$\mathbf{J} = \mathbb{T}(\epsilon, x)\tilde{\mathbf{J}} \quad \text{and} \quad \tilde{\mathbb{M}} = \tilde{\mathbb{T}}^{-1}\tilde{\mathbb{M}}\tilde{\mathbb{T}} - \tilde{\mathbb{T}}^{-1}\partial_x\tilde{\mathbb{T}}, \tag{C.2}$$

resulting in a transformed differential system,

$$\partial_x \tilde{\mathbf{J}}(x) = \tilde{\mathbb{M}}(\epsilon, x)\tilde{\mathbf{J}}(x). \tag{C.3}$$

One then needs to determine $\mathbb{T}$ such that it factors out the ϵ-dependence,

$$\partial_x \tilde{\mathbf{J}}(x) = \epsilon\tilde{\mathbb{S}}(x)\tilde{\mathbf{J}}(x). \tag{C.4}$$

This can be achieved in many cases [387] and in general one requires that $\tilde{\mathbb{S}}$ be Fuschian,

$$\tilde{\mathbb{S}}(x) = \sum_k \frac{A_k}{x - x_k}, \tag{C.5}$$

with A_k being constant, k finite and only simple poles in x present. This form of differential system then simply lends itself to a an iterative solution in terms of MPLs which has a nested sum representation,

$$\mathrm{Li}_{a_1,\ldots,a_n}(x_1, \ldots, x_n) = \sum_{i_1 > \ldots > i_n > 0} \frac{x_1^{i_1}}{i_1^{a_1}} \cdots \frac{x_n^{i_n}}{i_n^{a_n}}. \tag{C.6}$$

A special case of which are the so-called *Harmonic Polylogarithms* (HPLs) [304],

$$H_{a_1,\ldots,a_n}(x) = \mathrm{Li}_{a_1,\ldots,a_n}(x, 1, \ldots, 1), \tag{C.7}$$

with,

$$H_{0,\ldots,0}(x) = \frac{1}{n!}\ln^n(x). \tag{C.8}$$

In general however, there will be MIs in $\mathbf{J}(x)$ that are independent of x and thus differentiate to zero. These MIs along with x-dependent MIs at a pole in x must be determined as they define the boundary conditions and enforce regularity at all values of x. Otherwise one solely has the integrals up to an integration constant. Thus boundary integrals, which are simpler to determine, must be found with other means, for instance Feynman parametrisation, Mellin-Barnes representations [409], or dimensional recurrence relations [77, 79, 80], which we discuss in Appendix C.2.

C.2 Dimensional Recurrence Relations

As was originally formulated by Tarasov in Ref. [77], one can evaluate multi-loop integrals through dimensional recurrence relations and analyticity properties in $\mathcal{D}$, their space-time dimensionality. We employ the *dimensional recurrence algorithm* (DRA) first suggested by Lee in Refs. [79, 80] to evaluate our boundary integrals in Chapter 8. This approach is useful as we wish to provide boundary integrals to all orders in ϵ, for general applications. Given boundary integrals to all orders, the differential equations algorithm discussed in Section C.1 can then be employed to determine the remaining integrals to any desired order in ϵ.

The DRA method to determine multi-loop integrals can be broken down into five steps. For a more detailed review we recommend Ref. [80]. Before going through each step one must make sure that all multi-loop integrals which are *sub-topologies* of the one of interest are known as these will be necessary. Once these are determined one can proceed, given an MI, $J^{(\mathcal{D})}$, to be determined the DRA method proceeds in the following systematic way:

1. Examine the pole structure of $J^{(\mathcal{D})}$ and make certain that there exists a so-called *basic stripe* of integer width two between a set of poles. This is necessary as the integral needs to be finite in such a stripe. If the integral does not contain a basic stripe, make the integral suitable by increasing powers of certain propagators and relating the new integral to the original through IBP identities.

2. Given an appropriate MI for DRA treatment, $J^{(\mathcal{D})}$, one can now proceed to constructing its DRR which can in general be written as,

$$J^{(\mathcal{D}-2)} = C(\mathcal{D})J^{(\mathcal{D})} + R(\mathcal{D}). \tag{C.9}$$

   The first term on the right-hand side contains a rational factor, $C(\mathcal{D})$, and the second terms is known as the inhomogenous part of the relation, $R(\mathcal{D})$, and is made of MIs in sub-topologies of $J(\mathcal{D})$.

3. Given the recurrence relation in Eq. (C.9), one can write down a general solution as,

$$J^{(\mathcal{D})} = \Sigma^{-1}(\mathcal{D})\omega(z) + J_{\mathrm{I}}^{(\mathcal{D})}. \tag{C.10}$$

   The terms in this solution are to be determined individually where, $\Sigma^{-1}(\mathcal{D})$ is the *homogenous solution* also known as the summing factor and $J_{\mathrm{I}}^{(\mathcal{D})}$ is a particular solution to the *inhomogenous part*. The goal at this stage is to obtain the general solution by first finding a suitable homogenous solution, $\Sigma^{-1}(\mathcal{D})$, within the basic stripe and with this determining a particular solution, $J_{\mathrm{I}}^{(\mathcal{D})}$, for the inhomogenous part. The function, $\omega(z)$, is a periodic function in dimensionality with $z = e^{i\pi\mathcal{D}}$.

4. What remains at this stage is fixing the singularities of the periodic function, $\omega(z)$, which is done by studying the analytic properties of the MIs in Eq. (C.9) and the summing factor, $\Sigma(\mathcal{D})$, in the general solution.

5. If there are any remaining constants that are not yet fixed in Eq. (C.10) the last step is to fix these. This can also be done by studying analytic properties further, or evaluating the MI in a space-time dimension, $\mathcal{D}$, which is especially simple.

The main procedure which requires careful consideration in the DRA method is given in the fourth step. To fix the singularities in $\omega(z)$ one needs to analyse the pole structure of $\Sigma(\mathcal{D})J^{(\mathcal{D})}$ in the basic stripe of the complex plane of $\mathcal{D}$. One can attain this data, i.e. the position and order of the poles of $\Sigma(\mathcal{D})J^{(\mathcal{D})}$, either by inspection if trivial, or semi-analytically with the help of an algorithm automated in `FIESTA` [411]. What one finds in general is that the pole ordering is dependent on the summing factor, $\Sigma(\mathcal{D})$ and the basic stripe chosen given the MI being evaluated. Whence, step five may not be necessary in the case of such requirements being appropriately chosen. In this thesis we evaluate all our boundary MIs with the DRA method for completeness and check the results to high numerical precision with `FIESTA`.

C.3 Differential Systems in ϵ-form

In this section we present the reduced Fuschian systems of differential equations present in Chapter 8. The vertex diagrams are given in ϵ-form and the off-shell self-energy diagrams are given in $(A + B\epsilon)$-form. The original system described by $\mathbb{M}$ and the transformation matrix required for reduction, $\mathbb{T}$, are provided for all cases in an arXiv ancillary file of Ref. [381].

Heavy-Heavy:

$$\tilde{A}'_5 = \epsilon\left(-\frac{\tilde{A}_1\beta}{9(w-1)} + \frac{2\tilde{A}_5 w}{w^2-1} - \frac{\tilde{A}_7\beta}{2(w-1)}\right), \tag{C.11}$$

$$\tilde{A}'_6 = \epsilon\left(-\frac{12\tilde{A}_2\beta}{7(w-1)} + \frac{15\tilde{A}_3\beta}{4(w-1)w} - \frac{2\tilde{A}_6\left(w^2-2\right)}{w\left(w^2-1\right)}\right), \tag{C.12}$$

$$\tilde{A}'_7 = \epsilon\left(-\frac{4\tilde{A}_1}{9w} - \frac{16\tilde{A}_5\beta}{w-1} - \frac{4\tilde{A}_7}{w}\right), \tag{C.13}$$

$$\tilde{A}'_8 = \frac{\tilde{A}_1\beta\epsilon}{3(w-1)}, \tag{C.14}$$

$$\tilde{A}'_9 = \frac{\tilde{A}_1\beta\epsilon}{w-1}, \tag{C.15}$$

$$\tilde{A}'_{10} = \epsilon\left(\frac{3\tilde{A}_2\beta}{7(w-1)} + \frac{\tilde{A}_6 w}{2\left(w^2-1\right)}\right), \tag{C.16}$$

$$\tilde{A}'_{11} = -\frac{7\tilde{A}_6\epsilon}{6\left(w^2-1\right)}, \tag{C.17}$$

$$\tilde{A}'_{12} = \epsilon\left(-\frac{18\tilde{A}_5\beta}{w-1} - \frac{3\tilde{A}_8\beta}{w-1} - \frac{\tilde{A}_9\beta}{w-1}\right), \tag{C.18}$$

$$\tilde{A}'_{17} = \epsilon\left(-\frac{\tilde{A}_1\beta}{16(w-1)} + \frac{9\tilde{A}_{15}\beta}{32(w-1)} + \frac{2\tilde{A}_{17}w}{w^2-1} + \frac{\tilde{A}_{20}\beta}{4(w-1)} - \frac{9\tilde{A}_7\beta}{16(w-1)}\right), \tag{C.19}$$

$$\tilde{A}'_{18} = \epsilon \left(-\frac{9\tilde{A}_{14}\beta}{2w^2-w-1} + \frac{2\tilde{A}_{18}(w+2)}{2w^3+w^2-2w-1} + \frac{3\tilde{A}_2\beta}{2w^2-w-1} - \frac{15\tilde{A}_3\beta}{4\left(2w^2-w-1\right)} + \frac{7\tilde{A}_6}{2(2w+1)} \right), \tag{C.20}$$

$$\tilde{A}'_{19} = \epsilon \left(-\frac{\tilde{A}_1\beta\left(16w^2-7\right)}{4\left(4w^3-4w^2-w+1\right)} + \frac{2\tilde{A}_{13}\beta}{w-1} + \frac{9\tilde{A}_{15}\beta(4w+1)}{8\left(4w^3-4w^2-w+1\right)} + \frac{6\tilde{A}_{19}w}{4w^4-5w^2+1} + \frac{\tilde{A}_{20}\beta}{4w^3-4w^2-w+1} + \frac{27\tilde{A}_7\beta}{4\left(4w^3-4w^2-w+1\right)} \right), \tag{C.21}$$

$$\tilde{A}'_{20} = \epsilon \left(-\frac{\tilde{A}_1\left(10w^2-1\right)}{\left(4w^2-1\right)w} - \frac{9\tilde{A}_{15}(w+1)}{4w^2-1} + \frac{16\tilde{A}_{17}\beta}{w-1} + \frac{12\tilde{A}_{19}\beta}{4w^3-4w^2-w+1} - \frac{8\tilde{A}_{20}w}{4w^2-1} - \frac{108\tilde{A}_5\beta}{w-1} - \frac{9\tilde{A}_7\left(10w^2-1\right)}{\left(4w^2-1\right)w} \right) \tag{C.22}$$

$$\tilde{A}'_{21} = \epsilon \left(\frac{\tilde{A}_{13}\beta}{w-1} - \frac{\tilde{A}_1\beta}{3(w-1)} \right) \tag{C.23}$$

$$\tilde{A}'_{22} = \epsilon\frac{\tilde{A}_2\beta\epsilon}{w-1} \tag{C.24}$$

$$\tilde{A}'_{23} = \frac{\tilde{A}_{18}\epsilon}{2\left(w^2-1\right)} \tag{C.25}$$

$$\tilde{A}'_{26} = \epsilon\frac{\tilde{A}_{24}\beta\epsilon}{w-1} \tag{C.26}$$

Heavy-Light:

$$\tilde{B}'_3 = \epsilon \left(\frac{32\beta\tilde{B}_4}{5(w-1)} - \frac{6\tilde{B}_3w}{w^2-1} \right), \tag{C.27}$$

$$\tilde{B}'_4 = \epsilon \left(\frac{32\beta\tilde{B}_4}{5(w-1)} - \frac{6\tilde{B}_3w}{w^2-1} \right), \tag{C.28}$$

$$\tilde{B}'_6 = \epsilon \left(\frac{4\beta\tilde{B}_1}{3(w-1)} - \frac{2\tilde{B}_6w}{w^2-1} \right), \tag{C.29}$$

$$\tilde{B}'_7 = \epsilon \left(-\frac{2\beta\tilde{B}_2}{w-1} - \frac{49\beta\tilde{B}_4}{2(w-1)} + \frac{2\tilde{B}_7w}{w^2-1} \right), \tag{C.30}$$

$$\tilde{B}'_8 = \epsilon \left(\frac{16\beta\tilde{B}_2}{7(w-1)} - \frac{4\tilde{B}_8w}{w^2-1} \right), \tag{C.31}$$

$$\tilde{B}'_9 = \epsilon \left(-\frac{\beta\tilde{B}_1}{252(w-1)} + \frac{7\beta\tilde{B}_{10}}{2(w-1)} + \frac{5\beta\tilde{B}_4}{42(w-1)} + \frac{5\beta\tilde{B}_5}{288(w-1)} + \frac{2\tilde{B}_9w}{w^2-1} \right), \tag{C.32}$$

$$\tilde{B}'_{10} = \epsilon \left(\frac{\tilde{B}_1w}{441\left(w^2-1\right)} - \frac{4\tilde{B}_{10}w}{w^2-1} - \frac{75\beta\tilde{B}_3}{392(w-1)} - \frac{55\tilde{B}_4w}{147\left(w^2-1\right)} - \frac{5\tilde{B}_5(8w+3)}{2016\left(w^2-1\right)} + \frac{16\beta\tilde{B}_9}{7(w-1)} \right), \tag{C.33}$$

$$\tilde{B}'_{11} = \epsilon \left(-\frac{4\tilde{B}_1 w}{9\,(w^2-1)} - \frac{4\tilde{B}_{11} w}{w^2-1} - \frac{35\tilde{B}_5}{12\,(w^2-1)} + \frac{4\beta\tilde{B}_6}{3(w-1)} \right), \tag{C.34}$$

$$\tilde{B}'_{12} = \epsilon \left(-\frac{4\tilde{B}_{12} w}{w^2-1} + \frac{60\tilde{B}_2 w}{77\,(w^2-1)} + \frac{105\tilde{B}_4 w}{11\,(w^2-1)} + \frac{180\beta\tilde{B}_7}{77(w-1)} \right), \tag{C.35}$$

$$\tilde{B}'_{13} = \epsilon \left(-\frac{\beta\tilde{B}_1}{8(w-1)} + \frac{2\tilde{B}_{13} w}{w^2-1} - \frac{2\beta\tilde{B}_{14}}{w-1} + \frac{15\beta\tilde{B}_2}{28(w-1)} - \frac{105\beta\tilde{B}_4}{16(w-1)} \right), \tag{C.36}$$

$$\tilde{B}'_{14} = \epsilon \left(-\frac{4\beta\tilde{B}_{13}}{w-1} - \frac{4\tilde{B}_{14} w}{w^2-1} - \frac{525\beta\tilde{B}_3}{128(w-1)} + \frac{3\beta\tilde{B}_6}{8(w-1)} - \frac{15\beta\tilde{B}_8}{8(w-1)} \right), \tag{C.37}$$

$$\tilde{B}'_{15} = \epsilon \left(\frac{8\tilde{B}_1 w}{9\,(w^2-1)} - \frac{4\tilde{B}_{15} w}{w^2-1} - \frac{8\beta\tilde{B}_6}{3(w-1)} \right), \tag{C.38}$$

$$\tilde{B}'_{17} = -\frac{4\beta\tilde{B}_{18}\epsilon}{w-1}, \tag{C.39}$$

$$\tilde{B}'_{18} = \epsilon \left(-\frac{2\beta\tilde{B}_{17}}{w-1} - \frac{6\tilde{B}_{18} w}{w^2-1} \right), \tag{C.40}$$

$$\tilde{B}'_{19} = \epsilon \left(\frac{4\beta\tilde{B}_1}{3(w-1)} - \frac{2\tilde{B}_{19} w}{w^2-1} \right), \tag{C.41}$$

$$\tilde{B}'_{20} = \epsilon \left(\frac{\beta\tilde{B}_1}{42(w-1)} - \frac{5\beta\tilde{B}_{17}}{32(w-1)} + \frac{2\tilde{B}_{20} w}{w^2-1} - \frac{7\beta\tilde{B}_{21}}{12(w-1)} - \frac{5\beta\tilde{B}_5}{84(w-1)} \right), \tag{C.42}$$

$$\tilde{B}'_{21} = \epsilon \left(\frac{4\tilde{B}_1 w}{49\,(w^2-1)} - \frac{15\beta\tilde{B}_{18}}{14(w-1)} - \frac{96\beta\tilde{B}_{20}}{7(w-1)} - \frac{4\tilde{B}_{21} w}{w^2-1} - \frac{5\tilde{B}_5(32w-21)}{392\,(w^2-1)} \right), \tag{C.43}$$

$$\tilde{B}'_{22} = \epsilon \left(-\frac{49\beta\tilde{B}_{17}}{16(w-1)} + \frac{2\beta\tilde{B}_2}{w-1} + \frac{2\tilde{B}_{22} w}{w^2-1} \right), \tag{C.44}$$

$$\tilde{B}'_{23} = \epsilon \left(-\frac{19\beta\tilde{B}_1}{240(w-1)} + \frac{\beta\tilde{B}_{16}}{4(w-1)} + \frac{2\tilde{B}_{23} w}{w^2-1} + \frac{3\beta\tilde{B}_{24}}{10(w-1)} + \frac{7\beta\tilde{B}_5}{64(w-1)} \right), \tag{C.45}$$

$$\tilde{B}'_{24} = \epsilon \left(\frac{19\tilde{B}_1}{12w} - \frac{5\tilde{B}_{16}}{w} - \frac{2\beta\tilde{B}_{19}}{3(w-1)} + \frac{40\beta\tilde{B}_{23}}{w-1} - \frac{2\tilde{B}_{24}\left(3w^2-2\right)}{w\,(w^2-1)} - \frac{35\tilde{B}_5(3w-2)}{48(w-1)w} \right), \tag{C.46}$$

$$\tilde{B}'_{25} = \epsilon \left(-\frac{16\beta\tilde{B}_2}{7(w-1)} - \frac{4\tilde{B}_{25} w}{w^2-1} \right), \tag{C.47}$$

$$\tilde{B}'_{26} = \epsilon \left(\frac{4\tilde{B}_1 w}{9\,(w^2-1)} - \frac{4\beta\tilde{B}_{19}}{3(w-1)} - \frac{4\tilde{B}_{26} w}{w^2-1} + \frac{35\tilde{B}_5}{12\,(w^2-1)} \right), \tag{C.48}$$

$$\tilde{B}'_{27} = \epsilon \left(\frac{\beta\tilde{B}_1}{8(w-1)} - \frac{105\beta\tilde{B}_{17}}{128(w-1)} - \frac{15\beta\tilde{B}_2}{28(w-1)} + \frac{2\tilde{B}_{27} w}{w^2-1} + \frac{\beta\tilde{B}_{28}}{w-1} \right), \tag{C.49}$$

$$\tilde{B}'_{28} = \epsilon \left(-\frac{105\beta\tilde{B}_{18}}{32(w-1)} + \frac{3\beta\tilde{B}_{19}}{4(w-1)} + \frac{15\beta\tilde{B}_{25}}{4(w-1)} + \frac{8\beta\tilde{B}_{27}}{w-1} - \frac{4\tilde{B}_{28} w}{w^2-1} \right), \tag{C.50}$$

$$\tilde{B}'_{29} = \epsilon \left(-\frac{60\tilde{B}_2 w}{77\,(w^2-1)} - \frac{4\tilde{B}_{29} w}{w^2-1} - \frac{105\tilde{B}_4 w}{11\,(w^2-1)} - \frac{180\beta\tilde{B}_7}{77(w-1)} \right), \tag{C.51}$$

$$\tilde{B}'_{30} = \epsilon \left(\frac{4\tilde{B}_1 w}{9\,(w^2-1)} - \frac{4\tilde{B}_{30} w}{w^2-1} - \frac{35\tilde{B}_5}{12\,(w^2-1)} - \frac{4\beta\tilde{B}_6}{3(w-1)} \right), \tag{C.52}$$

$$\tilde{B}'_{31} = \epsilon \left(\frac{105\tilde{B}_{17} w}{88\,(w^2-1)} - \frac{60\tilde{B}_2 w}{77\,(w^2-1)} + \frac{180\beta\tilde{B}_{22}}{77(w-1)} - \frac{4\tilde{B}_{31} w}{w^2-1} \right), \tag{C.53}$$

$$\tilde{B}'_{32} = \epsilon \left(-\frac{4\tilde{B}_1 w}{9\,(w^2-1)} + \frac{4\beta\tilde{B}_{19}}{3(w-1)} - \frac{4\tilde{B}_{32} w}{w^2-1} + \frac{35\tilde{B}_5}{12\,(w^2-1)} \right), \tag{C.54}$$

$$\tilde{B}'_{33} = \epsilon \left(-\frac{105\tilde{B}_{17} w}{88\,(w^2-1)} + \frac{60\tilde{B}_2 w}{77\,(w^2-1)} - \frac{180\beta\tilde{B}_{22}}{77(w-1)} - \frac{4\tilde{B}_{33} w}{w^2-1} \right), \tag{C.55}$$

Heavy Propagator:

$$\tilde{C}'_3 = \epsilon \left(-\frac{4\beta\tilde{C}_1}{3(w-1)} - \frac{2\tilde{C}_3 w}{(w-1)(w+1)} \right), \tag{C.56}$$

$$\begin{aligned}
\tilde{C}'_4 = \epsilon \Bigg(& -\frac{8\tilde{C}_1(7w-8)}{(w-2)w(w+2)} - \frac{16\tilde{C}_4 w}{(w-2)(w+2)} + \frac{32\tilde{C}_4}{(w-2)(w+2)} - \frac{48\tilde{C}_4}{(w-2)w(w+2)} \\
& - \frac{28\tilde{C}_5 w}{(w-2)(w+2)} + \frac{64\tilde{C}_5}{(w-2)(w+2)} - \frac{112\tilde{C}_5}{(w-2)w(w+2)} \Bigg) + \frac{4\tilde{C}_1(7w-8)}{(w-2)w(w+2)} \\
& + \frac{7\tilde{C}_4 w}{(w-2)(w+2)} - \frac{29\tilde{C}_4}{(w-2)(w+2)} + \frac{24\tilde{C}_4}{(w-2)w(w+2)} + \frac{14\tilde{C}_5 w}{(w-2)(w+2)} \\
& - \frac{65\tilde{C}_5}{(w-2)(w+2)} + \frac{56\tilde{C}_5}{(w-2)w(w+2)},
\end{aligned} \tag{C.57}$$

$$\begin{aligned}
\tilde{C}'_5 = \epsilon \Bigg(& \frac{8\tilde{C}_1(3w-4)}{(w-2)w(w+2)} + \frac{6\tilde{C}_4 w}{(w-2)(w+2)} - \frac{16\tilde{C}_4}{(w-2)(w+2)} + \frac{24\tilde{C}_4}{(w-2)w(w+2)} \\
& + \frac{10\tilde{C}_5 w}{(w-2)(w+2)} - \frac{32\tilde{C}_5}{(w-2)(w+2)} + \frac{56\tilde{C}_5}{(w-2)w(w+2)} \Bigg) - \frac{4\tilde{C}_1(3w-4)}{(w-2)w(w+2)} \\
& - \frac{3\tilde{C}_4 w}{(w-2)(w+2)} + \frac{13\tilde{C}_4}{(w-2)(w+2)} - \frac{12\tilde{C}_4}{(w-2)w(w+2)} - \frac{6\tilde{C}_5 w}{(w-2)(w+2)} \\
& + \frac{29\tilde{C}_5}{(w-2)(w+2)} - \frac{28\tilde{C}_5}{(w-2)w(w+2)},
\end{aligned} \tag{C.58}$$

$$\begin{aligned}
\tilde{C}'_6 = \epsilon \Bigg(& -\frac{4\beta\tilde{C}_1 w^2}{(w-2)(w-1)(w+2)} - \frac{8\beta\tilde{C}_1}{(w-2)(w-1)(w+2)} - \frac{4\beta\tilde{C}_2}{w-1} \\
& - \frac{12\beta\tilde{C}_4 w}{(w-2)(w-1)(w+2)} - \frac{24\beta\tilde{C}_5 w}{(w-2)(w-1)(w+2)} - \frac{2\tilde{C}_6 w}{(w-1)(w+1)} \Bigg) \\
& + \frac{12\beta\tilde{C}_1}{(w-2)(w-1)(w+2)} + \frac{3\beta\tilde{C}_4 w}{(w-2)(w-1)(w+2)} - \frac{9\beta\tilde{C}_4}{(w-2)(w-1)(w+2)} \\
& + \frac{6\beta\tilde{C}_5 w}{(w-2)(w-1)(w+2)} - \frac{21\beta\tilde{C}_5}{(w-2)(w-1)(w+2)},
\end{aligned} \tag{C.59}$$

$$\tilde{C}'_7 = \epsilon \left(-\frac{8\beta\tilde{C}_1\left(w^2+2\right)}{(w-2)(w-1)(w+2)w} - \frac{3\beta\tilde{C}_4 w}{(w-2)(w-1)(w+2)} - \frac{24\beta\tilde{C}_4}{(w-2)(w-1)(w+2)} \right.$$

$$+\frac{12\beta\tilde{C}_4}{(w-2)(w-1)(w+2)w}-\frac{7\beta\tilde{C}_5 w}{(w-2)(w-1)(w+2)}-\frac{48\beta\tilde{C}_5}{(w-2)(w-1)(w+2)}$$
$$+\frac{28\beta\tilde{C}_5}{(w-2)(w-1)(w+2)w}-\frac{2\tilde{C}_7 w}{(w-1)(w+1)}\Bigg)+\frac{4\beta\tilde{C}_1\left(w^2+2\right)}{(w-2)(w-1)w(w+2)}$$
$$-\frac{3\beta\tilde{C}_4 w}{(w-2)(w-1)(w+2)}+\frac{6\beta\tilde{C}_4}{(w-2)(w-1)(w+2)}-\frac{6\beta\tilde{C}_4}{(w-2)(w-1)w(w+2)}$$
$$-\frac{7\beta\tilde{C}_5 w}{(w-2)(w-1)(w+2)}+\frac{12\beta\tilde{C}_5}{(w-2)(w-1)(w+2)}-\frac{14\beta\tilde{C}_5}{(w-2)(w-1)w(w+2)}, \quad \text{(C.60)}$$

$$\tilde{C}_8'=\epsilon\left(\frac{8\tilde{C}_1 w}{9(w-1)(w+1)}+\frac{8\beta\tilde{C}_3}{3(w-1)}-\frac{4\tilde{C}_8 w}{(w-1)(w+1)}\right), \quad \text{(C.61)}$$

$$\tilde{C}_9'=\epsilon\Bigg(\frac{12\tilde{C}_1 w}{4w^2-3}+\frac{12\beta\tilde{C}_3}{(w-1)\left(4w^2-3\right)}-\frac{6\tilde{C}_4 w}{4w^2-3}-\frac{14\tilde{C}_5 w}{4w^2-3}-\frac{4\beta\tilde{C}_6}{(w-1)\left(4w^2-3\right)}$$
$$-\frac{2\beta\tilde{C}_7 w}{(w-1)\left(4w^2-3\right)}-\frac{18\tilde{C}_8 w}{4w^2-3}-\frac{8\tilde{C}_9 w}{4w^2-3}\Bigg), \quad \text{(C.62)}$$

$$\tilde{C}_{11}'=-\frac{4\tilde{C}_{11}\epsilon}{w}, \quad \text{(C.63)}$$

$$\tilde{C}_{12}'=\epsilon\left(-\frac{4\beta\tilde{C}_{10}}{3(w-1)}-\frac{35\beta\tilde{C}_{11}}{6(w-1)}-\frac{2\tilde{C}_{12}w}{(w-1)(w+1)}\right). \quad \text{(C.64)}$$

C.4 Heavy Boundary Integrals

In this section we present exact results for all the boundary integrals in Chapter 8. In our notation, $\nu=d/2$ with $d=4-2\epsilon$ and we take mass scale to unity as is conventionally done for conciseness.

Heavy-Heavy:

$$A_1=a_1=\Gamma(1-\nu)^2, \quad \text{(C.65)}$$

$$A_2=a_2=\pi\left(-2^{2\nu-1}\right)\Gamma(2-2\nu), \quad \text{(C.66)}$$

$$A_3=a_3=-\frac{\pi 4^{\nu-1}\Gamma\left(\frac{5}{2}-2\nu\right)\Gamma\left(\frac{3}{2}-\nu\right)}{\Gamma(2-\nu)}, \quad \text{(C.67)}$$

$$A_4=a_4=\frac{\pi^3\sec^2(\pi\nu)}{2\Gamma\left(\nu-\frac{1}{2}\right)^2}, \quad \text{(C.68)}$$

$$A_{13}=a_5=\frac{\pi^{5/2}4^{\nu-1}\,{}_2\tilde{F}_1\left(1,\frac{5}{2}-\nu;3-\nu;\frac{3}{4}\right)\csc(2\pi\nu)\Gamma\left(\frac{5}{2}-\nu\right)}{\Gamma(2\nu-2)}-\frac{16\pi^3 3^{\nu-3}\csc(2\pi\nu)}{\Gamma(2\nu-2)}, \quad \text{(C.69)}$$

$$A_{14}=a_6=\frac{\pi^3 2^{2\nu-7}(4\nu-5)\sec^2(\pi\nu)\Gamma\left(\frac{7}{2}-2\nu\right)\,{}_3\tilde{F}_2\left(1,\frac{7}{4}-\nu,\frac{9}{4}-\nu;\frac{5}{2}-\nu,3-\nu;\frac{3}{4}\right)}{\Gamma\left(\nu-\frac{1}{2}\right)^2}$$
$$-\frac{3\pi^3 2^{2\nu-9}\sec^2(\pi\nu)\Gamma\left(\frac{11}{2}-2\nu\right)\,{}_3\tilde{F}_2\left(2,\frac{11}{4}-\nu,\frac{13}{4}-\nu;\frac{7}{2}-\nu,4-\nu;\frac{3}{4}\right)}{\Gamma\left(\nu-\frac{1}{2}\right)^2}$$
$$+\frac{\pi 4^{\nu-1}\,{}_2F_1\left(1,2-\nu;\frac{5}{2}-\nu;\frac{3}{4}\right)\Gamma(3-2\nu)}{2\nu-3}+\frac{\pi^3 2^{3-2\nu}3^{\nu-\frac{3}{2}}\sec^2(\pi\nu)}{\Gamma\left(\nu-\frac{1}{2}\right)^2}, \quad \text{(C.70)}$$

$$A_{15} = \frac{3\pi^3 \sec^2(\pi\nu)}{2\Gamma\left(\nu - \frac{1}{2}\right)^2}, \tag{C.71}$$

$$A_{16} = \frac{4\pi^2 3^{\nu-\frac{3}{2}} \csc(2\pi\nu)}{\Gamma(2\nu-1)} - \frac{3\pi\, {}_2F_1\left(1, 2-\nu; \frac{5}{2}-\nu; \frac{3}{4}\right) \csc(2\pi\nu)\Gamma(2-\nu)^2}{\Gamma(4-2\nu)\Gamma(2\nu-1)}, \tag{C.72}$$

$$A_{24} = a_7 = -2\pi \csc(\pi\nu)\Gamma(2-2\nu), \tag{C.73}$$

$$A_{25} = a_8 = \frac{\pi^3 2^{3-2\nu} \csc(\pi\nu)\sec(2\pi\nu)}{\Gamma\left(\nu - \frac{1}{2}\right)^2}. \tag{C.74}$$

Heavy-Light:

$$B_1 = b_3 = \Gamma(1-\nu)^2, \tag{C.75}$$

$$B_2 = b_1 = \frac{\pi \csc(\pi\nu)\Gamma(3-2\nu)\Gamma(\nu-1)\Gamma(4\nu-5)}{\Gamma(2\nu-2)\Gamma(3\nu-3)}, \tag{C.76}$$

$$B_5 = b_4 = \frac{\pi^2 16^{\nu-1} \csc(\pi\nu)\csc(4\pi\nu)\Gamma\left(3\nu - \frac{7}{2}\right)}{\Gamma\left(\nu - \frac{1}{2}\right)\Gamma(4\nu-4)}, \tag{C.77}$$

$$\begin{aligned} B_{16} = b_5 = {} & -11\pi^{3/2} 3^{3\nu-\frac{17}{2}} 4^{\nu+1}(\nu-2)^3\Gamma(4-3\nu)\Gamma(3-2\nu)\, {}_4\tilde{F}_3\left(2, 3-\nu, 3-\nu, 3-\nu; \frac{10}{3}\right. \\ & \left. -\nu, \frac{7}{2}-\nu, \frac{11}{3}-\nu; \frac{16}{27}\right) + \pi^{3/2} 3^{3\nu-\frac{11}{2}} 4^{\nu-1}(19-11\nu)\Gamma(4-3\nu)\Gamma(3-2\nu)\, {}_4\tilde{F}_3\left(1, 2\right. \\ & \left. -\nu, 2-\nu, 2-\nu; \frac{7}{3}-\nu, \frac{5}{2}-\nu, \frac{8}{3}-\nu; \frac{16}{27}\right) - \frac{3\pi 64^{\nu-1}\tan(\pi\nu)\Gamma(\nu-1)\Gamma(\nu)^2}{(2\cos(2\pi\nu)+1)\Gamma(2\nu-1)\Gamma(3\nu-2)}, \end{aligned} \tag{C.78}$$

$$b_2 = -\frac{\pi^2 2^{4\nu-3} \sin\left(\frac{1}{6}(\pi-6\pi\nu)\right)\left(\cot(\pi\nu)+\sqrt{3}\right)\csc(4\pi\nu)\Gamma\left(3\nu-\frac{7}{2}\right)}{\Gamma\left(\nu-\frac{1}{2}\right)\Gamma(4\nu-4)}. \tag{C.79}$$

Heavy Propagator:

$$C_1 = c_1 = \Gamma(1-\nu)^2, \tag{C.80}$$

$$C_2 = c_2 = -\frac{\pi 4^{\nu-1}\Gamma\left(\frac{5}{2}-2\nu\right)\Gamma\left(\frac{3}{2}-\nu\right)}{\Gamma(2-\nu)}, \tag{C.81}$$

$$C_{10} = c_9 = -2\pi \csc(\pi\nu)\Gamma(2-2\nu), \tag{C.82}$$

$$c_3 = \pi\left(-2^{2\nu-1}\right)\Gamma(2-2\nu), \tag{C.83}$$

$$c_4 = \frac{\pi^{5/2} 4^{\nu-1}\, {}_2\tilde{F}_1\left(1, \frac{5}{2}-\nu; 3-\nu; \frac{3}{4}\right)\csc(2\pi\nu)\Gamma\left(\frac{5}{2}-\nu\right)}{\Gamma(2\nu-2)} - \frac{16\pi^3 3^{\nu-3}\csc(2\pi\nu)}{\Gamma(2\nu-2)}, \tag{C.84}$$

$$\begin{aligned} c_5 = {} & \frac{\pi^3 2^{2\nu-7}(4\nu-5)\sec^2(\pi\nu)\Gamma\left(\frac{7}{2}-2\nu\right)\, {}_3\tilde{F}_2\left(1, \frac{7}{4}-\nu, \frac{9}{4}-\nu; \frac{5}{2}-\nu, 3-\nu; \frac{3}{4}\right)}{\Gamma\left(\nu-\frac{1}{2}\right)^2} \\ & - \frac{3\pi^3 2^{2\nu-9}\sec^2(\pi\nu)\Gamma\left(\frac{11}{2}-2\nu\right)\, {}_3\tilde{F}_2\left(2, \frac{11}{4}-\nu, \frac{13}{4}-\nu; \frac{7}{2}-\nu, 4-\nu; \frac{3}{4}\right)}{\Gamma\left(\nu-\frac{1}{2}\right)^2} \\ & + \frac{\pi 4^{\nu-1}\, {}_2F_1\left(1, 2-\nu; \frac{5}{2}-\nu; \frac{3}{4}\right)\Gamma(3-2\nu)}{2\nu-3} + \frac{\pi^3 2^{3-2\nu} 3^{\nu-\frac{3}{2}}\sec^2(\pi\nu)}{\Gamma\left(\nu-\frac{1}{2}\right)^2}, \end{aligned} \tag{C.85}$$

$$c_6 = \frac{\pi^3 \sec^2(\pi\nu)}{2\Gamma\left(\nu-\frac{1}{2}\right)^2}, \tag{C.86}$$

$$c_7 = \frac{3\pi^3 \sec^2(\pi\nu)}{2\Gamma\left(\nu - \frac{1}{2}\right)^2}, \tag{C.87}$$

$$c_8 = \frac{2\pi^2\, {}_2F_1\left(1, \frac{5}{2} - \nu; 3 - \nu; \frac{3}{4}\right) \csc(2\pi\nu)\Gamma\left(\frac{5}{2} - \nu\right)^2}{\Gamma(5 - 2\nu)\Gamma(2\nu - 2)} - \frac{8\pi^3 3^{\nu-3} \csc(2\pi\nu)}{\Gamma(2\nu - 2)}, \tag{C.88}$$

$$c_{10} = \frac{\pi^3 4^{2-\nu}}{(\sin(3\pi\nu) - \sin(\pi\nu))\Gamma\left(\nu - \frac{1}{2}\right)^2}. \tag{C.89}$$

$$\tag{C.90}$$

We can see the introduction of new functions in some of the boundary integrals of this section. These are the *hypergeometric functions* [412], and generalisations thereof. The hypergeometric function is defined for complex $|z|< 1$ as a power series expansion,

$${}_2F_1(a, b; c; z) = \sum_{n=0}^{\infty} \frac{(a)_n (b)_n}{(c)_n} \frac{z^n}{n!}, \tag{C.91}$$

with $(q)_n$ denoting the Pochhammer symbol defined by,

$$(q)_n = \begin{cases} 1 & n = 0 \\ q(q+1)\cdots(q+n-1) & n > 0 \end{cases} \tag{C.92}$$

For $|z|\geq 1$ the hypergeometric function can be analytically continued, avoiding branch points at unity and infinity. We also have the appearance of the *regularised generalised hypergeometric function* which is defined by,

$${}_p\tilde{F}_q(a_1, \ldots, a_p; b_1, \ldots, b_q; z) = \sum_{n=0}^{\infty} \frac{\Pi_{j=1}^{p} (a_j)_n}{\Pi_{j=1}^{q} \Gamma(n + b_j)} \frac{z^n}{n!}, \tag{C.93}$$

which is the maximal extension of the hypergeometric function and thus defines all forms that appear in our work. Such functions are common in multi-loop integrals and thus, there exist a variety of methods and associated tools to deal with them. In our case, for the remaining MIs we solve by differential equations we need to expand the hypergeometric functions present in the boundary integrals in $\nu = 2 - \epsilon$ for $\epsilon \to 0$. This can be done with automatically with `HypExp2`, which is what we employed in our study [406].

Bibliography

[1] G. Aad, T. Abajyan, B. Abbott, *et al.*, "Observation of a new particle in the search for the standard model higgs boson with the ATLAS detector at the LHC," *Physics Letters B*, vol. 716, no. 1, pp. 1–29, 2012.

[2] S. Chatrchyan, V. Khachatryan, A. M. Sirunyan, *et al.*, "Observation of a new boson at a mass of 125 GeV with the CMS experiment at the LHC," *Physics Letters B*, vol. 716, no. 1, pp. 30–61, 2012.

[3] P. W. Higgs, "Broken symmetries and the masses of gauge bosons," *Physical Review Letters*, vol. 13, no. 16, p. 508, 1964.

[4] F. Englert and R. Brout, "Broken symmetry and the mass of gauge vector mesons," *Physical Review Letters*, vol. 13, no. 9, p. 321, 1964.

[5] Q. Ahmad, R. Allen, T. Andersen, *et al.*, "Measurement of the rate of $\nu_e + d \rightarrow p + p + e^-$ interactions produced by ^8b solar neutrinos at the Sudbury Neutrino Observatory," *Phys. Rev. Lett*, vol. 87, no. 7, p. 071301, 2001.

[6] Y. Fukuda, T. Hayakawa, E. Ichihara, K. Inoue, K. Ishihara, H. Ishino, Y. Itow, T. Kajita, J. Kameda, S. Kasuga, *et al.*, "Evidence for oscillation of atmospheric neutrinos," *Physical Review Letters*, vol. 81, no. 8, p. 1562, 1998.

[7] B. Pontecorvo, "Mesonium and antimesonium," *Zhur. Eksptl'. i Teoret. Fiz.*, vol. 33, 1957.

[8] S. M. Faber and J. Gallagher, "Masses and mass-to-light ratios of galaxies," *Annual review of astronomy and astrophysics*, vol. 17, no. 1, pp. 135–187, 1979.

[9] A. Einstein, "The general theory of relativity," in *The Meaning of Relativity*, pp. 54–75, Springer, 1922.

[10] J. P. Ostriker, P. Peebles, and A. Yahil, "The size and mass of galaxies, and the mass of the universe," *The Astrophysical Journal*, vol. 193, pp. L1–L4, 1974.

[11] J. Einasto, A. Kaasik, and E. Saar, "Dynamic evidence on massive coronas of galaxies," *Nature*, vol. 250, no. 5464, pp. 309–310, 1974.

[12] C. A. Mead, "Possible connection between gravitation and fundamental length," *Physical Review*, vol. 135, no. 3B, p. B849, 1964.

[13] C. J. Isham, "Prima facie questions in quantum gravity," in *Canonical gravity: From classical to quantum*, pp. 1–21, Springer, 1994.

[14] H.-H. Borzeszkowski and H.-J. Treder, *The meaning of quantum gravity*, vol. 20. Springer Science & Business Media, 2012.

[15] J. Scherk and J. H. Schwarz, "Dual models for non-hadrons," *Nuclear Physics B*, vol. 81, no. 1, pp. 118–144, 1974.

[16] L. Bombelli, J. Lee, D. Meyer, and R. D. Sorkin, "Space-time as a causal set," *Physical review letters*, vol. 59, no. 5, p. 521, 1987.

[17] K. Becker, M. Becker, and J. H. Schwarz, *String theory and M-theory*. Cambridge university press, 2006.

[18] C. Rovelli, "Loop quantum gravity," *Living reviews in relativity*, vol. 11, no. 1, pp. 1–69, 2008.

[19] A. M. Sirunyan, A. Tumasyan, W. Adam, *et al.*, "Combination of searches for heavy resonances decaying to WW, WZ, ZZ, WH, and ZH boson pairs in proton-proton collisions at $\sqrt{s} = 8$ and 13 TeV," *Physics letters B*, vol. 774, pp. 533–558, 2017.

[20] N. Arkani-Hamed, S. Dimopoulos, and G. Dvali, "The hierarchy problem and new dimensions at a millimeter," *Physics Letters B*, vol. 429, no. 3-4, pp. 263–272, 1998.

[21] S. Weinberg, "The cosmological constant problem," *Reviews of modern physics*, vol. 61, no. 1, p. 1, 1989.

[22] A. J. Buras, J. Ellis, M. K. Gaillard, and D. V. Nanopoulos, "Aspects of the grand unification of strong, weak and electromagnetic interactions," *Nuclear Physics B*, vol. 135, no. 1, pp. 66–92, 1978.

[23] R. Aaij, B. Adeva, M. Adinolfi, Z. Ajaltouni, S. Akar, J. Albrecht, F. Alessio, M. Alexander, A. A. Albero, S. Ali, *et al.*, "Test of lepton flavor universality by the measurement of the $B^0 \to D^{*-}\tau^+\nu_\tau$ branching fraction using three-prong τ decays," *Physical Review D*, vol. 97, no. 7, p. 072013, 2018.

[24] S. Wehle, I. Adachi, K. Adamczyk, H. Aihara, D. Asner, H. Atmacan, V. Aulchenko, *et al.*, "Test of lepton-flavor universality in $B \to K^* l^+ l^-$ decays at Belle," *Physical Review Letters*, vol. 126, no. 16, p. 161801, 2021.

[25] G. W. Bennett, B. Bousquet, H. Brown, G. Bunce, R. Carey, P. Cushman, G. Danby, P. Debevec, M. Deile, H. Deng, *et al.*, "Final report of the E821 muon anomalous magnetic moment measurement at BNL," *Physical Review D*, vol. 73, no. 7, p. 072003, 2006.

[26] B. Abi, T. Albahri, S. Al-Kilani, D. Allspach, L. Alonzi, A. Anastasi, A. Anisenkov, F. Azfar, K. Badgley, S. Baeßler, *et al.*, "Measurement of the positive muon anomalous magnetic moment to 0.46 ppm," *Physical Review Letters*, vol. 126, no. 14, p. 141801, 2021.

[27] R. Alonso, B. Grinstein, and J. M. Camalich, "Lepton universality violation with lepton flavor conservation in B-meson decays," *Journal of High Energy Physics*, vol. 2015, no. 10, pp. 1–30, 2015.

[28] A. Greljo, G. Isidori, and D. Marzocca, "On the breaking of lepton flavor universality in B-decays," *Journal of High Energy Physics*, vol. 2015, no. 7, pp. 1–22, 2015.

[29] D. Buttazzo, A. Greljo, G. Isidori, and D. Marzocca, "B-physics anomalies: a guide to combined explanations," *Journal of High Energy Physics*, vol. 2017, no. 11, p. 44, 2017.

[30] M. Bauer and M. Neubert, "Minimal leptoquark explanation for the R_{D^*}, R_K, and $(g-2)_\mu$ anomalies," *Physical review letters*, vol. 116, no. 14, p. 141802, 2016.

[31] L. L. Everett, G. L. Kane, S. Rigolin, and L.-T. Wang, "Implications of $(g-2)_\mu$ for supersymmetry and for discovering superpartners directly," *Physical Review Letters*, vol. 86, no. 16, p. 3484, 2001.

[32] M. Sher, "Electroweak Higgs potential and vacuum stability," *Physics Reports*, vol. 179, no. 5-6, pp. 273–418, 1989.

[33] S. Alekhin, A. Djouadi, and S. Moch, "The top quark and Higgs boson masses and the stability of the electroweak vacuum," *Physics Letters B*, vol. 716, no. 1, pp. 214–219, 2012.

[34] D. Buttazzo, G. Degrassi, P. P. Giardino, G. F. Giudice, F. Sala, A. Salvio, and A. Strumia, "Investigating the near-criticality of the Higgs boson," *Journal of High Energy Physics*, vol. 2013, no. 12, p. 89, 2013.

[35] A. Pak, "The toolbox of modern multi-loop calculations: novel analytic and semi-analytic techniques," in *Journal of Physics: Conference Series*, vol. 368, p. 012049, IOP Publishing, 2012.

[36] M. Steinhauser, "Results and techniques of multi-loop calculations," *Physics reports*, vol. 364, no. 4, pp. 247–357, 2002.

[37] T. Binoth and G. Heinrich, "Numerical evaluation of multi-loop integrals by sector decomposition," *Nuclear Physics B*, vol. 680, no. 1-3, pp. 375–388, 2004.

[38] P. Baikov, K. Chetyrkin, and J. Kühn, "Five-loop running of the QCD coupling constant," *Physical review letters*, vol. 118, no. 8, p. 082002, 2017.

[39] F. J. Dyson, "Divergence of perturbation theory in quantum electrodynamics," *Physical Review*, vol. 85, no. 4, p. 631, 1952.

[40] M. Peter, "Static quark-antiquark potential in QCD to three loops," *Physical Review Letters*, vol. 78, no. 4, p. 602, 1997.

[41] C. Anzai, Y. Kiyo, and Y. Sumino, "Static QCD potential at three-loop order," *Physical review letters*, vol. 104, no. 11, p. 112003, 2010.

[42] M. Voloshin and M. Shifman, "On production of D^* and D in B-meson decays," *Yadernaya Fizika*, vol. 47, no. 3, pp. 801–806, 1988.

[43] N. Isgur, D. Scora, B. Grinstein, and M. B. Wise, "Semileptonic B and D decays in the quark model," *Physical Review D*, vol. 39, no. 3, p. 799, 1989.

[44] S. Dimopoulos, L. J. Hall, and S. Raby, "Predictive framework for fermion masses in supersymmetric theories," *Physical Review Letters*, vol. 68, no. 13, p. 1984, 1992.

[45] M. Ciuchini, E. Franco, S. Mishima, and L. Silvestrini, "Electroweak precision observables, new physics and the nature of a 126 GeV Higgs boson," *Journal of High Energy Physics*, vol. 2013, no. 8, p. 106, 2013.

[46] ALEPH Collaboration and DELPHI collaboration and L3 Collaboration and OPAL Collaboration and LEP Electroweak Working Group *et al.*, "Electroweak measurements in electron-positron collisions at W-boson-pair energies at LEP," *Physics reports*, vol. 532, no. 4, pp. 119–244, 2013.

[47] M. Beneke, "Renormalons," *Physics Reports*, vol. 317, no. 1-2, pp. 1–142, 1999.

[48] S. Schael *et al.*, "ALEPH and DELPHI and L3 and OPAL and LEP Electroweak Collaborations," *Phys. Rept*, vol. 532, no. 119, p. 20, 2013.

[49] J. de Blas, M. Ciuchini, E. Franco, S. Mishima, M. Pierini, L. Reina, and L. Silvestrini, "Electroweak precision constraints at present and future colliders," *arXiv preprint: hep-ph/1611.05354*, 2016.

[50] A. Denner and S. Dittmaier, "Electroweak radiative corrections for collider physics," *Physics Reports*, 2020.

[51] F. Bezrukov, M. Y. Kalmykov, B. A. Kniehl, and M. Shaposhnikov, "Higgs boson mass and new physics," *Journal of High Energy Physics*, vol. 2012, no. 10, pp. 1–35, 2012.

[52] G. Degrassi, S. Di Vita, J. Elias-Miro, J. R. Espinosa, G. F. Giudice, G. Isidori, and A. Strumia, "Higgs mass and vacuum stability in the Standard Model at NNLO," *Journal of High Energy Physics*, vol. 2012, no. 8, p. 98, 2012.

[53] B. Grinstein, R. Springer, and M. B. Wise, "Strong-interaction effects in weak radiative B-meson decay," *Nuclear Physics B*, vol. 339, no. 2, pp. 269–309, 1990.

[54] M. J. Savage and M. B. Wise, "SU(3) predictions for non-leptonic B-meson decays," *Physical Review D*, vol. 39, no. 11, p. 3346, 1989.

[55] E. Braaten and J. Leveille, "Higgs-boson decay and the running mass," *Physical Review D*, vol. 22, no. 3, p. 715, 1980.

[56] I. Bigi, M. Shifman, N. Uraltsev, and A. Vainshtein, "High power n of m_b in beauty widths and $n = 5 \to \infty$ limit," *Physical Review D*, vol. 56, no. 7, p. 4017, 1997.

[57] M. Beneke, "A quark mass definition adequate for threshold problems," *Physics Letters B*, vol. 434, no. 1-2, pp. 115–125, 1998.

[58] A. H. Hoang, A. Jain, C. Lepenik, V. Mateu, M. Preisser, I. Scimemi, and I. W. Stewart, "The MSR mass and the renormalon sum rule," *Journal of High Energy Physics*, vol. 2018, no. 4, p. 3, 2018.

[59] A. H. Hoang, Z. Ligeti, and A. V. Manohar, "B decay and the Υ mass," *Physical Review Letters*, vol. 82, no. 2, p. 277, 1999.

[60] N. Brambilla, J. Komijani, A. S. Kronfeld, A. Vairo, T. Collaboration, *et al.*, "Relations between heavy-light meson and quark masses," *Physical Review D*, vol. 97, no. 3, p. 034503, 2018.

[61] H. Georgi, "Effective field theory," *Annual review of nuclear and particle science*, vol. 43, no. 1, pp. 209–252, 1993.

[62] R. Contino, A. Falkowski, F. Goertz, C. Grojean, and F. Riva, "On the validity of the effective field theory approach to SM precision tests," *Journal of High Energy Physics*, vol. 2016, no. 7, pp. 1–26, 2016.

[63] I. Brivio and M. Trott, "The Standard Model as an effective field theory," *Physics Reports*, vol. 793, pp. 1–98, 2019.

[64] H. Georgi, "An effective field theory for heavy quarks at low energies," *Physics Letters B*, vol. 240, no. 3-4, pp. 447–450, 1990.

[65] B. Grinstein, "The static quark effective theory," *Nuclear Physics B*, vol. 339, no. 2, pp. 253–268, 1990.

[66] A. F. Falk, B. Grinstein, and M. E. Luke, "Leading mass corrections to the heavy quark effective theory," *Nuclear Physics B*, vol. 357, no. 1, pp. 185–207, 1991.

[67] R. Machleidt and D. R. Entem, "Chiral effective field theory and nuclear forces," *Physics Reports*, vol. 503, no. 1, pp. 1–75, 2011.

[68] E. V. Shuryak, "The structure of hadrons containing a heavy quark," *Physics Letters B*, vol. 93, no. 1-2, pp. 134–136, 1980.

[69] V. A. Khoze and M. A. Shifman, "Heavy quarks," *Physics-Uspekhi*, vol. 26, no. 5, pp. 387–424, 1983.

[70] S. Nussinov and W. Wetzel, "Comparison of exclusive decay rates for $b \to u$ and $b \to c$ transitions," *Physical Review D*, vol. 36, no. 1, p. 130, 1987.

[71] H. D. Politzer and M. B. Wise, "Leading logarithms of heavy quark masses in processes with light and heavy quarks," *Physics Letters B*, vol. 206, no. 4, pp. 681–684, 1988.

[72] N. Isgur and M. B. Wise, "Weak decays of heavy mesons in the static quark approximation," *Physics Letters B*, vol. 232, no. 1, pp. 113–117, 1989.

[73] W. E. Caswell and G. P. Lepage, "Effective lagrangians for bound state problems in qed, QCD, and other field theories," *Physics Letters B*, vol. 167, no. 4, pp. 437–442, 1986.

[74] G. T. Bodwin, E. Braaten, and G. P. Lepage, "Rigorous QCD analysis of inclusive annihilation and production of heavy quarkonium," *Physical Review D*, vol. 51, no. 3, p. 1125, 1995.

[75] B. Jantzen and V. A. Smirnov, "The two-loop vector form factor in the Sudakov limit," *The European Physical Journal C-Particles and Fields*, vol. 47, no. 3, pp. 671–695, 2006.

[76] J.-y. Chiu, F. Golf, R. Kelley, and A. V. Manohar, "Electroweak corrections to high energy processes using effective field theory," *Physical Review D*, vol. 77, no. 5, p. 053004, 2008.

[77] O. V. Tarasov, "Connection between Feynman integrals having different values of the space-time dimension," *Physical Review D*, vol. 54, no. 10, p. 6479, 1996.

[78] E. Remiddi, "Differential equations for Feynman graph amplitudes," *Il Nuovo Cimento A (1971-1996)*, vol. 110, no. 12, pp. 1435–1452, 1997.

[79] R. Lee, "Calculating multiloop integrals using dimensional recurrence relation and d-analyticity," *arXiv preprint: hep-ph/1007.2256*, 2010.

[80] R. Lee, "Space-time dimensionality $\mathcal{D}$ as complex variable: Calculating loop integrals using dimensional recurrence relation and analytical properties with respect to $\mathcal{D}$," *Nuclear Physics B*, vol. 830, no. 3, pp. 474–492, 2010.

[81] A. Kotikov, "Differential equation method. The calculation of N-point Feynman diagrams," *Physics Letters B*, vol. 267, no. 1, pp. 123–127, 1991.

[82] A. V. Kotikov, "Differential equations method. new technique for massive Feynman diagram calculation," *Physics Letters B*, vol. 254, no. 1-2, pp. 158–164, 1991.

[83] A. Kotikov, "New method of massive Feynman diagrams calculation," *Modern Physics Letters A*, vol. 6, no. 08, pp. 677–692, 1991.

[84] M. D. Schwartz, *Quantum field theory and the standard model*. Cambridge University Press, 2014.

[85] D. J. Gross and F. Wilczek, "Ultraviolet behavior of non-abelian gauge theories," *Physical Review Letters*, vol. 30, no. 26, p. 1343, 1973.

[86] S. Weinberg, "Non-abelian gauge theories of the strong interactions," *Physical Review Letters*, vol. 31, no. 7, p. 494, 1973.

[87] H. Fritzsch, M. Gell-Mann, and H. Leutwyler, "Advantages of the color octet gluon picture," *Physics Letters B*, vol. 47, no. 4, pp. 365–368, 1973.

[88] H. D. Politzer, "Reliable perturbative results for strong interactions?," *Physical Review Letters*, vol. 30, no. 26, p. 1346, 1973.

[89] S. Weinberg, "A model of leptons," *Physical review letters*, vol. 19, no. 21, p. 1264, 1967.

[90] S. L. Glashow, "Partial-symmetries of weak interactions," *Nuclear physics*, vol. 22, no. 4, pp. 579–588, 1961.

[91] S. Abdus, "Weak and electromagnetic interactions, conf," *Proc. C*, vol. 680519, pp. 367–377, 1968.

[92] L. Wolfenstein, "Neutrino oscillations in matter," in *Solar Neutrinos*, pp. 294–299, CRC Press, 2018.

[93] F. Boehm, P. Vogel, and P. Vogel, *Physics of massive neutrinos*. Cambridge University Press, 1992.

[94] M. Veltman *et al.*, "Regularization and renormalization of gauge fields," *Nuclear Physics B*, vol. 44, no. 1, pp. 189–213, 1972.

[95] D. H. Sattinger and O. L. Weaver, *Lie groups and algebras with applications to physics, geometry, and mechanics*, vol. 61. Springer Science & Business Media, 2013.

[96] T.-D. Lee and C.-N. Yang, "Question of parity conservation in weak interactions," *Physical Review*, vol. 104, no. 1, p. 254, 1956.

[97] Y. S. Kim and M. Noz, *Theory and applications of the Poincaré group*, vol. 17. Springer Science & Business Media, 2012.

[98] J. Bardeen, L. N. Cooper, and J. R. Schrieffer, "Theory of superconductivity," *Physical review*, vol. 108, no. 5, p. 1175, 1957.

[99] L. Sadler, J. Higbie, S. Leslie, M. Vengalattore, and D. Stamper-Kurn, "Spontaneous symmetry breaking in a quenched ferromagnetic spinor Bose–Einstein condensate," *Nature*, vol. 443, no. 7109, pp. 312–315, 2006.

[100] A. Albrecht and P. J. Steinhardt, "Cosmology for grand unified theories with radiatively induced symmetry breaking," *Physical Review Letters*, vol. 48, no. 17, p. 1220, 1982.

[101] J. Goldstone, "Field theories with superconductor solutions," *Il Nuovo Cimento (1955-1965)*, vol. 19, no. 1, pp. 154–164, 1961.

[102] J. Goldstone, A. Salam, and S. Weinberg, "Broken symmetries," *Physical Review*, vol. 127, no. 3, p. 965, 1962.

[103] G. t Hooft and M. Veltman, "Combinatorics of gauge fields," *Nuclear Physics B*, vol. 50, no. 1, pp. 318–353, 1972.

[104] S. L. Glashow, J. Iliopoulos, and L. Maiani, "Weak interactions with lepton-hadron symmetry," *Physical review D*, vol. 2, no. 7, p. 1285, 1970.

[105] N. Cabibbo, "Unitary symmetry and leptonic decays," *Physical Review Letters*, vol. 10, no. 12, p. 531, 1963.

[106] M. Kobayashi and T. Maskawa, "CP-violation in the renormalizable theory of weak interaction," *Progress of theoretical physics*, vol. 49, no. 2, pp. 652–657, 1973.

[107] L.-L. Chau and W.-Y. Keung, "Comments on the parametrization of the Kobayashi-Maskawa matrix," *Physical Review Letters*, vol. 53, no. 19, p. 1802, 1984.

[108] T. Ibrahim and P. Nath, "CP violation from the Standard Model to strings," *Reviews of Modern Physics*, vol. 80, no. 2, p. 577, 2008.

[109] M. Drewes, "The phenomenology of right handed neutrinos," *International Journal of Modern Physics E*, vol. 22, no. 08, p. 1330019, 2013.

[110] S. Weinberg, "Phenomenological lagrangians," *Physica a*, vol. 96, no. 1-2, pp. 327–340, 1979.

[111] R. P. Feynman, "Mathematical formulation of the quantum theory of electromagnetic interaction," *Physical Review*, vol. 80, no. 3, p. 440, 1950.

[112] F. J. Dyson, "The s matrix in quantum electrodynamics," *Physical Review*, vol. 75, no. 11, p. 1736, 1949.

[113] S. Weinberg, "New approach to the renormalization group," *Physical Review D*, vol. 8, no. 10, p. 3497, 1973.

[114] G. Martinelli, C. Pittori, C. T. Sachrajda, M. Testa, and A. Vladikas, "A general method for non-perturbative renormalization of lattice operators," *Nuclear Physics B*, vol. 445, no. 1, pp. 81–105, 1995.

[115] A. Denner, "Techniques for the calculation of electroweak radiative corrections at the one-loop level and results for W-physics at LEP 200," *Fortschritte der Physik/Progress of Physics*, vol. 41, no. 4, pp. 307–420, 1993.

[116] G. Prosperi, M. Raciti, and C. Simolo, "On the running coupling constant in QCD," *Progress in Particle and Nuclear Physics*, vol. 58, no. 2, pp. 387–438, 2007.

[117] A. Bednyakov, A. Pikelner, and V. Velizhanin, "Higgs self-coupling beta-function in the Standard Model at three loops," *Nuclear Physics B*, vol. 875, no. 3, pp. 552–565, 2013.

[118] J. Elias-Miro, J. R. Espinosa, G. F. Giudice, G. Isidori, A. Riotto, and A. Strumia, "Higgs mass implications on the stability of the electroweak vacuum," *Physics Letters B*, vol. 709, no. 3, pp. 222–228, 2012.

[119] A. Bednyakov, B. Kniehl, A. Pikelner, and O. Veretin, "Stability of the electroweak vacuum: gauge independence and advanced precision," *Physical review letters*, vol. 115, no. 20, p. 201802, 2015.

[120] M. Jung and D. M. Straub, "Constraining new physics in $b \to cl\nu$ transitions," *Journal of High Energy Physics*, vol. 2019, no. 1, p. 9, 2019.

[121] M. Chala, J. Santiago, and M. Spannowsky, "Constraining four-fermion operators using rare top decays," *Journal of High Energy Physics*, vol. 2019, no. 4, p. 14, 2019.

[122] A. X. El-Khadra and M. Luke, "The mass of the b quark," *Annual Review of Nuclear and Particle Science*, vol. 52, no. 1, pp. 201–251, 2002.

[123] M. Gronau, D. Pirjol, A. Soni, and J. Zupan, "Improved method for CKM constraints in charmless three-body B and B_s decays," *Physical Review D*, vol. 75, no. 1, p. 014002, 2007.

[124] A. J. Buras and R. Fleischer, "Constraints on the CKM angle γ and strong phases from $B \to \pi K$ decays," *The European Physical Journal C-Particles and Fields*, vol. 16, no. 1, pp. 97–104, 2000.

[125] C. T. Davies, E. Follana, A. Gray, G. Lepage, Q. Mason, M. Nobes, J. Shigemitsu, H. Trottier, M. Wingate, C. Aubin, *et al.*, "High-precision lattice QCD confronts experiment," *Physical Review Letters*, vol. 92, no. 2, p. 022001, 2004.

[126] S. Muroya, A. Nakamura, C. Nonaka, and T. Takaishi, "Lattice QCD at finite density: an introductory review,"

[127] Y. Nir, "The mass ratio m_c/m_b in semi-leptonic B-decays," *Physics Letters B*, vol. 221, no. 2, pp. 184–190, 1989.

[128] P. Ball, "Finite mass corrections to leptonic decay constants in the heavy quark effective theory," *Nuclear Physics B*, vol. 421, no. 3, pp. 593–612, 1994.

[129] E. Bagan, P. Ball, V. M. Braun, and H. G. Dosch, "QCD sum rules in the effective heavy quark theory," *Physics Letters B*, vol. 278, no. 4, pp. 457–464, 1992.

[130] M. Beneke and V. M. Braun, "Heavy quark effective theory beyond perturbation theory: Renormalons, the pole mass and the residual mass term," *Nuclear Physics B*, vol. 426, no. 2, pp. 301–343, 1994.

[131] A. Pineda, "Determination of the bottom quark mass from the $\Upsilon(1S)$ system," *Journal of High Energy Physics*, vol. 2001, no. 06, p. 022, 2001.

[132] A. Hoang and T. Teubner, "Top-quark pair production close to threshold: Top-quark mass, width, and momentum distribution," *Physical Review D*, vol. 60, no. 11, p. 114027, 1999.

[133] P. Marquard, A. V. Smirnov, V. A. Smirnov, and M. Steinhauser, "Quark mass relations to four-loop order in perturbative QCD," *Physical review letters*, vol. 114, no. 14, p. 142002, 2015.

[134] P. Marquard, A. V. Smirnov, V. A. Smirnov, M. Steinhauser, and D. Wellmann, "$\overline{\text{MS}}$-OS quark mass relation up to four loops in QCD and a general SU(N) gauge group," *Physical Review D*, vol. 94, no. 7, p. 074025, 2016.

[135] R. Tarrach, "The pole mass in perturbative QCD," *Nuclear Physics B*, vol. 183, no. 3, pp. 384–396, 1981.

[136] J. Breckenridge, M. Lavelle, and T. G. Steele, "The Nielsen identities for the two-point functions of QED and QCD," *Zeitschrift für Physik C Particles and Fields*, vol. 65, no. 1, pp. 155–164, 1995.

[137] A. S. Kronfeld, "Perturbative pole mass in QCD," *Physical Review D*, vol. 58, no. 5, p. 051501, 1998.

[138] M. Luke, M. J. Savage, and M. B. Wise, "Perturbative strong interaction corrections to the heavy quark semileptonic decay rate," *Physics Letters B*, vol. 343, no. 1-4, pp. 329–332, 1995.

[139] T. van Ritbergen, "The second order QCD contribution to the semileptonic $b \to u$ decay rate," *Physics Letters B*, vol. 454, no. 3-4, pp. 353–358, 1999.

[140] A. Hoang, A. Manohar, I. W. Stewart, and T. Teubner, "Threshold $t\bar{t}$ cross section at next-to-next-to-leading logarithmic order," *Physical Review D*, vol. 65, no. 1, p. 014014, 2001.

[141] M. E. Luke, A. V. Manohar, and I. Z. Rothstein, "Renormalization group scaling in non-relativistic QCD," *Physical Review D*, vol. 61, no. 7, p. 074025, 2000.

[142] N. Gray, D. J. Broadhurst, W. Gräfe, and K. Schilcher, "Three-loop relation of quark $\overline{\text{MS}}$ and pole masses," *Zeitschrift für Physik C Particles and Fields*, vol. 48, no. 4, pp. 673–679, 1990.

[143] K. Chetyrkin and M. Steinhauser, "The relation between the $\overline{\text{MS}}$ and the on-shell quark mass at order α_s^3," *Nuclear Physics B*, vol. 573, no. 3, pp. 617–651, 2000.

[144] K. Melnikov and T. van Ritbergen, "The three-loop relation between the $\overline{\text{MS}}$ and the pole quark masses," *Physics Letters B*, vol. 482, no. 1-3, pp. 99–108, 2000.

[145] R. Hempfling and B. A. Kniehl, "Relation between the fermion pole mass and $\overline{\text{MS}}$ Yukawa coupling in the Standard Model," *Physical Review D*, vol. 51, no. 3, p. 1386, 1995.

[146] B. A. Kniehl, "Dependence of electroweak parameters on the definition of the top-quark mass," *Zeitschrift für Physik C: Particles and Fields*, vol. 72, no. 3, p. 437, 1996.

[147] F. Jegerlehner, M. Y. Kalmykov, and B. A. Kniehl, "On the difference between the pole and the $\overline{\text{MS}}$ masses of the top quark at the electroweak scale," *Physics Letters B*, vol. 722, no. 1-3, pp. 123–129, 2013.

[148] B. A. Kniehl and O. L. Veretin, "Two-loop electroweak threshold corrections to the bottom and top yukawa couplings," *Nuclear Physics B*, vol. 885, pp. 459–480, 2014.

[149] B. A. Kniehl, A. F. Pikelner, and O. L. Veretin, "Two-loop electroweak threshold corrections in the standard model," *Nuclear Physics B*, vol. 896, pp. 19–51, 2015.

[150] S. Fanchiotti, B. Kniehl, and A. Sirlin, "Incorporation of QCD effects in basic corrections of the electroweak theory," *Physical Review D*, vol. 48, no. 1, p. 307, 1993.

[151] F. Jegerlehner, M. Y. Kalmykov, and B. A. Kniehl, "About the EW contribution to the relation between pole and MS-masses of the top-quark in the Standard Model," *arXiv preprint: hep-ph/1307.4226*, 2013.

[152] A. Hoang, M. Beneke, K. Melnikov, T. Nagano, A. Ota, A. Penin, A. Pivovarov, A. Signer, V. Smirnov, Y. Sumino, *et al.*, "Top-Antitop Pair Production Close to Threshold Synopsis of Recent NNLO Results," *EPJ direct*, vol. 2, no. 1, pp. 1–22, 2000.

[153] A. V. Manohar and M. B. Wise, *Heavy quark physics*, vol. 10. Cambridge university press, 2007.

[154] I. Bigi, M. Shifman, N. Uraltsev, and A. Vainshtein, "Sum rules for heavy flavor transitions in the small velocity limit," *Physical Review D*, vol. 52, no. 1, p. 196, 1995.

[155] I. Bigi, M. Shifman, and N. Uraltsev, "Aspects of heavy-quark theory," *Annual Review of Nuclear and Particle Science*, vol. 47, no. 1, pp. 591–661, 1997.

[156] M. A. Shifman and M. Voloshin, "On annihilation of mesons built from heavy and light quark and $\bar{B}_0 \leftrightarrow B_0$ oscillations," tech. rep., Gosudarstvennyj Komitet po Ispol'zovaniyu Atomnoj Ehnergii SSSR, 1986.

[157] M. Fael, K. Schönwald, and M. Steinhauser, "Kinetic heavy quark mass to three loops," *Physical review letters*, vol. 125, no. 5, p. 052003, 2020.

[158] A. Czarnecki, K. Melnikov, and N. Uraltsev, "Non-abelian dipole radiation and the heavy quark expansion," *Physical review letters*, vol. 80, no. 15, p. 3189, 1998.

[159] W. Fischler, "Quark-antiquark potential in QCD," *Nuclear Physics B*, vol. 129, pp. 157–174, 1977.

[160] L. D. Landau and E. M. Lifshitz, *Quantum mechanics: non-relativistic theory*, vol. 3. Elsevier, 2013.

[161] B. Assi and B. A. Kniehl, "Matching the standard model to HQET and NRQCD," *arXiv preprint: hep-ph/2011.06447*, 2020.

[162] A. Pineda and F. Yndurain, "Calculation of the quarkonium spectrum and m_b, m_c to order α_s^4," *Physical Review D*, vol. 58, no. 9, p. 094022, 1998.

[163] G. Altarelli and F. Feruglio, "Discrete flavor symmetries and models of neutrino mixing," *Reviews of Modern Physics*, vol. 82, no. 3, p. 2701, 2010.

[164] M. Dine and A. Kusenko, "Origin of the matter-antimatter asymmetry," *Reviews of Modern Physics*, vol. 76, no. 1, p. 1, 2003.

[165] J. F. Navarro, "The structure of cold dark matter halos," in *Symposium-international astronomical union*, vol. 171, pp. 255–258, Cambridge University Press, 1996.

[166] A. H. Guth, "Inflationary universe: A possible solution to the horizon and flatness problems," *Physical Review D*, vol. 23, no. 2, p. 347, 1981.

[167] M. Tanabashi, K. Hagiwara, K. Hikasa, K. Nakamura, Y. Sumino, F. Takahashi, J. Tanaka, K. Agashe, G. Aielli, C. Amsler, *et al.*, "Review of particle physics," *Physical Review D*, vol. 98, no. 3, p. 030001, 2018.

[168] P. Zyla, "Particle data group," *Prog. Theor. Exp. Phys.*, vol. 2020, p. 083C01, 2020.

[169] L. Wolfenstein, "Parametrization of the Kobayashi-Maskawa matrix," *Physical Review Letters*, vol. 51, no. 21, p. 1945, 1983.

[170] F. Cooper, A. Khare, and U. Sukhatme, "Supersymmetry and quantum mechanics," *Physics Reports*, vol. 251, no. 5-6, pp. 267–385, 1995.

[171] C. D. Froggatt and H. B. Nielsen, "Hierarchy of quark masses, Cabibbo angles and CP violation," *Nuclear Physics B*, vol. 147, no. 3-4, pp. 277–298, 1979.

[172] K. S. Babu, E. Ma, and J. Valle, "Underlying A_4 symmetry for the neutrino mass matrix and the quark mixing matrix," *Physics Letters B*, vol. 552, no. 3-4, pp. 207–213, 2003.

[173] P. Francesco, P. Mathieu, and D. Sénéchal, *Conformal field theory*. Springer Science & Business Media, 2012.

[174] A. E. Nelson and M. J. Strassler, "Suppressing flavor anarchy," *Journal of High Energy Physics*, vol. 2000, no. 09, p. 030, 2000.

[175] A. E. Nelson and M. J. Strassler, "Exact results for supersymmetric renormalization and the supersymmetric flavor problem," *Journal of High Energy Physics*, vol. 2002, no. 07, p. 021, 2002.

[176] R. Aaij, B. Adeva, Adinolfi, *et al.*, "Differential branching fractions and isospin asymmetries of $B \to K^* \mu^+ \mu^-$ decays," *Journal of High Energy Physics*, vol. 2014, no. 6, pp. 1–22, 2014.

[177] R. Aaij, B. Adeva, M. Adinolfi, A. Affolder, *et al.*, "Angular analysis and differential branching fraction of the decay $B_s^0 \to \phi \mu^+ \phi^-$," *Journal of High Energy Physics*, vol. 2015, no. 9, pp. 1–35, 2015.

[178] A. Bharucha, D. M. Straub, and R. Zwicky, "$B \to V l^+ l^-$ in the Standard Model from light-cone sum rules," *Journal of High Energy Physics*, vol. 2016, no. 8, pp. 1–64, 2016.

[179] R. Horgan, Z. Liu, S. Meinel, and M. Wingate, "Rare b decays using lattice QCD form factors," *arXiv preprint: hep-ph/1501.00367*, 2015.

[180] R. Aaij, C. A. Beteta, B. Adeva, M. Adinolfi, A. Affolder, Z. Ajaltouni, S. Akar, J. Albrecht, F. Alessio, M. Alexander, *et al.*, "Angular analysis of the $B_0 \to K^{*0} \mu^+ \mu^-$ decay using $3 f_b^{-1}$ of integrated luminosity," *Journal of High Energy Physics*, vol. 2016, no. 2, p. 104, 2016.

[181] A. Khodjamirian, T. Mannel, A. Pivovarov, and Y.-M. Wang, "Charm-loop effect in $B \to K^{*0} \mu^+ \mu^-$ and $B \to K^* \gamma$," *Journal of High Energy Physics*, vol. 2010, no. 9, pp. 1–36, 2010.

[182] M. Bordone, G. Isidori, and A. Pattori, "On the Standard Model predictions for R_K and R_{K^*}," *The European Physical Journal C*, vol. 76, no. 8, pp. 1–6, 2016.

[183] J. Lees, V. Poireau, V. Tisserand, J. G. Tico, E. Grauges, A. Palano, G. Eigen, B. Stugu, D. Brown, L. Kerth, *et al.*, "Evidence for an excess of $\bar{B} \to d^* \tau^- \bar{\nu}_\tau$ decays," *Physical review letters*, vol. 109, no. 10, p. 101802, 2012.

[184] E. Waheed, P. Urquijo, D. Ferlewicz, I. Adachi, K. Adamczyk, H. Aihara, S. Al Said, D. Asner, H. Atmacan, T. Aushev, *et al.*, "Measurement of the CKM matrix element $|V_{cb}|$ from $B^0 \to D^{*-} l^+ \nu_l$ at Belle," *Physical Review D*, vol. 100, no. 5, p. 052007, 2019.

[185] D. Bigi, P. Gambino, and S. Schacht, "$R(D^*)$, $|V_{cb}|$ and the Heavy Quark Symmetry relations between form factors," *Journal of High Energy Physics*, vol. 2017, no. 11, p. 61, 2017.

[186] W. Altmannshofer, P. Stangl, and D. M. Straub, "Interpreting hints for lepton flavor universality violation," *Physical Review D*, vol. 96, no. 5, p. 055008, 2017.

[187] T. Aoyama, N. Asmussen, M. Benayoun, J. Bijnens, T. Blum, M. Bruno, I. Caprini, C. C. Calame, M. Cè, G. Colangelo, *et al.*, "The anomalous magnetic moment of the muon in the Standard Model," *Physics reports*, 2020.

[188] F. Jegerlehner, "Muon $g-2$ theory: The hadronic part," in *EPJ Web of Conferences*, vol. 166, p. 00022, EDP Sciences, 2018.

[189] M. Davier, "Update of the hadronic vacuum polarization contribution to the muon $g-2$," *Nuclear and particle physics proceedings*, vol. 287, pp. 70–75, 2017.

[190] S. Borsanyi, Z. Fodor, J. Guenther, C. Hoelbling, S. Katz, L. Lellouch, T. Lippert, K. Miura, L. Szabo, F. Stokes, *et al.*, "Leading-order hadronic vacuum polarization contribution to the muon magnetic moment from lattice QCD," *arXiv preprint: hep-ph/2002.12347*, 2020.

[191] A. Crivellin, M. Hoferichter, C. A. Manzari, and M. Montull, "Hadronic vacuum polarization:$(g-2)_\mu$ versus global electroweak fits," *Physical review letters*, vol. 125, no. 9, p. 091801, 2020.

[192] A. Keshavarzi, W. J. Marciano, M. Passera, and A. Sirlin, "Muon $g-2$ and $\delta\alpha$ connection," *Physical Review D*, vol. 102, no. 3, p. 033002, 2020.

[193] P. Boyle, L. Del Debbio, E. Kerrane, and J. Zanotti, "Lattice determination of the hadronic contribution to the muon $g-2$ using dynamical domain wall fermions," *Physical Review D*, vol. 85, no. 7, p. 074504, 2012.

[194] H. Davoudiasl and W. J. Marciano, "Tale of two anomalies," *Physical Review D*, vol. 98, no. 7, p. 075011, 2018.

[195] J. Liu, C. E. Wagner, and X.-P. Wang, "A light complex scalar for the electron and muon anomalous magnetic moments," *Journal of High Energy Physics*, vol. 2019, no. 3, pp. 1–25, 2019.

[196] M. Bauer, M. Neubert, S. Renner, M. Schnubel, and A. Thamm, "Axionlike particles, lepton-flavor violation, and a new explanation of a a_μ and a_e," *Physical Review Letters*, vol. 124, no. 21, p. 211803, 2020.

[197] B. Dutta and Y. Mimura, "Electron $g-2$ with flavor violation in MSSM," *Physics Letters B*, vol. 790, pp. 563–567, 2019.

[198] M. Endo and W. Yin, "Explaining electron and muon $g-2$ anomaly in SUSY without lepton-flavor mixings," *Journal of High Energy Physics*, vol. 2019, no. 8, pp. 1–13, 2019.

[199] M. Badziak and K. Sakurai, "Explanation of electron and muon $g-2$ anomalies in the MSSM," *Journal of High Energy Physics*, vol. 2019, no. 10, pp. 1–19, 2019.

[200] R. D. Peccei, "The strong CP problem and axions," in *Axions*, pp. 3–17, Springer, 2008.

[201] C. Bonati, M. D'Elia, M. Mariti, G. Martinelli, M. Mesiti, F. Negro, F. Sanfilippo, and G. Villadoro, "Axion phenomenology and θ-dependence from $n_f = 2+1$ lattice QCD," *Journal of High Energy Physics*, vol. 2016, no. 3, p. 155, 2016.

[202] S. Borsányi, Z. Fodor, J. Guenther, K.-H. Kampert, S. Katz, T. Kawanai, T. Kovacs, S. Mages, A. Pasztor, F. Pittler, *et al.*, "Calculation of the axion mass based on high-temperature lattice QCD," *Nature*, vol. 539, no. 7627, pp. 69–71, 2016.

[203] J. E. Kim and G. Carosi, "Axions and the strong CP problem," *Reviews of Modern Physics*, vol. 82, no. 1, p. 557, 2010.

[204] C. Baker, D. Doyle, P. Geltenbort, K. Green, M. Van der Grinten, P. Harris, P. Iaydjiev, S. Ivanov, D. May, J. Pendlebury, *et al.*, "Improved experimental limit on the electric dipole moment of the neutron," *Physical Review Letters*, vol. 97, no. 13, p. 131801, 2006.

[205] R. D. Peccei and H. R. Quinn, "Constraints imposed by CP conservation in the presence of pseudoparticles," *Physical Review D*, vol. 16, no. 6, p. 1791, 1977.

[206] S. Weinberg, "A new light boson?," *Physical Review Letters*, vol. 40, no. 4, p. 223, 1978.

[207] F. Wilczek, "Problem of strong p and t invariance in the presence of instantons," *Physical Review Letters*, vol. 40, no. 5, p. 279, 1978.

[208] J. Redondo, "Solar axion flux from the axion-electron coupling," *Journal of Cosmology and Astroparticle Physics*, vol. 2013, no. 12, p. 008, 2013.

[209] K. Hirata, T. Kajita, M. Koshiba, M. Nakahata, Y. Oyama, N. Sato, A. Suzuki, M. Takita, Y. Totsuka, T. Kifune, *et al.*, "Observation of a neutrino burst from the supernova SN1987A," *Physical Review Letters*, vol. 58, no. 14, p. 1490, 1987.

[210] V. Anastassopoulos, S. Aune, K. Barth, A. Belov, H. Bräuninger, G. Cantatore, J. Carmona, J. Castel, S. Cetin, F. Christensen, *et al.*, "New CAST limit on the axion–photon interaction," *Nature Physics*, vol. 13, no. 6, p. 584, 2017.

[211] E. Armengaud, F. Avignone, M. Betz, P. Brax, P. Brun, G. Cantatore, J. Carmona, G. Carosi, F. Caspers, S. Caspi, *et al.*, "Conceptual design of the international axion observatory (IAXO)," *Journal of Instrumentation*, vol. 9, no. 05, p. T05002, 2014.

[212] E. Armengaud, D. Attié, S. Basso, P. Brun, N. Bykovskiy, J. Carmona, J. Castel, S. Cebrián, M. Cicoli, M. Civitani, *et al.*, "Physics potential of the international axion observatory (IAXO)," *Journal of Cosmology and Astroparticle Physics*, vol. 2019, no. 06, p. 047, 2019.

[213] N. Du, N. Force, R. Khatiwada, E. Lentz, R. Ottens, L. Rosenberg, G. Rybka, G. Carosi, N. Woollett, D. Bowring, *et al.*, "Search for invisible axion dark matter with the axion dark matter experiment," *Physical review letters*, vol. 120, no. 15, p. 151301, 2018.

[214] T. Braine, R. Cervantes, N. Crisosto, N. Du, S. Kimes, L. Rosenberg, G. Rybka, J. Yang, D. Bowring, A. Chou, *et al.*, "Extended search for the invisible axion with the axion dark matter experiment," *Physical review letters*, vol. 124, no. 10, p. 101303, 2020.

[215] K. Ehret, M. Frede, S. Ghazaryan, M. Hildebrandt, E.-A. Knabbe, D. Kracht, A. Lindner, J. List, T. Meier, N. Meyer, *et al.*, "New ALPS results on hidden-sector lightweights," *Physics Letters B*, vol. 689, no. 4-5, pp. 149–155, 2010.

[216] N. Crescini, C. Braggio, G. Carugno, P. Falferi, A. Ortolan, and G. Ruoso, "The QUAX-gpgs experiment to search for monopole-dipole axion interaction," *Nuclear Instruments and Methods in Physics Research Section A: Accelerators, Spectrometers, Detectors and Associated Equipment*, vol. 842, pp. 109–113, 2017.

[217] J. Preskill, M. B. Wise, and F. Wilczek, "Cosmology of the invisible axion," *Physics Letters B*, vol. 120, no. 1-3, pp. 127–132, 1983.

[218] A. V. Manohar, "Heavy quark effective theory and nonrelativistic QCD lagrangian to order α_s/m^3," *Physical Review D*, vol. 56, no. 1, p. 230, 1997.

[219] T. Appelquist and J. Carazzone, "Infrared singularities and massive fields," *Physical Review D*, vol. 11, no. 10, p. 2856, 1975.

[220] J. Gasser and H. Leutwyler, "Chiral perturbation theory to one loop," *Annals of Physics*, vol. 158, no. 1, pp. 142–210, 1984.

[221] P. Azzi, S. Farry, P. Nason, A. Tricoli, D. Zeppenfeld, R. A. Khalek, J. Alimena, N. Andari, L. A. Bella, A. Armbruster, *et al.*, "Standard Model physics at the HL-LHC and HE-LHC," *arXiv preprint: hep-ph/1902.04070*, 2019.

[222] R. M. Fonseca, "Enumerating the operators of an effective field theory," *Physical Review D*, vol. 101, no. 3, p. 035040, 2020.

[223] C. Hays, A. Martin, V. Sanz, and J. Setford, "On the impact of dimension-eight SMEFT operators on Higgs measurements," *Journal of High Energy Physics*, vol. 2019, no. 2, pp. 1–41, 2019.

[224] L. Lehman and A. Martin, "Low-derivative operators of the Standard Model effective field theory via Hilbert series methods," *Journal of High Energy Physics*, vol. 2016, no. 2, p. 81, 2016.

[225] S. Weinberg, "Larger Higgs-boson-exchange terms in the neutron electric dipole moment," *Physical Review Letters*, vol. 63, no. 21, p. 2333, 1989.

[226] S. Weinberg, "Baryon-and lepton-nonconserving processes," *Physical Review Letters*, vol. 43, no. 21, p. 1566, 1979.

[227] B. Grzadkowski, M. Iskrzyński, M. Misiak, and J. Rosiek, "Dimension-six terms in the standard model lagrangian," *Journal of High Energy Physics*, vol. 2010, no. 10, p. 85, 2010.

[228] B. Henning, X. Lu, T. Melia, and H. Murayama, "Higher dimension operators in the SM EFT," *Journal of High Energy Physics*, vol. 2017, no. 8, pp. 1–24, 2017.

[229] S. Willenbrock, "Symmetries of the standard model," in *Physics In D 4 Tasi 2004: TASI 2004*, pp. 3–38, World Scientific, 2006.

[230] B. Kayser and F. oise Gibrat-Debu, *The physics of massive neutrinos*, vol. 25. World Scientific, 1989.

[231] B. Henning, X. Lu, and H. Murayama, "How to use the Standard Model effective field theory," *Journal of High Energy Physics*, vol. 2016, no. 1, p. 23, 2016.

[232] J. Ellis, C. W. Murphy, V. Sanz, and T. You, "Updated global smeft fit to Higgs, di-boson and electroweak data," *Journal of High Energy Physics*, vol. 2018, no. 6, pp. 1–34, 2018.

[233] E. Eichten and B. R. Hill, "Static effective field theory: $1/m$ corrections," *Phys. Lett.*, vol. 243, no. Fermilab-pub-90-054-T, pp. 427–431, 1990.

[234] A. F. Falk, M. Neubert, and M. Luke, "The residual mass term in the heavy quark effective theory," *Nuclear Physics B*, vol. 388, no. 2, pp. 363–375, 1992.

[235] A. Czarnecki and K. Melnikov, "Two-loop QCD corrections to the heavy quark pair production cross section in e^+e^- annihilation near threshold," *Physical Review Letters*, vol. 80, no. 12, p. 2531, 1998.

[236] R. J. Hill, G. Lee, G. Paz, and M. P. Solon, "NRQED Lagrangian at order $1/M^4$," *Physical Review D*, vol. 87, no. 5, p. 053017, 2013.

[237] A. Gunawardana and G. Paz, "On HQET and NRQCD operators of dimension 8 and above," *Journal of High Energy Physics*, vol. 2017, no. 7, pp. 1–30, 2017.

[238] A. Grozin, P. Marquard, J. Piclum, and M. Steinhauser, "Three-loop chromomagnetic interaction in HQET," *Nuclear physics B*, vol. 789, no. 1-2, pp. 277–293, 2008.

[239] K. Chetyrkin and A. Grozin, "Three-loop anomalous dimension of the heavy-light quark current in HQET," *Nuclear Physics B*, vol. 666, no. 1-2, pp. 289–302, 2003.

[240] A. F. Falk, "Hadrons of arbitrary spin in the heavy-quark effective theory," *Nuclear Physics B*, vol. 378, no. 1-2, pp. 79–94, 1992.

[241] S. Alte, M. König, and M. Neubert, "Effective theory for a heavy scalar coupled to the SM via vector-like quarks," *The European Physical Journal C*, vol. 79, no. 4, p. 352, 2019.

[242] P. H. Damgaard, K. Haddad, and A. Helset, "Heavy black hole effective theory," *Journal of High Energy Physics*, vol. 2019, no. 11, pp. 1–27, 2019.

[243] M. Heiles, M. König, and M. Neubert, "Effective field theory for heavy vector resonances coupled to the standard model," *arXiv preprint: hep-ph/2011.08205*, 2020.

[244] Z. Bern, C. Cheung, R. Roiban, C.-H. Shen, M. P. Solon, and M. Zeng, "Black hole binary dynamics from the double copy and effective theory," *Journal of High Energy Physics*, vol. 2019, no. 10, pp. 1–135, 2019.

[245] G. P. Lepage, L. Magnea, C. Nakhleh, U. Magnea, and K. Hornbostel, "Improved nonrelativistic QCD for heavy-quark physics," *Physical Review D*, vol. 46, no. 9, p. 4052, 1992.

[246] M. Luke and A. V. Manohar, "Bound states and power counting in effective field theories," *Physical Review D*, vol. 55, no. 7, p. 4129, 1997.

[247] M. Beneke and V. A. Smirnov, "Asymptotic expansion of Feynman integrals near threshold," *Nuclear Physics B*, vol. 522, no. 1-2, pp. 321–344, 1998.

[248] B. Grinstein and I. Z. Rothstein, "Effective field theory and matching in nonrelativistic gauge theories," *Physical Review D*, vol. 57, no. 1, p. 78, 1998.

[249] M. Luke and M. J. Savage, "Power counting in dimensionally regularized nonrelativistic QCD," *Physical Review D*, vol. 57, no. 1, p. 413, 1998.

[250] A. Pineda, "NRQCD, effective field theories and potential models," *Nuclear Physics B-Proceedings Supplements*, vol. 93, no. 1-3, pp. 188–191, 2001.

[251] N. Brambilla, A. Pineda, J. Soto, and A. Vairo, "Potential NRQCD: An effective theory for heavy quarkonium," *Nuclear Physics B*, vol. 566, no. 1-2, pp. 275–310, 2000.

[252] T. Becher, A. Broggio, and A. Ferroglia, *Introduction to soft-collinear effective theory*, vol. 896. Springer, 2015.

[253] I. Korchemskaya and G. Korchemsky, "On light-like Wilson loops," *Physics Letters B*, vol. 287, no. 1-3, pp. 169–175, 1992.

[254] S. Mantry and F. Petriello, "Factorization and resummation of Higgs boson differential distributions in soft-collinear effective theory," *Physical Review D*, vol. 81, no. 9, p. 093007, 2010.

[255] C. W. Bauer, D. Pirjol, and I. W. Stewart, "Soft-collinear factorization in effective field theory," *Physical Review D*, vol. 65, no. 5, p. 054022, 2002.

[256] M. Beneke, A. P. Chapovsky, M. Diehl, and T. Feldmann, "Soft-collinear effective theory and heavy-to-light currents beyond leading power," *Nuclear Physics B*, vol. 643, no. 1-3, pp. 431–476, 2002.

[257] S. M. Freedman and M. Luke, "Soft collinear effective theory, QCD, and Wilson lines," *Physical Review D*, vol. 85, no. 1, p. 014003, 2012.

[258] C. W. Bauer, S. Fleming, and M. Luke, "Summing Sudakov logarithms in $B \to X_s\gamma$ in effective field theory," *Physical Review D*, vol. 63, no. 1, p. 014006, 2000.

[259] C. W. Bauer, S. Fleming, D. Pirjol, and I. W. Stewart, "An effective field theory for collinear and soft gluons: Heavy to light decays," *Physical Review D*, vol. 63, no. 11, p. 114020, 2001.

[260] C. W. Bauer and I. W. Stewart, "Invariant operators in collinear effective theory," *Physics Letters B*, vol. 516, no. 1-2, pp. 134–142, 2001.

[261] C. W. Bauer, S. Fleming, D. Pirjol, I. Z. Rothstein, and I. W. Stewart, "Hard scattering factorization from effective field theory," *Physical Review D*, vol. 66, no. 1, p. 014017, 2002.

[262] M. Beneke and T. Feldmann, "Multipole-expanded soft-collinear effective theory with non-abelian gauge symmetry," *Physics Letters B*, vol. 553, no. 3-4, pp. 267–276, 2003.

[263] R. J. Hill and M. Neubert, "Spectator interactions in soft-collinear effective theory," *Nuclear Physics B*, vol. 657, pp. 229–256, 2003.

[264] B. Assi, B. A. Kniehl, and O. Veretin, "Static Potential of the Standard Model and Spontaneously Broken Theories," *arXiv preprint: hep-ph/2011.06437*, 2020.

[265] A. V. Smirnov, V. A. Smirnov, and M. Steinhauser, "Three-loop static potential," *Physical review letters*, vol. 104, no. 11, p. 112002, 2010.

[266] M. Beneke, Y. Kiyo, P. Marquard, A. Penin, J. Piclum, and M. Steinhauser, "Next-to-next-to-next-to-leading order QCD prediction for the top antitop s-wave pair production cross section near threshold in e^+e^- annihilation," *Physical review letters*, vol. 115, no. 19, p. 192001, 2015.

[267] J. Maldacena, "Wilson loops in large N field theories," *Physical Review Letters*, vol. 80, no. 22, p. 4859, 1998.

[268] N. Arkani-Hamed, D. P. Finkbeiner, T. R. Slatyer, and N. Weiner, "A theory of dark matter," *Physical Review D*, vol. 79, no. 1, p. 015014, 2009.

[269] M. Beneke, R. Szafron, and K. Urban, "Wino potential and Sommerfeld effect at NLO," *arXiv preprint: hep-ph/1909.04584*, 2019.

[270] L. Susskind, "Weak and electromagnetic interactions at high energy," in *Les Houches lecture notes 1976*, North Holland, 1977.

[271] Y. Schröder, "The static potential in QCD to two loops," *Physics Letters B*, vol. 447, no. 3-4, pp. 321–326, 1999.

[272] N. Brambilla, J. Ghiglieri, and A. Vairo, "Three-quark static potential in perturbation theory," *Physical Review D*, vol. 81, no. 5, p. 054031, 2010.

[273] M. Bander, "Theories of quark confinement," *Physics Reports*, vol. 75, no. 4, pp. 205–286, 1981.

[274] T. Appelquist, M. Dine, and I. Muzinich, "The static potential in quantum chromodynamics," *Physics Letters B*, vol. 69, no. 2, pp. 231–236, 1977.

[275] K. Symanzik, "Small distance behaviour in field theory and power counting," *Communications in Mathematical Physics*, vol. 18, no. 3, pp. 227–246, 1970.

[276] D. Barry, J.-Y. Parlange, L. Li, H. Prommer, C. Cunningham, and F. Stagnitti, "Analytical approximations for real values of the lambert w-function," *Mathematics and Computers in Simulation*, vol. 53, no. 1-2, pp. 95–103, 2000.

[277] A. Kataev and V. Molokoedov, "Fourth-order QCD renormalization group quantities in the v scheme and the relation of the β function to the gell-mann–low function in QED," *Physical Review D*, vol. 92, no. 5, p. 054008, 2015.

[278] A. Pineda, "Static potential in $\mathcal{N} = 4$ supersymmetric yang-mills theory at weak coupling," *Physical Review D*, vol. 77, no. 2, p. 021701, 2008.

[279] M. Prausa and M. Steinhauser, "Two-loop static potential in $\mathcal{N} = 4$ supersymmetric Yang-Mills theory," *Physical Review D*, vol. 88, no. 2, p. 025029, 2013.

[280] E. Lifshitz, LD, and S. L. (JB), *Quantum Mechanics; Non-relativistic Theory*. Pergamon Press, 1959.

[281] V. Berestetskii, E. Lifshitz, and L. Pitaevskii, "Quantum electrodynamics," 1980.

[282] A. Pineda and J. Soto, "Effective field theory for ultrasoft momenta in NRQCD and NRQED," *arXiv preprint hep-ph/9707481*, 1997.

[283] S. J. Brodsky, G. P. Lepage, and P. B. Mackenzie, "On the elimination of scale ambiguities in perturbative quantum chromodynamics," *Physical Review D*, vol. 28, no. 1, p. 228, 1983.

[284] U. Aglietti and Z. Ligeti, "Renormalons and the quark potential," *Physics Letters B*, vol. 364, no. 2, pp. 75–77, 1995.

[285] M. Jeżabek, M. Peter, and Y. Sumino, "Relation between QCD potentials in momentum and position space," *Physics Letters B*, vol. 428, no. 3-4, pp. 352–358, 1998.

[286] I. I. Bigi, M. A. Shifman, N. Uraltsev, and A. Vainshtein, "Pole mass of the heavy quark: Perturbation theory and beyond," *Physical Review D*, vol. 50, no. 3, p. 2234, 1994.

[287] A. H. Hoang and I. W. Stewart, "Top mass measurements from jets and the tevatron top-quark mass," *Nuclear Physics B-Proceedings Supplements*, vol. 185, pp. 220–226, 2008.

[288] K. Melnikov and A. Yelkhovsky, "b quark low-scale running mass from Υ sum rules," *Physical Review D*, vol. 59, no. 11, p. 114009, 1999.

[289] C. Ayala, G. Cvetič, and A. Pineda, "The bottom quark mass from the Upsilon (1S) system at NNNLO," *Journal of High Energy Physics*, vol. 2014, no. 9, p. 45, 2014.

[290] T. Bringmann, F. Kahlhoefer, K. Schmidt-Hoberg, and P. Walia, "Strong constraints on self-interacting dark matter with light mediators," *Physical review letters*, vol. 118, no. 14, p. 141802, 2017.

[291] J. Wess and J. Bagger, *Supersymmetry and supergravity*. Princeton university press, 1992.

[292] T. Appelquist, H.-C. Cheng, and B. A. Dobrescu, "Bounds on universal extra dimensions," *Physical Review D*, vol. 64, no. 3, p. 035002, 2001.

[293] M. Kakizaki, S. Matsumoto, Y. Sato, and M. Senami, "Relic abundance of LKP dark matter in UED model including effects of second KK resonances," *Nuclear Physics B*, vol. 735, no. 1-3, pp. 84–95, 2006.

[294] S. Davidson and A. Ibarra, "A lower bound on the right-handed neutrino mass from leptogenesis," *Physics Letters B*, vol. 535, no. 1-4, pp. 25–32, 2002.

[295] S. Biondini, N. Brambilla, M. A. Escobedo, and A. Vairo, "An effective field theory for non-relativistic Majorana neutrinos," *Journal of High Energy Physics*, vol. 2013, no. 12, p. 28, 2013.

[296] S. Biondini, N. Brambilla, M. A. Escobedo, and A. Vairo, "CP asymmetry in heavy Majorana neutrino decays at finite temperature: the nearly degenerate case," *Journal of High Energy Physics*, vol. 2016, no. 3, p. 191, 2016.

[297] A. Palazzo, "Phenomenology of light sterile neutrinos: a brief review," *Modern Physics Letters A*, vol. 28, no. 07, p. 1330004, 2013.

[298] V. Shtabovenko, R. Mertig, and F. Orellana, "New developments in feyncalc 9.0," *Computer Physics Communications*, vol. 207, pp. 432–444, 2016.

[299] V. Shtabovenko, "FeynHelpers: connecting FeynCalc to FIRE and Package-X," *Computer Physics Communications*, vol. 218, pp. 48–65, 2017.

[300] A. Smirnov and F. Chukharev, "Fire6: Feynman integral reduction with modular arithmetic," *Computer Physics Communications*, vol. 247, p. 106877, 2020.

[301] H. H. Patel, "Package-x: A mathematica package for the analytic calculation of one-loop integrals," *Computer Physics Communications*, vol. 197, pp. 276–290, 2015.

[302] N. Brambilla, H. S. Chung, V. Shtabovenko, and A. Vairo, "Feynonium: Using feyncalc for automatic calculations in nonrelativistic effective field theories," *arXiv preprint: hep-ph/2006.15451*, 2020.

[303] P. Nogueira, "Automatic Feynman graph generation," *Journal of Computational Physics*, vol. 105, no. 2, pp. 279–289, 1993.

[304] J. A. Vermaseren, "New features of FORM," *arXiv preprint math-ph/0010025*, 2000.

[305] R. N. Lee, "Litered 1.4: a powerful tool for the reduction of the multiloop integrals," *arXiv preprint: hep-ph/1310.1145*, 2013.

[306] B. Assi and B. A. Kniehl, "Electro-weak corrections to heavy quark mass definitions," In Preparation.

[307] K. G. Chetyrkin, "Correlator of the quark scalar currents and $\Gamma_{\rm tot}(H \to \text{hadrons})$ at $\mathcal{O}(\alpha_s^3)$ in pQCD," *Physics Letters B*, vol. 390, no. 1-4, pp. 309–317, 1997.

[308] J. Vermaseren, S. Larin, and T. Van Ritbergen, "The 4-loop quark mass anomalous dimension and the invariant quark mass," *Physics Letters B*, vol. 405, no. 3-4, pp. 327–333, 1997.

[309] K. Chetyrkin and M. Steinhauser, "Short-distance mass of a heavy quark at order α_s^3," *Physical Review Letters*, vol. 83, no. 20, p. 4001, 1999.

[310] K. Chetyrkin, "Four-loop renormalization of QCD: Full set of renormalization constants and anomalous dimensions," *Nuclear Physics B*, vol. 710, no. 1-2, pp. 499–510, 2005.

[311] B. A. Kniehl and A. Sirlin, "Pole mass, width, and propagators of unstable fermions," *Physical Review D*, vol. 77, no. 11, p. 116012, 2008.

[312] E. G. Floratos, S. Narison, and E. de Rafael, "Spectral function sum rules in quantum chromodynamics:(i). charged currents sector," *Nuclear Physics B*, vol. 155, no. 1, pp. 115–149, 1979.

[313] A. H. Hoang, A. Jain, I. Scimemi, and I. W. Stewart, "Infrared renormalization-group flow for heavy-quark masses," *Physical review letters*, vol. 101, no. 15, p. 151602, 2008.

[314] M. Voloshin and M. Shifman *Soviet Journal of Nuclear Physics*, vol. 45, no. 2, pp. 292–294, 1987.

[315] A. V. Manohar and I. W. Stewart, "QCD heavy-quark potential to order v^2: One loop matching conditions," *Physical Review D*, vol. 62, no. 7, p. 074015, 2000.

[316] A. Pineda and J. Soto, "Matching at one loop for the four-quark operators in NRQCD," *Physical Review D*, vol. 58, no. 11, p. 114011, 1998.

[317] R. Frey, "Top quark physics at a future e^+e^- collider: Experimental aspects," *arXiv preprint hep-ph/9606201*, 1996.

[318] H. D. Politzer, "Power corrections at short distances," *Nuclear Physics B*, vol. 172, pp. 349–382, 1980.

[319] M. Beneke and V. A. Smirnov, "Asymptotic expansion of Feynman integrals near threshold," *arXiv preprint hep-ph/9711391*, 1997.

[320] T. Kinoshita and M. Nio, "Radiative corrections to the muonium hyperfine structure: The $\alpha(Z\alpha)^2$ correction," *Physical Review D*, vol. 53, no. 9, p. 4909, 1996.

[321] N. Brambilla, A. Vairo, and E. Mereghetti, "Hadronic quarkonium decays at order v^7," *Physical Review D*, vol. 79, no. 7, p. 074002, 2009.

[322] S. Pokorski and S. Pokorski, *Gauge field theories*, vol. 92. Cambridge University Press Cambridge, 2000.

[323] A. Pineda and J. Soto, "Matching the HQET to Coulomb-type bound states," *Physics Letters B*, vol. 361, no. 1-4, pp. 95–104, 1995.

[324] W. Kilian, T. Mannel, and T. Ohl, "Unimagined imaginary parts in heavy quark effective field theory," *arXiv preprint hep-ph/9303224*, 1993.

[325] B. Assi and B. A. Kniehl, "Electroweak Form Factor in Sudakov and Threshold Regimes with Effective Field Theories," *arXiv preprint: hep-ph/2011.14933*, 2020.

[326] J.-y. Chiu, A. Fuhrer, R. Kelley, and A. V. Manohar, "Factorization structure of gauge theory amplitudes and application to hard scattering processes at the LHC," *Physical Review D*, vol. 80, no. 9, p. 094013, 2009.

[327] M. Chiesa, G. Montagna, L. Barze, M. Moretti, O. Nicrosini, F. Piccinini, and F. Tramontano, "Electroweak Sudakov corrections to new physics searches at the LHC," *Physical review letters*, vol. 111, no. 12, p. 121801, 2013.

[328] T. Gehrmann, E. Glover, T. Huber, N. Ikizlerli, and C. Studerus, "Calculation of the quark and gluon form factors to three loops in QCD," *Journal of High Energy Physics*, vol. 2010, no. 6, p. 94, 2010.

[329] R. N. Lee, A. von Manteuffel, R. M. Schabinger, A. V. Smirnov, V. A. Smirnov, and M. Steinhauser, "Fermionic corrections to quark and gluon form factors in four-loop QCD," *arXiv preprint: hep-ph/2105.11504*, 2021.

[330] A. von Manteuffel and R. M. Schabinger, "Quark and gluon form factors to four-loop order in QCD: the n_f^3 contributions," *Physical Review D*, vol. 95, no. 3, p. 034030, 2017.

[331] B. Agarwal, A. von Manteuffel, E. Panzer, and R. M. Schabinger, "Four-loop collinear anomalous dimensions in QCD and $\mathcal{N} = 4$ super Yang-Mills," *Physics Letters B*, vol. 820, p. 136503, 2021.

[332] J. M. Henn, A. V. Smirnov, V. A. Smirnov, and M. Steinhauser, "A planar four-loop form factor and cusp anomalous dimension in QCD," *Journal of High Energy Physics*, vol. 2016, no. 5, pp. 1–17, 2016.

[333] J. Henn, R. N. Lee, A. V. Smirnov, V. A. Smirnov, and M. Steinhauser, "Four-loop photon quark form factor and cusp anomalous dimension in the large-n_c limit of QCD," *Journal of High Energy Physics*, vol. 2017, no. 3, pp. 1–13, 2017.

[334] S. Moch, B. Ruijl, T. Ueda, J. Vermaseren, and A. Vogt, "Four-loop non-singlet splitting functions in the planar limit and beyond," *Journal of High Energy Physics*, vol. 2017, no. 10, pp. 1–80, 2017.

[335] S. Moch, B. Ruijl, T. Ueda, J. Vermaseren, and A. Vogt, "On quartic colour factors in splitting functions and the gluon cusp anomalous dimension," *Physics Letters B*, vol. 782, pp. 627–632, 2018.

[336] R. N. Lee, A. V. Smirnov, V. A. Smirnov, and M. Steinhauser, "n_f^2 contributions to fermionic four-loop form factors," *Physical Review D*, vol. 96, no. 1, p. 014008, 2017.

[337] R. N. Lee, A. V. Smirnov, V. A. Smirnov, and M. Steinhauser, "Four-loop quark form factor with quartic fundamental colour factor," *Journal of High Energy Physics*, vol. 2019, no. 2, pp. 1–16, 2019.

[338] A. von Manteuffel and R. M. Schabinger, "Quark and gluon form factors in four-loop QCD: The n_f^2 and $n_{q\gamma}n_f$ contributions," *Physical Review D*, vol. 99, no. 9, p. 094014, 2019.

[339] W. Bernreuther, R. Bonciani, T. Gehrmann, R. Heinesch, T. Leineweber, and E. Remiddi, "Two-loop QCD corrections to the heavy quark form factors: Anomaly contributions," *Nuclear Physics B*, vol. 723, no. 1-2, pp. 91–116, 2005.

[340] J. Blümlein, P. Marquard, N. Rana, and C. Schneider, "Heavy quark form factors at three loops," 2019.

[341] J. Ablinger, J. Blümlein, P. Marquard, N. Rana, and C. Schneider, "Heavy quark form factors at three loops in the planar limit," *Physics Letters B*, vol. 782, pp. 528–532, 2018.

[342] N. Brambilla, A. Pineda, J. Soto, and A. Vairo, "Effective-field theories for heavy quarkonium," *Reviews of Modern Physics*, vol. 77, no. 4, p. 1423, 2005.

[343] M. Ciafaloni, P. Ciafaloni, and D. Comelli, "Bloch-Nordsieck violating electroweak corrections to inclusive TeV scale hard processes," *Physical review letters*, vol. 84, no. 21, p. 4810, 2000.

[344] P. Ciafaloni and D. Comelli, "Electroweak Sudakov form factors and nonfactorizable soft QED effects at NLC energies," *Physics Letters B*, vol. 476, no. 1-2, pp. 49–57, 2000.

[345] V. S. Fadin, L. Lipatov, A. D. Martin, and M. Melles, "Resummation of double logarithms in electroweak high energy processes," *Physical Review D*, vol. 61, no. 9, p. 094002, 2000.

[346] J. H. Kühn, A. A. Penin, and V. A. Smirnov, "Summing up subleading Sudakov logarithms," *The European Physical Journal C-Particles and Fields*, vol. 17, no. 1, pp. 97–105, 2000.

[347] B. Feucht, J. H. Kühn, A. A. Penin, and V. A. Smirnov, "Two-loop Sudakov form factor in a theory with a mass gap," *Physical review letters*, vol. 93, no. 10, p. 101802, 2004.

[348] B. Jantzen, J. H. Kühn, A. A. Penin, and V. A. Smirnov, "Two-loop high-energy electroweak logarithmic corrections in a spontaneously broken SU(2) gauge model," *Physical Review D*, vol. 72, no. 5, p. 051301, 2005.

[349] A. Denner and S. Pozzorini, "One-loop leading logarithms in electroweak radiative corrections," *The European Physical Journal C-Particles and Fields*, vol. 18, no. 3, pp. 461–480, 2001.

[350] M. Hori, H. Kawamura, and J. Kodaira, "Electroweak Sudakov at two loop level," *Physics Letters B*, vol. 491, no. 3-4, pp. 275–279, 2000.

[351] J. H. Kühn, S. Moch, A. Penin, and V. A. Smirnov, "Next-to-next-to-leading logarithms in four-fermion electroweak processes at high energy," *Nuclear Physics B*, vol. 616, no. 1-2, pp. 286–306, 2001.

[352] J.-y. Chiu, F. Golf, R. Kelley, and A. V. Manohar, "Electroweak Sudakov corrections using effective field theory," *Physical review letters*, vol. 100, no. 2, p. 021802, 2008.

[353] J.-y. Chiu, R. Kelley, and A. V. Manohar, "Electroweak corrections using effective field theory: Applications to the CERN LHC," *Physical Review D*, vol. 78, no. 7, p. 073006, 2008.

[354] A. M. M Czakon, P Fiedler, "Total top-quark pair-production cross section at hadron colliders through $\mathcal{O}(\alpha_s^4)$," *Physical Review Letters*, vol. 110, no. 25, p. 252004, 2013.

[355] M. Martinez and R. Miquel, "Multi-parameter fits to threshold observables at a future e^+e^- linear collider," *The European Physical Journal C-Particles and Fields*, vol. 27, no. 1, pp. 49–55, 2003.

[356] F. Simon, "Impact of theory uncertainties on the precision of the top quark mass in a threshold scan at future e^+e^--colliders," *arXiv preprint: hep-ph/1611.03399*, 2016.

[357] W. Beenakker, S. Brensing, M. Krämer, A. Kulesza, E. Laenen, and I. Niessen, "Supersymmetric top and bottom squark production at hadron colliders," *Journal of High Energy Physics*, vol. 2010, no. 8, p. 98, 2010.

[358] G. Ovanesyan, T. R. Slatyer, and I. W. Stewart, "Heavy dark matter annihilation from effective field theory," *Physical Review Letters*, vol. 114, no. 21, p. 211302, 2015.

[359] P. Ciafaloni, D. Comelli, A. Riotto, F. Sala, A. Strumia, and A. Urbano, "Weak corrections are relevant for dark matter indirect detection," *Journal of Cosmology and Astroparticle Physics*, vol. 2011, no. 03, p. 019, 2011.

[360] H. Georgi, "Heavy quark effective field theory," *Proc. of the Theoretical Advanced Study Institute*, p. 589, 1991.

[361] E. Braaten, A. Mohapatra, and H. Zhang, "Classical nonrelativistic effective field theories for a real scalar field," *Physical Review D*, vol. 98, no. 9, p. 096012, 2018.

[362] M. H. Namjoo, A. H. Guth, and D. I. Kaiser, "Relativistic corrections to nonrelativistic effective field theories," *Physical Review D*, vol. 98, no. 1, p. 016011, 2018.

[363] A. H. Guth, M. P. Hertzberg, and C. Prescod-Weinstein, "Do dark matter axions form a condensate with long-range correlation?," *Physical Review D*, vol. 92, no. 10, p. 103513, 2015.

[364] A. Pineda and J. Soto, "Effective field theory for ultrasoft momenta in NRQCD and NRQED," *Nuclear Physics B-Proceedings Supplements*, vol. 64, no. 1-3, pp. 428–432, 1998.

[365] H. Georgi, "D-$\bar{D}$ mixing in heavy quark effective field theory," *Physics Letters B*, vol. 297, no. 3-4, pp. 353–357, 1992.

[366] G. Hiller and F. Krüger, "More model-independent analysis of b$\to$ s processes," *Physical Review D*, vol. 69, no. 7, p. 074020, 2004.

[367] E. Jenkins and A. V. Manohar, "Baryon chiral perturbation theory using a heavy fermion lagrangian," *Physics Letters B*, vol. 255, no. 4, pp. 558–562, 1991.

[368] A. Hoang and A. Manohar, "Charm effects in the ms bottom quark mass from υ mesons," *Physics Letters B*, vol. 483, no. 1-3, pp. 94–98, 2000.

[369] A. V. Manohar, "Effective field theories," in *Perturbative and nonperturbative aspects of quantum field theory*, pp. 311–362, Springer, 1977.

[370] A. V. Manohar, "Deep inelastic scattering as $X \to 1$ using soft-collinear effective theory," *Physical Review D*, vol. 68, no. 11, p. 114019, 2003.

[371] M. E. Machacek and M. T. Vaughn, "Two-loop renormalization group equations in a general quantum field theory:(III). Scalar quartic couplings," *Nuclear Physics B*, vol. 249, no. 1, pp. 70–92, 1985.

[372] C. W. Bauer and A. V. Manohar, "Shape function effects in $B \to Xs\gamma$ and $B \to Xul\nu$ decays," *Physical Review D*, vol. 70, no. 3, p. 034024, 2004.

[373] A. K. Leibovich, Z. Ligeti, and M. B. Wise, "Comment on quark masses in SCET," *Physics Letters B*, vol. 564, no. 3-4, pp. 231–234, 2003.

[374] S. Fleming, A. H. Hoang, S. Mantry, and I. W. Stewart, "Jets from massive unstable particles: Top-mass determination," *Physical Review D*, vol. 77, no. 7, p. 074010, 2008.

[375] C. W. Bauer, A. V. Manohar, and M. B. Wise, "Enhanced nonperturbative effects in jet distributions," *Physical review letters*, vol. 91, no. 12, p. 122001, 2003.

[376] S. Dittmaier and C. Grosse-Knetter, "Integrating out the standard Higgs field in the path integral," *Nuclear Physics B*, vol. 459, no. 3, pp. 497–536, 1996.

[377] K. Chetyrkin, A. Kataev, and F. Tkachov, "New approach to evaluation of multiloop Feynman integrals: The gegenbauer polynomial x-space technique," *Nuclear Physics B*, vol. 174, no. 2-3, pp. 345–377, 1980.

[378] R. Lee, "Presenting litered: a tool for the loop integrals reduction," *arXiv preprint: hep-ph/1212.2685*, 2012.

[379] W. Van Neerven, "Dimensional regularization of mass and infrared singularities in two-loop on-shell vertex functions," *Nuclear Physics B*, vol. 268, no. 2, pp. 453–488, 1986.

[380] J. Fleischer and M. Y. Kalmykov, "ON-SHELL2: FORM based package for the calculation of two-loop self-energy single scale Feynman diagrams occurring in the Standard Model," *Computer physics communications*, vol. 128, no. 3, pp. 531–549, 2000.

[381] B. Assi, B. A. Kniehl, and A. Onischenko, "Massive two-loop heavy particle diagrams," In Preparation.

[382] M. Bauer, M. Neubert, S. Renner, M. Schnubel, and A. Thamm, "The low-energy effective theory of axions and ALPs," *arXiv preprint: hep-ph/2012.12272*, 2020.

[383] B. Mecaj and M. Neubert, "Effective field theory for leptoquarks," *arXiv preprint: hep-ph/2012.02186*, 2020.

[384] R. Aoude, K. Haddad, and A. Helset, "On-shell heavy particle effective theories," *Journal of High Energy Physics*, vol. 2020, no. 2001.09164, pp. 1–44, 2020.

[385] Z. Bern, D. Kosmopoulos, and A. Zhiboedov, "Gravitational effective field theory islands, low-spin dominance, and the four-graviton amplitude," *arXiv preprint: hep-ph/2103.12728*, 2021.

[386] R. N. Lee and V. A. Smirnov, "Evaluating the last missing ingredient for the three-loop quark static potential by differential equations," *Journal of High Energy Physics*, vol. 2016, no. 10, pp. 1–9, 2016.

[387] J. M. Henn, "Multiloop integrals in dimensional regularization made simple," *Physical review letters*, vol. 110, no. 25, p. 251601, 2013.

[388] R. N. Lee and A. A. Pomeransky, "Normalized Fuchsian form on Riemann sphere and differential equations for multiloop integrals," *arXiv preprint: hep-ph/1707.07856*, 2017.

[389] R. N. Lee, "Reducing differential equations for multiloop master integrals," *Journal of High Energy Physics*, vol. 2015, no. 4, p. 108, 2015.

[390] A. B. Goncharov, "Multiple polylogarithms, cyclotomy and modular complexes," *arXiv preprint: hep-ph/1105.2076*, 2011.

[391] E. Remiddi and J. A. Vermaseren, "Harmonic polylogarithms," *International Journal of Modern Physics A*, vol. 15, no. 05, pp. 725–754, 2000.

[392] A. Levin and A. Beilinson, "Elliptic polylogarithms," in *Proceedings of Symposia in Pure Mathematics*, vol. 55, pp. 126–196, 1994.

[393] S. Bloch and P. Vanhove, "The elliptic dilogarithm for the sunset graph," *Journal of Number Theory*, vol. 148, pp. 328–364, 2015.

[394] L. Adams, C. Bogner, A. Schweitzer, and S. Weinzierl, "The kite integral to all orders in terms of elliptic polylogarithms," *Journal of Mathematical Physics*, vol. 57, no. 12, p. 122302, 2016.

[395] E. Remiddi and L. Tancredi, "An elliptic generalization of multiple polylogarithms," *Nuclear Physics B*, vol. 925, pp. 212–251, 2017.

[396] J. Broedel, C. Duhr, F. Dulat, and L. Tancredi, "Elliptic polylogarithms and iterated integrals on elliptic curves. part i: general formalism," *Journal of High Energy Physics*, vol. 2018, no. 5, pp. 1–54, 2018.

[397] S. Weinzierl, "Modular transformations of elliptic Feynman integrals," *Nuclear Physics B*, vol. 964, p. 115309, 2021.

[398] M. Bezuglov, A. Onishchenko, and O. Veretin, "Massive kite diagrams with elliptics," *Nuclear Physics B*, vol. 963, p. 115302, 2021.

[399] S. Bloch, M. Kerr, and P. Vanhove, "A Feynman integral via higher normal functions," *Compositio Mathematica*, vol. 151, no. 12, pp. 2329–2375, 2015.

[400] L. Adams, E. Chaubey, and S. Weinzierl, "Planar double box integral for top pair production with a closed top loop to all orders in the dimensional regularization parameter," *Physical review letters*, vol. 121, no. 14, p. 142001, 2018.

[401] L. Adams, E. Chaubey, and S. Weinzierl, "Analytic results for the planar double box integral relevant to top-pair production with a closed top loop," *Journal of High Energy Physics*, vol. 2018, no. 10, pp. 1–77, 2018.

[402] A. Primo and L. Tancredi, "Maximal cuts and differential equations for Feynman integrals. an application to the three-loop massive banana graph," *Nuclear Physics B*, vol. 921, pp. 316–356, 2017.

[403] R. N. Lee, "Libra: a package for transformation of differential systems for multiloop integrals," *arXiv preprint: hep-ph/2012.00279*, 2020.

[404] M. Czakon, "Automatized analytic continuation of mellin–barnes integrals," *Computer physics communications*, vol. 175, no. 8, pp. 559–571, 2006.

[405] M. Ochman and T. Riemann, "MBsums-a Mathematica package for the representation of Mellin-Barnes integrals by multiple sums," *arXiv preprint: hep-ph/1511.01323*, 2015.

[406] T. Huber and D. Maitre, "Hypexp 2, expanding hypergeometric functions about half-integer parameters," *Computer Physics Communications*, vol. 178, no. 10, pp. 755–776, 2008.

[407] H. Ferguson, D. Bailey, and S. Arno, "Analysis of PSLQ, an integer relation finding algorithm," *Mathematics of Computation*, vol. 68, no. 225, pp. 351–369, 1999.

[408] N. Nakanishi, *Graph theory and Feynman integrals*. Gordon and Breach, 1971.

[409] R. B. Paris and D. Kaminski, *Asymptotics and mellin-barnes integrals*, vol. 85. Cambridge University Press, 2001.

[410] L. Adams, C. Bogner, and S. Weinzierl, "The iterated structure of the all-order result for the two-loop sunrise integral," *Journal of Mathematical Physics*, vol. 57, no. 3, p. 032304, 2016.

[411] A. Smirnov, V. Smirnov, and M. Tentyukov, "FIESTA 2: parallelizeable multiloop numerical calculations," *Computer Physics Communications*, vol. 182, no. 3, pp. 790–803, 2011.

[412] K. Aomoto, M. Kita, T. Kohno, and K. Iohara, *Theory of hypergeometric functions*. Springer, 2011.

Acronyms

$\overline{\text{MS}}$ Modified Minimal Subtracted. 17,

N^{m}LO Next-to-^{m}Leading Order.

AMM Anomalous Magnetic Moment. 2,

AS Approximate Symmetry. 36,

BE Binding Energy. 3,

BSM Beyond the Standard Model. 2,

CFT Conformal Field Theory. 29,

CKM Cabibbo-Kobayashi-Maskawa. 15,

COM Centre of Mass. 2,

CP Charge-Parity. 15,

DM Dark Matter. 1,

DRA Dimensional Recurrence Algorithm. 168,

DRR Dimensional Recurrence Relations. 123,

EFT Effective Field Theory. 3,

EM Electromagnetism. 8,

EOM Equation of Motion. 36,

EPL Elliptical Polylogarithms. 124,

EW Electroweak. 2,

EWSB Electroweak Symmetry Breaking. 14,

FCC Future Circular Collider. 29,

FN Froggatt-Nielsen. 28,

FP Faddeev-Popov. 89,

GF Gauge-fixing. 16,

GR General Relativity. 1,

GUT Grand Unified Theory. 28,

HPET Heavy Particle Effective Theory. 88,

HPL Harmonic Polylogarithms. 167,

HQET Heavy Quark Effective Theory. 4,

HSET Heavy Scalar Effective Theory. 92,

IBP Integration-By-Parts. 36,

IR Infrared. 3,

KE Kinetic Energy. 3,

KK Kaluza-Klein. 58,

LC Light-Cone. 39,

LHC Large Hadron Collider. 1,

LKP Lightest Kaluza-Klein Particle. 58,

LO Leading Order. 2,

MB Mellin-Barnes. 130,

MI Master Integral. 107,

MPL Multiple Polylogarithms. 124,

MRS Minimal Renormalon Subtracted. 71,

MS Minimal Subtracted. 17,

MSSM Minimal Supersymmetric Standard Model. 28,

NEDM Neutron Electric Dipole Moment. 31,

NLO Next-to Leading Order. 2,

NNLO Next-to-next-to Leading Order. 20,

NR Non-Relativistic. 3,

NRQCD Non-Relativistic Quantum Chromodynamics. 4,

OS On-Shell. 50,

pNRQCD Potential Non-Relativistic Quantum Chromodynamics. 48,

PQ Peccei-Quinn. 31,

PQSB Peccei-Quinn Symmetry Breaking. 31,

PS Potential-Subtracted. 26,

QCD Quantum Chromodynamics. 2,

QED Quantum Electrodynamics. 3,

QFT Quantum Field Theory. 1,

RG Renormalisation Group.

RGE Renormalisation Group Equations. 19,

RGI Renormalisation Group Improved. 71,

RS Renormalon Subtracted. 27,

SCET Soft-Collinear Effective Theory. 39,

SM Standard Model. 1,

SMEFT Standard Model Effective Field Theory. 35,

SSB Spontaneous Symmetry Breaking. 7,

SUSY Supersymmetry. 31,

SV Small-Velocity. 26,

SYM Supersymmetric Yang-Mills. 43,

US Ultrasoft. 92,

UV Ultraviolet. 3,

VEV Vacuum Expectation Value. 13,

WFR Wave-Function Renormalisation. 50,

YM Yang-Mills. 43,

Eidesstattliche Versicherung / Declaration on oath

Hiermit versichere ich an Eides statt, die vorliegende Dissertationsschrift selbst verfasst und keine anderen als die angegebenen Hilfsmittel und Quellen benutzt zu haben.

Hamburg, den 27.08.2021

Unterschrift der Doktorandin / des Doktoranden